Australian Government

Ansto

Nuclear-based science benefiting all Australians

Research Selections 2012

As the home to Australia's nuclear expertise, the Australian Nuclear Science and Technology Organisation (ANSTO) is one of Australia's largest research organisations.

Nuclear science and technology is a dynamic area of research that focuses on the building blocks of matter. Many of the most important questions society faces in areas such as health, climate change and industry are being investigated by ANSTO researchers.

At the heart of ANSTO's research capabilities is the OPAL reactor which is one of the world's newest and best multi-purpose research reactors. OPAL is used for scientific research, the production of medical radioisotopes, the activation of targets and the irradiation of silicon used for electronics.

ANSTO operates two particle accelerators, STAR and ANTARES, which are used to analyse materials to determine their elemental composition and age and are fundamental to advancing knowledge in human history and the environment.

As a Federal Government agency, ANSTO's provides policy advice to Government on all matters relating to nuclear science, technology and engineering, supporting its international roles and obligations. ANSTO is connected with all Australian and New Zealand universities through the Australian Institute of Nuclear Science and Engineering (AINSE), providing researchers access to Australia's nuclear science, technology and engineering expertise.

Table of contents

Foreword

ANSTO is an instrument of the Australian Government committed to Australian scientists and researchers, Australian innovation and Australia's future. ANSTO's existence is inextricably linked to efforts to protect and sustain Australia's environment, to improve our health, to find ways to better diagnose and treat diseases, to produce nuclear medicines and to make a contribution to the global progress of nuclear science and technology.

While ANSTO's world-class infrastructure and science platforms are a demonstration of the foresight of the Australian Government, through the work of our researchers - and our collaborative thinking and strong partnerships - we contribute significantly to momentum in scientific discovery: bringing ideas to life.

Through strong collaborations great advances are made. ANSTO's local and international partnerships, as evidenced by the articles in this year's *Research Selections*, are part of a scientific network that reaches into universities, government and industry and other research organisations – all of which have a crucial contribution to make to research outcomes and, by extension, our living world.

ANSTO is part of the international science and technology community and is a hub for a vibrant research engagement and discovery. Each year hundreds of the world's top researchers who use nuclear techniques to advance knowledge head to ANSTO. These collaborations enable us to magnify our influence and reach across the geography of possibilities. Not least of all through the mechanism of collaborative agreements with international organisations thereby ensuring a gateway for Australian scientists to the best international facilities, including CERN's Large Hadron Collider - home to the intrepid Higgs Boson particle physicists.

Research Selections is a small sample of the vast amount of great science being leveraged with our infrastructure. But science doesn't stand still. To continue to achieve great science and ensure Australia remains at the forefront of discovery and innovation, we need to develop, grow and build on existing foundations of knowledge.

ANSTO is already custodian of OPAL – Australia's only nuclear reactor and one of the best research reactors in the world. Thanks to OPAL, we are able to supply vital nuclear medicine for Australians, irradiate silicon for the global semi-conductor market and, importantly, provide neutrons enabling researchers to probe matter at the nano and atomic scale, unlocking mysteries that can lead to profound discovery.

While OPAL puts ANSTO streets ahead of where it otherwise would be, we cannot and are not resting on our laurels. In April 2012, approximately100 national and international experts attended the Second OPAL Guide Hall Workshop to discuss the medium- to long-term future of OPAL, an essential step towards the full exploitation of this world-leading research infrastructure. They discussed the extremely rapid advances in neutron beam instruments over the past few years and brainstormed strategies for using these advances and building a second suite of beamlines and instruments that will be at the forefront of neutron beam capabilities.

ANSTO is also taking great strides in accelerator science. Our particle accelerators ANTARES and STAR are well established for analysing the elemental composition and age of materials using ion beam analysis and accelerator mass spectrometry. Two new accelerators will be established at ANSTO, as part of our Centre for Accelerator Science which has been funded through investment by the Government. These will enhance our capabilities in, for example, radiocarbon dating on historical artefacts, environmental studies, and determining how fossil fuels are contributing to climate change. The formation of the Australian Collaboration for Accelerator Science between the Australian Synchrotron, the University of Melbourne and the Australian National University is aimed at creating and maintaining a national pool of world class facilities and accelerator expertise. This collaboration will ensure Australia remains at the leading edge of accelerator capabilities and facilities.

In presenting this year's *Research Selections*, which showcases achievements throughout the past 12 or so months, I congratulate the researchers who have been published this year.

Dr Adi Paterson
Chief Executive Officer
ANSTO

Life sciences and food

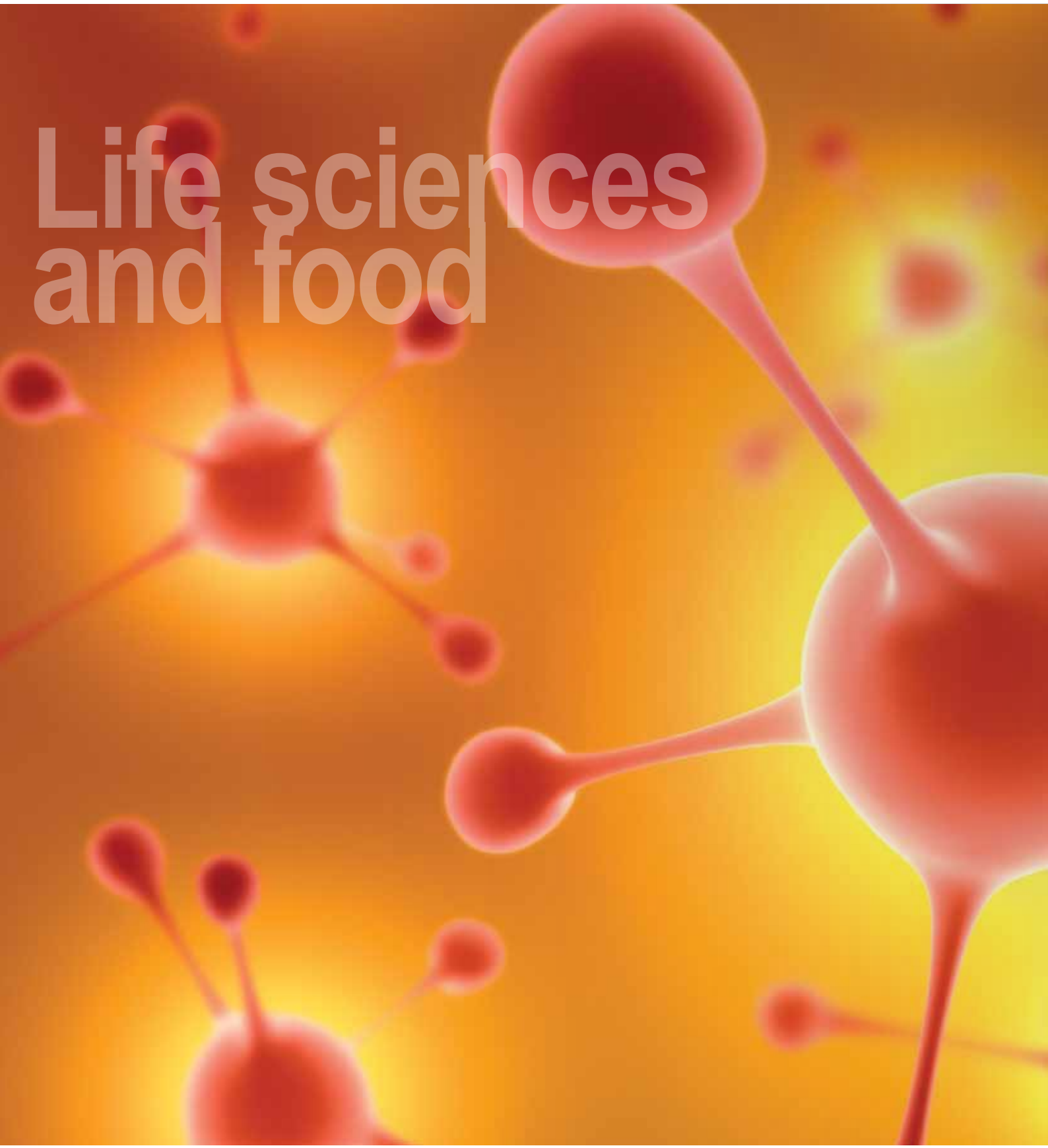

Life sciences and food

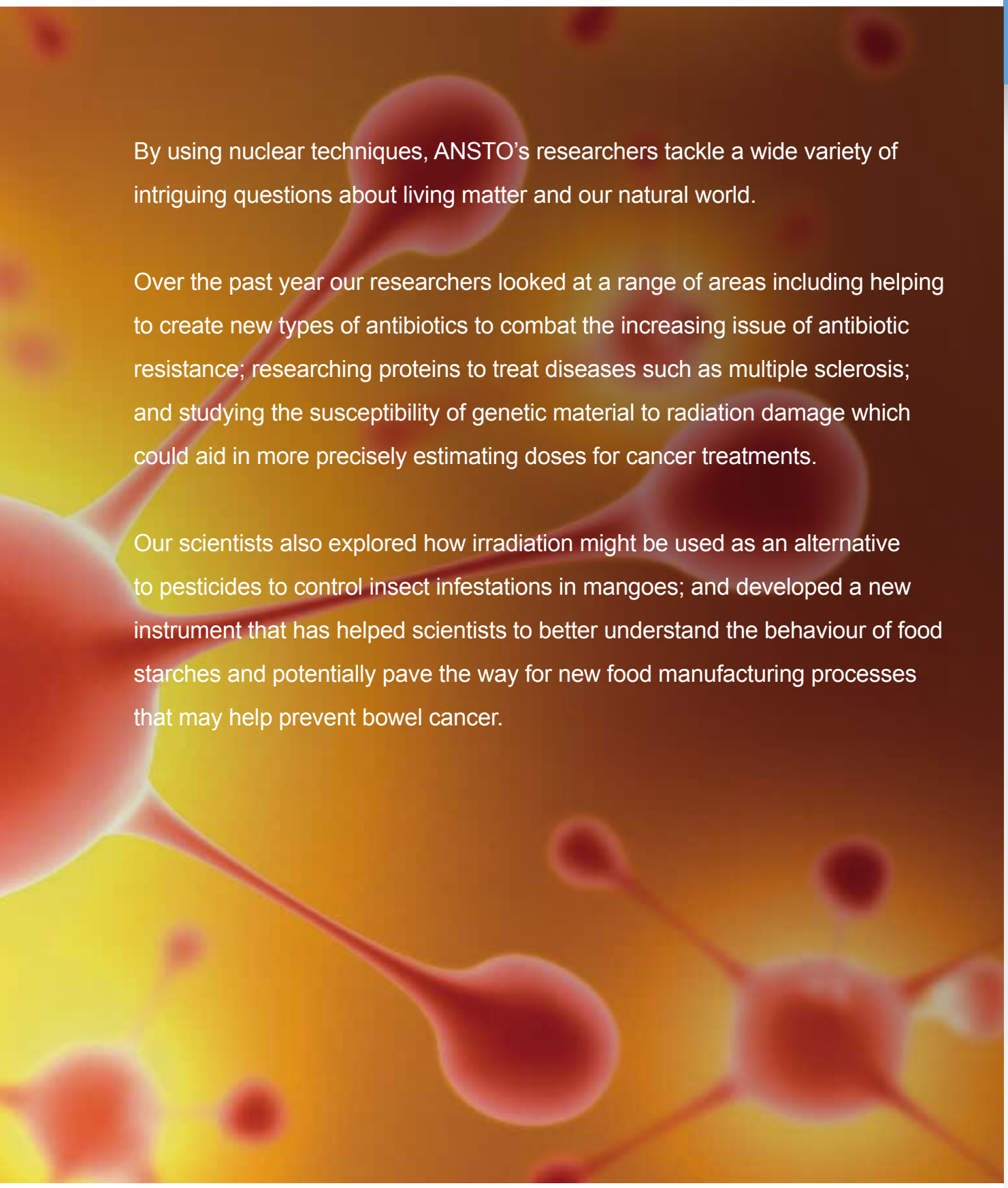

By using nuclear techniques, ANSTO's researchers tackle a wide variety of intriguing questions about living matter and our natural world.

Over the past year our researchers looked at a range of areas including helping to create new types of antibiotics to combat the increasing issue of antibiotic resistance; researching proteins to treat diseases such as multiple sclerosis; and studying the susceptibility of genetic material to radiation damage which could aid in more precisely estimating doses for cancer treatments.

Our scientists also explored how irradiation might be used as an alternative to pesticides to control insect infestations in mangoes; and developed a new instrument that has helped scientists to better understand the behaviour of food starches and potentially pave the way for new food manufacturing processes that may help prevent bowel cancer.

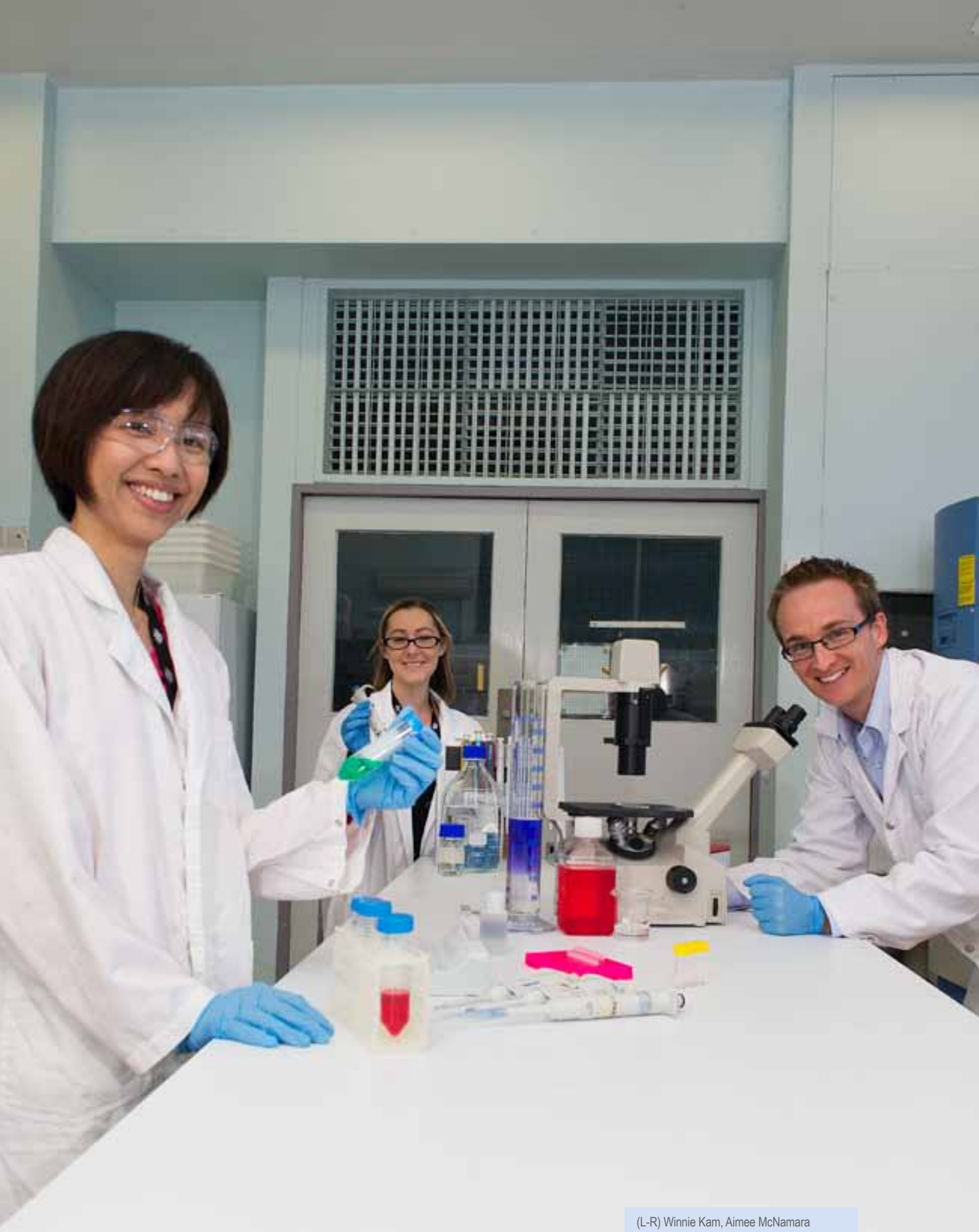

(L-R) Winnie Kam, Aimee McNamara and Justin Davies are working together to better understand the effects of radiation on genetic material.

Complex responses of extra-nuclear DNA and RNA after gamma irradiation

Winnie W.Y. Kam[1], Aimee L. McNamara[2], Connie Banos[1], Sohil Sheth[1], Justin B. Davies[1,2], Richard B. Banati[1,2]
[1]ANSTO, [2]University of Sydney.

The genetic information of a mammal cell is stored in two types of molecules: deoxyribonucleic acid (DNA) and ribonucleic acid (RNA).

Understanding the susceptibility of these molecules to radiation damage helps to more accurately estimate dose rates for cancer treatment.

While most research has focused on the effects of radiation on the DNA that is stored in the cell nucleus, our research shows that there are also significant effects on genetic material other than the cell nucleus i.e. mitochondria, the energy-producing units of the cell.

Our research shows that radiation has complex interactions with genetic material outside the nucleus and causes responses that are not yet captured by current dose estimation methods.

Genetic material outside the cell nucleus

Research into the impact of radiation on living matter is usually focused on its effect on the genetic material inside the cell nucleus, i.e. chromosomal DNA, and its repair mechanisms.

However, within the cytoplasm of the cell is an organelle, the mitochondrion which contains a small chromosome of its own, a small circular DNA coding for 37 genes. Sometimes referred to as the “power plants of the cell”, mitochondria generate adenosine triphosphate (ATP) as a source of energy. In addition to supplying cellular energy, mitochondria are involved in a range of other processes. They are also important for cell signalling, differentiation, growth, cell death, and the cell cycle.

Figs. 1A and 1B show electron microscope images of a cell (macrophages) containing numerous mitochondria; Figs. 1C to 1E show mitochondria in different functional states after cell activation. Fig. 2 shows mitochondria stained by a fluorescent dye. In many cell types, mitochondria take up a greater portion of the cell volume than the nucleus, as can be seen in Figs. 1 and 2. Thus, the likelihood of radiation being received by mitochondria is expected to be greater than for the nucleus.

There are two types of genetic material: deoxyribonucleic acid (DNA) and ribonucleic acid (RNA). DNA serves as the genetic blueprint. DNA is transcribed into RNA which is the messenger that translates into proteins. DNA is a relatively robust double-stranded, structure, which is either helical in the nucleus or circular in mitochondria. In contrast, RNA is single-stranded making it more vulnerable to various stresses, including radiation, see Fig. 3.

Despite the importance of RNA (for protein synthesis) and mitochondria (for energy production and hence cell survival), radiation-induced changes to the genetic material in mitochondria has so far received little attention.

Figure 1

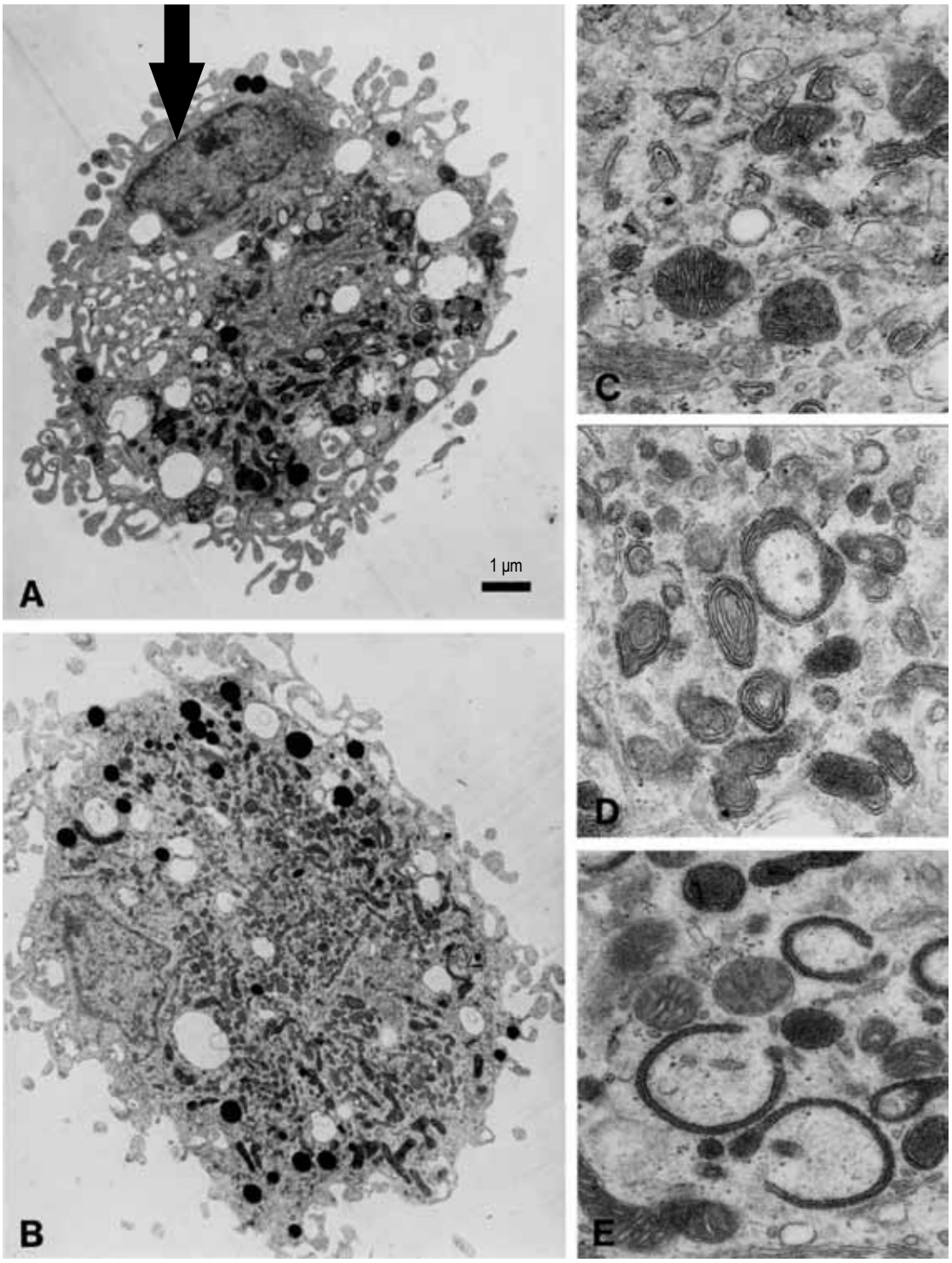

A mammalian brain macrophage (A & B): The arrow points to the cell nucleus. The mitochondria are the dark oval/elongated structures inside the cell. Scale bar: 1 µm.

The shape of the mitochondria reflects the functional state of the cell; (C) mitochondria in a resting cell; (D & E) mitochondria in activated cells (Image from [1]). Scale bar: 0.2 µm.

Figure 2

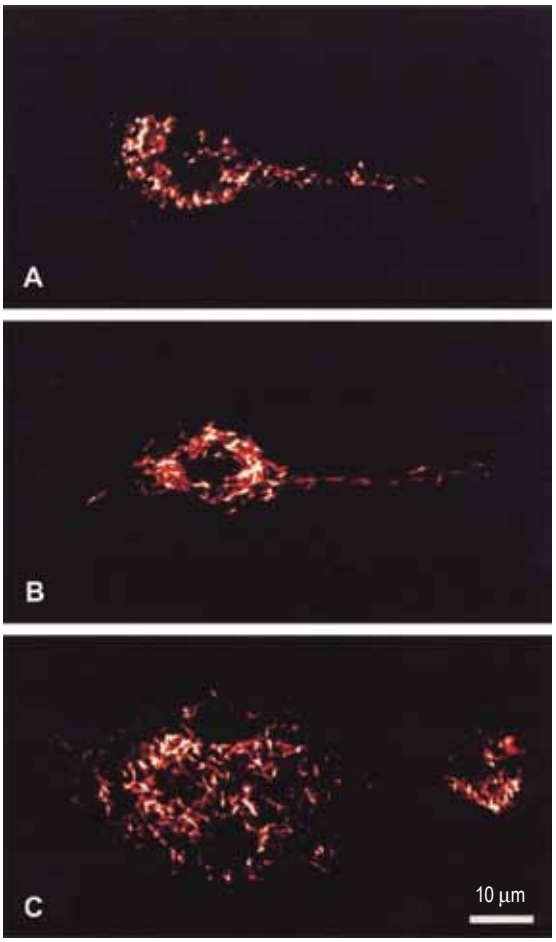

Visualization of mitochondria stained with a fluorescent mitochondrial dye. In contrast to a resting cell (A), activated cells have mitochondria, that form a dense network of often large elongated mitochondria (B & C). Scale bar: 10 µm (Image from [1]).

Figure 3

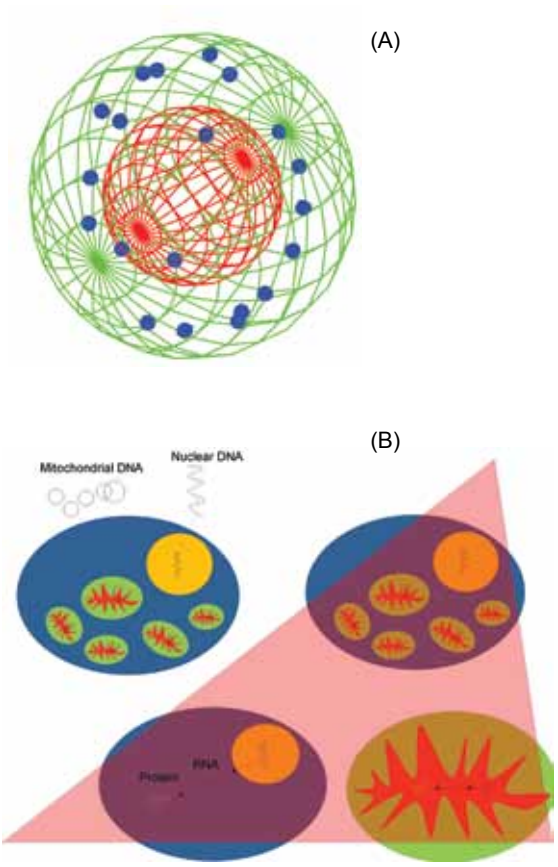

(A) A schematic view of the cell and the targets of our radiation experiment. Nucleus (red sphere) and mitochondria (blue spheres) are randomly distributed within the cell.

(B) Irradiation (red shadow) effects all components within the cell i.e. DNA in both nucleus (double-helical) and mitochondria (circular). Note that in mitochondria, the transcription from DNA into RNA and then translation into protein (protein synthesis) occurs within the space of the organelle; while for nuclear encoded genes, the protein synthesis occurs outside the nucleus in the cytosol.

Experimental gamma irradiation of cells

Mammalian cells (of lymphocytic lineage) were irradiated at room temperature using a cobalt-60 irradiator. ^{60}Co emits gamma rays, ionising, high-frequency electromagnetic radiation (similar to X-rays). Our control samples were kept at room temperature and were not irradiated. RNA and DNA extractions from the irradiated and non-irradiated cells were performed immediately after irradiation. The extracted RNA and DNA were analysed by quantifying the amount of mitochondrial gene present after irradiation using quantitative real-time polymerase chain reaction. This technique uses repeated amplification cycles to amplify minute quantities of target gene from a pool of nucleic acids (RNA or DNA template).

So far we have analysed 18 mitochondrial genes. Fig. 4 shows the results: After an irradiation dose of 100 Gy, 12 out of the 18 mitochondrial genes amplified from the mitochondrial RNA template showed an increase in the amplifiable amount.

This suggests that, in response to this particular radiation dose, there was already an early increase in the rate of transcription from the mitochondrial DNA into mitochondrial RNA during the period of irradiation itself (a period of ~2.5 minutes in our experiments).

Figure 4

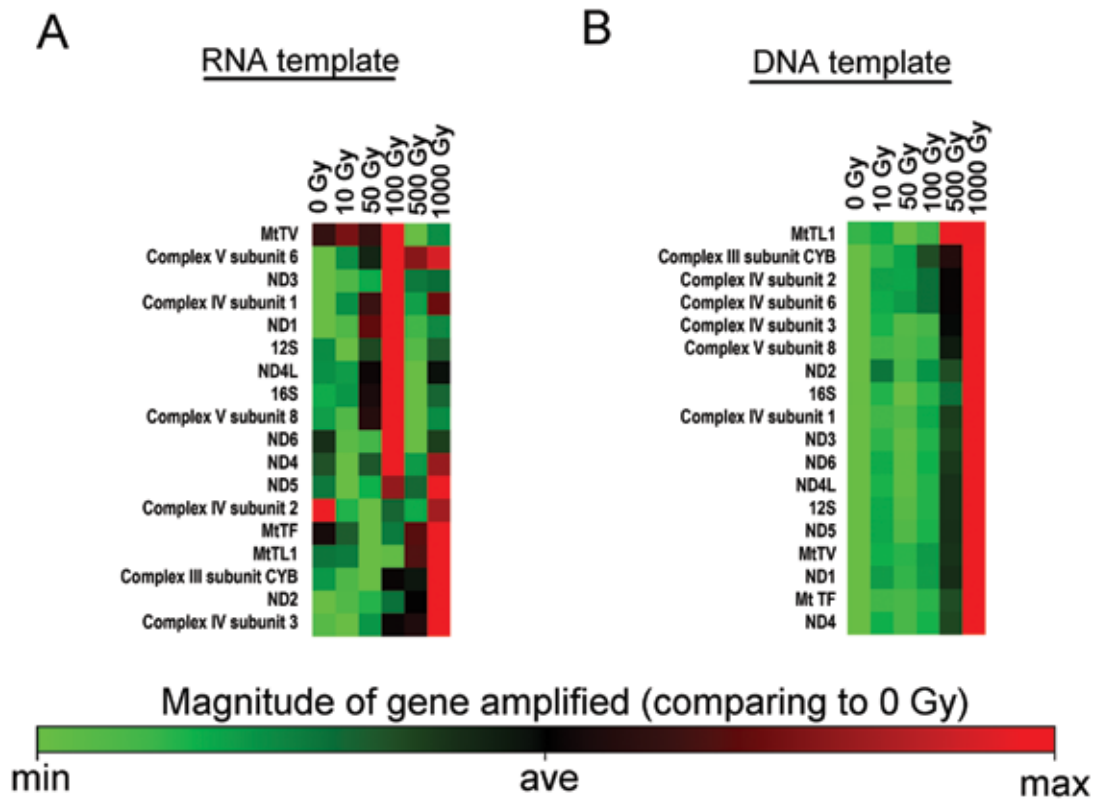

The acute response of mitochondrial RNA and DNA to gamma radiation. Genes were amplified from (A) RNA or (B) DNA template using a quantitative real-time polymerase chain reaction. The heat maps graphically represent the relative amount of the 18 selected mitochondrial genes amplified from each type of the template at each tested dose, when compared to the non-irradiated sample. The genes are sorted according to their overall similarity in quantity.

Interestingly, after irradiation, mitochondrial DNA also responded with an increase in the detectable amount. Unlike mitochondrial RNA, the multiplication of mitochondrial DNA was detectable only at the higher dose of 1000 Gy. We are currently dissecting the specific mechanism, such as time courses, temperature dependency and others, that lead to the changes in small mitochondrial chromosomes. This analysis also extends to the question of which pathways are likely to be affected by the differential regulation of mitochondrial RNA expression after radiation exposure. In summary, our data show that cell irradiation leads to a rich set of responses that relate to genetic material outside the cell nucleus. Since extra-nuclear DNA and RNA are crucial for vital cell functions, future radiation dose models will need to take into account the amount of radiation received by mitochondria as well as their complex dose-dependent response to it, see Fig. 5.

References

[1] Banati, R.B., Egensperger, R., Maassen, A., Hager, G., Kreutzberg, G.W. and Graeber, M.B., Mitochondria in activated microglia in vitro, Journal of Neurocytology, 33(5), 535-541 (2004).

Figure 5

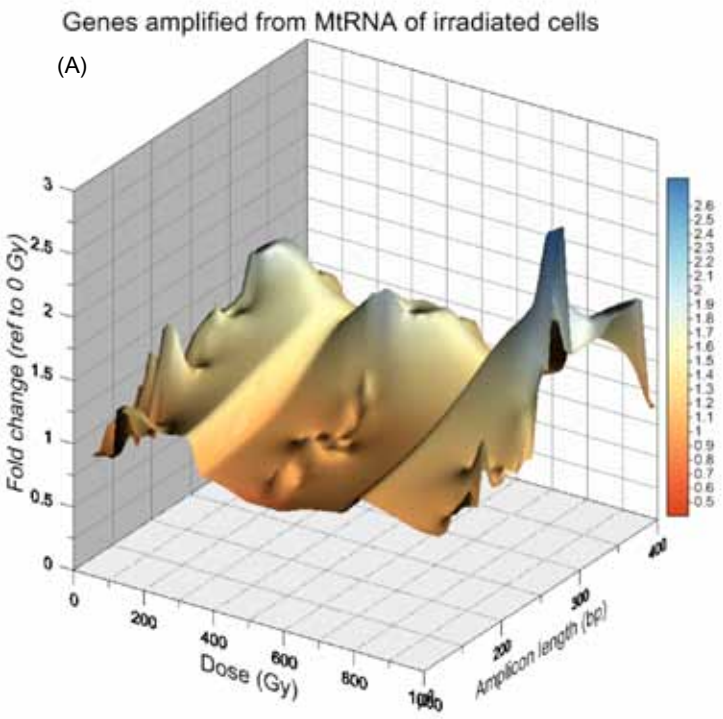

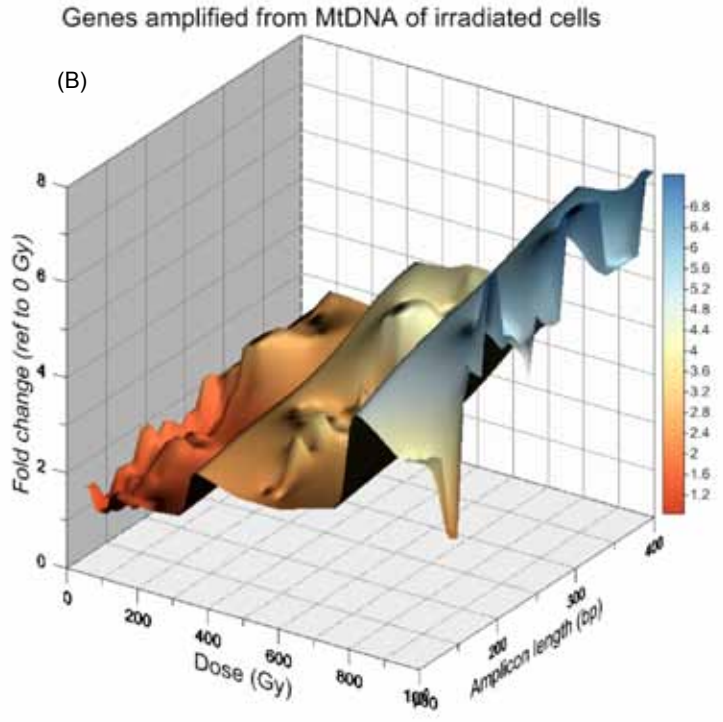

The relationship between the level of gene detectable (fold change reference to 0 Gy control), dose-delivered and the length of the amplified gene (amplicon length). 3D plots on the profiles of dose-dependent changes in amplifiable gene from (A) mitochondrial RNA and (B) mitochondrial DNA, demonstrating the complex highly differentiated response that varies significantly between different genes.

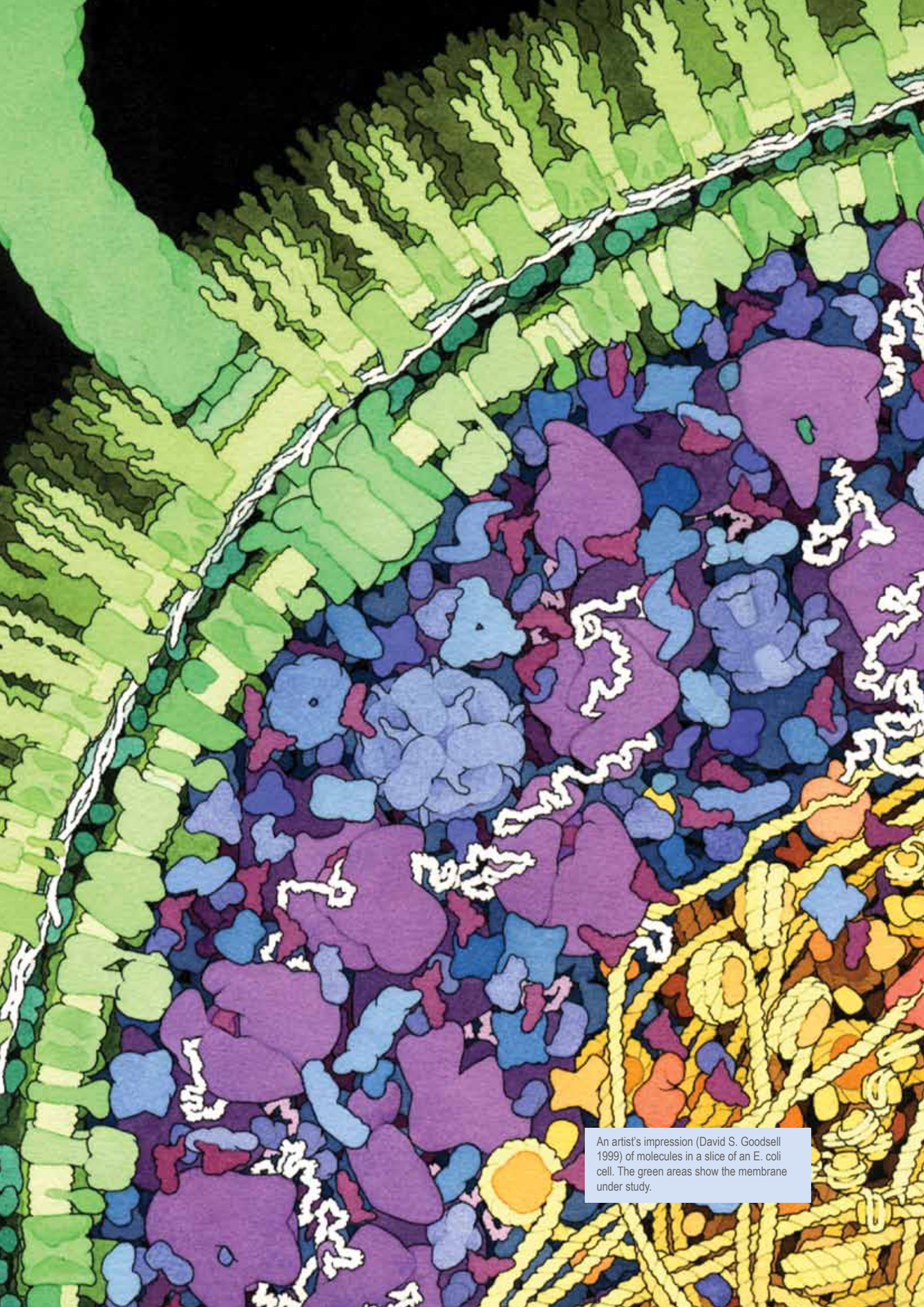

An artist's impression (David S. Goodsell 1999) of molecules in a slice of an E. coli cell. The green areas show the membrane under study.

Cell membrane studies helping to tackle antibiotic resistance

Tomas Mayfield, Anton Le Brun, Stephen Holt
ANSTO

Biological membranes are watertight barriers that regulate what gets in and out of cells. Some membranes have very specialised functions, such as insulation for nerve cells or capturing light in the rod cells of the eye. Currently, around the world, there are significant research efforts in developing antibiotics that can attack bacterial membranes to help combat the threat posed by antibiotic-resistant bacteria.

As membranes are highly complex structures models, or man-made copies of a bacterial membrane, are needed to better understand the effectiveness of a potential new drug.

In this study we have developed models of bacterial outer membranes and investigated their molecular structure using neutron reflectometry. The results show that the models we are creating of the bacterial outer membrane are biologically relevant, reproducible and can help test and develop better antibiotics.

All cells, whether bacterial or from higher organisms are surrounded by a membrane. The membrane is what separates the cell from its external environment. The membrane is made of a lipid bilayer which acts as a hydrophobic (water resistant) barrier. Distributed within the membrane are membrane proteins, which act as the cell's gate keepers, allowing nutrients into the cell and letting the waste products out. The importance of cell membranes is also underlined by the fact that over 60% of currently available drugs and 40% of new drugs target membrane proteins [1] and there is a large focus on antibiotics that attack the lipid-bilayer component of bacterial membranes. To better understand a membrane we need to understand the physical properties of the lipid bilayer and how membrane proteins function and assemble. This is not a trivial task. A cell membrane is a very complex structure with many different types of lipids and an even greater number of different proteins, all contributing to the function of the cell. To study biological membranes we take a reductionist approach i.e. we start with a very simple model, see how that works and then slowly build up in complexity. So our research seeks to investigate how to make these simple models and whether they mimic what is seen in nature.

So why use neutrons?

There are a number of reasons why scientists studying membranes want to use the neutrons produced by the OPAL reactor at ANSTO. The main neutron technique is neutron reflectometry, which provides a depth profile of the 5 to 6 nanometre thick membrane over a large area, whereas techniques such as microscopy only allow study of the initial membrane surface over small areas. Most proteins in the cell are surrounded by water. However, because membrane proteins reside in the water-resistant phospholipid bilayer this makes them difficult to study using many of the routine scientific techniques such as X-ray crystallography. Neutron reflectometry provides structural information on membrane proteins in their natural bilayer surrounding, by taking a slice through the depth of the membrane. Reflectometry tells us the thickness and distribution of the different components (typically lipids, proteins and water) as we measure through the depth of the bilayer.

Characterising model bacterial outer membranes

Bacteria that have a double membrane are classed as Gram-negative. Gram-negative bacteria include bacteria such as *E. coli* and *Salmonella*. They have an inner membrane and an outer membrane. The outer membrane is unusual in that it is asymmetric. An asymmetrical membrane is one in which the half of the membrane that faces the inside of the cell is very different from the half that faces the outside of the cell. We have made model membranes that replicate this asymmetry, using floating supported bilayers [2]. Floating supported bilayers are advantageous as the membrane is not physically bonded to the surface that supports it. This means that the properties of the

Figure 1

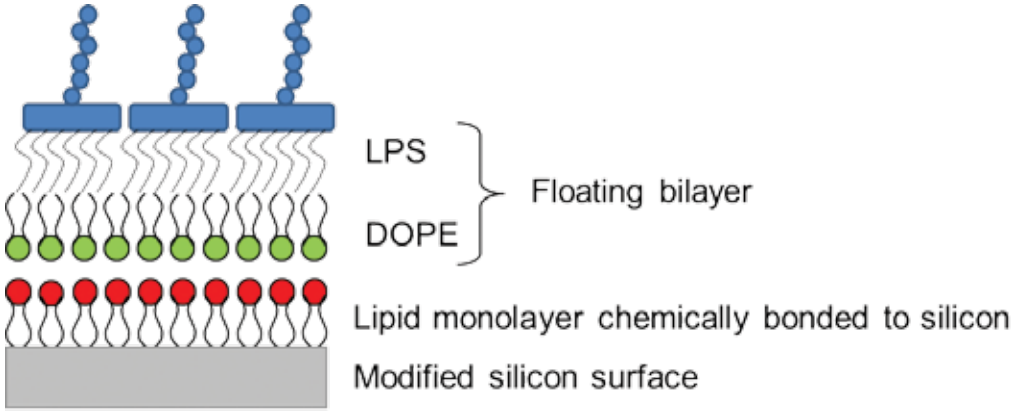

A schematic showing the principle of a floating supported bilayer. A lipid monolayer is chemically bonded to a modified silicon surface. Then using Langmuir-Blodgett deposition the lower lipid leaflet is deposited (in this case the DOPE layer) and then using Langmuir-Schaefer deposition an upper leaflet of lipids is deposited (the LPS layer).

model membrane are not influenced by the supporting surface and should behave more like a membrane found in nature. A silicon surface is used both because the surface can be made atomically flat, which is necessary for good neutron reflectometry measurements, and also because silicon is amenable to a number of different chemistries, making the surface easy to functionalise. To create the floating supported bilayer, a lipid monolayer is grafted onto a silicon surface. The bilayer that we wish to create then sits or floats above the grafted monolayer (Fig. 1). The membrane is created by using a series of Langmuir-Blodgett and Langmuir-Schaefer dipping techniques [3]. Using a state-of-the-art Langmuir dipping trough, the modified silicon surface is pushed through a monolayer of lipid on a liquid surface either vertically (Langmuir-Blodgett) or horizontally (Langmuir-Schaefer). When the silicon surface is passed through the lipid monolayer the material transfers from the liquid surface onto the silicon creating the floating bilayer. Using the dipping techniques we have managed to create for the first time asymmetric floating bilayers of di-oleoyl-phosphatidylethanolamine (DOPE) and lipopolysaccharide (LPS). DOPE is the most abundant lipid on the inner side of the membrane of the outer membrane, whilst LPS is the abundant molecule on the outer side of the outer membrane. These floating bilayers have been found to be good models, as they can replicate asymmetry, mimic the phase behaviour of lipids in nature and mimic the fluidity of bilayers. Using neutron reflectometry on the Platypus reflectometer at OPAL we have been able to characterise the structures of these model bacterial outer membranes. Fig. 2 shows the data collected on the reflectometer and the structure of the bilayer as a scattering-length, density profile. A neutron scattering-length density (SLD) can be considered as the “neutron refractive index” and we model the change in scattering-length density through each layer of the membrane to deduce its structure (Fig. 2).

Using deuteration to get further details

Neutron scattering in soft matter and biomolecular science can be made more advantageous if some components of a multi-component system are deuterated. Neutrons scatter from hydrogen very differently than from its heavier isotope deuterium. Therefore, if we label one of the components in the membrane system with deuterium, each component can be picked out of the complex system. Deuterated LPS was made in the bio-labs of the National Deuteration Facility at ANSTO. The deuterated LPS allows us to distinguish between it and the hydrogenous DOPE leaflet when we swap between a D_2O solvent and regular H_2O, adding further detail to our model, such as the surface coverage and molecular area of each component in the membrane.

Summary

We have created robust models of the outer membrane of Gram-negative bacteria. Using neutron reflectometry and molecular deuteration we have been able to characterise these model membranes to see if they reflect the properties of a membrane in nature. These model membranes are powerful tools for studying how membrane proteins function and how antibacterial agents and other drugs interact with membranes.

Figure 2

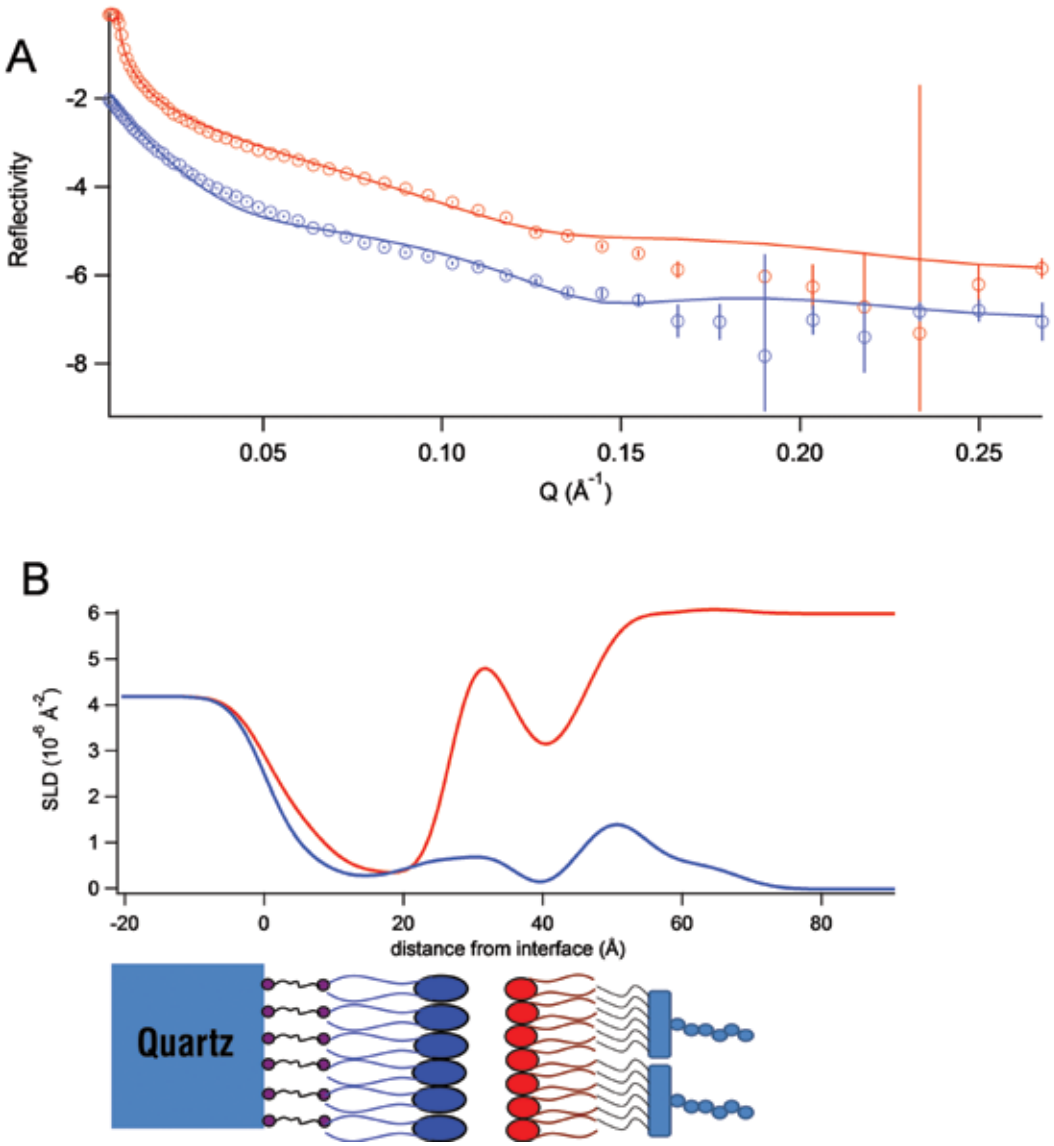

A) The reflectivity data (points with error bars) and model fits (lines) of a floating model membrane of DOPE and lipopolysaccharide under a D_2O (red) and H_2O (blue) solvent contrast. B) The corresponding neutron scattering-length density profile. The schematic below the profile shows the position of each component along the membrane.

References

[1] Yildirim, M. A., Goh, K.-I., Cusick, M. E., Barabasi, A.-L., and Vidal, M., Drug-target Network, Nature Biotechnology, 25(10), 1119-1126 (2007).

[2] Hughes, A. V., Howse, J. R., Dabkowska A., Jones, R. A. L., Lawrence M. J., Roser, S. J., Floating lipid bilayers deposited on chemically grafted phosphatidylcholine surfaces, Langmuir, 24(5), 1989-1999 (2008).

[3] Charitat, T., Bellet-Amalric, E., Fragneto, G., and Graner, F., Absorbed and free lipid bilayers at the solid-liquid interface. European Physical Journal B, 8(4), 583-593 (1999).

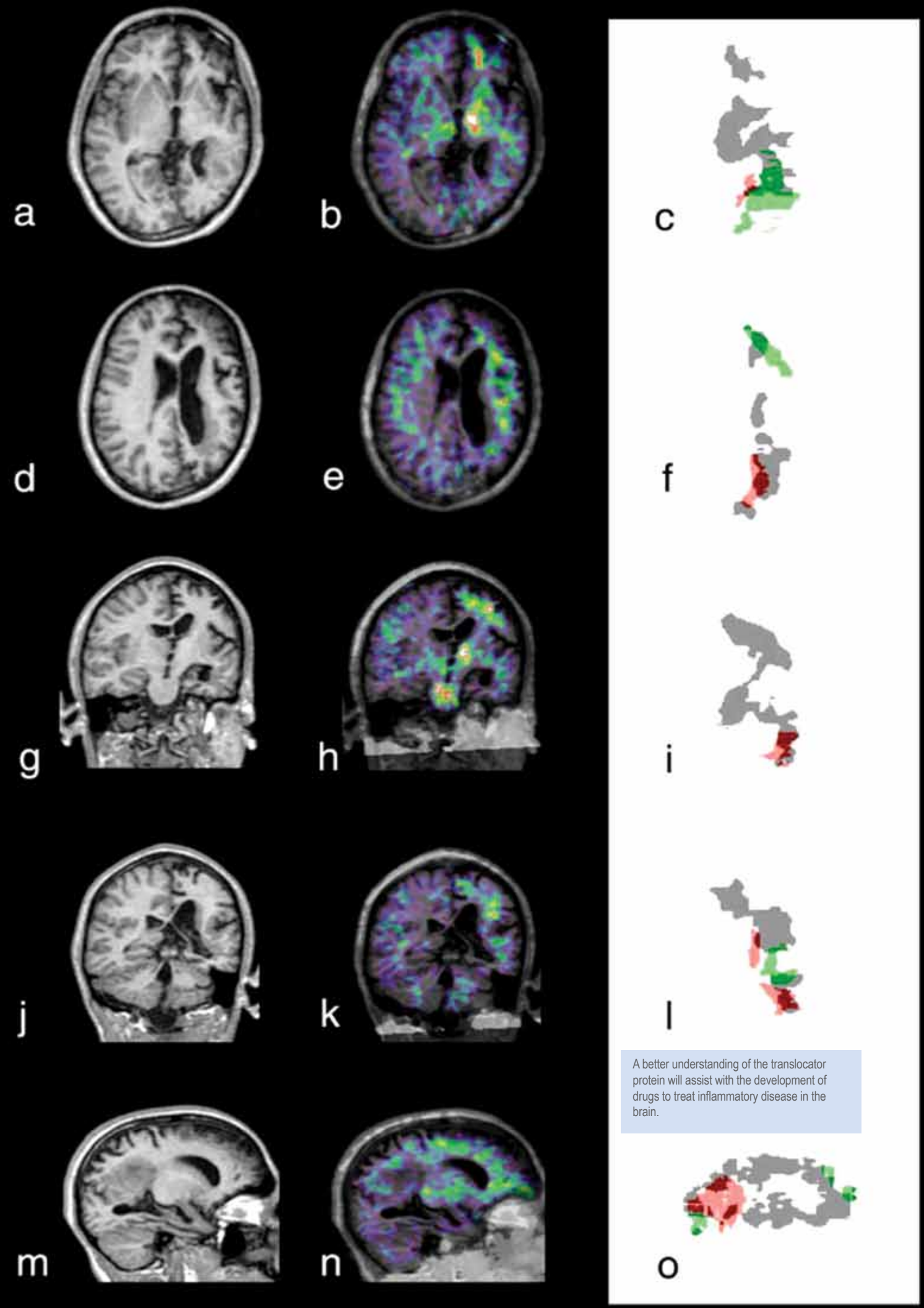

A better understanding of the translocator protein will assist with the development of drugs to treat inflammatory disease in the brain.

Learning more about inflammation by studying molecular mechanisms in the brain

Claire Hatty[1,2], Anton Le Brun[1], Vanessa Lake[1], Guo Jun Liu[1,2], Richard Banati[1,2]
[1]ANSTO, [2]University of Sydney

The translocator protein is a marker of inflammation in the brain, neuroinflammation, which is implicated in diseases such as multiple sclerosis and Alzheimer's disease.

An understanding of the structure and function of this protein is vital in developing drugs to treat neuroinflammation. ANSTO's research uses neutron reflectometry to study the structure of the translocator protein at the molecular level, to gain a deeper understanding of the protein and its interactions with potential drugs.

The translocator protein

The translocator protein (TSPO) is an integral membrane protein located primarily in the outer mitochondrial membrane of cells in a variety of peripheral tissue, and in immune cells in the brain [1]. It is highly conserved throughout evolution, indicating an important functional role for TSPO [1]. There is evidence that TSPO acts as a transport channel for cholesterol, a necessary step in steroid synthesis, and potentially acts as an ion channel [1]. Furthermore, TSPO has been implicated in inflammatory disease processes as it is greatly up-regulated in activated immune cells [2]. The synthetic TSPO ligand PK11195 has been shown to induce functional responses via TSPO, such as mitochondrial Ca^{2+} release, and potentially to modulate cholesterol transport and steroid production [1]. Despite the functional importance of TSPO, there is little structural data on the protein, due in large part to the difficulty of studying the structures of integral membrane proteins. The formation of a channel that can transport cholesterol was predicted using molecular dynamics [3], and a potential cholesterol recognition site was identified through nuclear magnetic resonance spectroscopy on a TSPO peptide [4]. However, further structural evidence of channel formation is needed, especially in relation to the effects of ligand binding on TSPO conformation, so that this can be correlated with the observed functional effects.

Using neutrons to study the TSPO

Neutron reflectometry makes it possible to study a membrane protein such as TSPO in a more natural lipid environment, which is extremely difficult using other structural techniques such as crystallography. The use of neutrons, in particular, allows contrast variation (the difference in scattering between hydrogen and deuterium) to be exploited. Measurements can be made with either deuterated lipids or deuterated protein, and in multiple solvent contrasts to 'match out' certain components. This aids in structural refinement, and allows for the selective analysis of the different components of the system that cannot be distinguished using other methods. We used neutron reflectometry in combination with our quartz crystal microbalance (Table 1) to study the formation of mixed TSPO – lipid bilayers, with a view to investigating changes associated with ligand binding.

Formation of TSPO – lipid bilayers

We used the quartz crystal microbalance with dissipation monitoring (QCM-D) technique to monitor the formation of protein – lipid bilayers. First, we immobilised mouse TSPO (mTSPO) solubilised in detergent to a surface engineered to bind the protein (Fig. 1a). Next, we formed a lipid bilayer around the protein layer by replacing detergent with lipid (Fig. 1b). The use of QCM-D allows us to monitor the adsorption of protein and lipid onto a resonating crystal surface. A decrease in frequency of the crystal indicates that mass has been added to the crystal surface. We observed a decrease in frequency when mTSPO binds to the crystal surface, indicating a protein surface coverage of approximately 75% (Fig. 2a). The final change in frequency, after replacing detergent with lipid, is consistent with the remaining area being filled by lipid (Fig. 2a). We then tested the effect of the TSPO ligand PK11195 on the frequency response, in an attempt to detect ligand binding. We incubated PK11195 with the protein-lipid bilayer, which resulted in a significant change ($p < 0.005$) in frequency compared to the interaction with the surface or lipid alone (Fig. 2b). The change was greater than expected for the mass of

Figure 1

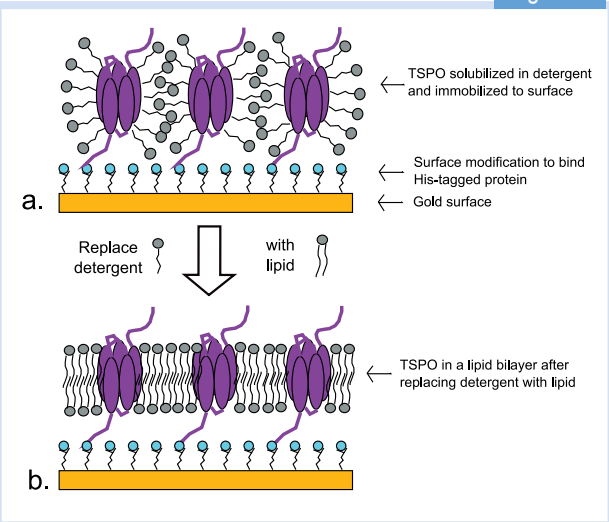

Process of forming a protein – lipid bilayer. Detergent solubilised protein is immobilised to the surface (a), and detergent is gradually replaced with lipid (b).

the ligand, indicating a possible conformational change of the protein, such as the opening of a channel and increased water content of the layer.

We proceeded to study this TSPO-lipid bilayer system with neutron reflectometry, with a view to detecting changes in the hydration of the protein-lipid layer as a result of ligand binding. Neutron reflectivity was measured at the major stages of TSPO-lipid bilayer formation (Fig. 3). There was indeed evidence of adsorption of a protein/detergent layer to the surface, with an approximate thickness of 50 Å. In addition, there was a change in reflectivity after exchanging detergent for lipid, indicating the addition of lipid to the protein layer. We are currently refining a model to describe the TSPO-lipid layer, and the effect of ligands on the hydration of the layer.

Outlook

Currently, we are working on improving the stability of the TSPO-lipid bilayer system for further studies with neutron reflectometry. The data collected on this system will make a valuable addition to the limited structural data available for the TSPO. In particular, it could provide evidence for channel formation induced by ligand interactions, making it possible to relate changes in conformation to observed functional changes. This fundamental information could have impact in the broader context of understanding the function of TSPO and how it relates to inflammatory disease.

Table 1

Technique	What does it measure?	What can we learn?
Quartz crystal microbalance with dissipation monitoring	The mass and rigidity of a film (such as a lipid bilayer) deposited on a surface.	We can follow the formation of a TSPO-lipid bilayer in real-time. We can learn whether the bilayer is rigid or “floppy”, estimate the protein / lipid coverage from the mass on the surface, and calculate the thickness of the layer. We can also follow changes in mass and rigidity during ligand binding.
Neutron reflectometry	The thickness and composition of films on a surface.	We can use the data to model the thickness and the composition of the TSPO-lipid bilayer. We can estimate the ratio of protein to lipid in the bilayer, and the thickness of the TSPO across the bilayer, giving us more information about the dimensions of the TSPO in the membrane environment.

Techniques used to study the TSPO in lipid bilayers.

Figure 2

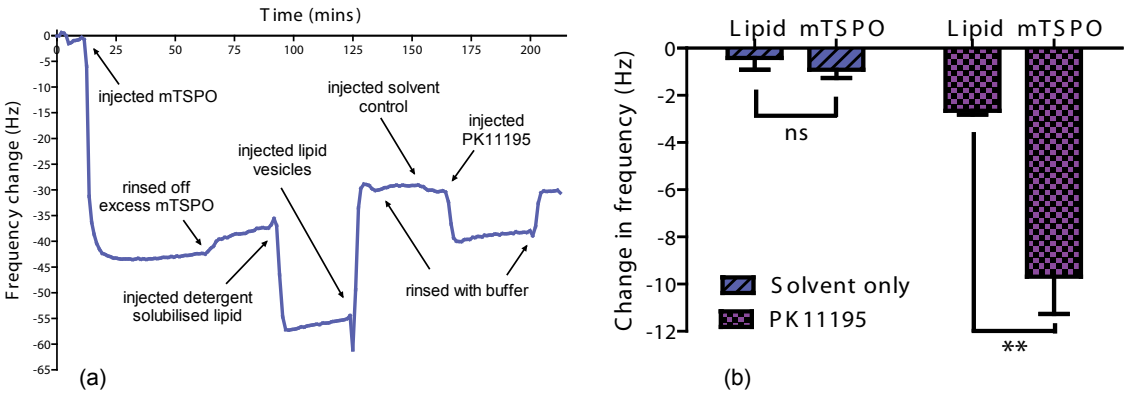

(a) The change in frequency at each step of the formation of a TSPO-lipid bilayer, and interaction with the ligand PK11195. (b) Comparison of the change in frequency as a result of interaction with solvent only or PK11195 on lipid bilayer with or without TSPO. Errors are standard deviations, n = 4 in each group.

Figure 3

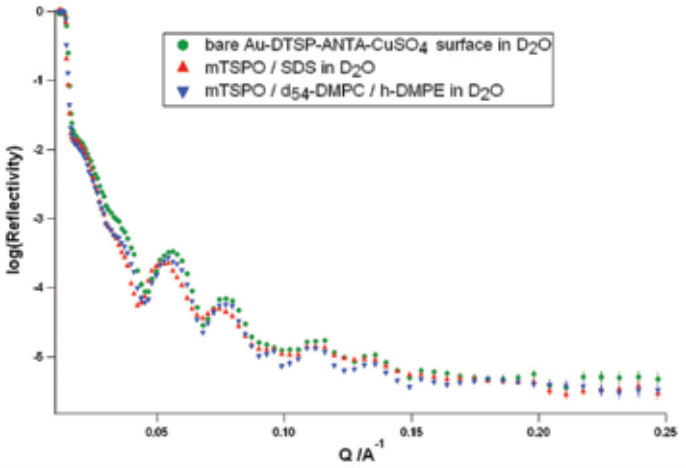

Neutron reflectivity profiles at each stage of protein – lipid bilayer formation, measured in D_2O. Measurements were taken of the bare surface (green), the surface after addition of protein solubilized in detergent (red), and after the replacement of detergent with lipid (blue). All measurements were made on the Surf reflectometer, ISIS, UK.

References

[1] Papadopoulos, V., Baraldi, M., Guilarte, T. R., Knudsen, T. B., Lacapere, J-J., Lindemann, P., Norenberg, M. D., Nutt, D., Weizman, A., Zhang, M-R., and Gavish, M., Translocator protein (18 kDa): new nomenclature for the peripheral-type benzodiazepine receptor based on its structure and molecular function, Trends in Pharmacological Sciences, 27(8), 402-409 (2006).

[2] Banati, R. B., Visualising microglial activation in vivo, Glia, 40(2), 206-217 (2002).

[3] Bernassau, J. M., Reversat, J. L., Ferrara, P., Caput, D., and Lefur, G., A 3D model of the peripheral benzodiazepine receptor and its implication in intra mitochondrial cholesterol transport, Journal of Molecular Graphics, 11, 236-244 (1993).

[4] Jamin, N., Neumann, J-M., Ostuni, M. A., Vu, T. K. M., Yao, Z-X., Murail, S., Robert, J-C., Giatzakis, C., Papadopoulos, V., and Lacapere, J-J., Characterization of the Cholesterol Recognition Amino Acid Concensus Sequence of the Peripheral-Type Benzodiazepine Receptor, Molecular Endocrinology, 19(3), 588-594 (2005).

Winnie Kam studying the effect of the translocator protein in diseases such as schizophrenia and psychosis.

The translocator protein in response to cannabinoids

Ronald Chan[1,2], Winnie Kam[1], Guo Jun Liu[1,2], Katerina Zavitsanou[1,3], Richard Banati[1,2]
[1]ANSTO, [2]University of Sydney, [3]Schizophrenia Research Institute, Sydney

The translocator protein is a vital component in stress and anxiety regulation. As cannabis has the potential to alter anxiety, stress levels and also trigger psychosis and schizophrenia, this study investigates the influence of continuous administration of cannabinoid on the translocator protein in both adult and adolescent rats.

Since the translocator protein is mainly expressed outside of the brain, a variety of organs were studied. The results show that cannabinoids have a negative impact on the testicular translocator protein. However importantly, this finding was only observed in the adult rats and not in the adolescent rats. The implications of observing a specifically different effect in the adult compared to adolescent rats suggests adults were most affected by cannaboid treatment whereas adolescent rats showed little change. It is possible that the failure to regulate the translocator protein in adolescents may lead to diseases such as schizophrenia and psychosis in later life.

The translocator protein

The translocator protein (TSPO) is an ancient protein, with analogues found in almost all living organisms studied to date. In mammals, it is expressed in nearly all tissues with important physiological and pathophysiological roles. Currently, known roles and functions of this protein include cholesterol transport, steroid production (steroids are organic compounds found in plants, animals and humans), stress regulation, cell proliferation, apoptosis (normal process leading to cell death), heme (a large ring-shaped molecule with an iron atom at its centre) transport and immune modulation [1]. However, perhaps the best studied function is TSPO's role in steroid production and stress regulation. It has been recognised that TSPO is involved in the transport of cholesterol across the mitochondrial membranes (mitochondria are the energy productive sites of a cell). Once transported inside the matrix side of the mitochondria, enzymes begin converting cholesterol into steroid precursors. Thus, the ability of the TSPO to assist in the transport of cholesterol is critical for the health and development of an organism; this is particularly so as the cholesterol transport process is also the rate limiting step of all new steroid production [2].

Studies on the impact of stress and anxiety have noted that TSPO expression is dramatically decreased upon exposure to prolonged periods of stress. The type of stress does not appear to be limited to psychological stress, but also applies to physical stress including forced swimming and electric shocks [1]. In this context, TSPO appears to be a general marker for prolonged stress, with decreases in expression correlating to the degree of stress experienced. The mechanistic process for which TSPO contributes towards stress and anxiety regulation is still being investigated. One theory is that since TSPO is involved in the rate-limiting step of cholesterol transport, the expression of TSPO is able to regulate steroid production within the brain. These neurosteroids, such as allopregnanolone and allotetrahydrodeoxycorticosterone, have been shown to regulate the primary inhibitory neurotransmitter, GABA transmissions, within the brain. The GABA neurotransmitter system is well known for its stress and anxiety regulating properties (Fig. 1) [3]. Other researchers have suggested the influences of peripheral organs including the kidneys and adrenal glands, citing the high expression of TSPO in the periphery compared to the brain.

Studying chronic cannabinoid treatment

Understanding the roles of TSPO particularly in steroid production, we sought to investigate the effect of a chronic cannabinoid treatment on the expression of TSPO. In this light, cannabinoids are interesting not only due to their psychoactive and anxiety altering nature, but also due to their peripheral effects, namely those on testosterone production and sperm production. Cannabinoids have negative effects on both testosterone production and sperm production. Previous literature reports reduced testosterone production after both acute and chronic exposure to either cannabis and/or cannabinoids. Further, sperm production is decreased along with increases in the incidences of abnormalities and defects.

We used a rat model [4] previously established at ANSTO, to examine the effects of chronic cannabinoids on the expression of TSPO in a variety of organs including the spleen, kidneys, liver and testes. Further, we also examined the effect on adult and adolescent rats since cannabinoids are known to affect adults and adolescents differently.

Figure 1

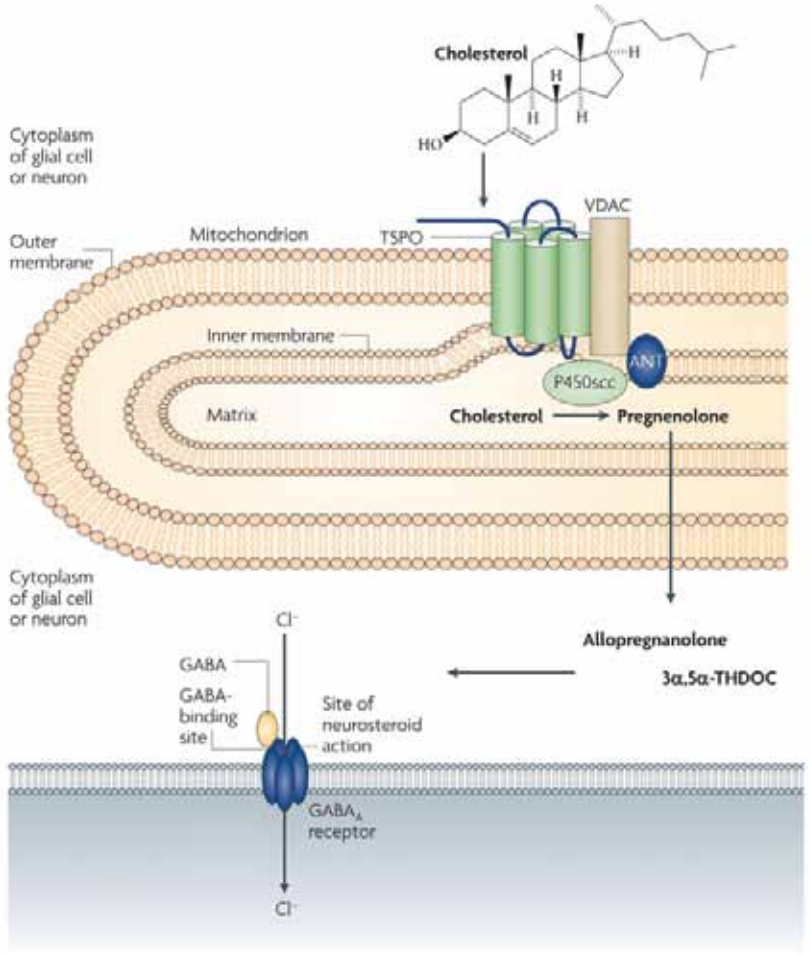

A schematic diagram of how TSPO might modulate stress and anxiety. Within the brain, cholesterol is transported into the matrix side of the mitochondrion with the help from TSPO and other proteins. Once inside, side-chain-cleaving cytochrome P450 enzyme (P450scc) converts cholesterol into pregnenolone. Here it diffuses into the cytoplasm and is converted by a series of other enzymes (not shown) into allopregnanolone and allotetrahydrodeoxycorticosterone (3α,5α-THDOC). These neurosteroids are then able to modulate the binding of GABA to GABAA receptors which in turn alters the receptor's function and affect stress and anxiety responses. Figure appropriated from [3].

Different effects for adults and adolescents

Administration of chronic cannabis (daily over two weeks) clearly elicited a general stressful response, with dramatic decreases in weight across both adult and adolescent treated groups (Fig. 2). Our investigations into the expression of TSPO confirmed that changes in expression were indeed stress-stimulus dependent. We failed to find any changes in the renal, liver or spleen tissues; results from the renal tissues are particularly interesting as they are the classical responders to either electric shock or forced swim stress. In response to cannabinoid treatment, variations within the testicular tissues were found. However this was not too surprising since it has already been confirmed that cannabinoids produce alterations within testosterone levels [5]. It does confirm that cannabinoids act on a very basic level at suppressing testosterone production through the TSPO.

However, what is much more interesting and surprising is that we found a differential effect between adult and adolescent rats (Fig. 3).

In most cases, early-age drug use, particularly during adolescence, can have long lasting negative impacts resulting in neurological and behavioural deficits. Here, we found that adults were most affected by cannabinoid treatment whereas adolescent rats showed little difference from controls. It is possible that, with respect to the effect of cannabinoids on TSPO expression, it is the failure of regulation that may lead to these deficits later in life. Given that cannabis consumption is strongly linked with the development of schizophrenia and psychosis [6], the inability of adolescent animals to regulate testosterone levels through the TSPO may represent a novel avenue of future research in elucidating the developmental causes of various psychiatric illnesses.

Figure 2

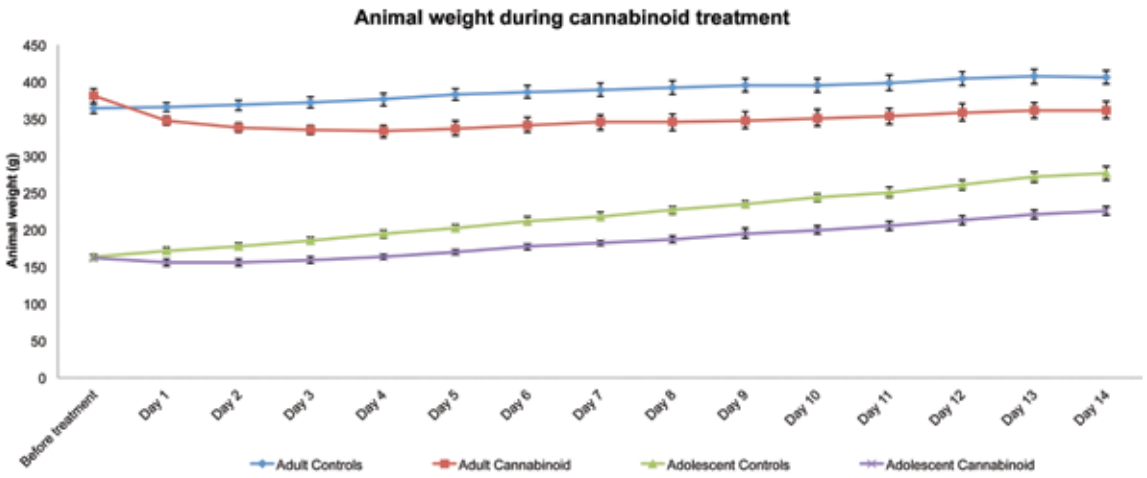

Alterations in animal weights during a 14 day chronic cannabinoid treatment, each group contained six animals. Following cannabinoid treatment, a decrease in body weight was seen across both adult and adolescent groups. Animal weights remained lower over the course of cannabinoid treatment with no marked improvement or adaptation seen.

Figure 3

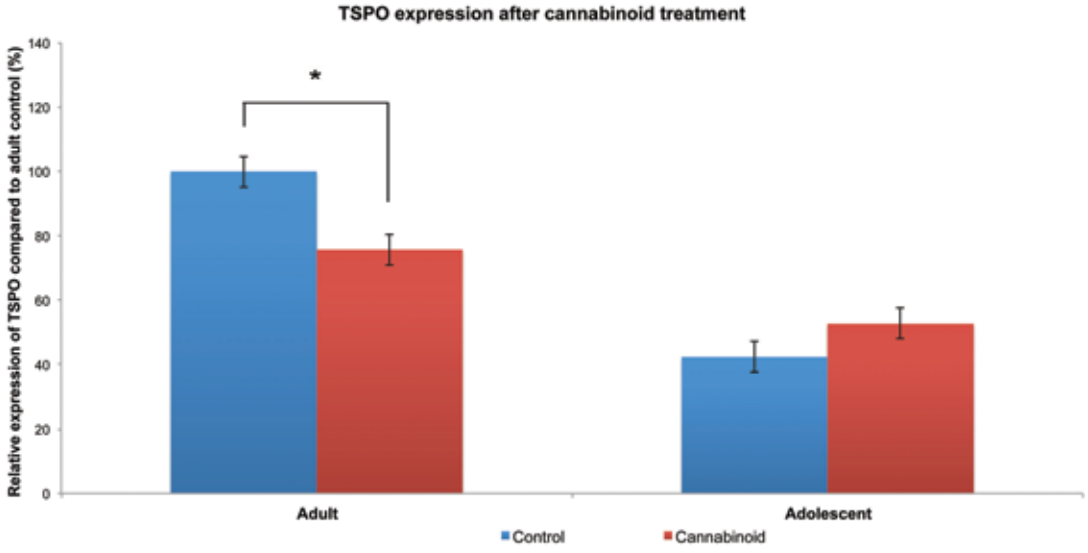

Relative expression of TSPO in testicular tissues following chronic cannabinoid treatment. Expression is significantly different in the adult group with decreases in cannabinoid treated animals (*$p < 0.01$). In contrast, no significant differences are seen in the adolescent group. Expression is relative to adult control.

References

[1] Gavish. M., Bachman. I., Shoukrun. R., Katz. Y., Veenman. L., Weisinger. G., Weizman. A., Enigma of the peripheral benzodiazepine receptor, Pharmacological Reviews, 51(4), 629-650 (1999).

[2] Pandak. W.M., Ren. S., Marques. D., Hall. E., Redford. K., Mallonee. D., Bohdan. P., Heuman. D., Gil. G., Hylemon. P., Transport of cholesterol into mitochondria is rate-limiting for bile acid synthesis via the alternative pathway in primary rat hepatocytes, Journal of Biological Chemistry, 277(50), 48158-48164 (2002).

[3] Rupprecht. R., Papadopoulos. V., Rammes. G., Baghai. T.C., Fan. J., Akula. N., Groyer. G., Adams. D., Schumacher. M., Translocator protein (18 kDa) (TSPO) as a therapeutic target for neurological and psychiatric disorders, Nature reviews. Drug Discovery, 9(12), 971-988 (2010).

[4] Dalton. V.S., Wang. H.Q., Zavitsanou. K., HU210-induced downregulation in cannabinoid CB1 receptor binding strongly correlates with body weight loss in the adult rat. Neurochemical Research, 34(7), 1343-1353 (2009).

[5] Gorzalka, B.B., Hill, M.N., Chang, S.C., Male–female differences in the effects of cannabinoids on sexual behavior and gonadal hormone function, Hormones and behavior, 58(1), 91-99 (2010).

[6] Smit. F., Bolier. L., Cuijpers. P., Cannabis use and the risk of later schizophrenia: a review, Addiction, 99(4), 425-430 (2004).

ANSTO's studies are helping to sustain Australia's growing mango industry.

Non-destructive assessment of gamma irradiation on internal mango quality

Roger Bourne[2], Connie Banos[1], Justin Davies[1,2] Richard Banati[1,2,] Robert Henriod[3]
[1]ANSTO, [2]University of Sydney, [3]Queensland Department of Employment, Economic Development and Innovation

The Australian mango fruit grower's market is a substantial industry sector that is anticipated to grow by 20% in 2014. The ripening, transportation, and saleable life-span of mangoes depends on keeping the fruit free from pests and disease.

Worldwide, the use of irradiation is emerging as a viable, chemical-free alternative to traditional pesticides.

This research builds upon our knowledge in understanding the physiological responses of three new Australian mango fruit hybrids to varying doses of gamma irradiation following harvest. Of particular interest is the question of whether irradiation may degrade the fruit, such as cause damage to lenticels (small pores) on the fruit's outer skin.

The study illustrates how ANSTO's expertise makes a crucial contribution to the development of Australia's national food security by providing new insight into the viability of irradiation to achieve safe phytosanitary (pest and disease) protocols for the agriculture industry.

Using magnetic resonance imaging for studying mangoes

Magnetic resonance imaging (MRI) offers a means of non-destructively examining fruit for internal and surface defects and has been used here to monitor changes in the water status of tissues of fruits and flowers [1-4]. MRI is distinct from most other imaging modalities in being able to provide multiple methods of contrast formation dependent on biophysical properties across a wide range of spatial scales. For example, T_2-weighted MRI is dependent on the interactions of water molecules with their immediate molecular environment. In fruit, interactions with macromolecules including carbohydrates and proteins predominate. Alternatively, diffusion-weighted MRI produces images in which contrast depends on the displacement of water molecules over a specific time period (typically 10-100 ms) in a specific direction. As water movement is restricted by intracellular structures and cell walls DWI can be used as a probe of tissue pathology and degradation.

The mangoes investigated

In this trial, we investigated the effect of gamma irradiation on internal browning and bruising of a small number of NMBP1243 mangoes, see Fig.1. Eight mangoes were gamma-irradiated with doses of 0, 200 or 800 Gy using ANSTO's cobalt-60 irradiation facility, at a dose rate of 10.1 Gy.min^{-1}. Fricke (ferrous ammonium sulphate) dosimeters were used to monitor the irradiation doses. Tissue changes were assessed by MRI immediately after (0 hr) and 43 hrs after irradiation, see Fig. 2. MR images of mango 2 (800 Gy, indicated with red square in photo) are shown. The images illustrate internal mango flesh (mesocarp) browning developed over two days but not visible as defect or discolouration on the skin (epicarp). There was no evidence of tissue damage relative to the two unirradiated samples.

In diffusion-weighted imaging, signal strength (image contrast) is dependent on the physical restriction of water movement especially by cell walls and organelles. Fig. 3 demonstrates an extensive region of increased water diffusivity (orange pixels).

Figure 1

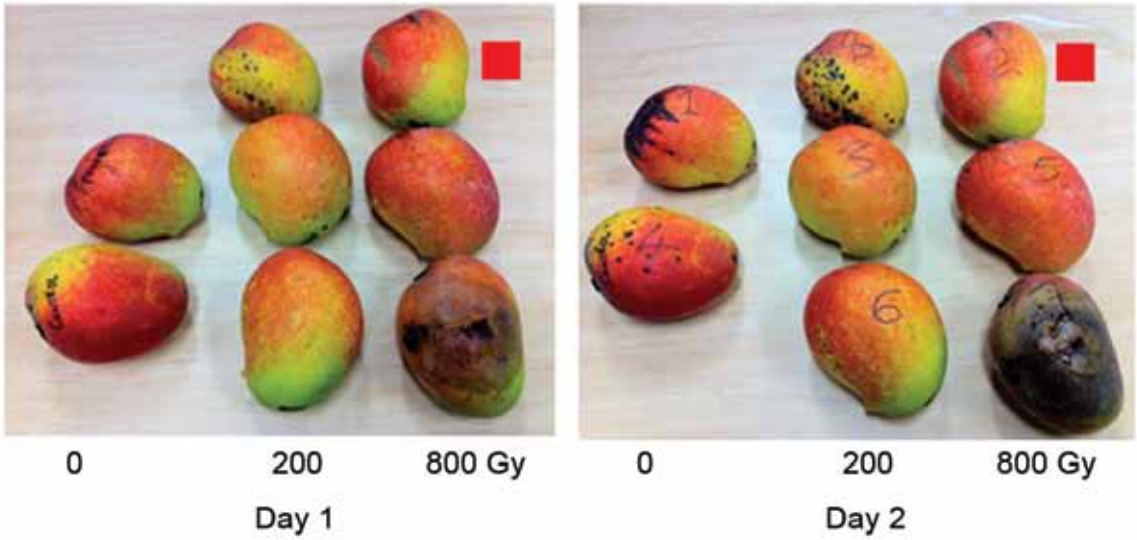

The mangoes investigated: NMBP1243 mangoes gamma-irradiated with doses of either 0, 200, or 800 Gy; on the right after two days.

Conclusion

Both T_2 and diffusion-weighted MRI clearly illustrated mango tissue changes associated with internal browning, some of which were not visible on the skin. There was no evidence of changes in tissue properties associated with irradiation.

MRI may also be valuable in investigations of radiation damage to lenticels. In this case samples of mango skin would be imaged at very high spatial resolution in an 11.5 or 16 Tesla microimaging system.

References

[1] Joyce, D.C., et al., H-1-Nuclear magnetic resonance imaging of ripening 'Kensington Pride' mango fruit. Functional Plant Biology, 2002. 29(7): p. 873-879.

[2] Clark, C.J. and MacFall, J.S., Quantitative magnetic resonance imaging of 'Fuyu' persimmon fruit during development and ripening. Magnetic Resonance Imaging, 2003. 21(6): p. 679-685.

[3] Musse, M., et al., Monitoring the postharvest ripening of tomato fruit using quantitative MRI and NMR relaxometry. Postharvest Biology and Technology, 2009. 53(1-2): p. 22-35.

[4] Yooyongwech, S., et al., Changes in aquaporin gene expression and magnetic resonance imaging of water status in peach tree flower buds during dormancy. Physiologia Plantarum, 2008. 134(3): p. 522-533.

Figure 2

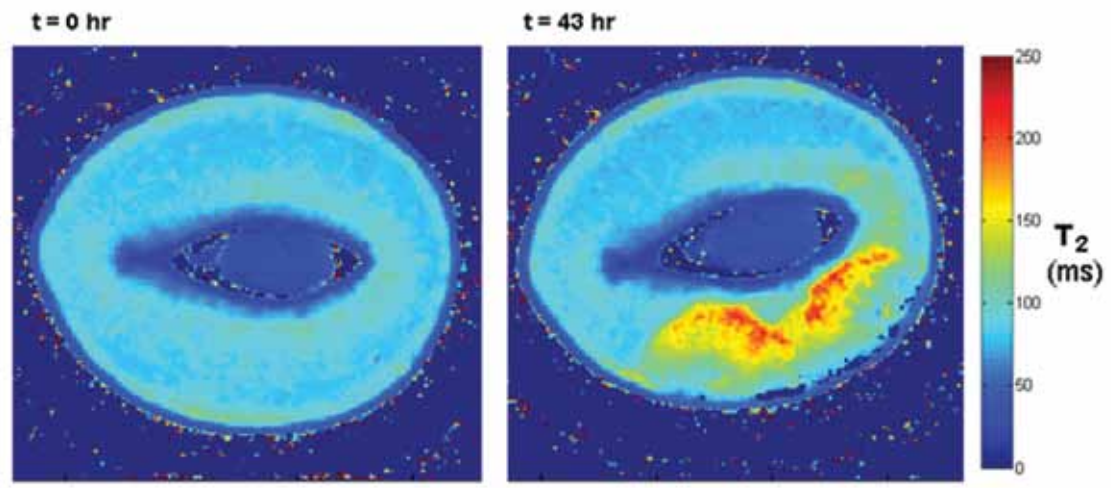

Quantitative imaging (T_2 weighted) of the development of internal mango browning (imaging was performed on a GE Syngo 3T MRI system with 8-channel transmit/receive knee coil). Mesocarp (internal) browning (yellow and red area), evident as a 50-100% increase (in T_2), is consistent with sugar hydrolysis and decreased local sugar concentration. In this example the absence of change in extent of the dark blue (low-T_2) 'halo' around the seed illustrates the absence of significant ripening progression over the 43 hour measurement interval (consistent with absence of change in skin colour of this specimen).

Figure 3

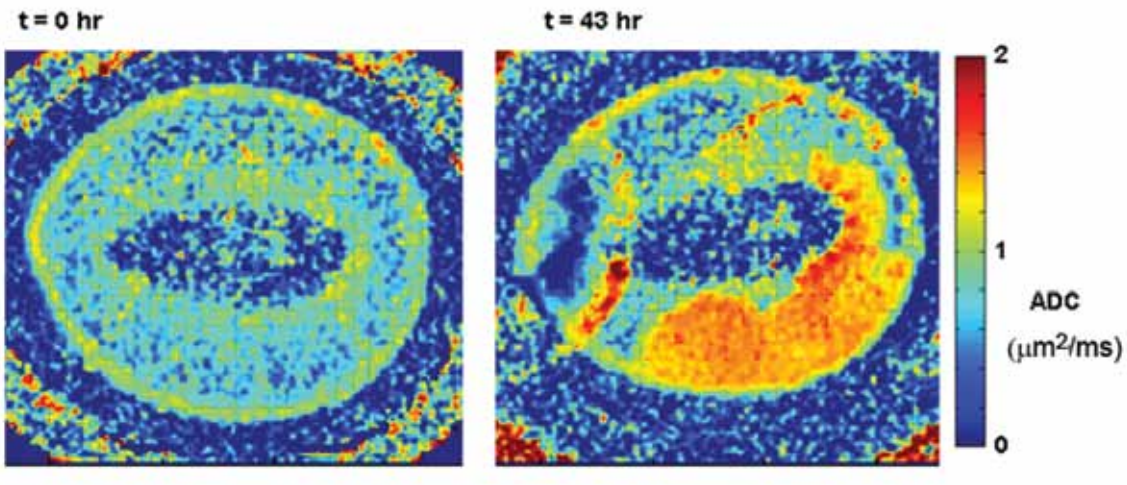

Apparent diffusion coefficient (ADC) image of the development of mango browning (cf. Fig. 2). Mesocarp (internal) browning is evident as 50-100% increase in ADC consistent with the breakdown of cell walls over an extended volume of tissue. (Concentric rings are a parallel image artefact which can be eliminated by use of an alternative imaging protocol).

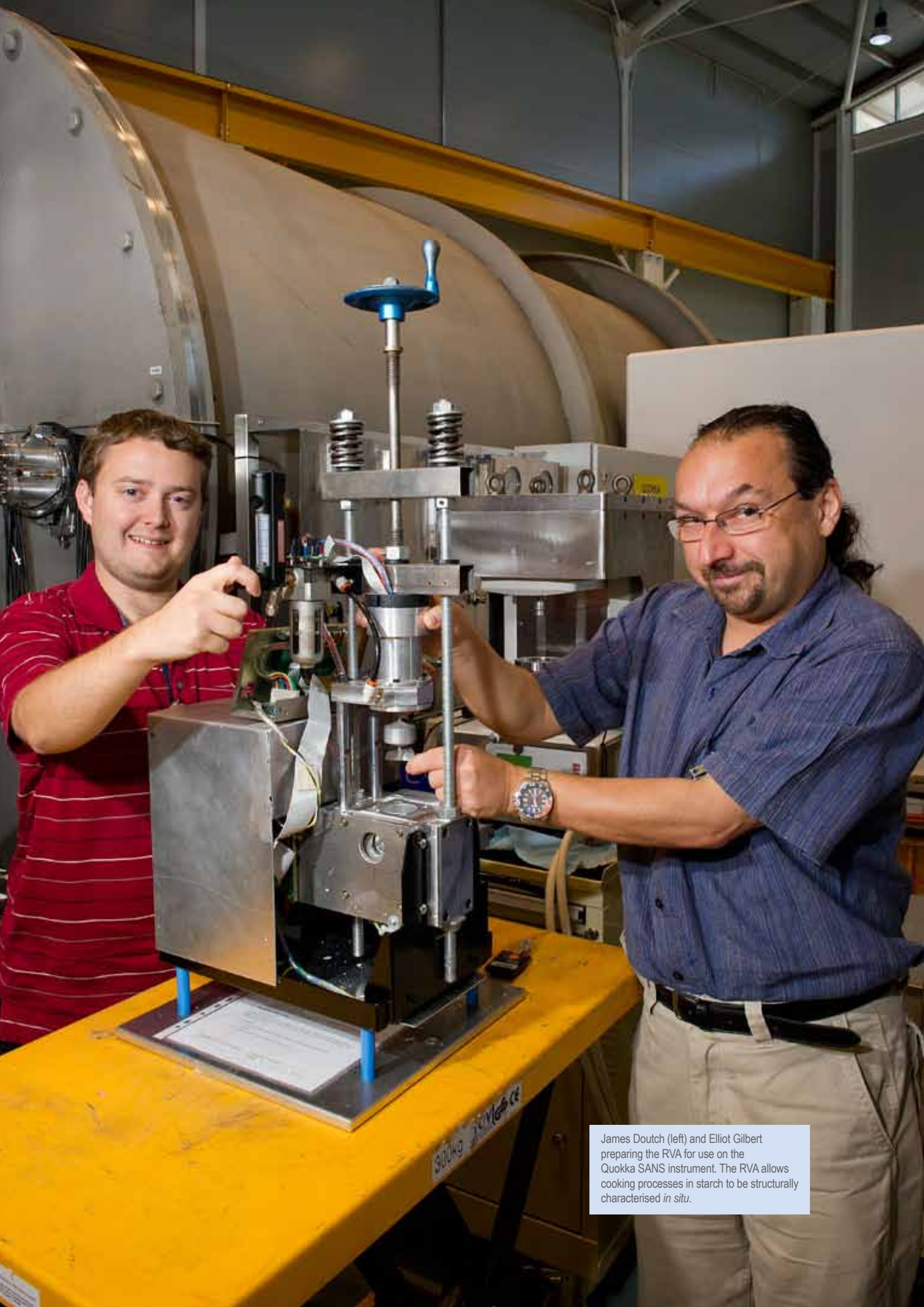

James Doutch (left) and Elliot Gilbert preparing the RVA for use on the Quokka SANS instrument. The RVA allows cooking processes in starch to be structurally characterised *in situ*.

Simultaneous measurement of structure and viscosity changes during starch cooking

James Doutch[1], Mark Bason[2], Ferdi Franceschini[1], Kevin James[2], Douglas Clowes[1], Elliot P. Gilbert[1]
[1]ANSTO, [2]Perten Instruments

Starch is the key carbohydrate in the human diet and the major storage structure in plants.

The structure of the starch granule is surprisingly complex and has a number of hierarchical levels extending from the micron- to nano-scale. These structural characteristics confirm considerable botanic variation, or differences between plants and this, in turn, causes considerable differences in the nutritional and industrial properties of different starches which form part of our diet. This particularly manifests itself with differences in cooking properties. This study characterised this behaviour using simultaneous Rapid Visco Analysis (RVA) and small-angle neutron scattering [1].

Starch granules and pasting

Starch is deposited by plants in granules that show considerable botanical variation in shape and size distribution; generally granules range from 2 µm to 100 µm in dimension. Most of the granule is composed of essentially linear amylose and highly branched amylopectin. The ratio varies considerably between plant species. The granules are further subdivided into growth ring structures, which alternate between amorphous and semi-crystalline structures. The semi-crystalline rings have a repeating lamellar structure of periodicity 90 – 100 Å. This is easily observed using neutron scattering (small-angle neutron scattering – SANS) and x-ray scattering (small-angle X-ray scattering – SAXS) [2]. Other sub-structures such as superhelices and blocklets are thought to exist within the granule [3].

The pasting properties of starch are readily studied using the RVA unit, in which slurries of starch are subjected to a defined program of heating and cooling cycles which allows the cooking properties of starches to be reproducibly tested, for example, prior to sale. This allows for grain quality control and can be used to assess viscosity changes during innovative processing techniques.

During a heating and cooling cycle in excess water, several changes in the RVA profile are observed. Firstly, a sufficient number of starch granules undergo such rapid swelling and partial amylose leaching, particularly following gelatinisation, that a rapid rise in viscosity is observed. Under conditions of both heat and shear, the granules are partially disrupted and the leached amylose aligns, leading to a reduction in viscosity in most cases. On subsequent cooling, the hydrated polymers re-associate and the material undergoes a transition to a gel, which is observed as a 'setback' or increase in viscosity. The corresponding changes in nanostructure however had not previously been characterised.

Simultaneous SANS and RVA

Neutrons have several key advantages for analysing the nanostructure of food systems, in particular their relatively high penetration through dense or concentrated samples and sample environments, as well as the ability to avoid beam damage.

An industrial RVA unit, modified to allow a neutron beam to pass through it, is shown in Fig. 1. This was then used on the Quokka SANS instrument at OPAL to collect simultaneous SANS and RVA data using a typical industrial test cycle of heating and cooling, while hydrated with deuterated water. The cycle used in this study was 13 minutes long with the starch heated to 95°C over the course of 5 minutes, held at that temperature for 2 minutes and then subjected to a gradual cooling for the remainder of the profile.

Figure 1

Modified Rapid Visco Analyser assembly for SANS study. (B) indicates hollow impeller assembly through which neutrons pass.

Figure 2

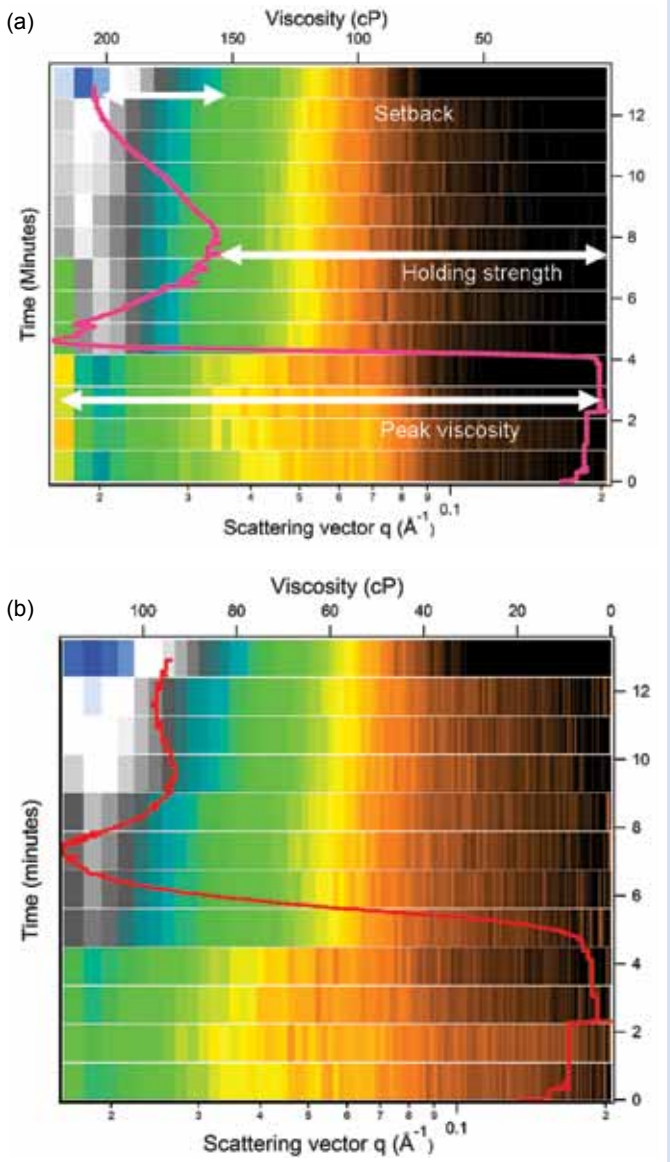

SANS data transposed with RVA viscosity profiles as a function of time - (a) waxy maize (b) maize; Black and white regions denote low and high intensity respectively (logarithmic scale).

A fractal structure in the gels

Fig. 2 shows simultaneous scattering and RVA profiles for two starches: the scattering at low-q values increases quite dramatically for both starches at the point at which the viscosity first starts to rise. This implies the formation of large scale structures and occurs after approximately 4 minutes. The scattering for waxy (amylopectin only) maize is shown in detail in Fig. 3. Here, the periodic lamellar structure is destroyed after 4 minutes and replaced by power law scattering, in which the scattered intensity decays by some negative power with increasing q. This power law scattering shows variation through the remaining time of the experiment.

Power law behaviour in small-angle scattering experiments can indicate a number of structural possibilities; for example, regular shapes like cylinders, spheres or fractal structures. We were able to differentiate between these possibilities by placing the data on an absolute scale, a task easily achieved with SANS. This clearly demonstrated that the gel structures had the form of fractals on the nanometre scale. The data was analysed using the method of Teixeira [4]. In contrast to other structural interpretations in the literature, only this structural model is able to yield the correct volume fractions expected for the systems studied.

Figure 3

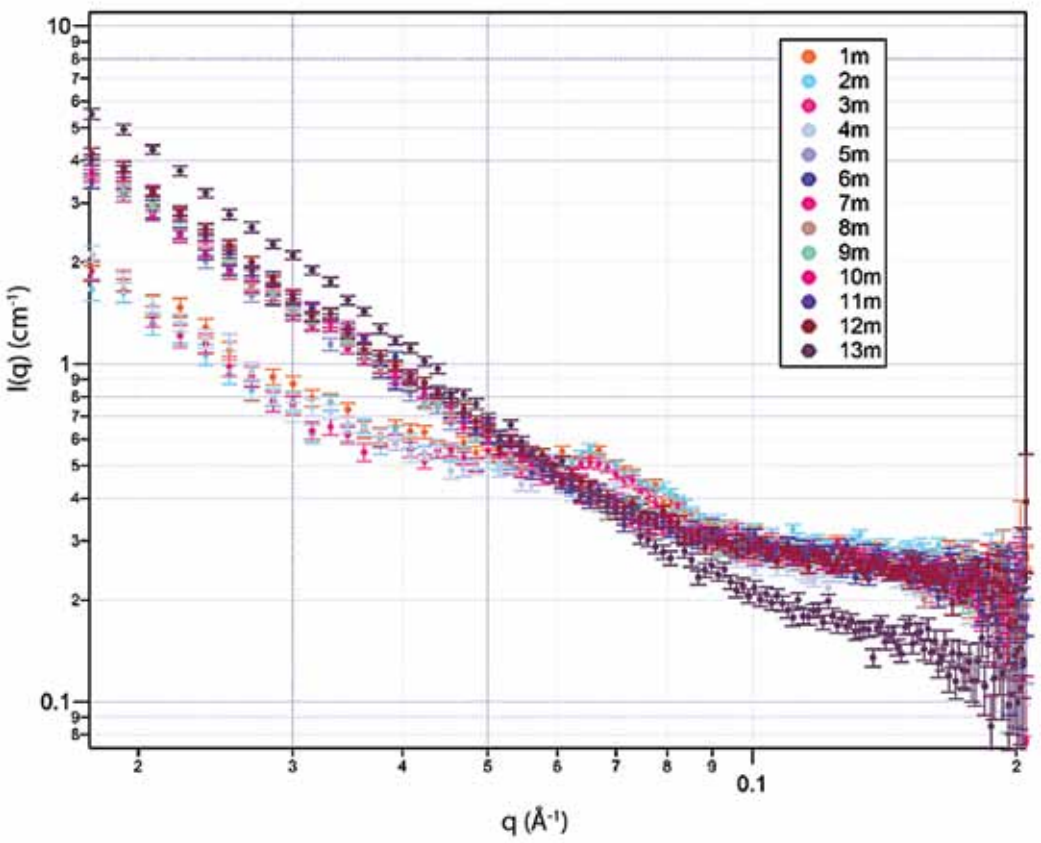

SANS data as a function of time during RVA measurement for waxy maize. The lamellar peak at ~0.065Å^{-1} is seen to disappear after 4 minutes, being replaced by decays that follow a power law with variable exponent between -2.24 to -2.32.

This analysis yielded some interesting variations between different botanical starch varieties. In particular, potato, tapioca and waxy maize form aggregates which are relatively large (~200 Å) compared with wheat and normal maize (~90 Å). There were also interesting differences in fractal or Hausdorff dimension. This gives an indication of the morphological complexity of the system. We deduced that tapioca and potato gels appear to have quite linear and relatively simple structure, whereas maize and wheat gels are much more complex and the aggregates quite polydisperse, while waxy maize is intermediate between the two groups. These nanoscale characteristics show excellent correlation with the macroscopic properties of the gels and invite further study. The nanoscale parameters obtained from simultaneous SANS/RVA can be used to better understand structural transitions during starch gelation, across a wide variety of industrially relevant conditions.

References

[1] Doutch, J., Bason, M., Franceschini, F., James, K., Clowes, D., Gilbert, E. P. (2012). Structural changes during starch pasting using simultaneous Rapid Visco Analysis and small-angle neutron scattering. Carbohydrate Polymers, 88(3), 1061-1071.

[2] Blazek, J., & Gilbert, E. P. (2011). Application of small-angle X-ray and neutron scattering techniques to the characterisation of starch structure: A review. Carbohydrate Polymers, 85, 281–293.

[3] Perez, S, Bertoft, E, (2010), The molecular structures of starch components and their contribution to the architecture of starch granules: A comprehensive review, Starch, 62, 389-420.

[4] Teixeira, J, (1988) Small-Angle Scattering by Fractal Systems, Journal of Applied Crystallography, 21, 781-785.

Environment and climate change

Environment and climate change

Understanding and improving our environment is essential for the continuing prosperity of our planet. ANSTO's studies look at many aspects of our environmental systems from the impact of humans on the environment to how we can mitigate and adapt to climate change.

Over the past 12 months, ANSTO's studies have investigated ways of improving groundwater management in Western Australia; looked inside the feathers of migratory Mutton Birds to better inform our understanding of trace metal pollutants in our marine environment; and performed sustainability studies on forest soils subject to severe bushfires followed by high intensity storms.

Our researchers have also undertaken studies to better understand and predict the increasing number of high-intensity tropical cyclones to help reduce the widespread flooding, economic and social disruption and potential loss of life they cause for Australia's coastal communities.

Karina Meredith in the Institute for Environmental Research working in the Isotope Ratio Mass Spectrometry Laboratory.

Groundwater 'age' assessment in the Gnangara Mound, Western Australia

Karina Meredith[1], Dioni I. Cendón[1], Jon-Philippe Pigois[2], Suzanne Hollins[1], Geraldine Jacobsen[1]
[1]ANSTO, [2]Government of Western Australia, Department of Water

ANSTO's study of the Perth Basin aquifers determined the age of groundwater to be 23,000 to 35,000 years old. Although this result was expected, what was surprising was the identification of an area of younger modern groundwater at a depth of 300 metres below ground level. This area is of prime interest for water resource managers because fresh water is replenishing the otherwise isolated underground system.

The Gnangara groundwater system is the largest utilised source of groundwater in the southwest of Australia and supplies up to 70% of Perth's potable water during periods of drought. Its sustainable use is crucial for future development in and around Perth. Naturally occurring radioactive isotopes such as tritium and radiocarbon are ideal tools to date the groundwater. By understanding the age of the groundwater, we can then determine how frequently the water is being replenished and how much of the resource is available for use. Strong competition for this limited water resource means that understanding its hydrology is essential for sustainable groundwater management.

The Gnangara Mound and groundwater system

The Gnangara groundwater system covers an area of approximately 2,200 km^2 and constitutes the largest utilised source of groundwater in the southwest of Australia (Fig. 1). These aquifers can supply up to 70% of Perth's potable water when river water is not available (such as during drought periods) and its sustainable use is of major importance for future development in the Perth Basin. Aquifers are rock structures or sediments located beneath the ground that are saturated and permeable enough to allow economic quantities of groundwater to be extracted. Groundwater from these vast aquifer systems support agriculture, industry and private domestic use, and also sustain significant groundwater dependent ecosystems that carry social, cultural and environmental values. There is increasing pressure on this supply, resulting from irrigation demands and urban development. Strong competition for this limited water resource, along with warmer weather and a decrease in rainfall from climate change has led to reduced groundwater levels.

Information obtained from the analysis of stable isotopes of O, H and C, and the radioactive isotopes of C and H, used together with hydrochemical information, provides the necessary tools for understanding groundwater age and hence recharge patterns within this large water resource system.

How is groundwater dated?

It is important to understand how frequently water is being replenished in the aquifers. This can be achieved by determining the age of the water, and to do this we use two naturally occurring radioactive isotopes that are found in water. Tritium, ^{3}H is a short-lived isotope of hydrogen with a half-life of 12.43 years. It forms part of the water molecule and therefore can be used to directly date the water. Radiocarbon dating is the most accessible and widely used technique to date 'older' groundwater resources. Radiocarbon (^{14}C) is the radioactive isotope of carbon and has a half-life of around 5,700 years. It is produced naturally in the atmosphere by cosmic rays and is subsequently oxidised to CO_2, where it mixes into the lower atmosphere and is then incorporated into the biosphere and hydrosphere. The ubiquity of carbon in groundwater makes it an ideal isotope for dating groundwater.

Dating groundwater using radiocarbon (^{14}C) is complicated by the fact that the carbon may come from a variety of sources of different ages, for example some carbonates may come from very old sources and contain no radiocarbon. The presence of this 'dead' carbon must be corrected for, in order to get a reliable age. This can be overcome by accounting for the major hydrochemical and physical processes that are likely to influence the carbon chemistry of a groundwater sample [1].

Figure 1

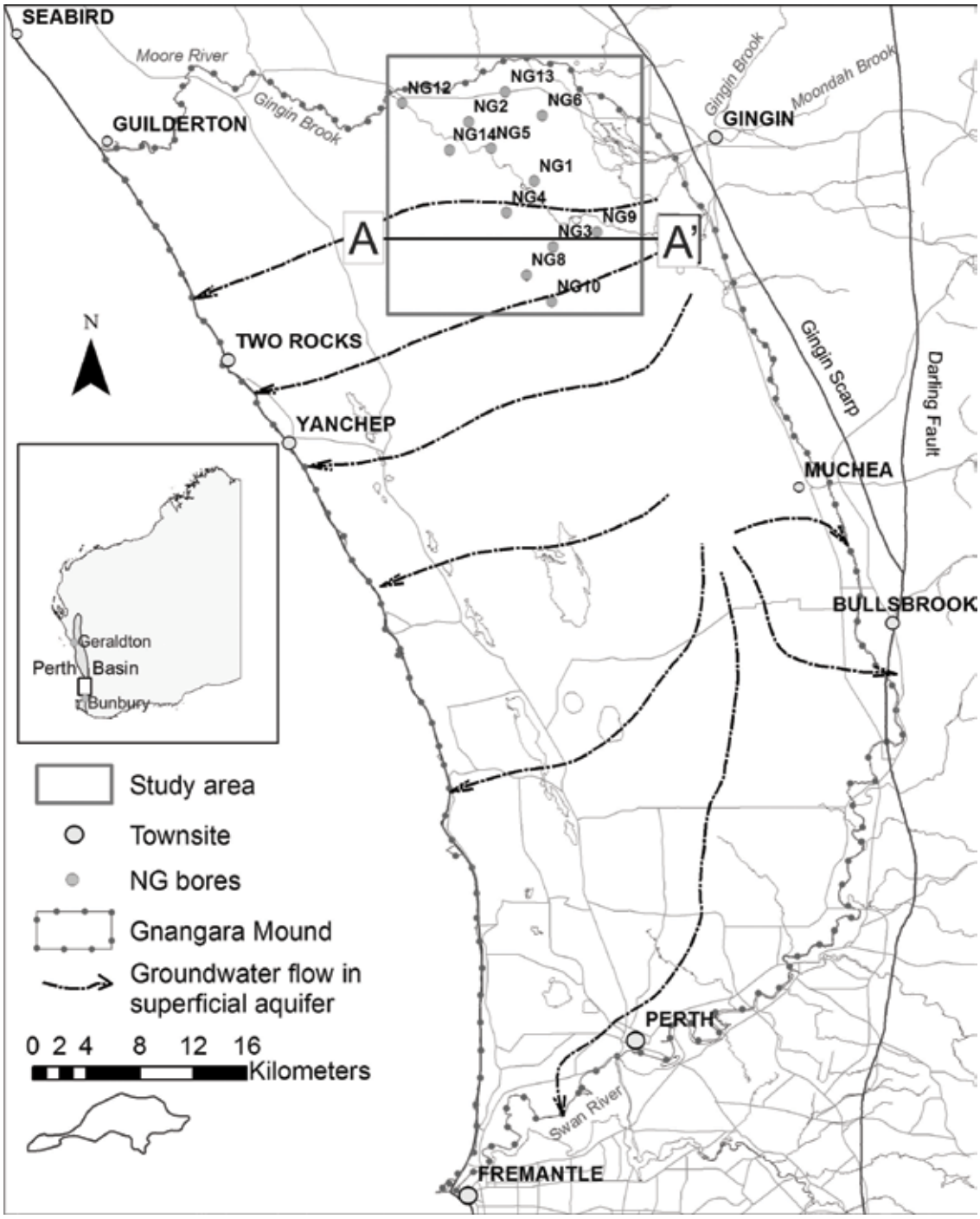

Location map of the North Gnangara Mound study area with well locations and generalised groundwater flow direction for the Gnangara Mound in relation to the Perth Basin.

How do we analyse groundwater chemistry and isotopes?

The chemical composition of water samples is measured by inductively coupled plasma-atomic emission spectroscopy for cations and ion chromatography for anions. Stable isotopes of dissolved inorganic carbon ($\delta^{13}C_{DIC}$) are analysed by liberating CO_2 from each sample and injecting it into an isotope ratio mass spectrometer. For ^{3}H analysis, water samples are distilled and electrolytically enriched prior to being analysed by the liquid scintillation method. For ^{14}C analysis, the total DIC (dissolved inorganic carbon) is processed into CO_2 by acidifying the samples and

Figure 2

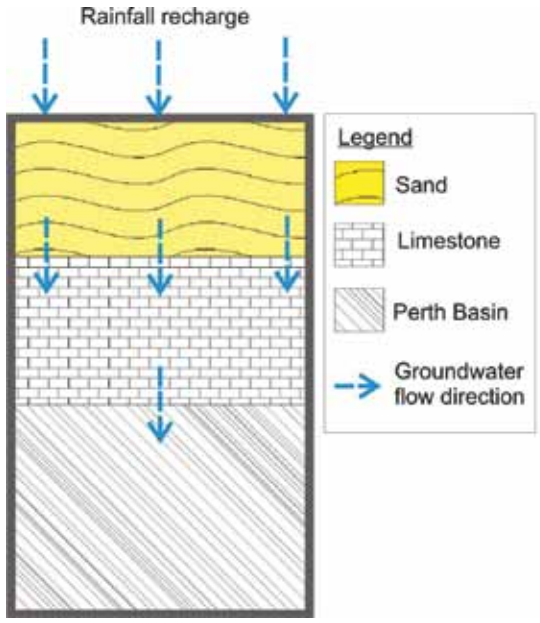

Groundwater recharge path into the Perth Basin aquifers through the sandy aquifer and carbonate unit.

extracting the liberated CO_2 gas using a custom-built extraction line. The ^{14}C activities were measured by accelerator mass spectrometry using ANSTO's 2MV tandetron accelerator, STAR.

Groundwater recharge and carbon evolution

Hydrochemical variability was observed in groundwaters abstracted from the different aquifers within the Gnangara groundwater system [2]. Fig. 2 shows the recharge path of rainfall and/or river waters through the various aquifer units until it forms groundwater in the interconnected pores of the sand and limestone units. Once groundwater from these units reaches the Perth Basin aquifers (located more than 200 m below the ground surface) they generally form palaeowater or old groundwater.

The groundwater is recharged by rainfall which passes through the soil zone, and dissolves carbon on the way. Thus, groundwater in the sandy aquifer inherits a $\delta^{13}C_{DIC}$, which is similar to the signature of soil zone CO_2 (i.e. ~25%). Groundwater from this unit also had

Figure 3

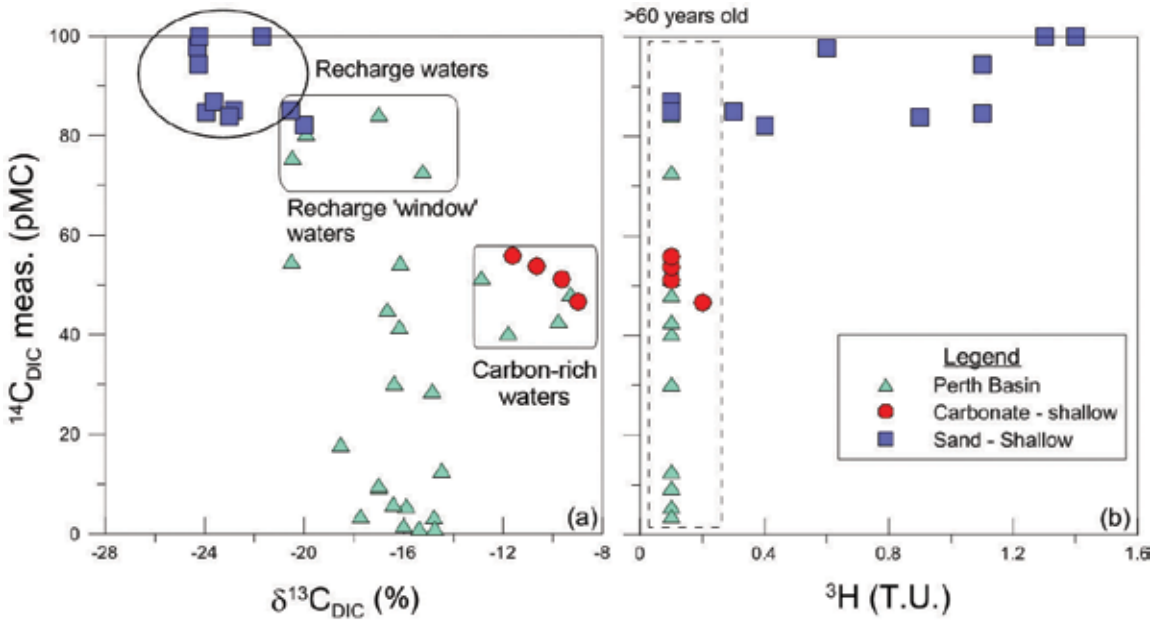

Bivariate plots of measured ^{14}C activity vs. (a) $\delta^{13}C_{DIC}$ and (b) ^{3}H activity.

Figure 4

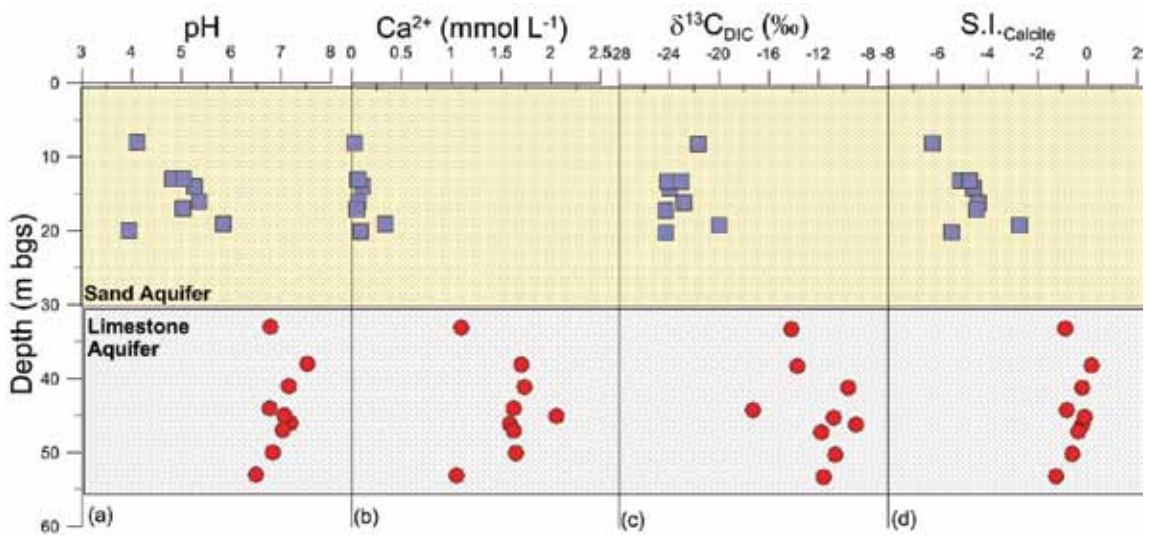

Bivariate plots of depth vs. (a) pH (b) Ca^{2+} (c) $\delta^{13}C_{DIC}$ and (d) saturation indices for calcite for groundwaters from the top ~60 m of the study area.

high measured ^{14}C activities (70 to ~100 pMC) and detectable ^{3}H activities (Fig. 3) indicating exchange with the ^{14}C-active soil zone, leaving it open to modern carbon exchange.

Groundwaters originating from the overlying sandy aquifer have high concentrations of CO_2 liberated from the oxidation of organic matter. As this acidic recharge enters the carbonate aquifer, dissolution is enhanced. Consequently, groundwater pH, Ca^{2+} concentration and $\delta^{13}C_{DIC}$ values increase (Fig. 4). Groundwaters also move towards carbonate saturation further implying a shift from open to closed system conditions. Groundwater infiltrating through limestone units such as these found in Gnangara, can have up to 50% of its HCO_3^- contributed from a 'dead' carbon source making the waters appear older. Therefore, uncorrected radiocarbon results can appear much older and are not considered representative ages in this groundwater environment.

Identification of recharge areas within the Gnangara Mound

Radiocarbon corrections were applied to all groundwater samples according to the main hydrogeochemical processes identified [3]. The corrected radiocarbon ages of groundwater from the Perth Basin aquifers were generally found to be old (23,000 to 35,000 years old). However, in the south-eastern corner of the study area (sites NG03 and NG09, see Fig.1) they were much younger than anticipated, ranging from modern to ~2,000 years old. Fig. 5 is a geological cross-section running east to west through the study site showing the location of younger groundwaters recharged into the Perth Basin. This is occurring where low permeability units are not present, forming a recharge 'window'.

The identified recharge area is of prime interest for water resource management because not only is it important that it is left to actively recharge fresh water into the deep aquifers, but it also needs to be protected from point-source contamination. For example, application of pesticides to soils in this area could lead to a higher risk of contamination in an otherwise protected groundwater resource.

Identification of areas of recharge into confined aquifers is important for managing water allocations and will help with calibrating physical hydrogeological models of a groundwater system. The understanding of aquifer interaction in this area is crucial to sustainable management of confined aquifer abstraction in a drying climate.

Acknowledgements

The authors would like to thank the Government of Western Australia, Department of Water (DoW) for providing the funding and support for this project. Thank you to Geoff Sadgrove from DoW for his field work contribution and technical assistance.

Figure 5

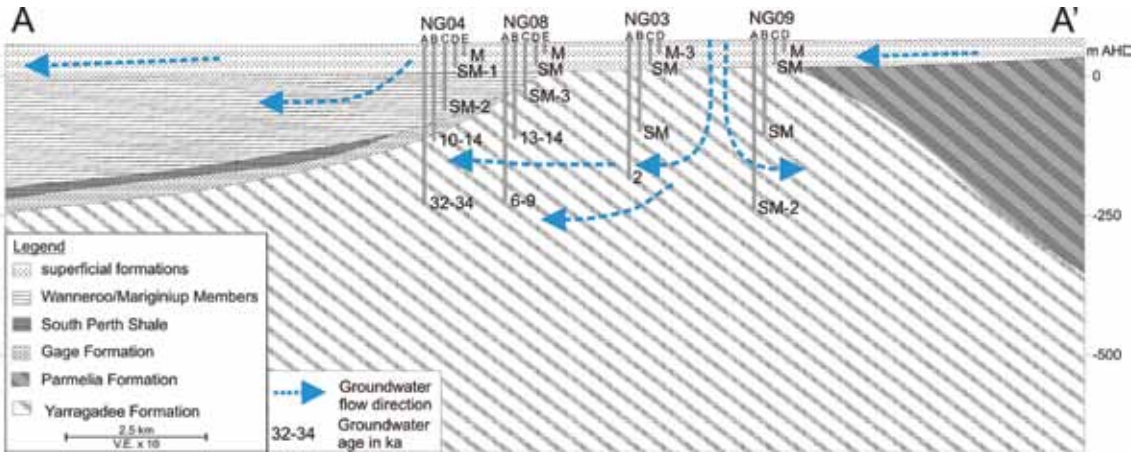

Geological cross-section with corrected groundwater age and flow direction (arrows) for the study site (refer to Figure 1 for cross section location A-A'). M = modern (<60 years old) and SM = sub-modern (>60 but <1,000 years old).

(1) In field set-up for sample collection and analysis for groundwater dating, middle, (2) Groundwater sampling in Gnangara Mound (Karina Meredith), (3) Groundwater sampling in Gnangara Mound (Jon-Philippe Pigois [foreground] and Geoff Sadgrove [background], Department of Water, WA, (4) Aerial photo of Yeal Lake in the study area, (5) Yeal Lake dry 12/3/2007. Photos courtesy of Sarah Bourke.

References

[1] Kalin, R.M., Radiocarbon dating of groundwater systems. In: Cook P.G., Herczeg A.L. (Ed.) Environmental tracers in subsurface hydrology. Kluwer, Boston, pp 112–144 (1999).

[2] Meredith, K., Cendón, D., Hollins, S. North Gnangara Groundwater Dating, Western Australia. A report prepared for The Government of Western Australia (WA), Department of Water. ANSTO/C-1084 (2010).

[3] Meredith, K., Cendón, D.I., Pigois, J.-P., Hollins, S., Jacobsen, G., Using ^{14}C and ^{3}H to delineate a recharge 'window' into the Perth Basin aquifers, North Gnangara groundwater system, Western Australia, Science of The Total Environment, 414, 456-469 (2012).

Studies of the Flesh-footed Shearwater are helping scientists understand the effects of plastic waste on sea birds.

Trace metal distribution in feathers from migratory, pelagic birds using high-resolution synchrotron X-ray fluorescence microscopy

Nicholas Howell[1], Jennifer Lavers[2], David Paterson[3] Richard Garrett[1], Richard Banati[1,4]
[1]ANSTO, [2]Institute for Marine & Antarctic Studies, University of Tasmania, [3]Australian Synchrotron, [4]University of Sydney

Increased trace metal concentrations in feathers from migratory birds are regularly used in ecotoxicology (the study of the effects of toxic chemicals on biological organisms) as indicators of individual, population and environmental health. For most routine sampling and analysis, usually only parts of feathers are sampled.

However such sampling procedures have major short-comings because they ignore variations in feather development and how the contaminant enters the bird's cells during feather growth.

In order to gain a better understanding of contaminant distribution along the full length of a feather, ANSTO used the X-ray fluorescent microprobe at the Australian Synchrotron to obtain high resolution elemental images of breast feathers collected from chicks of Flesh-footed Shearwater (*Puffinus carneipes*) also known locally as Mutton Birds.

The study revealed, with exceptional clarity, previously unknown distribution patterns of trace metals necessary for healthy development as well as showing how the birds absorb metals that come from major pollutants such as micro-plastics, disintegrating plastic waste that is increasingly affecting a wide range of marine animals including sea birds.

The Flesh-footed Shearwater

The Flesh-footed Shearwater is a trans-equatorial migrant seabird that is a common local visitor to the waters of the continental shelf and slope of south-west Australia and around Lord Howe Island, which both serve as breeding and foraging grounds [1]. The Flesh-footed Shearwater is listed under the Japan-Australia Migratory Bird Agreement (JAMBA) and is categorised as 'vulnerable' by the *Threatened Species Conservation Act (1995)* in NSW, 'rare' in South Australia and 'in decline' in New Zealand. Surveys of populations only go back ~40 years but decline is evident through more recent work [1]. Flesh-footed Shearwaters generally pair for life and will return to the same burrow every year to breed from September to May. Upon completion of the breeding season, birds from Western Australian colonies migrate north across the Indian ocean to the Arabian Sea and the Gulf of Oman while birds from Lord Howe Island and New Zealand move north across the Pacific Ocean to the Sea of Japan and southern Sea of Okhotsk (Fig.1,2) [1].

Due to their global distribution and reliance on marine resources, sea birds function as indicators of marine environmental contamination. Ecotoxicology often uses feather chemistry and composition to infer information about the individual, population and environment of the bird during the period of feather growth [2-6]. As most feathers are replaced yearly, they contain valuable indicators of the state of the bird and its environment over this period, which can be days to weeks [4].

The distinct yet consistent migratory patterns of the Flesh-footed Shearwater allow avian chemoecological methods to be used to gain complementary data from distinct locations across the globe. Flesh-footed Shearwater breast feathers are replaced on the wintering grounds in the southern hemisphere [7]. The breast feathers that were used in this experiment were collected from the Lord Howe Island colonies. These samples contain information regarding the overall health of the bird during the breeding season when the birds are foraging within the Tasman Sea.

Figure 1

Flesh-footed Shearwater (Puffinus Carnepes). Documented and proposed migratory patterns of some breeding colonies of Flesh-footed Shearwater off Lord Howe Island and south-west Western Australia.

Marine birds and micro-plastics

During migration, birds pick up plastics floating on the ocean surface. Decaying plastics have become a globally widespread and abundant marine environmental contaminant [7,8] and a major source of persistent organic pollutants and heavy metals. These bio-accumulate particularly through the course of feeding of the birds' offspring [3].

The ingestion of plastic by marine birds has been well-documented [8], particularly in Flesh-footed Shearwaters, often leading to gastrointestinal blockage and death [3].

While larger pieces of plastic are mostly a mechanical hazard for the ingesting bird, microplastics are particles of synthetic organic polymers <5mm in size; typically too small to cause physical damage [9]. However, while floating in the marine environment for many years or decades, plastic items act as sorbents for other contaminants, such as persistent organic pollutants and heavy metals [9]. The impact of microplastic contamination is yet to be fully realised, though it may lead to higher accumulation of persistent organic pollutants and heavy metals in marine surface feeders as the bird is likely to ingest much more over a lifetime [9].

Figure 2

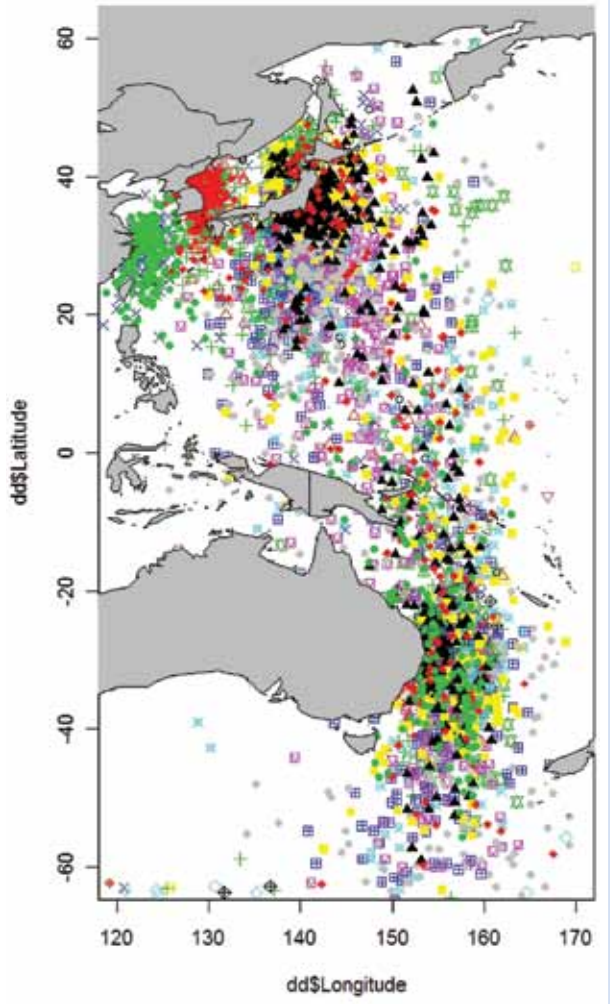

The map shows the tracks of individual Flesh-footed Shearwater birds tagged with light loggers follows their migration to the Sea of Japan from Lord Howe Island (courtesy Dr Tim Reid, University of Tasmania).

Elemental imaging using X-ray fluorescence microscopy

The X-ray fluorescence microscopy beamline [10] at the Australian Synchrotron (Fig.3) was used to produce high-definition elemental images (Fig. 4) of breast feathers collected from Flesh-footed Shearwater chicks on Lord Howe Island. The scanning X-ray fluorescence microprobe used a 16 keV incident energy beam focussed to several microns to create images with pixel sizes between 5-70 µm. This technique allowed us to reconstruct quantitative elemental concentration maps or images of the feathers for a wide range of elements with an atomic number greater than 19 (potassium) as well as look at patterns of distribution within regions of interest (Fig. 5). Fig. 6 indicates the anatomy of a feather.

Figure 3

Nicholas Howell and Jennifer Lavers from the University of Tasmania, used the Australian Synchrotron's XFM beamline for their research. Photo courtesy the Australian Synchrotron.

Figure 4

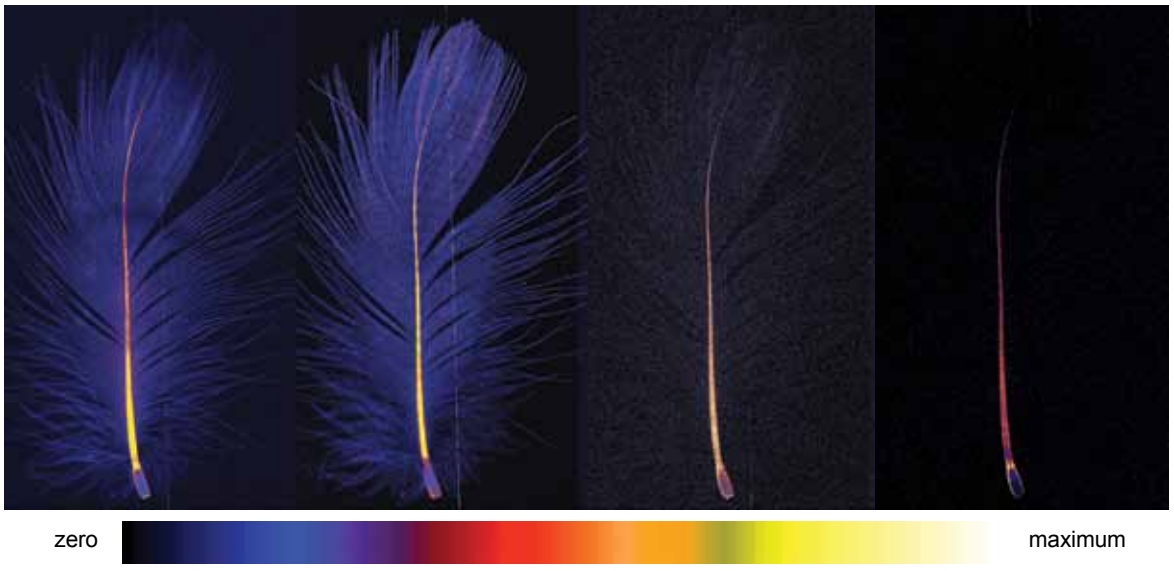

X-ray fluorescence microscopy images of Flesh-footed Shearwater chick breast feathers showing distributions of (left to right) Bromine, Zinc, Arsenic, Calcium.

It is a common sampling procedure, such as in stable isotope measurement, to only sub-sample the feather by cutting off the tip and using it for further analysis [2]. However, our results show intricate patterns that reflect growths pattern Fleshfooted Shearwater chicks that sub-sampling and analysis would normally miss. A better understanding of the hitherto unknown within-sample heterogenity of the elemental distribution in individual feathers reduce the risk of over- or underestimation of population parameters.

Of particular interest is the distribution of elements that are known to be essential for healthy plumage growth. When reconstructing the image based on zinc (Zn) concentration, a striking regular banding pattern is

Figure 5

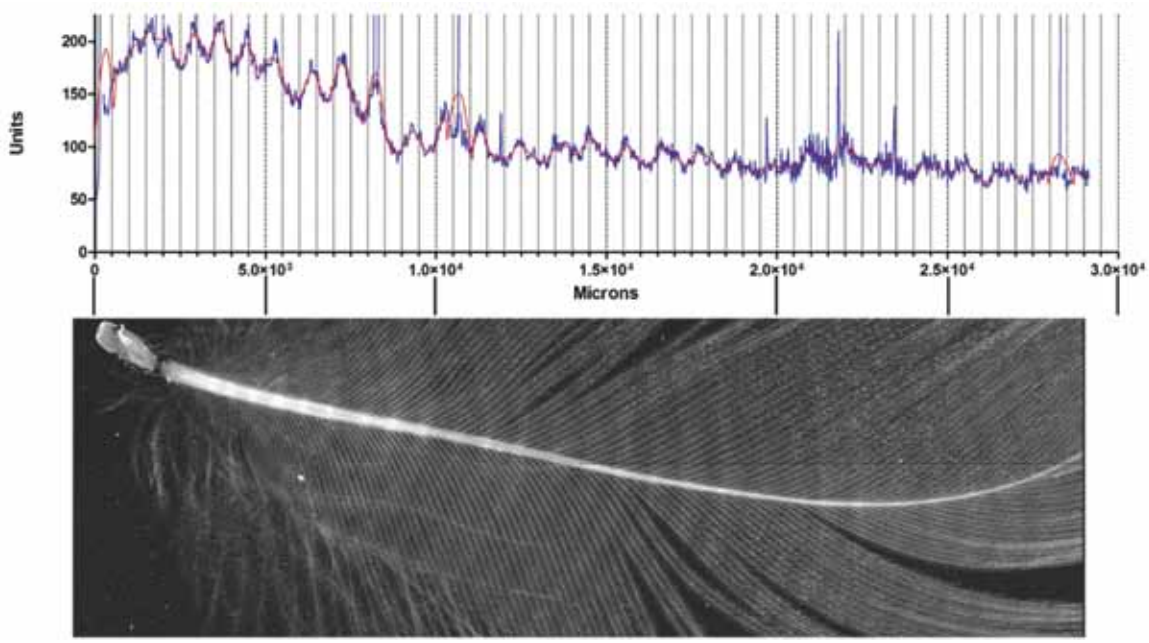

X-ray fluorescence microscopy image showing Zn banding patterns along the length of the feather.

observed running the length of the feather and radiating out from the calamus and rachis into the vanes (Fig. 5). This shape of the banding is consistent with the established mechanism of feather growth [11] The distribution of Calcium is localised in high concentrations to the base of the calamus. It forms a corset-shaped structure at the calamus to skin interface but is scarce along the length of the rachis. Arsenic can be observed uniformly along the length of the rachis but is diminished in the calamus. The most abundant element observed using this technique is Bromine (Br). Br is present in high concentrations throughout the feather structure. It is readily concentrated from sea water by marine algae and bacteria which are then ingested by organisms feeding at the surface [12-14]. Iron (Fe) can be observed almost exclusively in the vanes of the feather and is barely detectable in the rachis. Occasional spots of iron detected on the calamus correspond to contamination from blood or tissue remaining after plucking.

Outlook

The challenges facing the Flesh-footed Shearwater include plastic ingestion, contamination, habitat loss, and by-catch in fisheries [1]. The species represents a convenient indicator of marine environmental health, locally and internationally, therefore further efforts made to understand challenges to its physiology are of interest from a conservation and environmental monitoring point of view. High-resolution X-ray fluorescence microscopy allows the acquisition of so far unseen two-dimensional elemental distribution maps and highlights the significant uptake of contaminants by migratory birds.

Together with knowledge about the birds' migratory route, elemental distribution data from individual feathers can provide new and more detailed information about the time period of up-take and thus the origin of the bio-accumulated contamination. If the up-take pattern of a normal trace element is found to be disturbed, there may potentially also be an opportunity to develop a biomarker for any adverse health effects of pollutants. Future scope of work includes the more systematic study of species variations as well as variations in the distribution maps for normal and contaminant elements due to changes in feed intake.

Acknowledgement

We acknowledge funding from the W.V. Scott Charitable Trust and field assistance provided by Ian Hutton, Curator of the Lord Howe Island Museum.

Figure 6

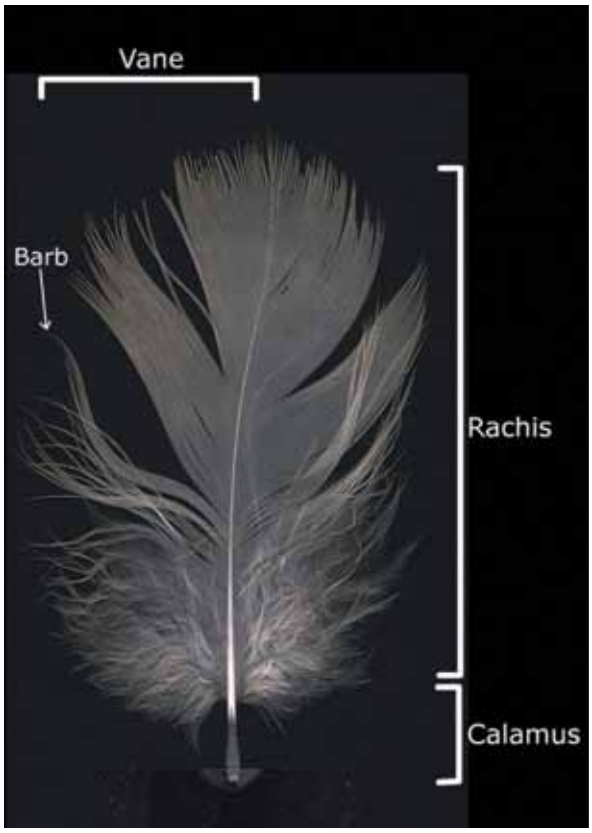

Photograph of a Flesh-footed Shearwater feather showing the calamus, rachis, vanes and barbs.

References

[1] Department of Sustainability, E., Water, Population and Communities, Ardenna carneipes in Species Profile and Threats Database, in Species Profile and Threats Database 2012, Department of Sustainability, Environment, Water, Population and Communities.

2] Bortolotti, G.R., Flaws and pitfalls in the chemical analysis of feathers: bad news-good news for avian chemoecology and toxicology. Ecological Applications, 2010. 20(6): p. 9.

[3] Bond, A.L. and J.L. Lavers, Trace Element Concentration in Feathers of Flesh-footed Shearwaters (Puffinus carneipes) from Across Their Breeding Range. Archives of Environmental Contamination Toxicology, 2011. 61: p. 318-326.

[4] Bortolotti, G.R. and J.C. Barlow, Potential use of feather chemistry as an indicator of relative growth. Wilson Bulletin, 1986. 98(4): p. 516-525.

[5] Bortolotti, G.R., et al., Mineral profiles of Spruse Grouse feathers show habitat affinities. Journal of Wildlife Management, 1989. 53(3): p. 811-817.

[6] Moreno, R., et al., Seabird feathers as monitors of the levels and persistence of heavy metal pollution after the Prestige oil spill. Environmental Pollution, 2011. 159(10): p. 2454-2460.

[7] Marchant, S. and P.J.H. (eds), Handbook of Australian, New Zealand and Antarctic Birds. Volume 1: Ratites to Ducks. 1990, Melbourne: Oxford University Press.

[8] Azzarello, M.Y., Van Vleet, E. S., Marine birds and plastic pollution Marine Ecology Progress Series, 1987. 37: p. 295-303.

[9] Cole, M., et al., Microplastics as contaminants in the marine environment: A review. Marine Pollution Bulletin, 2011. 62(12): p. 2588-2597.

[10] Paterson, D., et al., The X-ray Fluorescence Microscopy Beamline at the Australian Synchrotron. AIP Conference Proceedings, 2011. 1365(1): p. 219-222.

[11] Prum, R.O., Development and evolutionary origin of feathers. Journal of Experimental Zoology, 1999. 285(4): p. 291-306.

[12] Moore, M.R., et al., Trace organic compounds in the marine environment. Marine Pollution Bulletin, 2002. 45(1–12): p. 62-68.

[13] Saenko, G.N., et al., Concentration of Iodine and bromine by plants in the seas of Japan and Okhotsk. Marine Biology, 1978. 47(3): p. 243-250.

[14] Wan, Y., et al., Contribution of Synthetic and Naturally Occurring Organobromine Compounds to Bromine Mass in Marine Organisms. Environmental Science & Technology, 2010. 44(16): p. 6068-6073.

The ANTARES accelerator, used by Michael Hotchkis, is used for tracing plutonium fallout in the Australian environment.

Forest soil erosion in the wake of major bushfires

Michael Hotchkis[1], Hugh Smith[2,3], Gary Sheridan[3], Petter Nyman[3], Patrick Lane[3], David Child[1], Geraldine Jacobsen[1]
[1]ANSTO, [2]University of Plymouth, UK, [3]University of Melbourne

Severe bushfires, such as Australia's 2009 Victorian 'Black Saturday' bushfires, expose the soil in bushland. Subsequent high intensity storms – possibly once-in-a-hundred year events – can then cause significant erosion with massive debris flows. This can happen even in small creek systems.

This study used fallout radionuclides (radioactive atoms) as tracers to better understand the processes that influence the evolution of landscapes experiencing these events.

The fate of the forest soil is particularly important because it can tell us whether or not existing conditions are sustainable. For example, if severe bushfires followed by severe storms causes soil depletion, we know there will be damage to the soil and subsequently, the forest, rather than a sustainable equilibrium.

Fallout plutonium isotopes, measured at trace levels using the ANTARES accelerator, were used for the first time in this kind of study.

Study area

The upper part of Myrtle Creek, in the Ovens River basin of North East Victoria, forms a small 23 hectare catchment, covered in dry open eucalypt forest (see map, Fig. 1). This area was completely burnt by one of the numerous high severity bushfires which swept Victoria in February 2009. In the first few days of March 2009, several storm cells passed over the catchment, producing short duration, high intensity rainfall (around 50 mm per hour rainfall rate). Even in a small catchment such as Myrtle Creek, the water pouring off the hillsides into the creek generated significant debris flows, moving hundreds of tons of material including gravel, sediments, tree trunks and small boulders (see Fig. 2).

Fallout radionuclides as tracers

Fallout from atmospheric nuclear weapons tests, carried out mainly in the late 1950s and early 1960s, distributed radionuclides all around the world. Certain longer lived radionuclides remain where they fell, in soil, sediments and elsewhere in the environment. These radionuclides act as markers in the soil or sediment and can then be used to trace the movements of such material. Of these, ^{137}Cs fallout has been used widely in erosion studies, as it tends to be firmly attached to the fine particles in soil or sediment. ^{137}Cs has a half-life of 30 years, so this marker is diminishing as the years go by. Plutonium, in particular ^{239}Pu and ^{240}Pu, also forms a major component of fallout and, like caesium, binds well to fine particles. With half-lives of several thousand years, the fallout signal from Pu isotopes provides a long-term marker in soils and sediments. Plutonium has only recently been used in this kind of work [1], as a result of the recent development of accelerator mass spectrometry for actinides. In the present study, both caesium and plutonium were used.

Sampling and measurements

^{137}Cs can be measured by gamma spectrometry in large samples. Pu is not detectable in this way, but can be measured with high sensitivity, even in small samples, by accelerator mass spectrometry. For this work, the Pu isotopes were measured using ANSTO's ANTARES accelerator. We could easily measure samples with 0.1 picogram of Pu per gram of soil.

Three different types of locations in the catchment were sampled:

1) Hillslope surface soils, to identify typical material which may contribute to downstream deposition. These samples had the highest levels of fallout radionuclides.

Figure 1

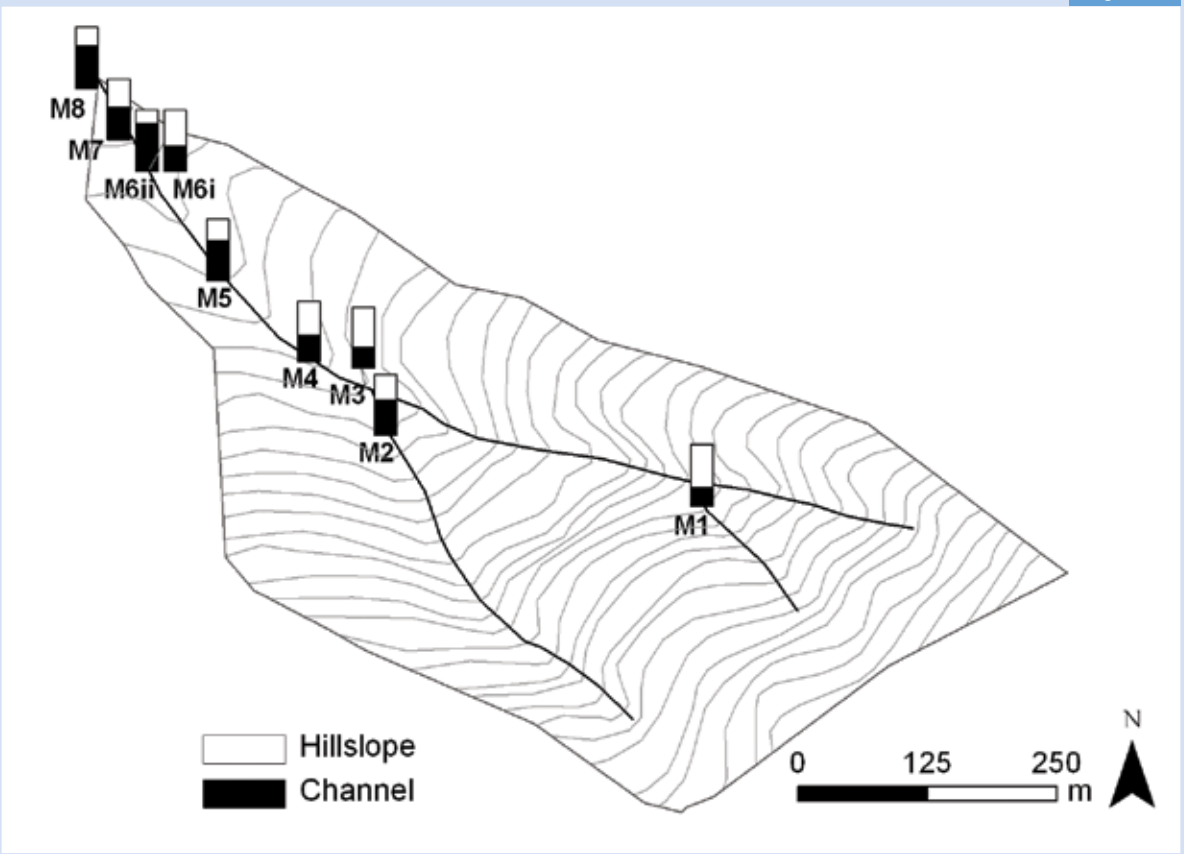

Contour map of the Myrtle Creek catchment, ranging in elevation from 430 to 770m. Sampled sediment deposition sites are shown, with the relative contribution from hillslope and channel bank source contributions.

2) Channel banks. As the creek floods, it cuts into the banks and stream bed, deepening the watercourse. Hence, material from the banks is swept into the flow and is also deposited downstream. These samples are comprised of sub-soil material and contain the least amount of fallout.
3) Deposits were sampled, such as levees left behind at the height of the storm flow. In all cases, we extracted fine sediments from the sampled material for our measurements.

Results

Fig. 3 shows that caesium (^{137}Cs) and plutonium (^{239}Pu+^{240}Pu) are well-correlated, confirming that plutonium is as valid as the more commonly used caesium for sediment tracing. As expected, the highest and the lowest activities are seen, respectively, in the hillslope and the channel bank samples. The activities of the deposits fall in between; the relative contributions to each deposit site sampled can be derived from a simple mixing model with relative contributions shown on the map in Fig. 1.

Further study of the results with respect to the types of locations sampled shows that hillslope erosion is the major contributor to sediment deposition during the peak of the storm. Subsequent deposition, following the peak flow, accumulated in inner channel deposits and in the terminal fan, is dominated by channel bank sourced material.

Carbon dating, using the STAR accelerator, has also been performed on past debris flows at Myrtle Creek. These show that severe erosion events, such as those observed here in 2009, might occur at intervals of several hundred years in susceptible locations.

In combination, these observations allow conclusions to be drawn about the erosion processes occurring at this site. Despite the low frequency of these events, the results indicate that they are major contributors to the long-term erosion of forest soils. Although the data here are limited, there are indications that the erosion rate exceeds the soil formation rate in this situation, leading to net soil loss. Soil loss leads to long-term environmental impacts.

This study, along with that of another site in Victoria, is reported in detail in a recent issue of the journal *Geomorphology* [2].

Figure 2

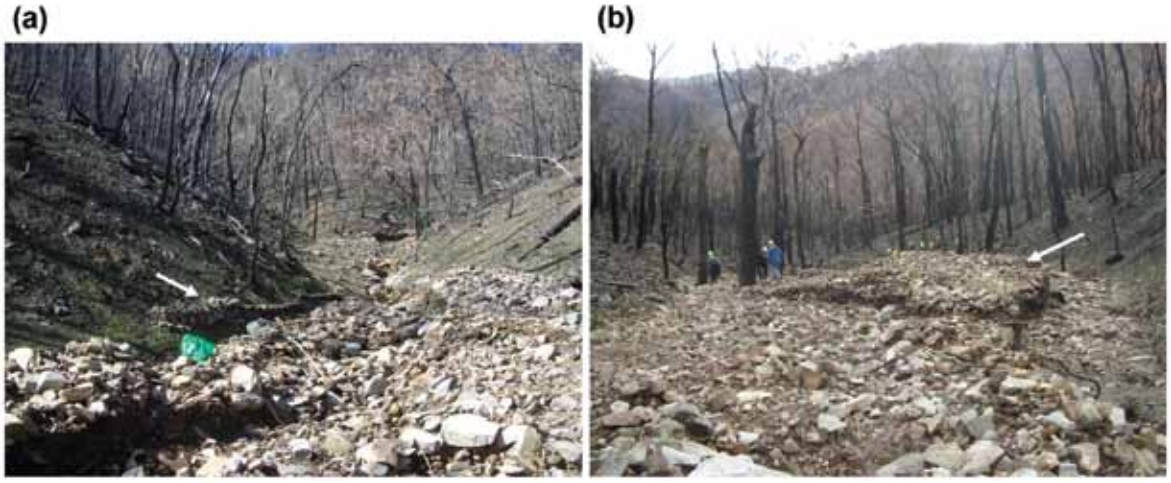

Photos of Myrtle Creek showing significant debris deposits left behind after sudden intense storm events in 2009. (b) Sampling locations are indicated with arrows. Note the burnt-out trees and denuded hill slopes resulting from the bushfires (photos courtesy Hugh Smith).

Figure 3

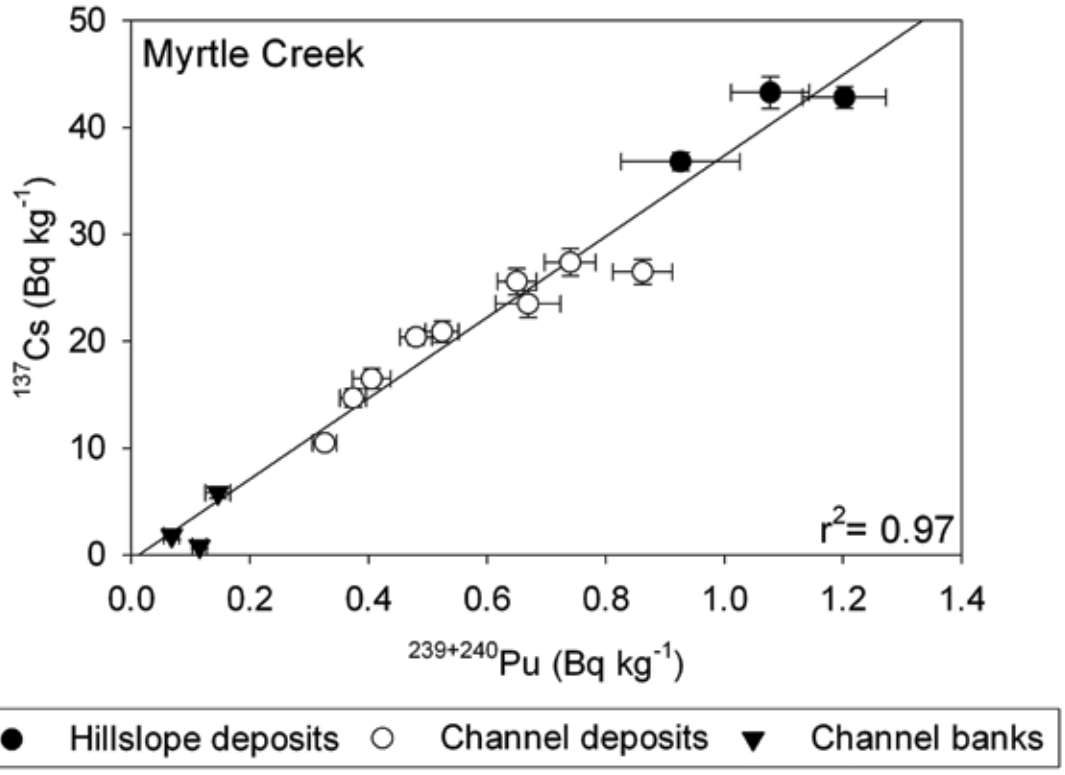

^{137}Cs and $^{239+240}$Pu activities of samples from the Myrtle Creek catchment.

References

[1] Everett, S. E., Tims, S. G., Hancock, G. J., Bartley, R. and Fifield, L. K., Comparison of Pu and ^{137}Cs as tracers of soil and sediment transport in a terrestrial environment. J. Environ. Radioact. 99, 383-393 (2008).

[2] Smith, H.G., Sheridan, G.J., Nyman, P., Child, D.P., Lane, P.N.J., Hotchkis, M.A.C., and Jacobsen, G.E., Quantifying sources of fine sediment supplied to post-fire debris flows using fallout radionuclide tracers, Geomorphology 139–140, 403-15 (2012).

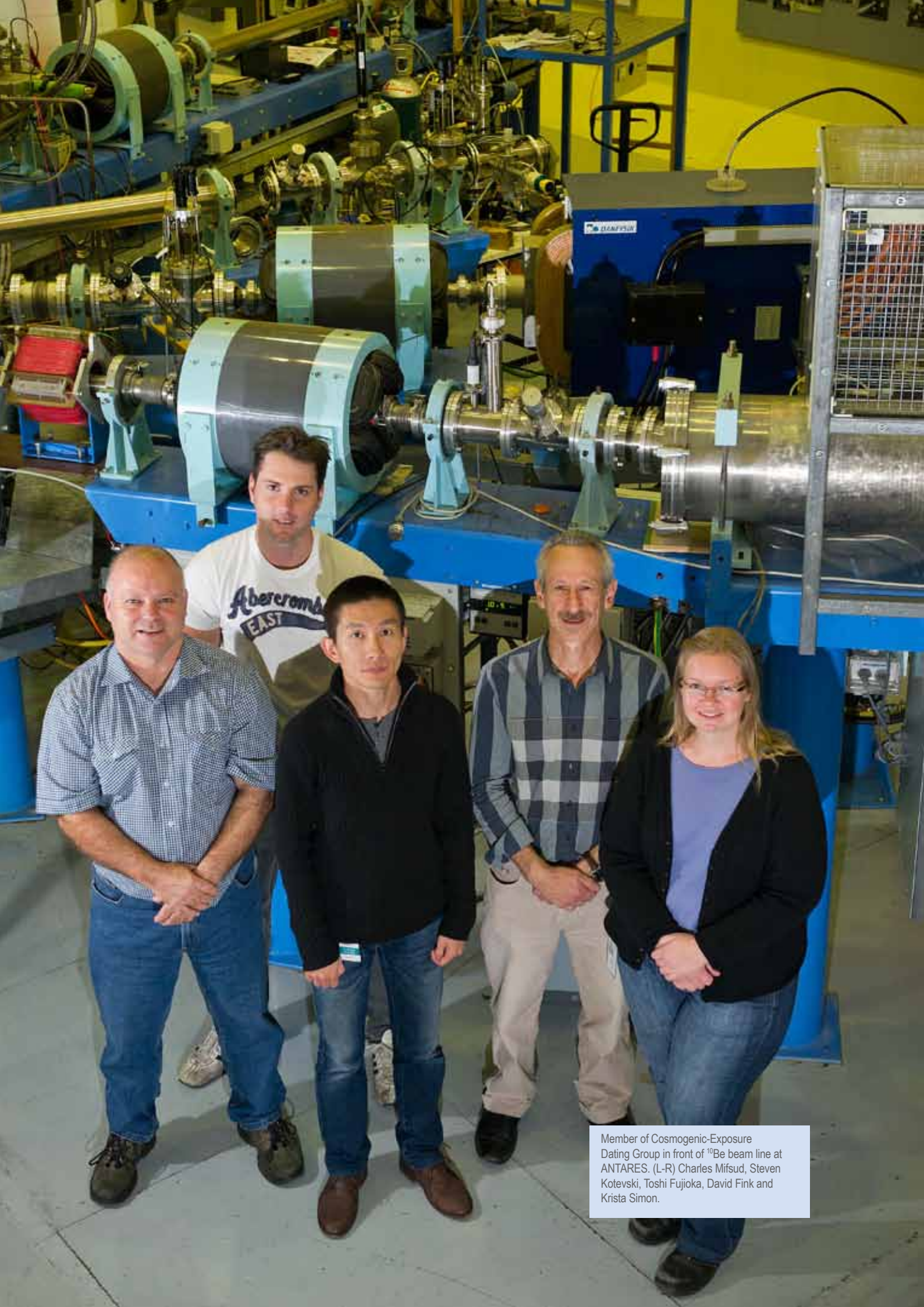

Member of Cosmogenic-Exposure Dating Group in front of ^{10}Be beam line at ANTARES. (L-R) Charles Mifsud, Steven Kotevski, Toshi Fujioka, David Fink and Krista Simon.

Ancient mega floods in the monsoon tropics of Australia coincide with climatic instability

Toshiyuki Fujioka[1], David Fink[1], Gerald Nanson[2], Charles Mifsud[1]
[1]ANSTO, [2]University of Wollongong

Recent climate predictions suggest Australia will experience more high-intensity tropical cyclones and flooding leading to extensive economic and social disruption.

These predictions are based on modelling global warming scenarios using short-duration historical cyclonic records. In order to improve future modelling of cyclone frequency, we need to find evidence of extreme events occurring over the past few tens of thousands of years.

At Jacks Waterhole, a narrow gorge about 500 m wide along the Durack River, in the Kimberley region of north-west Australia, numerous sets of meter-sized, mega-ton boulders are found stacked into semi-circular piles. These piles of imbricated boulders are due to massive storms and floods occurring during the past when rainfall conditions were vastly different from today. Using the novel technique of *in situ* cosmogenic-exposure dating and ANSTO's Accelerator Mass Spectrometry ANTARES Facility, ANSTO scientists were able to measure the time when these massive boulders were plucked from bedrock and flipped into piles. Initial results indicate that mega floods in the Kimberley region occurred about 15,000, 130,000 and 250,000 years ago - exactly during the period when earth's climate was changing rapidly at the end of the last 3 major ice ages. During these periods, sea-surface temperatures were increasing leading to increased atmospheric moisture supply and sea level rise associated with polar-ice melt. These results indicate that rapid increase of global temperature and future increases in global sea-level, may increase the magnitude of tropical cyclones and extreme flood events.

Assessing the floods

Australia has recently experienced a series of catastrophic floods associated with tropical cyclones and storms. While enhanced rainfall potentially helps agriculture to recover from long-standing drought, it can cause tremendous damage to urban communities and natural environments. Assessing risks of such hazardous events is of significant public concern in terms of the sustainable use of resources under our current rapidly changing climate.

There have been numerous investigations on how current global warming affects the occurrence of tropical cyclones and thus flood events [1], but the outcome is somewhat controversial. Although tropical cyclone activity appears to have increased in Australia over the past decade, the short nature of the historical and instrumental records prevents climate scientists from unambiguously decoupling the anthropogenic influence from the natural cyclone systems, thus making future predictions difficult.

In this study, we determined the timing of extreme floods in the monsoon tropics of Australia that displaced and overturned massive boulders plucked from underlying bedrock. The dating technique utilises the measurement of the concentration of the long-lived radioactive nuclide, ^{10}Be (half-life ~1.39 million years), which is produced in Earth's surface rocks via continuous bombardment of cosmic-ray particles. We applied this technique to imbricated clusters of gigantic boulders at Jack's Waterhole along the Durack River in the Kimberley in northern Australia.

The study site

The Kimberley belongs to the monsoon tropics of northern Australia; its climate is highly seasonal ranging from tropical to semi-arid where the region receives 90% of annual rainfall during the summer monsoon period (November–April). Occasional, but often intense, storms and cyclones lead to river flooding causing one of the main natural hazards for the local population.

Figure 1

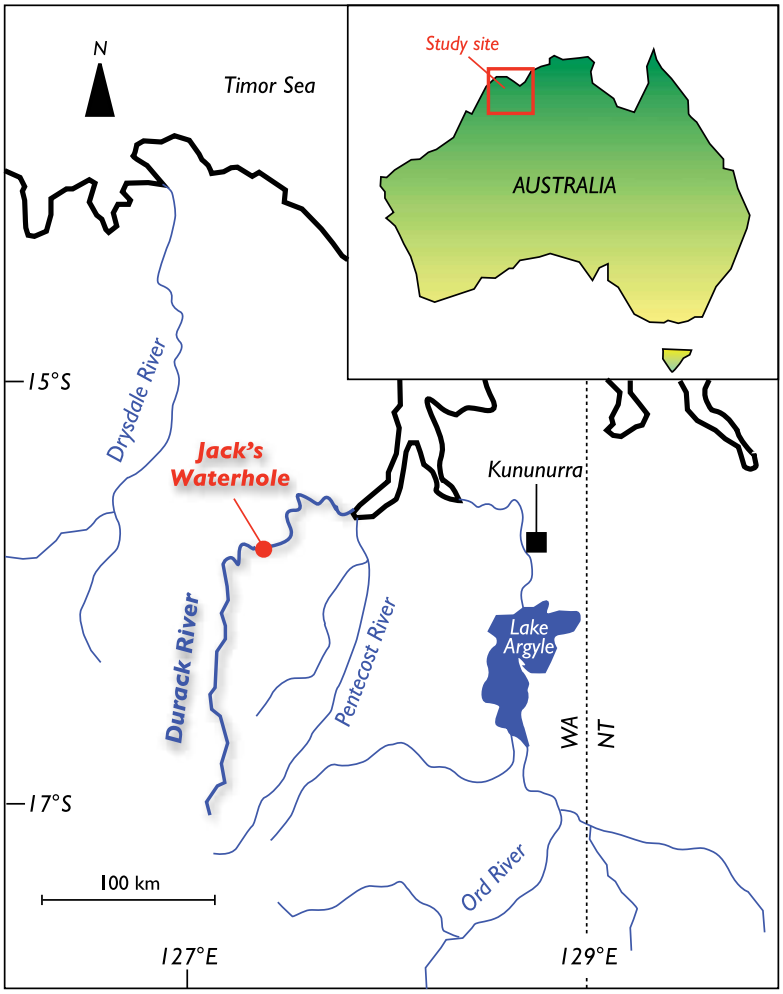

Location of the massive flood-generated boulder site at Jack's Waterhole in the Durack River, the Kimberley, northern Australia; the exposed and hidden surfaces of six boulders were sampled for dating of mega floods using cosmic-ray-produced radionuclide ^{10}Be.

Jack's Waterhole is located in the middle to lower sections of the Durack River, about 70 km upstream from its outlet to the Cambridge Gulf (Fig. 1). The flow derived from the upper catchment of 12,000 km^2 is funnelled through a narrow gorge, 500 m wide and ~1.5 km long, which has been formed by long-term incision of the Durack River into resistant sandstone. Along the flanks of the gorge and slightly above the modern river channel, numerous hydraulically-plucked rock slabs have been stacked into discontinuous, semi-circular patterns of imbricated piles that resemble toppled rows of dominoes (Fig. 2a-d). Based on surface erosional features (e.g., weathering pits, smoothness, rock vanish coating) and freshness of joint breaks and fracturing, some of these boulders have clearly been overturned. The layered bedding matrix of sandstone results in platy boulder shapes of a few to several metres in the long-axis and 0.5 to 2 m thick. The blocky quasi-square nature of the boulders results from the vertical jointing of the local bedrock.

A hydrological and channel morphological study of the site by Wende [2] suggested that only extreme floods with exceptionally high-flow velocities of up to 10 m/sec can dislodge and move these massive boulders. Such climatic events have not been documented in the palaeoclimate and environmental archives since the mid-Holocene (past 5,000 years), and we speculate that the overturning events may result from major changes in global climate associated with the waxing and waning of past ice ages. But, how can we 'date' when a boulder flipped?

Figure 2

(a) View looking upstream of a portion of the field of massive imbricated boulders at Jack's Waterhole. White arrow represents flow direction. (b) Prof Gerald Nanson next to boulder JW-1 (surface area 5.5 x 5 m, thickness ~70 cm, weight ~20 t), which was sampled on upper and lower surfaces for ^{10}Be that gave a model overturning age of 11,400 years. (c) David Fink next to imbricated boulder clusters. The boulder at the extreme left (JW-2, surface area 3.5 x 3.5 m, thickness ~70 cm, weight ~20 t) was sampled for ^{10}Be that gave an overturning age of 140,000 years. (d) Toshi Fujioka (left) and Gerald Nanson (right) on boulder JW-5 (surface area 7 x 3 m, thickness ~1 m, weight ~50 t). The boulder is among the largest we sampled that gave the oldest overturning age of 235,000 years.

Model concept

Cosmogenic ^{10}Be is produced via a spallation nuclear reaction of secondary cosmic-ray particles (neutrons and muons) on oxygen atoms within the mineral quartz (SiO_2 is the most abundant mineral on Earth) in rocks. The longer the surface is bombarded the more ^{10}Be accumulates. Given that the production rate of ^{10}Be (atoms per gram of quartz per year) is known and the extremely low concentration of resultant ^{10}Be in rocks can be measured by accelerator mass spectrometry, we can calculate the exposure ages of rock surfaces. In addition, by knowing how the cosmic-ray intensity attenuates with depth in the rock, we can predict a ^{10}Be concentration 'depth profile' by simply measuring ^{10}Be in the top few centimetres of rock surfaces. However, when a boulder is overturned, the predictable depth profile no longer applies, and the deviation of the predicted value from the measured one can be used to estimate the time when it overturned.

We sampled both the upper (exposed) and lower (hidden) surface of six boulders deemed to have been overturned by field observation. If our identification is correct, the previously buried surface is now exposed and the previously exposed surface is now buried after the event (Fig. 3), making the ^{10}Be ratio of the two surfaces deviate from the predicted value. Immediately after the event, the ^{10}Be concentration of the now hidden surface (i.e., the previously exposed surface) must exceed that at the exposed surface (i.e., the previously buried surface) (Fig. 3b). This inverse relationship will, with time, gradually tend to revert to the *normal* relationship (i.e., as if the boulder had never overturned) as the current upper surface continues to receive a higher cosmic-ray dose (Fig. 3c). Thus, the longer the elapsed time since overturning, the more difficult it is to uniquely determine whether the boulder has been overturned or not. Our modelling shows that we are able to determine overturning events for the time range between 1,000 to 300,000 years for boulders of 1 m thickness.

Figure 3

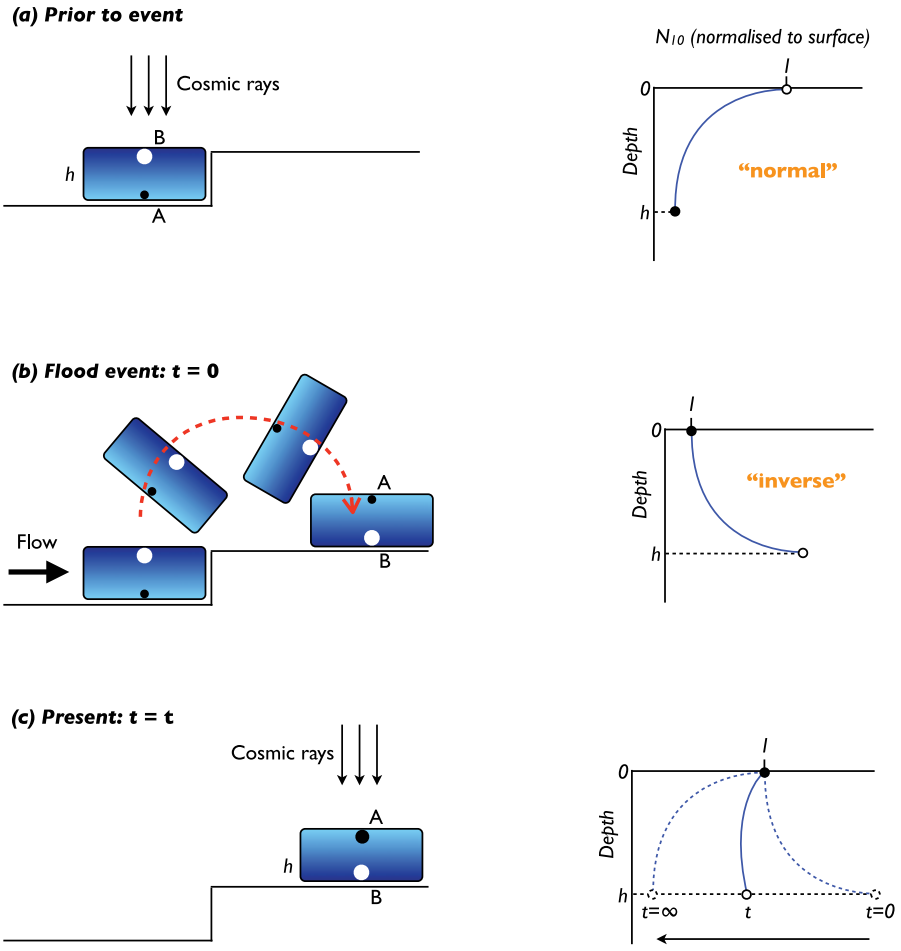

Schematic diagrams of an interpretive boulder-overturning model (left) and associated cosmogenic-^{10}Be vertical depth profiles through the boulder (right). (a) Just prior to the event (designated as t = 0): long-term continual irradiation of the intact boulder has resulted in an exponentially decreasing ("normal") ^{10}Be concentration profile, which is controlled by the cosmic-ray attenuation rate and boulder thickness, h. (b) At the flood event (t = 0): the upstream face of the rock slab is plucked from its bedrock contact, detached, rotated about a pivot point at its downstream face and overturned, exposing a previously-buried surface (surface A). The ^{10}Be profile immediately after overturning (t ~ 0) will be an inverted curve ("inverse" profile) similar to that given in (a). (c) As the cosmic-ray irradiation time continues, the ^{10}Be profile tends progressively to resemble the "normal" profile (dashed curves). During this time period, prior to re-establishing a "normal" depth profile, the overturning age, t, can be calculated by comparing the ratio of ^{10}Be on the lower to upper surface with that the predicted ratio based on the upper-surface ^{10}Be concentration with boulder thickness. The size of black and white dots denotes the relative difference in the ^{10}Be concentration between the surface A and B.

Determining the age of floods

Four out of six boulders we sampled show an inverse relationship in ^{10}Be concentrations between their upper and lower surfaces, indicating that they have been overturned. Within our measurement uncertainty, we could not unequivocally determine if the remaining two boulders were overturned. Our model gave overturning ages of 6,300, 11,400, 140,000 and 235,000 years with ~15% uncertainty for the four boulders [3].

These ages largely coincide with the last three major transitions of global climate from glacial to interglacial periods, termed glacial terminations, i.e., T-I (18,000–11,000), -II (136,000–124,000) and -III (252,000–238,000 years ago) [4] (Fig. 4). These transitions are characterised by a rapid increase in global temperature (~2°C per 1,000 years) associated with sea-level rise in parallel to a reorganisation of atmospheric and ocean circulations. We believe that the relative climatic instability at glacial terminations led to temporal enhancement of tropical cyclone and storm activities, consequently generating devastating floods along northern Australia.

Figure 4

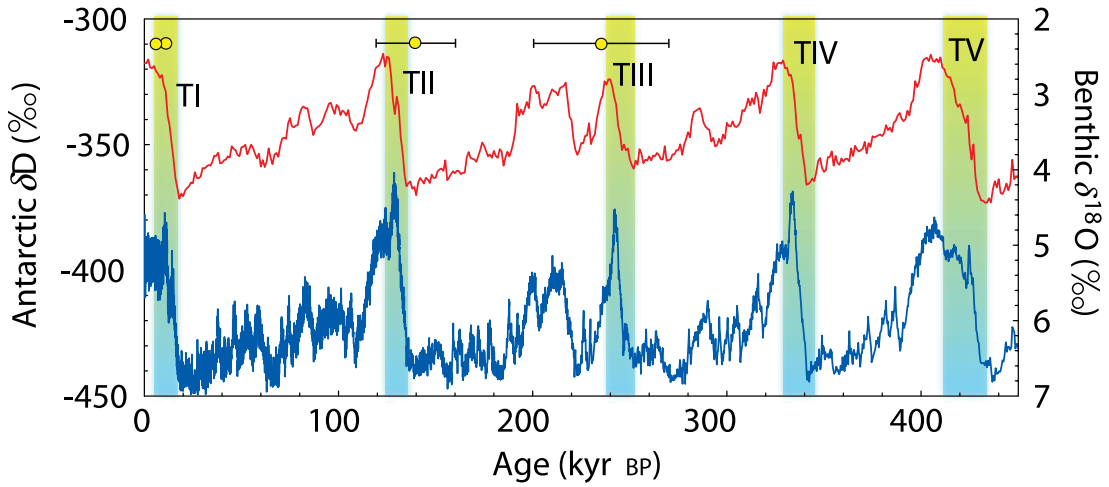

The model overturning ages of the mega-flood-generated boulders at Jack's Waterhole, the Kimberley, overlayed on major climate records over the past 450,000 years (after [4]). Benthic $\delta^{18}O$ stack (red curve, representing global deepwater temperature and ice volume); deuterium excess (δD) from the EPICA Dome C ice core, Antarctica (blue curve, representing Antarctic temperature). T-I to T-V (yellow-blue bands) denote glacial terminations. Our model overturning ages (yellow-dots; measurements taken on ANSTO's ANTARES accelerator) coincide with the three recent terminations which involve major oceanic and atmospheric reorganisation.

The youngest model age (6,300 years) corresponds to a period of relative warmer and wetter conditions associated with final sea-level adjustment to Antarctic-ice melt since the last glacial maximum (~20,000 years ago). This is supported by sediment records near Darwin indicating intense floods during early to mid-Holocene with much higher magnitude than those during the last 4,000 years [5].

In summary, we conclude that the palaeo-hydrological regime in northern Australia over the past 250,000 years has responded to the major global climate changes during periods of glacial terminations, as evidenced in this study by massive boulder overturing during increased river flow. This result has implications for assessing the effect of future global warming on the frequency and magnitude of cyclones and storms in the monsoon tropics of Australia.

References

[1] Knutson, T.R. et al. (2010). Tropical cyclones and climate change. Nature Geoscience, 3, 157-163.

[2] Wende, R. (1999). Boulder bedforms in jointed-bedrock channels. In: Miller, A.J. and Gupta, A., eds., Varieties of fluvial form, John Wiley and Sons Ltd, 189-216.

[3] Fujioka et al., in prep. Modelling of massive boulder overturning by palaeo-flood events in the tropics Australia, using *in situ* cosmogenic ^{10}Be. Quaternary Geochronology.

[4] Wolff et al. (2009). Glacial terminations as southern warmings without northern control. Nature Geoscience, 2, 206-209.

[5] Nott and Price (1999). Waterfalls, floods and climate change: evidence from tropical Australia. Earth and Planetary Science Letters, 171, 267-276.

Novel materials

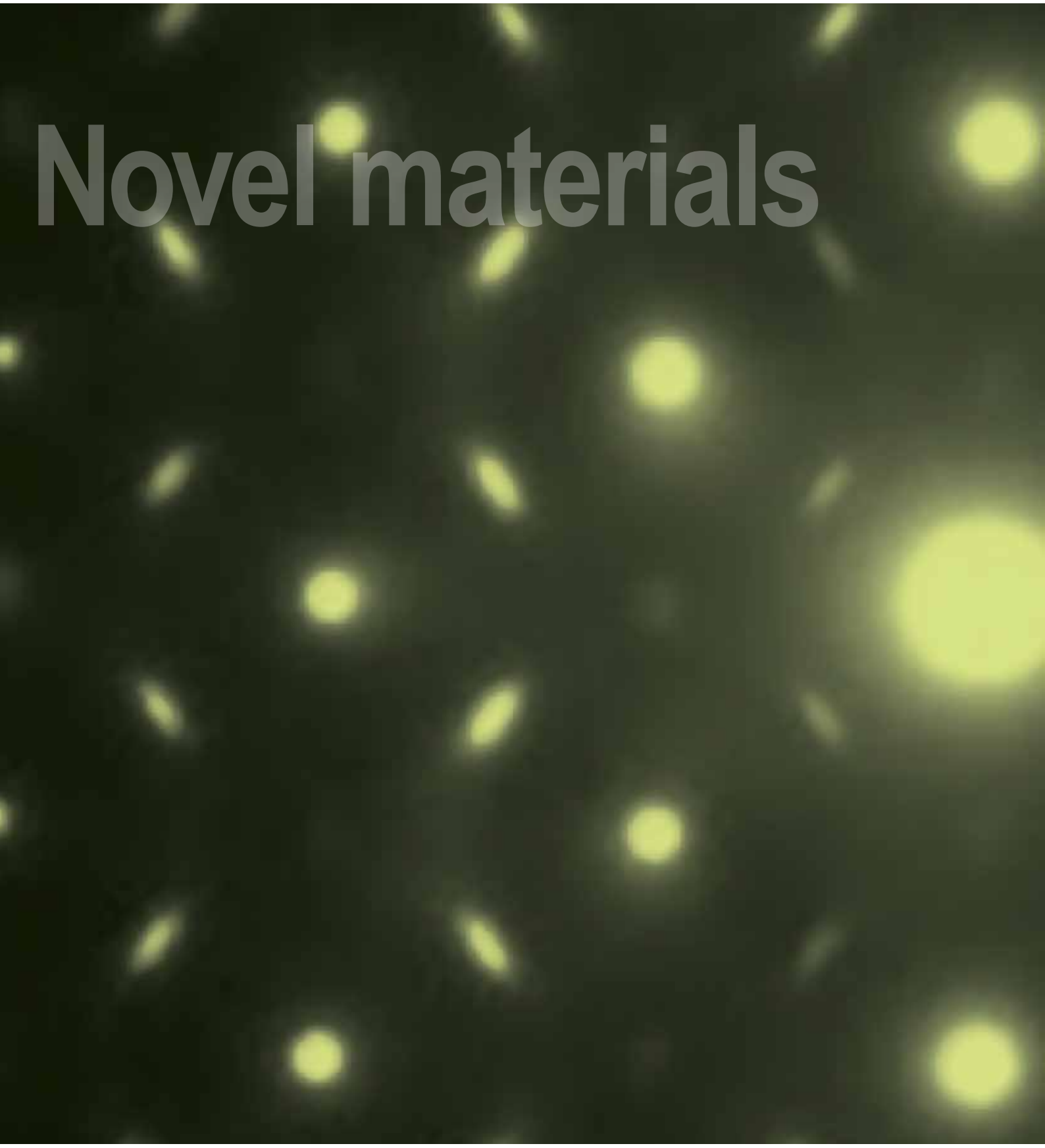

Novel materials

The novel material research conducted at ANSTO is aimed at developing and characterising new materials to tackle industry problems and create innovative and improved products in industries as diverse as health care, electronics and construction.

Research into novel materials includes plastics, metals and ceramics– essentially materials that are designed to exhibit new properties and improve performance.

ANSTO's recent novel material studies are helping improve the performance of the next generation of electronic devices such as television and mobile phone screens; finding the best way to store hydrogen, which could be the answer to producing cleaner, greener energy; and aiding the design of the nuclear materials of the future by studying how materials respond to extreme levels of radiation.

Tamim Darwish is setting up a hydrothermal deuteration reaction in a Parr high pressure reactor.

Studying the morphology and stability of organic light-emitting diode devices

Tamim A. Darwish[1] Michael James[1], Peter J. Holden[1], Arthur R. G. Smith,[2] Ian R. Gentle[2], Paul L. Burn[2].
[1]ANSTO, [2]University of Queensland

Organic light-emitting diodes (OLEDs) are extensively used in devices such as television and mobile phone screens, but their life-time depends significantly on the stability of the chemical layers that form these devices. Structural changes at the interfaces between these layers, which can occur during production or when the device heats up, dramatically affect how electrical charge travels through the device leading to changes in its performance.

ANSTO's research used neutron reflectometry and specifically synthesised deuterated molecules that are typically used in OLEDs, to study the combining of layers and the structural changes that take place on the nanoscale, or sub-microscopic level, to improve the performance of the next generation of these devices.

What is an OLED?

Organic light-emitting diodes (OLEDs) are generally made of thin layers of organic or organometallic (macro) molecules sandwiched between two electrodes (Fig.1). The devices emit light when an electric current flows through them. OLEDs are under intense investigation for use in the next generation of display and lighting technologies. These devices are used already in television screens, computer monitors and small portable system screens such as mobile phones and personal digital assistants.

How does an OLED work?

The simplest OLED has the emissive layer sandwiched between two electrodes (anode and cathode), one of which must be transparent to let the light escape. The anode injects holes into the device while the cathode injects electrons. When an appropriate voltage (typically a few volts) is applied to the cell the injected positive and negative charges recombine in the emissive layer to produce light (electroluminescence). However, for the devices to work well there needs to be balanced injection and charge transport of holes and electrons and to do this, additional charge transport layers are often introduced between the electrodes and the emissive layer. Fig. 2 shows a typical device that contains an 'electron transport layer' and a 'hole transport layer' in addition to the light-emitting layer.

Scope of study

While efficiencies of OLEDs have risen quickly the task of preparing such devices with lifetimes suitable for displays and lighting has proved challenging. The morphological stability of the layers in the device can affect both device efficiency and lifetime. Heat generated during operation is one of the critical factors which can contribute to the instability of the layers at the molecular interfaces. This is particularly important for OLEDs based on small molecule phosphorescent iridium(III) complexes such as *fac*-tris(2-phenylpyridyl)iridium(III) [Ir(ppy)$_3$] due to the different thermal properties of the materials in the adjacent layers, and also due to the fact that the complex is blended into a host material [e.g., 4,4-bis(*N*-carbazolyl)biphenyl = 'CBP']. In blends, it is difficult to elucidate whether the guest is evenly distributed throughout the film or whether there are concentration variations in parts of the film. Investigations of functioning devices with buried interfaces present numerous difficulties using conventional surface-science techniques and so neutron reflectometry along with deuteration of specific molecular layers has become the key method for the study of the morphology, diffusion and interfacial behaviour in organic thin-film semiconducting devices. These phenomena and the performance of organic optoelectronic devices are the subject of ongoing investigations by Paul Burn, Ian Gentle and their co-workers at the University of Queensland. They have developed a combined *in situ* neutron reflectometry/ photoluminescence measurement that allows the simultaneous collection of the neutron reflectivity data and emission spectra from functioning OLEDs [1]. An additional feature of the experiment is that the sample can be heated *in situ* thus enabling the direct determination of the effect of annealing on the physical and photophysical properties.

Figure 1

A flexible OLED device (photo courtesy of Andrew Liszewski).

Figure 2

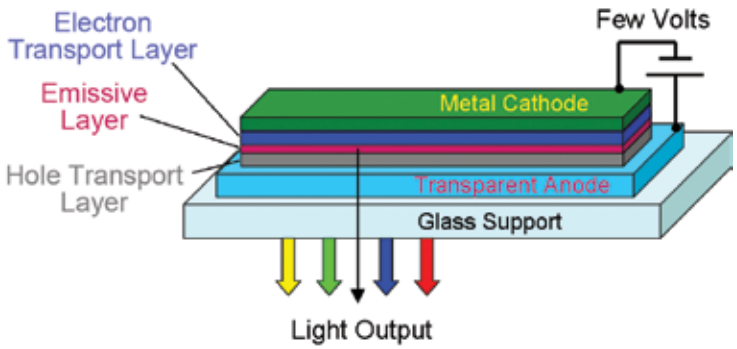

Schematic of an OLED device.

Why use neutrons and deuteration?

Neutron reflectometry is an excellent method for investigating the internal structure of thin (typically < 100 nm) films. In blended films, where there may be out-of-plane phase separation of the components within the blend, careful deuteration enables differentiation of components and allows any separation to be observed. Deuteration is the process where all or part of the hydrogen (^1H) content of a molecule is replaced by the stable (non-radioactive) isotope deuterium (^2H = D). Materials containing hydrogen (^1H) are said to be protonated whilst those containing deuterium (^2H = D) are said to be deuterated. The properties of the hydrogen and deuterium nuclei mean they scatter neutrons quite differently. This difference manifests as a variation in a quantity called the neutron scattering-length density. Neutron-beam studies exploit this difference in scattering-length density to probe the structures of individual components in multicomponent systems. In multi-layer films, a combination of deuterated and protonated layers can give excellent contrast in a neutron reflectometry experiment.

Deuteration of the OLED components

The National Deuteration Facility at ANSTO has the capability and expertise to deuterate a variety of (macro) molecules: this includes biodeuteration of proteins and polymers, as well as chemical deuteration including the synthesis and deuteration of a range of compounds such as surfactants, lipids, fatty acids, sugars and other small organic molecules.

Conjugated aromatic heterocycles such as bathocuproine (BCP) and tris(4-carbazoyl-9-ylphenyl) amine (TCTA) (Fig. 3) are widely used in OLEDs as electron and hole transport materials respectively. Deuteration of these aromatic and heterocyclic molecules enables the characterisation of the film structure typically found in multilayer OLEDs, due to a substantial increase in neutron scattering-length density of the deuterated material compared to their equivalent protonated forms. In addition, we can probe interdiffusion between the different molecular layers under thermal stress [1-3].

A combination of spectroscopic techniques such as nuclear magnetic resonance (NMR) and mass spectroscopy (MS) were used to calculate the total deuterium content in the molecules and the relative occurrence of hydrogen and deuterium atoms at specific sites within the molecule. NMR is a particularly useful analytical tool as experiments can be designed that discriminate between resonances of the various types of carbon molecules present: fully deuterated groups (CD, CD_2, CD_3), partially deuterated groups (CHD, CHD_2, CH_2D), and non-deuterated groups (C, CH, CH_2, CH_3), thus allowing the full characterisation of the deuterated molecules, and hence the calculation of the scattering-length density of the different materials in the OLED layers for the neutron experiments [3].

Hydrothermal deuterium labelling

Deuteration of the molecules for this work was achieved either by H/D exchange reactions with deuterium oxide (D_2O) catalysed by Pt/C and Pd/C under hydrothermal conditions, or by synthesis from deuterated precursors produced by the same method. Hydrothermal deuteration involves heating the protonated version of the molecule in D_2O, which acts as the solvent and deuterium source, in the presence of metal catalysts under high temperatures and pressures using a Parr reactor (see image p.58). These reactors are designed to heat aqueous solutions to temperatures approaching water's supercritical temperature under pressure. This induces H/D exchange between sites on the protonated molecule to produce a deuterated version which is then isolated, purified and characterised.

Inter-diffusion and phase separation in OLEDs

Thin films of the desired protonated and deuterated compounds were prepared by thermal evaporation under high vacuum onto silicon wafers at the University

Figure 3

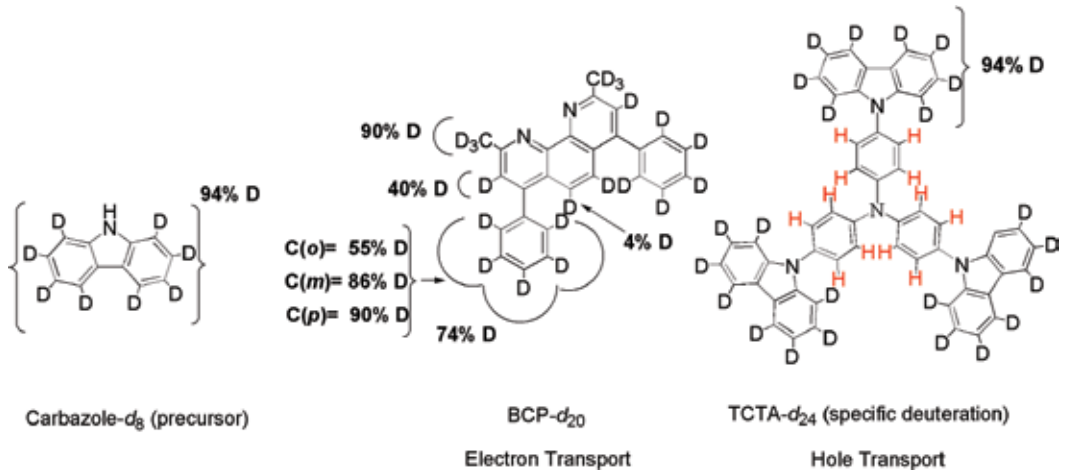

Deuterated molecules used in this study.

of Queensland for neutron reflectivity measurements on the Platypus time-of-flight neutron reflectometer at the OPAL 20 MW research reactor at ANSTO [4]. Analysis of neutron reflectivity data from a BCP-d_{20} / (Ir(ppy)$_3$:CBP) / TCTA-d_{24} trilayer film on silicon (Si) measured at room temperature gave thicknesses of 15 nm, 35 nm and 27 nm respectively with excellent contrast between the BCP-d_{20} and TCTA-d_{24} layers (SLD~5x10^{-6} Å^{-2}) and the (Ir(ppy)$_3$:CBP) layer (SLD~2.5x10^{-6} Å^{-2}). The three-layer structure was stable at temperatures up to 90°C. At 100°C the Ir(ppy)$_3$:CBP and BCP-d_{20} layers were found to interdiffuse, while the (TCTA-d_{24}) / Ir(ppy)$_3$:CBP interface remained stable (Fig. 4). Only by using deuterated BCP-d_{20} and TCTA-d_{24} could we study this behaviour as the protonated forms of BCP and TCTA in these thin-film devices would not have provided adequate scattering contrast between the CBP emissive layer, the BCP and the TCTA layer.

In addition, our study found that as prepared blended films of Ir(ppy)$_3$ in CBP were uniformly mixed. However the stability of the films with respect to phase separation was strongly dependent on the weight ratio of the Ir(ppy)$_3$ in CBP. When films comprised of 6 wt% Ir(ppy)$_3$ in CBP (typically used in OLEDs) were heated to a moderate temperature (at 80°C) they were found to phase separate. In contrast, simply increasing the weight percent to 12wt% caused the film to become stable such that on heating no significant separation occurred.

These results have important implications for materials and device design, not only for OLEDs but also for stacked organic photovoltaic devices. It is important to identify the temperature at which these devices can work reproducibly and most efficiently, as well as the environment in which these devices are being used or stored.

Figure 4

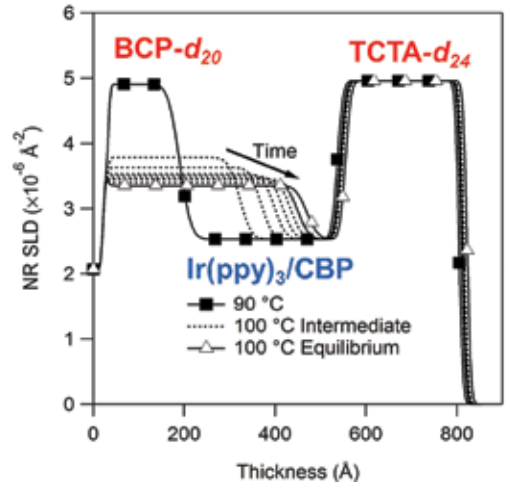

Neutron scattering-length density profile from an OLED trilayer from neutron reflectivity data showing interdiffusion of BCP-d_{20} and Ir(ppy)$_3$:CBP layers at 100°C.

References

[1] Smith, A. R. G., Ruggles, J. L., Cavaye, H., Shaw, P., Darwish, T. A., James, M., Gentle, I. R., Burn, P. L., Morphology and Stability of *Fac*-tris(2-phenylpyridyl) iridium(III) Blended Films: a Neutron Reflectometry Study, Advanced Functional Materials, 21(12), 2225-2231 (2011).

[2] Smith, A. R. G., Lee, K. H., Nelson, A., James, M., Burn, P. L., and Gentle, I. R., Diffusion – the Hidden Menace in Organic Optoelectronic Devices, Advanced Materials, 24(6), 822-826 (2012).

[3] Darwish, T. A., Smith, A. R. G., Gentle, I. R., Burn, P. L., Luks, E., Moraes, G., Gillon, M., Holden, P. J., and James, M, Deuteration of conjugated aromatic heterocycles for morphological studies of organic light emitting devices, Tetrahedron Letters, 53, 931–935 (2012).

[4] James, M, Nelson, A, Holt, SA, Saerbeck, T, Hamilton, WA and Klose, F, The multipurpose time-of-flight neutron reflectometer "Platypus" at Australia's OPAL reactor, Nucl. Instrum. Methods Phys. Res., Sect. A 632(1), 112-123 (2011).

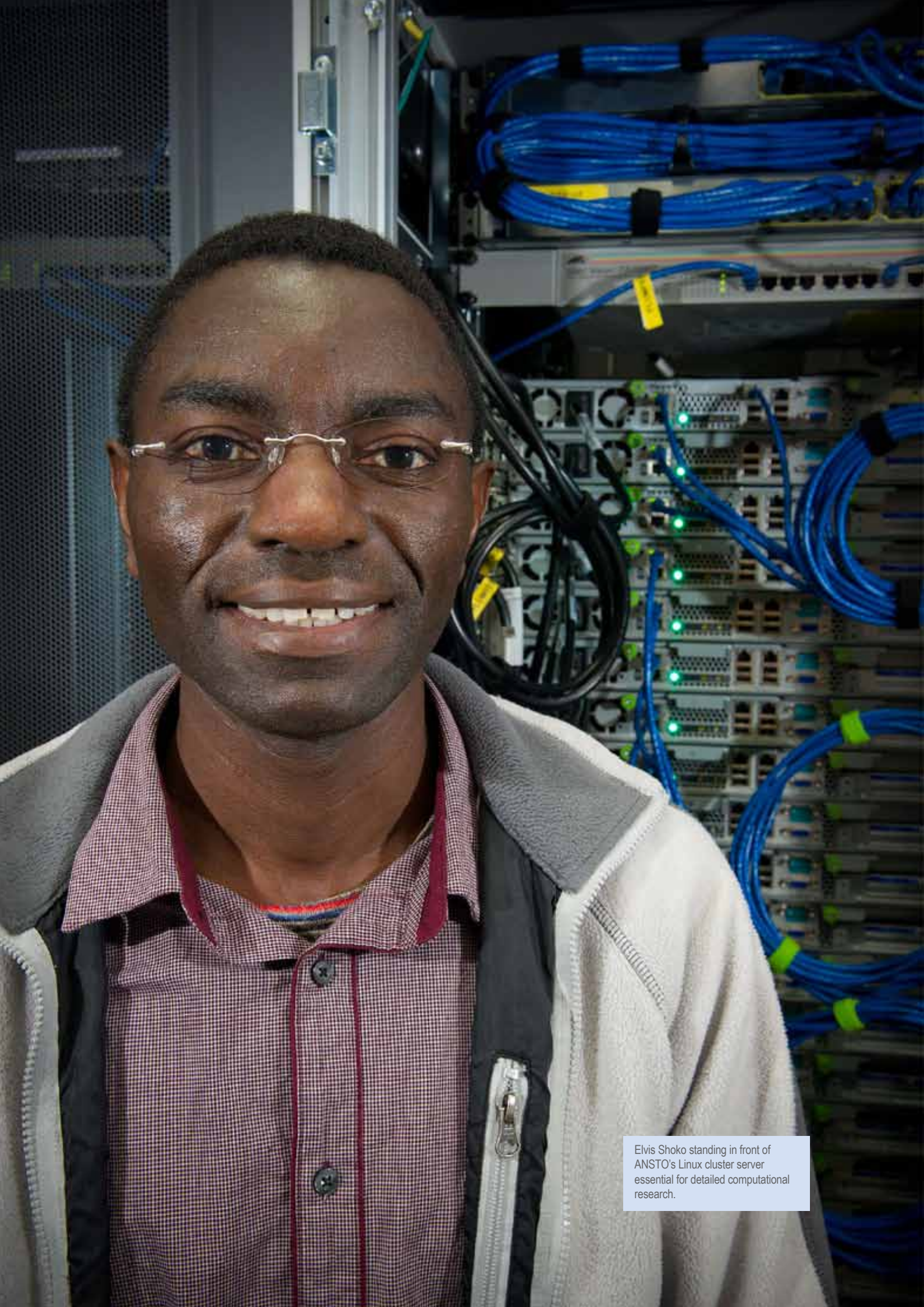

Elvis Shoko standing in front of ANSTO's Linux cluster server essential for detailed computational research.

When the guest rattles the host

Elvis Shoko, Vanessa K. Peterson, Gordon J. Kearley
ANSTO

Environmental sustainability is driving energy production and use towards cleaner and greener technologies such as using hydrogen as a fuel. However, this raises the problem of how best to safely store hydrogen.

This study investigated trapping hydrogen molecules (H_2) in ice. This forms a clathrate hydrogen hydrate, which is essentially an ice cage which can hold hydrogen. Although this research focuses on ice, there are other options for cage materials and we need to understand how the hydrogen interacts with the container carrying it. This is best done by analysing how the hydrogen molecules move around in the cage. The research also tackled the question of whether the cage's own thermal motion is also important.

Although complex, these questions must be understood because they relate directly to the performance and safety of the hydrogen storage material. This research used a more rigorous approach than has been commonly used previously, taking into account the cage's flexibility rather than assuming that the cage is rigid. This has highlighted the shortcomings of previous experiments. It is crucial to correctly calculate the interaction between the hydrogen and the cage so that we can work towards ice composite materials that can safely store more hydrogen.

Hydrogen in a clathrate hydrate cage: A hydrogen-storage system

Environmental sustainability is driving energy production and use towards cleaner and greener technologies. This has brought to the forefront of research the prospect of a hydrogen economy, in which the hydrogen molecule is the primary energy carrier with its conversion to power through fuel-cell technologies.

An important challenge in moving to a hydrogen economy for the automotive industry is the onboard storage of hydrogen through a technology which meets both power (as capacity) and delivery time (fuelling) requirements of the vehicle. The small hydrogen-molecule is energy-intensive to compress, and the limitations of high pressure storage tanks have been circumvented by storage of hydrogen within another material. Candidate materials include metal hydrides, chemical hydrides, and porous materials such as coordination frameworks and hydrogen clathrates [2], but to be of practical use, these should meet the US Department of Energy (DOE) targets [3] for both storage capacity and delivery of the hydrogen, and should be be cheap, non-toxic, compact, and light, for viable commercialisation.

The structure of type II pure hydrogen clathrates, (Fig. 1), form and remain stable only at 200 MPa and 273 K [4]. This pressure is high, but can be reduced by incorporating other molecules in the nanocages, e.g. tetrahydrofuran [4]. However, adding other molecules into the clathrate means that there is less room for the hydrogen and the conflicting requirements of structural stability and storage capacity are difficult to reconcile. For a pure hydrogen hydrate, the theoretical maximum storage capacity is close to the 5.5 w/w% DOE storage requirement for 2015 [3], assuming 2 and 4 hydrogen molecules in the small and large cages respectively (see Fig. 1) [5]. The prospect of reaching this maximum relies on an understanding of the nature of the interactions between a guest molecule and the cage containing it.

Figure 1

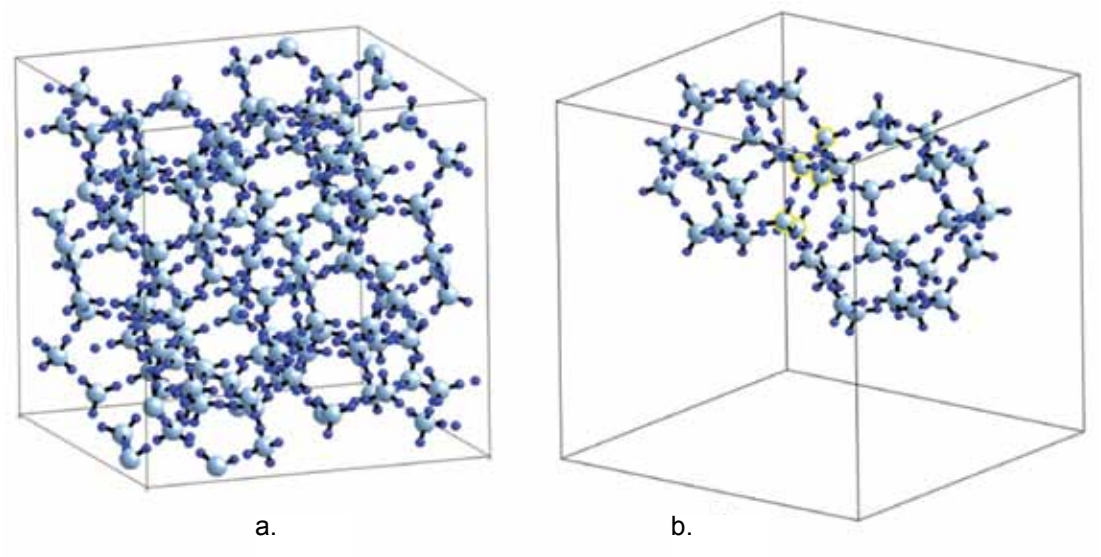

Schematic of structure II hydrogen hydrate cages as (a) the unit cell, and (b) part of the unit cell highlighting small and large cages. There are 16 small and 8 large cages in a unit cell. The small dark blue circles are H atoms and the large light blue are O atoms. The two cage types share a pentagonal face which is highlighted in yellow. Guest hydrogen molecules are not shown for clarity.

There is a sweet spot in the interaction between the hydrogen guest and the cage that maximises storage capacity and allows the gas to be released for subsequent use. When the hydrogen molecule is loosely held, it undergoes a fascinating phenomenon known as quantum translation/rotation that has been widely studied theoretically [6]. However, these studies assume that the cage is rigid in order to simplify the problem computationally, since including the movements of the cage complicate these calculations [7]. We resolve these difficulties by taking an axiomatic approach which enables us to model this quantum system classically, at 15 K, using *ab initio* molecular dynamics (MD) in VASP [8]. Quantum systems are more sensitive to changes in the hydrogen-cage interaction than classical systems. By treating the system classically (which is easy) and comparing results from a flexible-cage calculation with that for a fixed-cage calculation, we can assess any differences and judge if ignoring cage flexibility in the real quantum system will cause a serious error.

There are four types of motion that are of importance here. The hydrogen may rotate around its centre (twist) and translate (rattle) in the cage. The cage is more restricted in its motion and we consider libration, which is restricted rotation (or twisting) of the two H-atoms about an axis through the O-atoms. We also consider a translation (more like shaking) of the water molecule about its average position in the cage.

A useful quantitative measure of the interaction between the hydrogen guest and the cage is the potential of mean force (PMF) which is calculated from the MD atomic trajectories as the negative logarithm of the population density of the hydrogen molecule within the cage. In the following sections we look in detail at the atomic and molecular motions obtained from the MD simulations to extract what interactions exist and their origins.

Where is the guest?

Fig. 2 shows the first and perhaps most convincing result from the MD simulations for a hydrogen molecule in a fixed and flexible cage. There are clear differences: Firstly, the PMF of the hydrogen in the flexible cage shows that the hydrogen covers a larger spatial range compared to that of the hydrogen in the fixed cage. Secondly, whereas the fixed cage PMF is approximately isotropic, the flexible cage PMF has a more complex structure, which shows that there are important interactions in the guest-host dynamics.

This result demonstrates that the fixed cage computational approach fails to capture some essential physics of the guest-host interactions and is a poor starting point for understanding the technologically important storage-capacity issues.

Figure 2

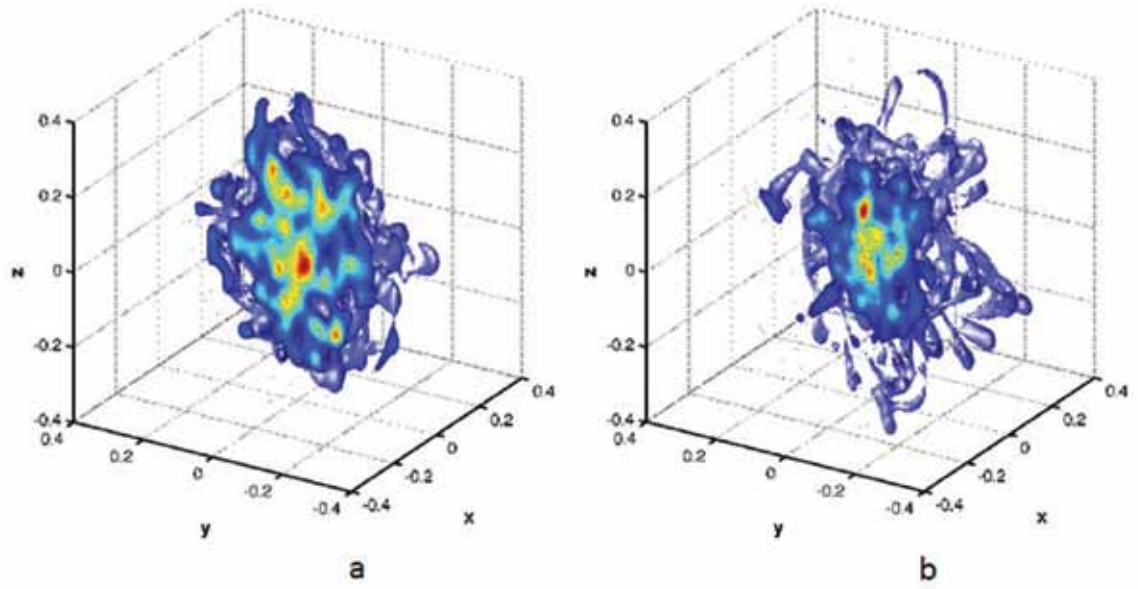

Cross-sections through the 3D potential of mean force (PMF) for the H_2 guest in the (a) fixed cage and (b) the flexible cage, where the contours show greater depth in energy from red to blue.

This result demonstrates that the fixed cage computational approach fails to capture some essential physics of the guest-host interactions and is a poor starting point for understanding the technologically important storage-capacity issues.

Figure 3

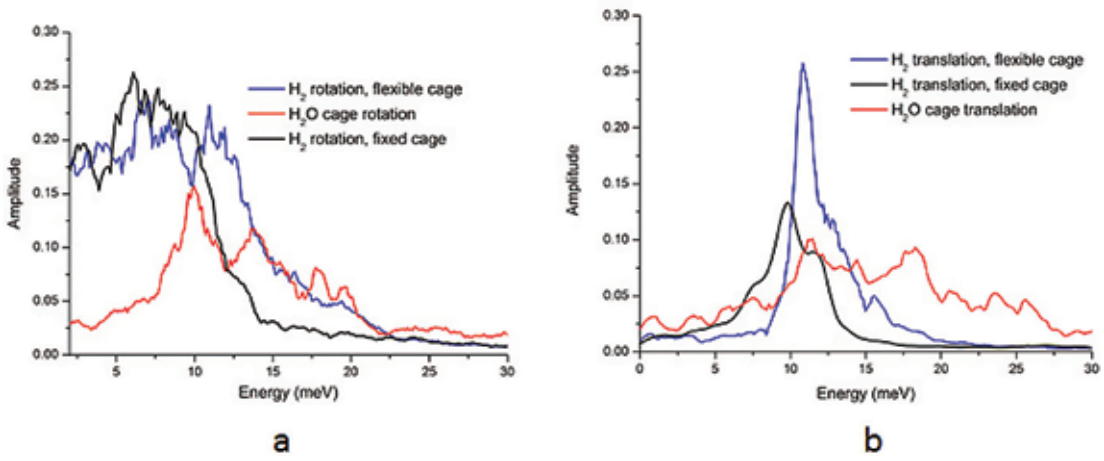

Frequency spectra of the (a) rotational/librational and (b) translational motions of the H_2 and the H_2O cage molecules.

It is important to understand the mode coupling because this affects the total energy (stability) of the system via the entropy; a key factor in the storage capacity and temperature range in which the material is useful.

Figure 4

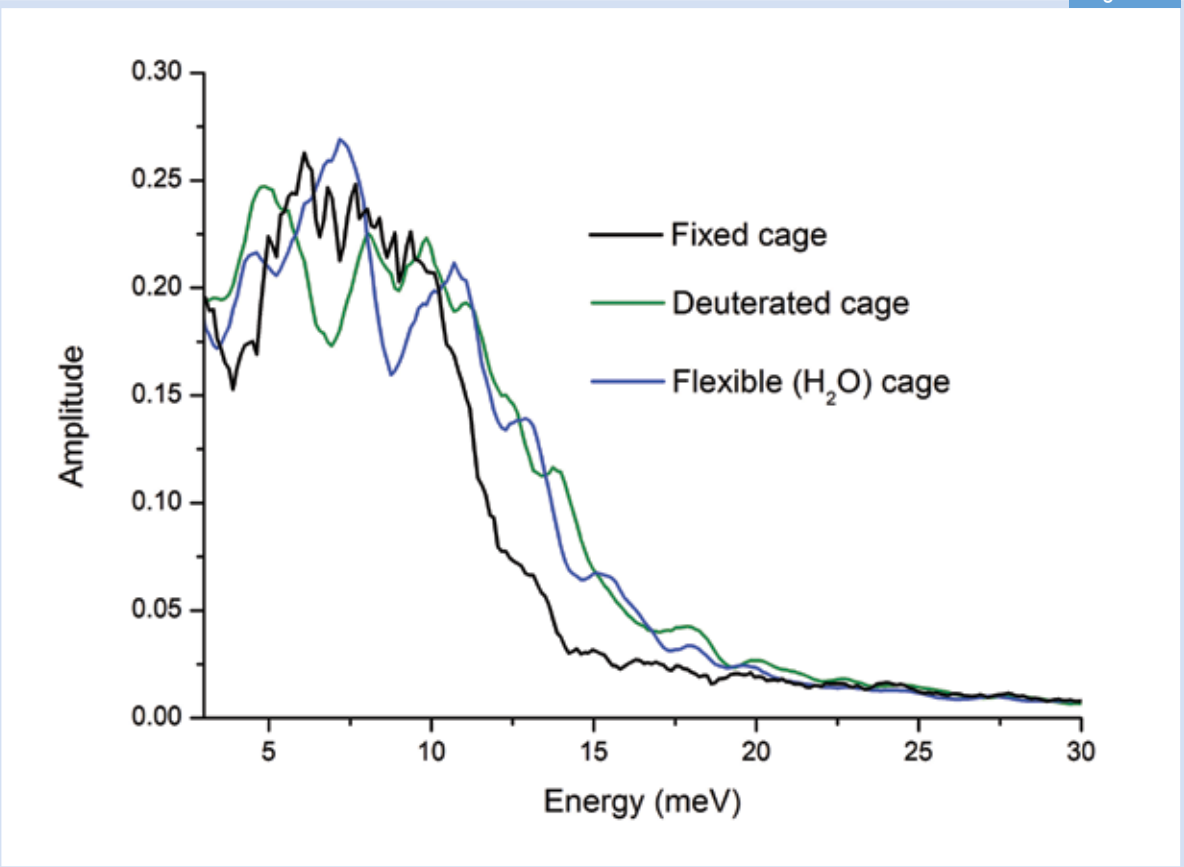

Rotational spectra of H_2 in the fixed, flexible deuterated and flexible H_2O cages. The fixed and deuterated cages exhibit similar spectral features in the region around 10 meV.

Does the guest rattle the host?

Dynamical coupling between the guest and the cage requires the motions for the two to have similar frequencies and to examine this, we extracted the frequencies of selected dynamical modes of the hydrogen and the flexible cage H_2O molecules from the MD trajectories. The results in Fig. 3 show that both the librational and translational modes of the cage H_2O overlap considerably with the rotational and translational modes of the hydrogen, respectively, pointing to significant coupling. A striking feature of Fig. 3 is the peak at approximately 10 meV which corresponds closely to the well-known peak at 9.86 meV observed experimentally using inelastic neutron scattering. This peak is normally attributed to the translational motion of the hydrogen ("rattling") but the current work suggests that this mode contains a rotational contribution, at least from the H_2O cage.

How does the guest behave in a heavy host?

Substitution of the hydrogen atoms of the cage with deuterium is routine in inelastic neutron scattering experiments because it effectively removes the signal from the ice. This makes it easier to study the movements of the hydrogen molecule, but implicitly makes the assumption that movements of the hydrogen guest and the cage are independent. We investigate the effect of this cage deuteration on the rotational dynamics of the hydrogen (Fig. 4). Compared to the normal H_2O cage, the deuterated cage gives rise to a rather different (classical) rotational spectrum for the hydrogen because the coupling to the cage has changed. It is particularly important to note that the normal H_2O and deuterated-cage spectra differ in the region around 10meV. Our results suggest that deuteration of the cage shifts the cage dynamics to be closer to that observed for the fixed cage system, giving a "false agreement" with a calculated spectrum in which the cage is fixed and that for the experimentally measured deuterated cage. This is an exciting result that we intend to verify experimentally.

Conclusion

Quantum systems are delicate and it is risky to assume that substituting a normal ice cage by a heavy-water ice cage will not affect the motions of the guest in the cage. Clearly, it does. This is an important warning because it is common (and convenient) practice to use deuterium substitution to remove the incoherent signal from hydrogen that would otherwise clutter the signal from the H-atoms of interest. Simulation (as we use) is probably the simplest method of guarding against this mistake.

Previous studies have used analytical expressions for the potential-energy surface for the hydrogen molecule that give very accurate results, but for a fixed-cage model that we have shown to be inadequate. It would be difficult to use these analytical methods for a model in which the cage is flexible, but we have shown that the more tractable potential of mean force (PMF) for the hydrogen molecule (which is very close to the potential-energy surface) is very different in the cases of flexible and rigid cages. This arises because the frequencies of the low-energy motions of the cages almost coincide with the period of the hydrogen motions, which could ultimately be used as a method for tuning hydrogen-storage capacity.

References

[1] Peterson, V. K., Shoko, E., and Kearley, G. J., The Effect of Host Relaxation and Dynamics on Guest Molecule Dynamics in H_2/tetrahydrofuran-hydrate, Faraday Discuss., 151, 37-46 (2011).

[2] David, W. I. F., Effective Hydrogen Storage: A Strategic Chemistry Challenge, Faraday Discuss., 151, 399-414 (2011).

[3] DOE. http://www1.eere.energy.gov/hydrogenandfuelcells/storage/pdfs/targets_onboard_hydro_storage_explanation.pdf, the targets for a future hydrogen economy as defined by the Department of Energy.

[4] Struzhkin, V. V., Militzer, B., Mao, W. L., Mao, H-K., and Hemley, R. J., Hydrogen Storage in Molecular Clathrates, Chem. Rev. 107, 4133-4151 (2007).

[5] Schuth, F., Hydrogen and Hydrates, Nature, 434, 712-713 (2005).

[6] Xu, M., and Bacic, Z., Inelastic Neutron Scattering Spectra of a Hydrogen Molecule in a Nanocavity: Methodology for Quantum Calculations Incorporating the Coupled Five-Dimensional Translation-Rotation Eigenstates, Phys. Rev. B, 84, 195445 (2011).

[7] Patchkovskii, S., and Tse, J. S., Thermodynamic Stability of Hydrogen Clathrates, Proc. Natl. Acad. Sci. USA, 100 (25), 14645-14650 (2003).

[8] Kresse, G., and Furthmuller, J., Efficient Iterative Schemes for ab initio Total-energy Calculations Using a Plane-wave Basis Set, Phys. Rev. B54, 11169-11186 (1996); Bloechl, P. E., The Projector Augmented-wave Method, Phys. Rev. B, 50, 17953-17979 (1994); Kresse, G., and Joubert, J., From Ultrasoft Pseudopotentials to the Projector Augmented-wave Method, Phys. Rev. B, 59, 1758-1775 (1999).

Greg Lumpkin's work is helping develop tomorrow's materials for future nuclear applications.

Understanding radiation damage at the atomic scale

Marc Robinson[2], Nigel Marks[2], Karl Whittle[1], Greg Lumpkin[1]
[1]ANSTO, [2]Curtin University

Materials for future nuclear applications all share one important property: the ability to maintain functionality during exposure to extreme levels of irradiation. Developing such materials requires an in-depth understanding of the atomic processes that attribute to the build-up of radiation damage.

ANSTO's study used atomistic scale simulations to discover the mechanisms of initial defect formation. Allowing a first-hand look at which factors contribute to a material's radiation tolerance or susceptibility will help us understand and design prospective nuclear materials.

The virtual microscope

To aid the understanding of a macroscopic process, it is important to isolate and study the contributing microscopic factors. Applying this philosophy to understanding how a material responds to radiation, inevitably leads us to the investigation of the fundamental atomic-level phenomena. However, the dynamics of radiation damage cannot be observed directly even using the best experimental techniques: the processes are simply too small and too fast. This is where 'virtual' experiments can take over.

Atomistic computer simulations are becoming increasingly popular, aided by advances in High Performance Computing (HPC). The ability to model the motions of millions of atoms over the nanosecond time-scale has resulted in simulation becoming a powerful tool to complement experiment.

The investigation of radiation damage is well suited to computer simulation, in particular molecular dynamics (MD). In MD, each atom in the system is treated individually, allowing us to follow the trajectories of energetic atoms and reveal the mechanisms of damage accumulation (see Fig. 1).

In our research, we develop new techniques based on MD computer simulation. We study low-energy radiation events with the goal to understand which factors contribute to changes in initial defect formation.

Combining this methodology with thousands of processors from HPC facilities has allowed us to gain a very high level of statistics enabling precise calculation of important quantities such as the threshold displacement energy.

Figure 1

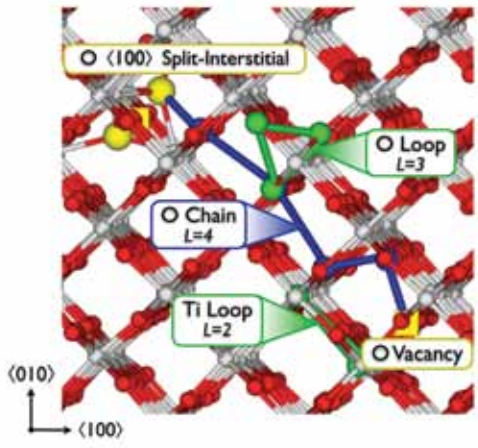

A snapshot of an MD simulation in rutile. By tracking the trajectories of the atoms, the mechanisms of defect production and recombination are revealed. In this simulation, an oxygen split-interstitial is formed (yellow) by a succession of knock-on events referred to as a replacement chain (blue). When these chains form loops (green), no defects are produced.

The threshold displacement energy

What is the kinetic energy required to permanently displace an atom in a particular system? This question forms the basis for numerous models of radiation damage and the answer is known as the threshold displacement energy or E_d.

A common use of E_d is in SRIM (The Stopping and Range of Ions in Matter)[1] a popular computer simulation program. SRIM is used extensively by the semiconductor industry and ion-implantation community to calculate ion-implantation depths, defect production and sputtering yield. However, the accuracy of models such as SRIM hinge on ascertaining an accurate value of E_d.

To precisely determine E_d requires a methodology that can capture the onset of defect creation. This methodology would be required to sample numerous variables such as impact energy and direction. Due to the probabilistic nature of defect production at low

Figure 2

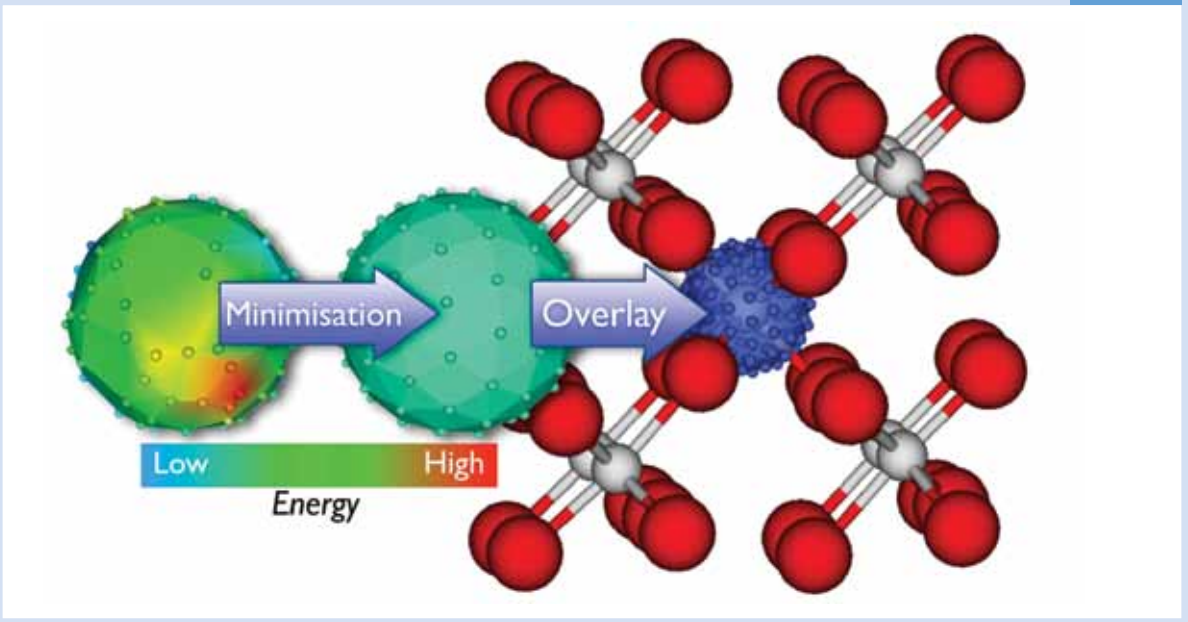

The generation of directions of initial impact from solutions to 'The Thomson Problem'. Firstly the points are randomly distributed on the surface of the sphere. After assigning a repulsive potential to each point, the configuration is minimized to produce a uniform distribution. The sphere is then centred on an atom (as shown for a Ti atom in the rutile lattice) so that each point creates a vector of initial impact.

energies, a very high level of statistics is required to enable an accurate extrapolation of E_d [2,3].

The methodology we have developed not only meets the above criterion but does so in a generalised and transferable manner. This allows us to seamlessly change the material under investigation and generate readily comparable results.

New solutions to an old problem

The main feature of our methodology that enables transferability is the automated generation of directions of initial impact. This allows any crystal type to be the subject of investigation, regardless of the complexity of the structure. To achieve this, inspiration was drawn from a problem of historical significance, namely "*The Thomson Problem*".

In 1904, J.J. Thomson outlined the problem of uniformly distributing points on the surface of a sphere whilst attempting to determine the arrangement of point charges in the atom [4]. Since then the problem has become a significant area of research, applicable to a multitude of real-world problems from the structure of fullerenes to the morphology of viruses.

Importantly, solutions to the Thomson Problem can be employed as a method of sampling directions of initial impact. This is shown in Fig. 2, where 100 points are uniformly distributed on the surface of a sphere and then superimposed on top of an atom providing vectors of initial velocity.

Taking a look at TiO_2

The three common polymorphs of TiO_2: rutile, brookite and anatase, provide ideal candidates to test our new methodology, allowing us to study the effect of crystal structure on initial defect formation. Furthermore, rutile TiO_2 is a constituent phase in Synroc, the wasteform developed by ANSTO for the immobilisation of radioactive waste. Experiments by ANSTO researchers have shown surprising differences between the polymorphs, with rutile being highly radiation tolerant, while anatase was easily amorphised [5]. This important result provides a solid foundation for comparison to our simulations.

Our study into the TiO_2 polymorphs involved over a quarter of a million MD simulations, with Fig. 3 demonstrating the importance of good statistical sampling. Displacement events along a single direction (Fig. 3a) suffer large uncertainties due to the chaotic nature of the collision process. However, the problem is eliminated (see Fig. 3b) when the directions are sampled using solutions to the Thomson Problem.

Another benefit from achieving a high level of statistics is the capability to carry out detailed analysis. A prime example of this is shown in Fig. 4, which shows a comprehensive categorisation of the residual defect clusters created from simulations in rutile. The calculated defect proportions give quantitative support to an observation common to all polymorphs, that significantly more isolated oxygen point defects are created than titanium point defects. This relates to the ease at which displacements occur on the oxygen sublattice resulting in long-range replacement chains.

Figure 3

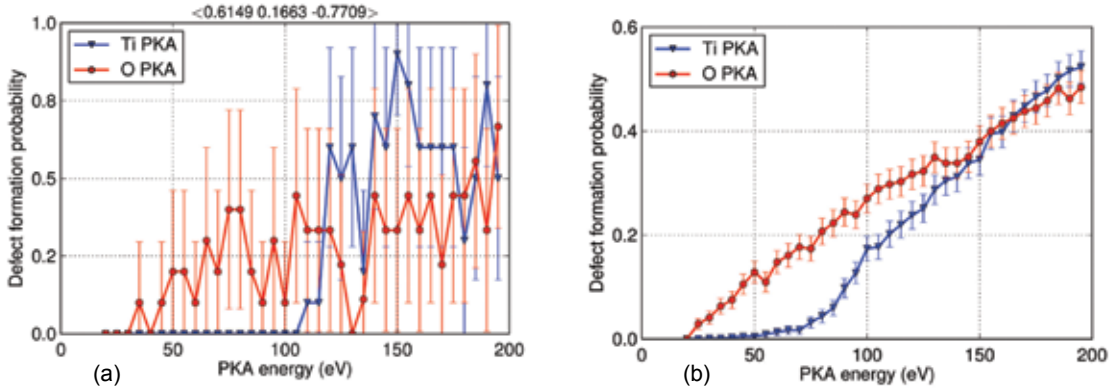

Defect formation probability as a function of energy of the impacted atom here referred to as the PKA (primary knock-on atom). (a) Sampling a single impact direction. (b) Sampling 100 directions uniformly distributed on the surface of a sphere.

Figure 4

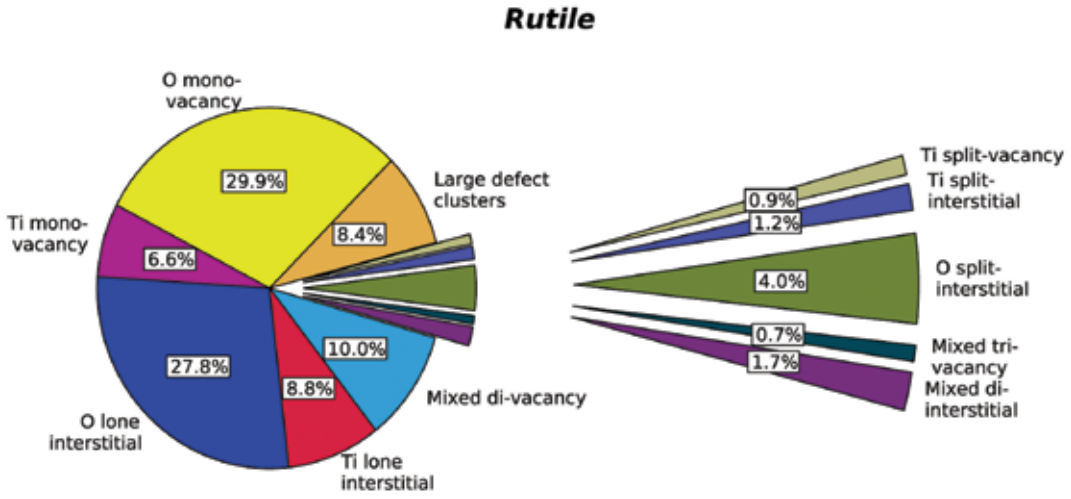

Residual defect clusters in rutile. Note the large proportion of isolated oxygen vacancies and interstitials, a result of long chains of atomic replacements on the oxygen sublattice.

Future directions

The methodology we have developed is applicable to any crystal structure, enabling a quantitative approach to investigating radiation damage. In future studies, we will employ this approach to study complex materials such as pyrochlores to aid the understanding and design of prospective nuclear materials.

The present work also forms the foundation for further studies into the dynamics of defect recombination over longer time scales. Working in conjunction with Los Alamos National Laboratory, we aim to build the complete picture of the atomic-level response to radiation damage.

References

[1] J. F. Ziegler, M. D. Ziegler, and J. P. Biersack, Nuclear Instruments and Methods in Physics Research Section B: Beam Interactions with Materials and Atoms 268, 1818-1823 (2010).

[2] K. Nordlund, J. Wallenius, and L. Malerba, Nuclear Instruments and Methods in Physics Research Section B: Beam Interactions with Materials and Atoms 246, 322-332 (2006).

[3] L Malerba, JM Perlado, A. Sánchez-Rubio, I. Pastor, L. Colombo, and T. Diaz de la Rubia, Journal of Nuclear Materials 283, 794–798 (2000).

[4] J. J. Thomson, Philosophical Magazine Series 6 7, 237-265 (1904).

[5] G. R. Lumpkin, K. L. Smith, M. G. Blackford, B. S. Thomas, K. R. Whittle, N. A. Marks, and J. Z. Zaluzec, Physical Review B 77, 1-9 (2008).

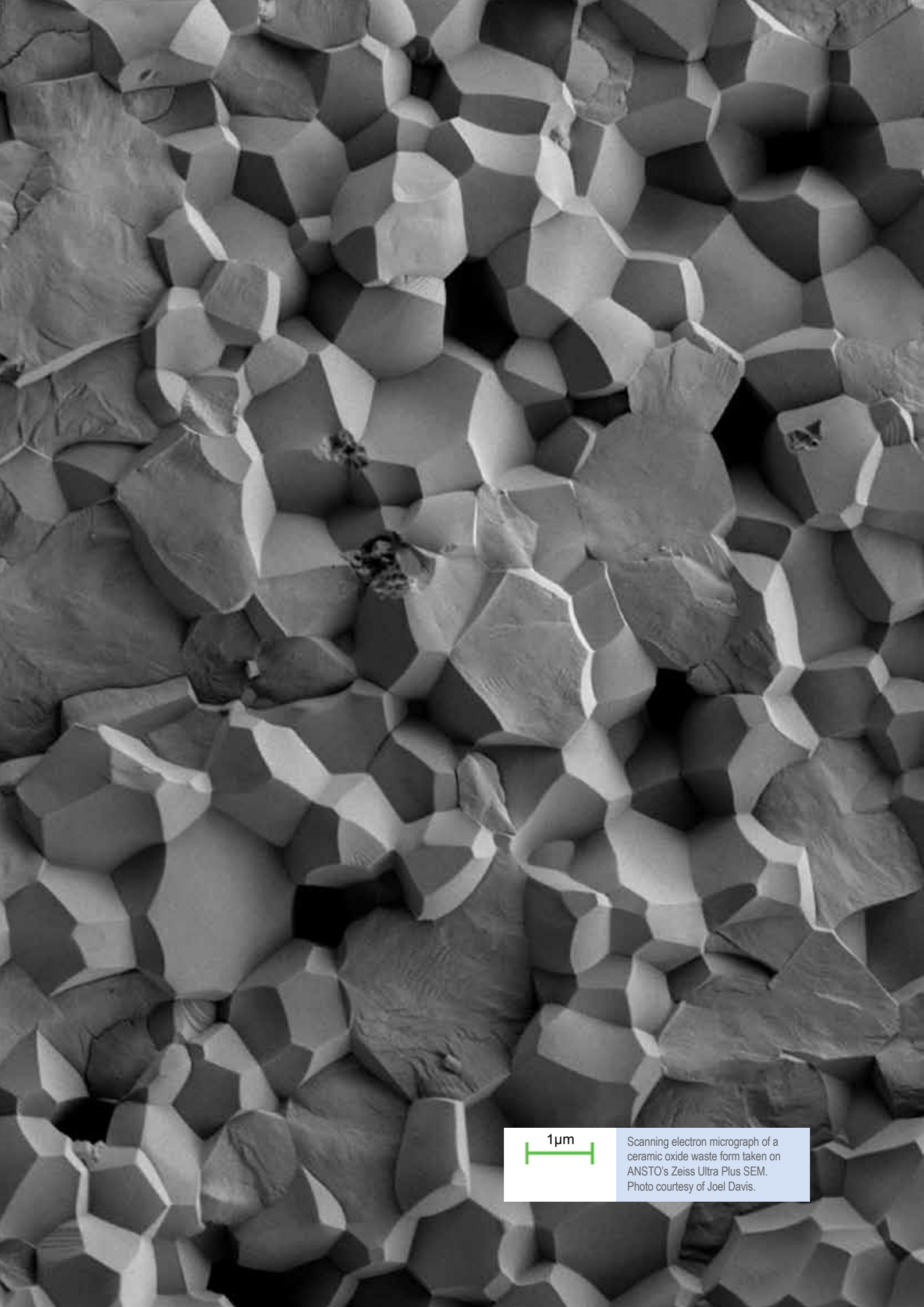

Scanning electron micrograph of a ceramic oxide waste form taken on ANSTO's Zeiss Ultra Plus SEM. Photo courtesy of Joel Davis.

Advanced nuclear waste forms

Daniel Gregg, Yingjie Zhang, Zhaoming Zhang, Inna Karatchevtseva, Linggen Kong, Mark Blackford, Gerry Triani, Karl Whittle, Gregory Lumpkin, Eric Vance.
ANSTO

Since the 1980s, ANSTO has been a world leader in nuclear waste form research and is now extending its waste form activities into developing nuclear materials for the next generation of reactor technologies. This includes developing materials for advanced nuclear waste forms, and inert-matrix targets for actinide burning.

Such materials have the potential to address the worldwide growing stockpiles of plutonium and minor actinides, and to provide long-term nuclear waste management solutions. A key scientific focus is to acquire fundamental knowledge on the crystal chemistry of actinides within suitable materials and to provide an understanding of how the materials behave during the extreme conditions of the advanced fuel cycle.

This research covers current strategies to fabricate and characterise these systems as well as future research directions, and demonstrates the viability of the studied material as a waste form and host for actinides.

Nuclear energy with waste minimisation

To prepare for future generation nuclear systems (so-called Gen IV reactors) and a 'closed fuel cycle', it is necessary to provide long-term waste management solutions and address the growing stockpile of plutonium and minor actinides (neptunium, americium and curium) contained in spent nuclear fuel. Most of the longer term radioactive hazard from irradiated nuclear fuel originates from these four chemical elements (the actinides, see Fig. 1), as well as some long-lived fission products such as iodine and technetium [1]. At ANSTO, we are developing materials which can encapsulate the actinides for use in two different and complementary waste management concepts, (1) conditioning and (2) transmutation:

1. **Advanced nuclear waste forms (conditioning)**

Actinides are incorporated into the lattice of specific crystalline solids which have high radiation resistance and aqueous durability. These 'waste forms' can then be sent to a geological repository for long-term storage.

2. **Inert matrix and transmutation targets (transmutation)**

Partitioning and transmutation of the actinides potentially reduces the burden on a geological repository. The actinides are removed from the waste (partitioned) and fissioned in a reactor (transmutation). For example, plutonium-239 (half-life of 24,000 years) is transmuted to various fission products, the vast majority of which have significantly shorter half-lives. This concept not only utilses resources (plutonium is an essential energy resource) but also provides enhanced resistance to proliferation. Importantly, this approach would potentially reduce average high-level nuclear waste lifetimes from tens of millennia to a few centuries. Candidate materials to encapsulate the actinides for transmutation will be required to fulfil a range of criteria including radiation tolerance and desirable thermophysical properties. Not only will these materials experience high radiation fields in the reactor, but also extremely high temperatures.

Here we report our investigations into the incorporation of actinides within one such promising candidate material which has use in both the conditioning and transmutation concepts.

Radiation tolerance in crystalline solids

Material choice draws on computer models and in-house experiments. Element choice is closely tied to the on-going separation research program, resulting in a combined approach to actinide separation and waste form or transmutation target design. This has pointed to zirconia-based compounds which are considered suitable for both the transmutation and conditioning

Figure 1

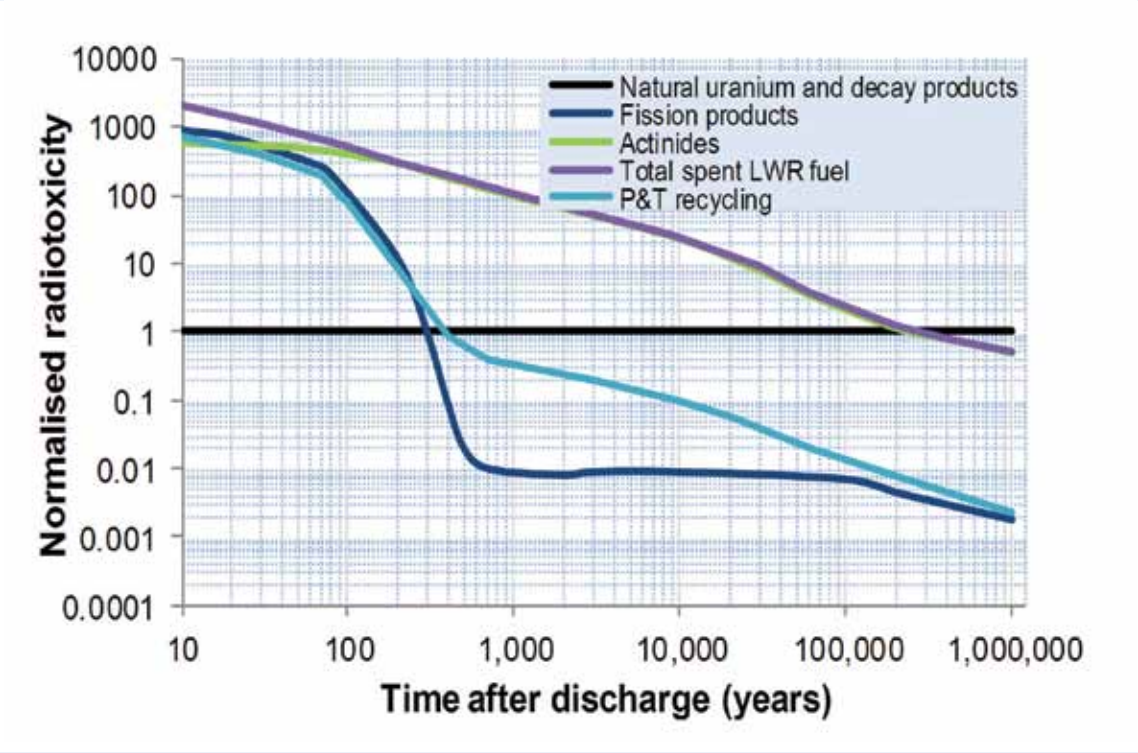

Ingestion radiotoxicity for typical spent UOX fuel (total radiotoxicity is broken up into fission products and actinides) and for the same spent fuel following P&T recycling with 99.9% removal of actinides from the waste stream. Values are normalised to natural uranium ore and its decay products [1].

strategies. Ordered derivatives of cubic zirconia are the pyrochlore-structured zirconates, $Ln_2Zr_2O_7$ (Ln = lanthanides from La to Gd) and members of this family have been found to have remarkable resistance to amorphisation under ion-beam irradiation [2]. The cationic and anionic ordering within the pyrochlore crystal structure is an extremely important variable and has been linked to this significant radiation tolerance [3]. The ordering can also be affected by actinide-doping, with the oxidation state of the actinide primarily determining its location within the structure. Therefore it is important to study the effect of actinide doping on the ordering in the crystal structure and to determine the actinide location and oxidation state within the pyrochlore matrix.

Incorporating actinides into the crystal structure

Uranium- and plutonium-incorporated samples are prepared in designated facilities within ANSTO's Institute of Materials Engineering. Small samples (~1 g) are prepared and are sectioned for various characterisation techniques. X-ray diffractometry and scanning electron microscopy are used to determine the phase composition, sample purity and microstructure. The porous nature of the samples is clearly visible in the scanning electron microscope images (Fig. 2(a) and (b)), however high density is an essential requirement for application as transmutation targets and durable waste forms. This has formed the catalyst for the group to develop a novel, simple, low-temperature chemical synthetic route for the preparation of dense, homogeneous zirconate ceramics. The method allows intimate mixing in the aqueous phase at ambient temperature and produces zirconate pyrochlores with high density. Fig. 2(c) illustrates our extremely successful processing result.

The actinide oxidation state in each sample can be determined using a combination of diffuse reflectance and X-ray absorption near edge structure (XANES) spectroscopies. See Fig. 3 for typical XANES spectra (carried out on the Australian Synchrotron) for two such uranium-doped matrices sintered in air. We found that all the air-sintered samples were consistent with a U^{6+} oxidation state, whilst those sintered in argon or H_2/N_2 atmospheres revealed mixed U^{5+}/U^{6+} oxidation states. Interestingly, this occurred even when Ca^{2+} was added to try to charge balance for U^{4+}.

There are two cationic crystallographic sites in the pyrochlore structure and the actinide element can potentially be accommodated on either. Clues provided from oxidation-state information along with refinement of high-resolution X-ray diffraction data can be used to

Figure 2

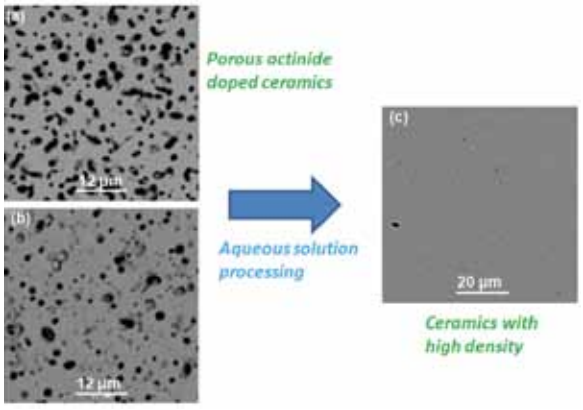

Backscattered scanning electron micrographs of (a) uranium-doped and (b) plutonium-doped pyrochlore ceramic matrices after sintering at 1400°C. The dark areas are pores. Micrograph (c) shows the increased density achieved for a sample formed using our novel chemical synthesis approach after sintering at a similar temperature.

Figure 3

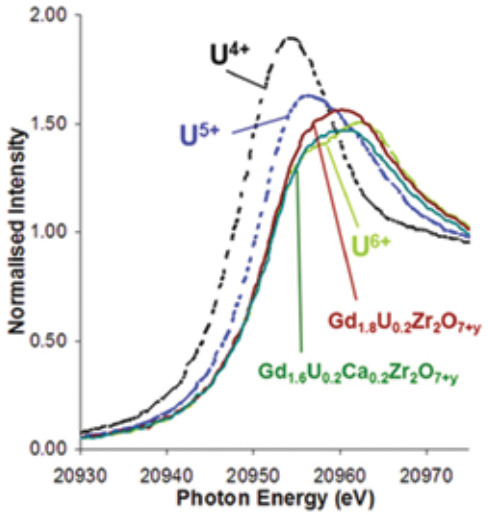

Normalised uranium (U) L_2-edge XANES spectra of two uranium-doped samples sintered in air indicating a U^{6+} oxidation state. U^{4+}, U^{5+} and U^{6+} standards are included for reference.

determine the location of the actinide within the matrix structure, i.e. on which cationic site does the actinide sit? Transmission electron microscopy can then provide specific information on the cationic/anionic ordering in the structure following actinide doping, as shown in Fig. 4.

Where to from here?

Considering the ability of the pyrochlore-structure phase to accommodate uranium and plutonium, zirconate pyrochlores are promising host matrices for use as actinide transmutation targets and specialised nuclear waste forms. In future work we plan to investigate the radiation tolerance of this system through the synthesis and characterisation of ^{238}Pu-doped samples. The long-term effects of α-decay events can be simulated by incorporating short-lived actinides, such as ^{238}Pu (half-life of 87.7 years) [4]. This provides information on the radiation tolerance to α-decay events at accelerated dose rates in laboratory time scales (~2 years) and will place ANSTO amongst a handful of organisations worldwide that can undertake this type of research.

Figure 4

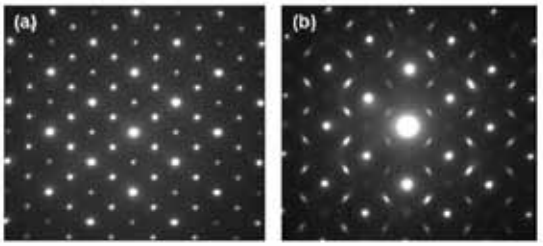

Selected area diffraction patterns of two actinide-doped zirconate pyrochlores, viewing down the [110] zone axis. (a) shows sharp spots characteristic of the ordered pyrochlore, while (b) shows diffuse scattering indicating incommensurate ordering within the structure.

References

[1] "Potential Benefits and Impacts of Advanced Nuclear Fuel Cycles with Actinide Partitioning and Transmutation", 2011 Nuclear Energy Agency report available online at: http://www.oecd-nea.org/science/reports/2011/6894-benefits-impacts-advanced-fuel.pdf.

[2] Ewing, R. C.; Weber, W. J.; Lian, J. J. Appl. Phys. 2004, 95, 5949.

[3] Zhang, J.; Lian, J.; Zhang, F.; Wang, J.; Fuentes, A. F.; Ewing, R. C. J. Phys. Chem. C 2010, 114, 11810.

[4] Weber, W. J.; Ewing, R. C.; Catlow, C. R. A.; Diaz de La Rubia, T.; Hobbs, L. W.; Kinoshita, C.; Matzke, Hj.; Motta, A. T.; Nastasi, M.; Salje, E. H. K.; Vance, E. R.; Zinkle, S. J. J. Mater. Res. 1998, 13, 1434.

Materials engineering

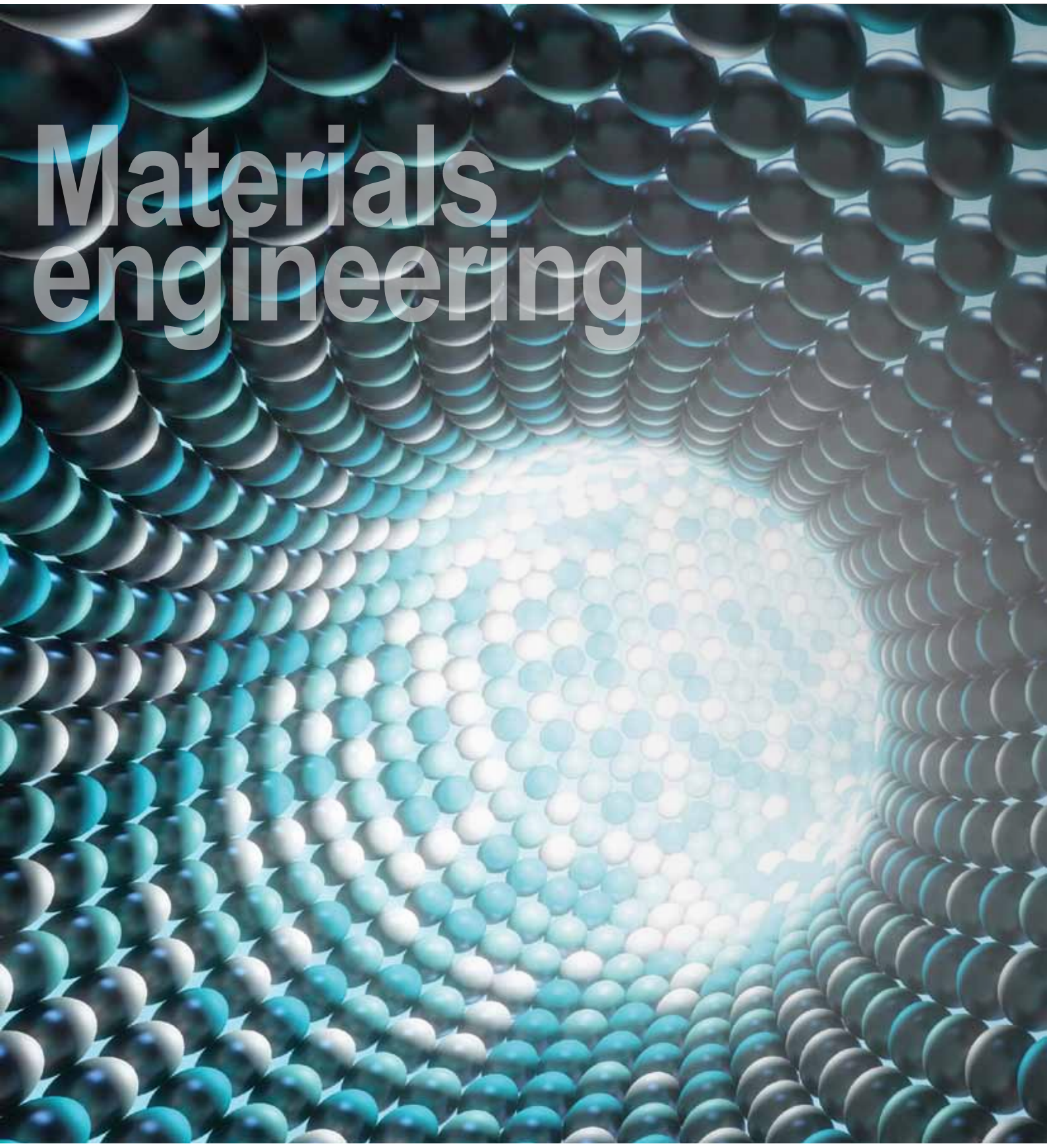

Materials engineering

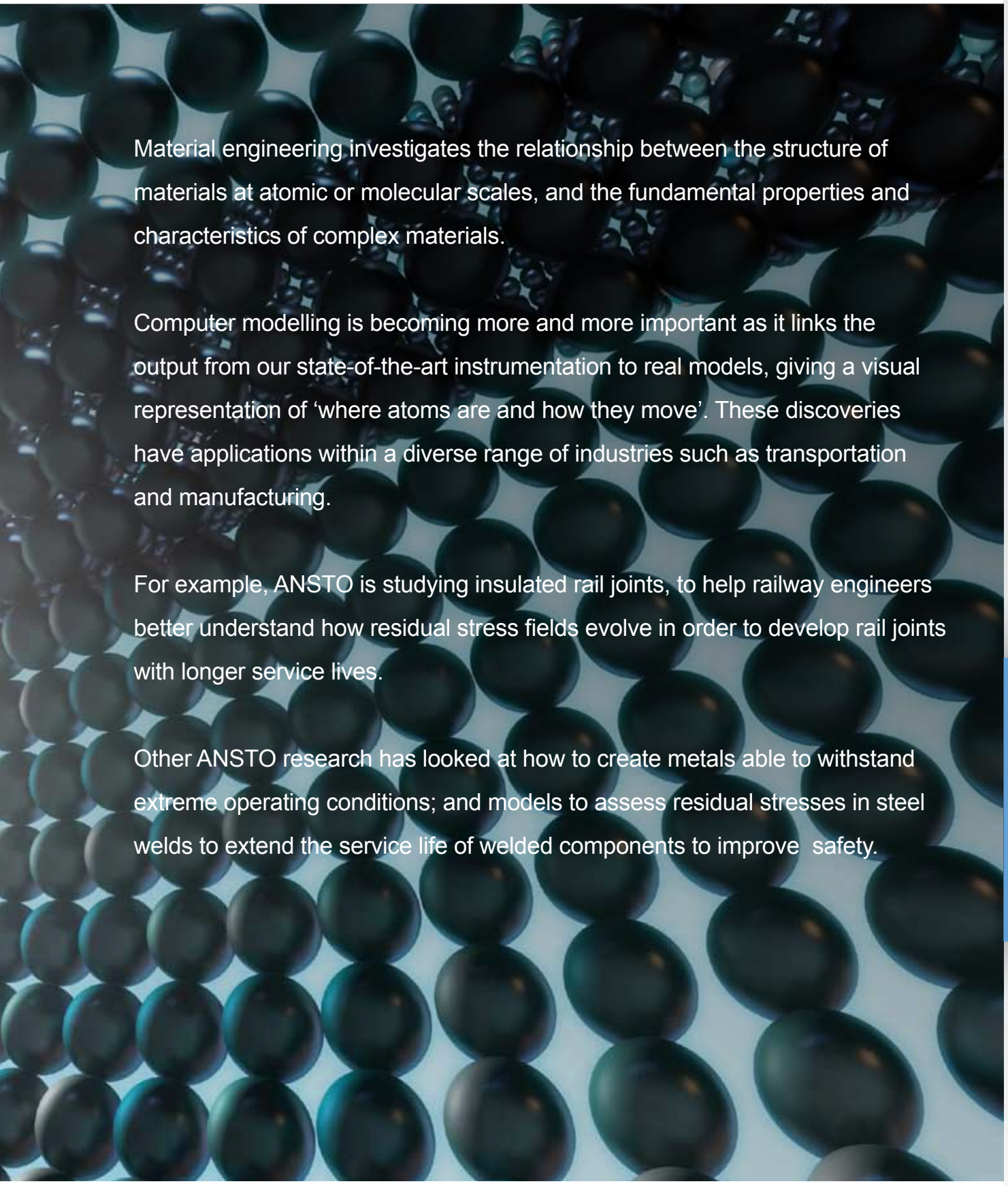

Material engineering investigates the relationship between the structure of materials at atomic or molecular scales, and the fundamental properties and characteristics of complex materials.

Computer modelling is becoming more and more important as it links the output from our state-of-the-art instrumentation to real models, giving a visual representation of ‘where atoms are and how they move’. These discoveries have applications within a diverse range of industries such as transportation and manufacturing.

For example, ANSTO is studying insulated rail joints, to help railway engineers better understand how residual stress fields evolve in order to develop rail joints with longer service lives.

Other ANSTO research has looked at how to create metals able to withstand extreme operating conditions; and models to assess residual stresses in steel welds to extend the service life of welded components to improve safety.

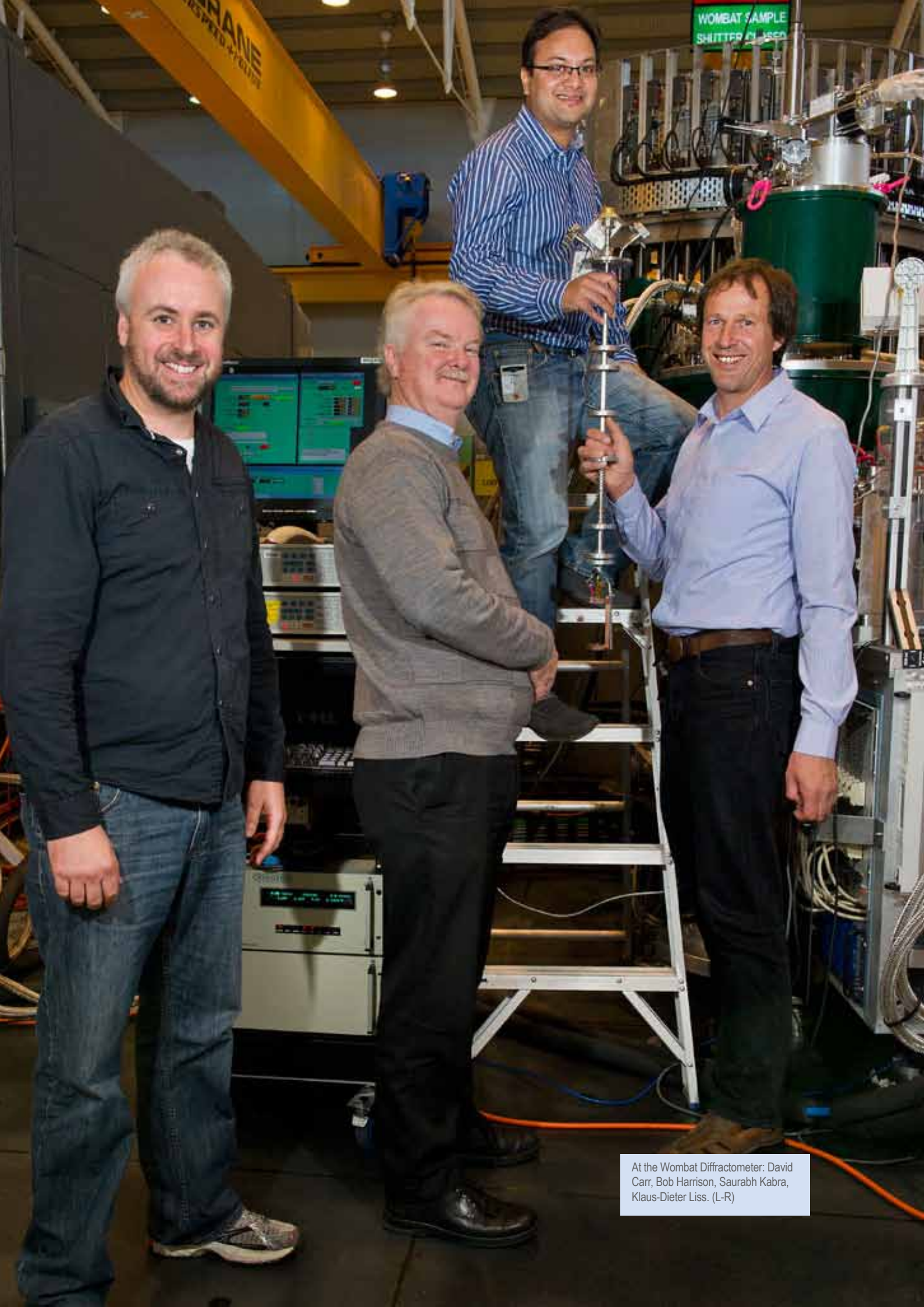

At the Wombat Diffractometer: David Carr, Bob Harrison, Saurabh Kabra, Klaus-Dieter Liss. (L-R)

Viewing metals' evolution at high temperature

Klaus-Dieter Liss[1], Kun Yan[1,2], Saurabh Kabra[1], Lisa Thoennessen[1,2], David G. Carr[1], Robert P. Harrison[1], Rian Dippenaar[2]
[1]ANSTO, [2]University of Wollongong

The performance of metals under extreme operating conditions, such as high temperature, pressure, shock and mechanical load, is strongly linked to their microscopic structure. Modern research aims to make materials withstand even tougher conditions. While conventional metallurgical analysis uses quench-arrest (rapid cooling) techniques to study microstructural evolution, neutron and synchrotron X-ray facilities allow the study of those as well as the response of a material to mechanical deformation *in situ* and in real time. This tremendously advances the field, as many deformation mechanisms occurring at the atomic scale cannot be observed in other ways. One example relates to changes that occur in a zirconium alloy at high temperatures.

Why research on metals

Since the Bronze Age humans have melted and processed metals to manufacture advanced products for the most diverse applications in our daily life, with demanding mechanical strength, ductility, durability and ease of use. Examples of materials that have been developed to be used under these extreme conditions are high-strength steels to produce thinner, and therefore lighter automotive parts in addition to improved shock-absorbing capacity upon impact; high-strength, light-weight alloys for the aerospace industry to reduce fuel costs; high-temperature materials for more effective turbine performance; radiation-resistant materials for applications in the nuclear industry; materials possessing bio-compatibility in addition to complying with mechanical demands for medical implants; and micro-mechanical components for mechatronic devices.

Influence of microstructure on mechanical properties

Most metals comprise crystallite grains, which form the building blocks of a useful piece of material. These crystallites can be arranged in a multitude of ways and the same or multiple phases can be moulded and shaped by a variety of mechanical deformation processes. The atomic mechanisms by which plastic deformation can occur are slip, twinning, vacancy diffusion, grain boundary sliding and stress-induced phase transformations. Resistance to plastic deformation can be enhanced by invoking distortions into the crystal structure and creating barriers to lattice dislocation motion. Examples are solute elements, precipitates, grain boundaries, dislocation structures, and phase boundaries which must be circumvented in order to cause permanent deformation.

Microstructure evolution through heat treatment

Thermo-mechanical processing influences the microstructure of metals, and heat treatment at elevated temperature can, for example, create precipitates making the material stronger. On the other hand, heat treatment of already deformed material might lead to recovery, recrystallisation and grain growth, which softens the material – a problem often encountered upon welding and joining. In order to assess the impact of deformation and heat treatment on the resulting mechanical properties of a material, one must fully understand the underpinning fundamental physical mechanisms such as dislocation movement, phase transformations that might occur, diffusional processes and the response of the material to local stress concentrations.

In situ neutron diffraction

In our present studies, we analyse the thermo-physical behaviour of metallic materials by the use of *in situ* neutron diffraction techniques. These techniques allow us to probe in real time the evolution and changes in microstructure, which are then correlated with complementary characterisation methods in order to better understand the fundamental driving forces for the material behaviour. Most of the *in situ* data, recorded while the material was heated, held at temperature and cooled, was acquired using the high-intensity diffractometer Wombat [1] at the OPAL facility at ANSTO. In addition high-resolution scans at pre-selected holding temperatures were obtained using the Echidna diffractometer [2].

Figure 1

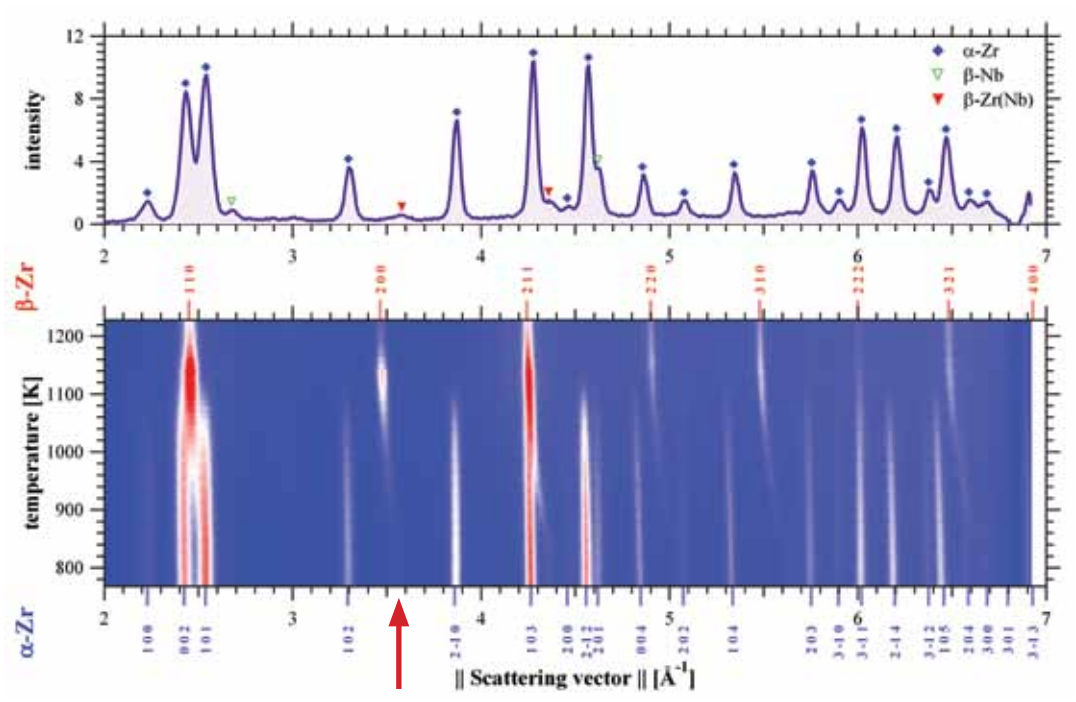

Diffraction pattern of Zr-2.5Nb at room temperature (top) and its temperature evolution (bottom) with intensities coded in color levels.

Materials that have been studied by these techniques include zirconium alloys used in the nuclear industry; titanium alloys for use in bio-medical applications, as well as in high-strength, light-weight applications in the aerospace industry; titanium-aluminium intermetallics for use in high-temperature turbines in aerospace engines [3]; and high-strength steels designed to reduce mass and increase safety in the transportation industry [4]. A common theme in these investigations is the attempt to better understand how enhanced mechanical properties can be obtained by alloying, heat treatment and thermo-mechanical processing. In addition, we have studied the way in which both diffusive and displacive phase-transformations play a role in the development of microstructrue.

Example: neutron diffraction of a zirconium alloy [5]

In thermodynamic equilibrium, the important nuclear reactor material, Zr-2.5Nb (mass %) consists of an α-Zr-rich phase with a hexagonal close-packed structure and a β-Nb-rich phase with a body-centered cubic structure at room temperature. This two-phase material has been widely researched with respect to microstructural characterisation following a variety of, high-temperature deformation and variant selection during phase transformation. However, the underlying crystalline properties, e.g. the lattice parameters and thermal expansion of the different phases during the phase transformations, have not been determined *in situ* and in real time. Using a vacuum furnace on Wombat, we recorded for the first time, the crystalline properties of Zr-2.5Nb during the α-β phase transformation.

Fig. 1 shows a stacked sequence of individual diffraction patterns with temperatures on the vertical axis, and intensity indicated by colour. The fraction of the β-Zr(Nb) phase starts to increase above the eutectoid temperature of T_{eu} = 883 K, i.e. the lowest temperature and specific concentration, at which the system undergoes the transformation, while the α-Zr vanishes totally at T_{β} = 1133 K; in accordance with the phase diagram. Apart from the structures, the effect of the alloying element Nb on this phase transformation process has been investigated. The arrow in Fig. 1 locates the 200 peak of retained β-Zr(Nb). During the phase transformation the β-Zr(Nb) peak shifts to the position of the expected β-solid solution peak.

The strong changes in lattice parameter testify to variations in the Nb concentration of the β-Zr(Nb) phase during the α−β transformation.

We can evaluate the change in lattice parameter by a combination of Vegard's law (the linear variation of lattice parameter with concentration) and thermal expansion, Fig. 2, to obtain the Nb concentration in the β-Zr(Nb) phase, which is superimposed as a trace on the phase diagram in Fig. 3. Initially, the β-Zr(Nb) phase contains 28% Nb, but as atomic diffusion becomes

Figure 2

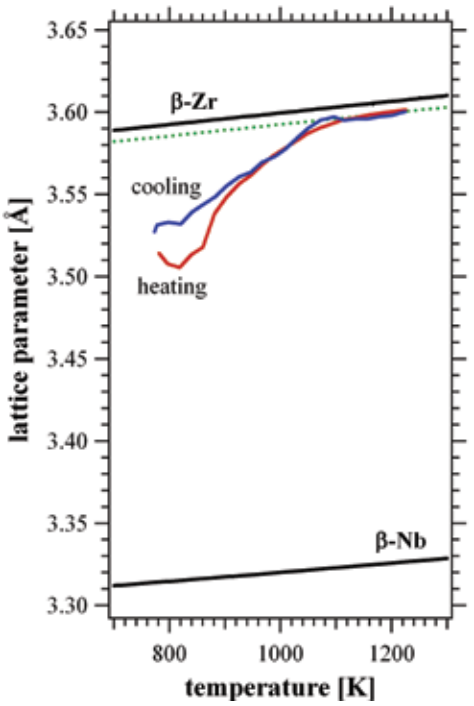

Lattice parameters for the pure element β-phases as a function of temperature, including the experimental data of the β-Zr(Nb) alloy upon heating and cooling. The dotted line would correspond to a homogeneous solid solution of Zr-2.5Nb.

Figure 3

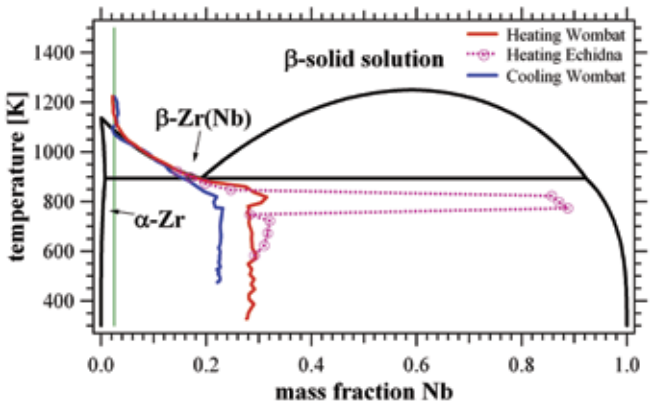

Nb concentration of β-Zr(Nb) phase during heating and cooling with the rate of 2 K/min. The black line is the accepted Zr-Nb phase diagram; the red line represents the continuous heating process; the blue line represents the continuous cooling process while the dotted pink line is obtained by data acquired during 60 min temperature holding steps.

more important during heating, Nb segregates up to 90% on 60 min holding steps. It then dilutes again to meet the eutectoid point at 18.5% and T_{eu}, following from there on the β-transus line and eventually reaching the composition of the solid solution. The path reverses upon cooling and the concentration is quenched, in this case at 23% for the applied cooling rate. Since composition influences the microstructure, such knowledge of the kinetics is extremely important for the establishment and prediction of heat treatment in a manufacturing or welding process. Desired concentrations can be fine-tuned and the operating temperatures for a work piece can be defined in a more accurate way.

Conclusion

Neutron diffraction studies not only provide quantitative phase analysis, but are also a method of analysing the migration of alloying elements and their kinetics during phase transformations *in situ* and in real time. Evolution of lattice-parameter changes elucidate the variation of atomic concentrations during the phase transformation, which are dramatic during the eutectoid reaction in the Zr-2.5Nb system. Through analysis of the diffracted intensity and peak positions of different phases, a complementary image of the phase transformation process can be produced during heat treatment. The significance of this study is to disclose the transient behaviour relevant to the phase transformations in a Zr-2.5%Nb alloy. Detailed knowledge of phase diagrams is vital for any materials studies. Here, we have clearly recorded the decomposition behaviour in a fast, uncomplicated and concise way; this cannot be achieved by conventional studies which are usually obtained from *ex-situ* X-ray diffraction or dilatometric tests. This approach benefits investigations of a multitude of multi-phase materials, and is not just limited to metals.

References

[1] A.J. Studer, M.E. Hagen, T.J. Noakes, Physica B: Condensed Matter 2006, 385-386, 1013.

[2] K.-D. Liss, B. Hunter, M. Hagen, T. Noakes, S. Kennedy: "Echidna—the new high-resolution powder diffractometer being built at OPAL", Physica B: condensed matters 385-386/part 2 (2006), p. 1001-1002. Doi/10.1016/j.physb.2006.05.322.

[3] Saurabh Kabra, Kun Yan, Svea Mayer, Thomas Schmoelzer, Mark Reid, Rian Dippenaar, Helmut Clemens, Klaus-Dieter Liss: "Phase transition and ordering behavior of ternary Ti–Al–Mo alloys using *in situ* neutron diffraction", International Journal of Materials Research 102/6 (2011), p. 697- 702, doi/10.3139/146.110528.

[4] K. Yan, D.G. Carr, M.D. Callaghan, K-D. Liss, H. Li: "Deformation mechanisms of twinning induced plasticity steels: *In situ* synchrotron characterization and modeling", Scripta Materialia 62/5 (2010), p. 246-249. doi/10.1016/j.scriptamat.2009.11.008.

[5] Kun Yan, David G. Carr, Saurabh Kabra, Mark Reid, Andrew Studer, Robert P. Harrison, Rian Dippenaar, Klaus-Dieter Liss: "*In situ* Characterization of Lattice Structure Evolution during Phase Transformation of Zr-2.5Nb", Advanced Engineering Materials, 13/9 (2011), p. 882-886 (+ Back Cover Page). doi/10.1002/adem.201000350 + doi/10.1002/adem.201190023.

ANSTO's research into welding is helping industry develop welding processes the will extend the service life and safety of welded components.

Simulating phase transformations during the welding of ferritic steels

Cory Hamelin, Ondrej Muránsky, Philip Bendeich, Lyndon Edwards
ANSTO

Numerical analysis of welded structures is becoming more commonly accepted in the field of engineering safety. This brings new challenges, such as assessing residual stresses in ferritic (iron) steel welds, which are complex due to the structural changes that occur during welding. The following research highlights a solid state phase transformation model that has been developed to predict these structural changes.

Ultimately, this weld model may be used to optimise the welding process used for ferritic steels, which may help extend the service life of welded components.

The numerical analysis of welded structures

The study of welds – most importantly, the residual stresses induced during welding – is receiving greater attention within a wide range of engineering fields. In general, residual stresses are confined internal stresses that exist in a structural component in the absence of external loading or thermal gradient. Weld-induced residual stresses are a particular concern in safety-critical components and assemblies, since these stresses may lead to the premature failure of a given system. One of the most common failure methods is the creation and propagation of cracks that develop in or near welds; the problem of premature cracking is exacerbated by the presence of a severe thermal or corrosive environment. For this reason, the effects of welds are considered when performing remaining-life assessments and safety inspection schedules for the power generation industry, where a complex system of welded components and piping are used to produce and deliver steam to turbines. As the cost associated with extensive experimental analyses can be prohibitive, simulations via numerical analyses are employed to predict the weld-induced residual stress field in a component. These predicted stresses may then be used to study the in-service structural integrity of an object.

The importance of solid-state phase transformations

Currently, finite-element models are capable of accurately predicting the residual stress field (and the resultant distortion) in a wide variety of welds. Preliminary benchmark studies were performed in single-pass welded structures, where a weld is made by depositing filler metal during a solitary pass of the welding torch. Subsequent work has been successfully performed in multi-pass welds, where tens or hundreds of weld passes may be required to deposit the necessary amount of filler metal; these welds are more complex due to thermal cycling in the metal surrounding the weld, as the welding torch repeatedly heats the material and it then cools between each pass.

To a similar extent, the types of materials involved in a welding process display a varying level of complexity when simulating their behaviour. Most weld studies have focused on commonly used pressure vessel and piping materials, including austenitic stainless steel and nickel-based superalloys. However, austenitic steel welds are well understood, straightforward processes to model when compared to their ferritic steel counterparts (which are also frequently used for piping); the reason for this discrepancy stems from the crystal structure found in each material. As illustrated in Fig. 1, austenite possesses a face-centred cubic (fcc) lattice, whereas ferritic steel is predominantly body-centred cubic (bcc). The iron (Fe) atoms are arranged closer in a fcc steel relative to a bcc steel; should a bcc-fcc transformation of phases occur, volumetric shrinkage of the transforming material is observed. In contrast, the occurrence of an fcc-bcc transformation would result in a volumetric expansion of the transformed material. While austenitic steels are stable through a wide range of temperatures, the extreme heating and cooling encountered during welding of ferritic steels causes a phase transition in the metal (Fig. 1); from a bcc structure to an fcc structure

Figure 1

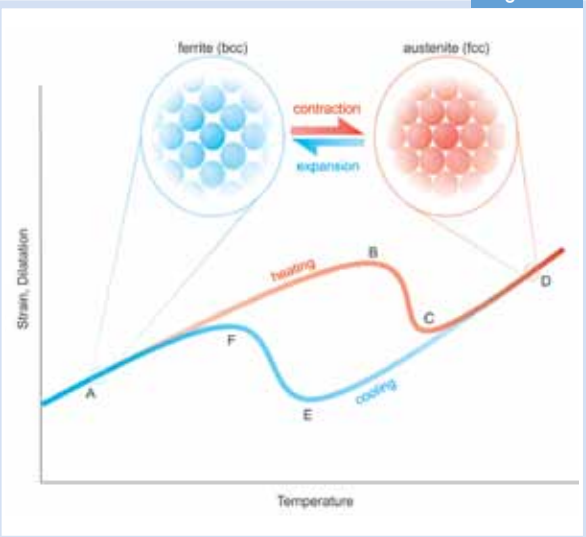

Representative thermo-mechanical cycle in ferritic steel welding processes. The weldment first undergoes heating (line A-B-C-D): as bcc ferrite is heated to point B, the metal experiences thermal expansion. Between points B and C, the crystal structure transforms from ferrite to austenite, resulting in a contraction of the metal due to the increased atomic density of fcc metal. The inverse cycle occurs upon cooling (line D-E-F-A); a variation in transformation temperatures exists (point E vs. point B) due to the rapid heating and cooling rates involved in the welding process, which delays the transformation process.

during heating/welding and an inverse transition upon cooling. The structural changes associated with these phase transformations can have a dramatic effect on the final residual stress field in a ferritic steel weldment. The transformation kinetics involved are complex and dependent on a number of variables, which is why many current numerical weld analyses use simplified approximations of the phenomena, or exclude these transformations entirely.

Developing a model

Research conducted within ANSTO's Structural Integrity group is currently focused on identifying the key material parameters required to predict solid-state phase transformation kinetics during welding of ferritic steels. The present approach employs a semi-empirical methodology developed by Kirkaldy and Venugopalan [1], whereby the chemical composition and the average grain size of the steel are the main parameters required to calibrate the model. Such an approach is advantageous because many other models require a set of experimental analyses be carried out for model calibration. The essentials of the Kirkaldy-Venugopalan model have been integrated into a user-defined subroutine for the ABAQUS finite-element package, which is the software package currently used within our Institute to predict weld-induced residual stresses [2].

Model validation

To test the accuracy of the ABAQUS subroutine, a weld model has been constructed in collaboration with the European Network on Neutron Techniques Standardisation for Structural Integrity (NeT), via a Task Group (TG5) that is concerned primarily with the analysis of ferritic steel welds. Within this task group, a series of autogenous beam welds have been laid on specimens of ferritic steel commonly used for power plant components (SA508 Gr.3 Cl.1 steel) using a conventional gas metal arc welding technique; Fig. 2 shows one of the welded samples. Two sets of samples were produced, with the primary variable being the speed at which the welding torch passes across the weldment (i.e. the torch speed). One set of samples was prepared with a torch speed of 5 mm/s, while a second set of samples was prepared using a torch speed of 1.25 mm/s. These variations in the welding torch speed have resulted in different heating and cooling rates during welding, and consequently in different steady-state microstructures observed in each sample set.

Predictions of these phase compositions have been made using an ABAQUS thermal analysis, calibrated using thermocouple data taken during the welding studies. Once an accurate thermal history is reproduced in the model, the predicted phase composition is captured. Using an approach developed by Maynier et al. [3], the phase distribution and chemical composition of the steel can be used to predict the local hardness of the heat-affected weld metal. This phase-specific hardness data can then be compared to measured microhardness data, which has been collected from the samples using a Nano Indenter G300 [4]. Fig. 3 compares the predicted hardness profiles of both sample sets to measured values. Good agreement can be seen in each study, thus validating the phase-transformation subroutine developed.

Outlook

The successful prediction of phase composition in ferritic steel welds is merely the first step of a comprehensive structural integrity analysis for safety-critical engineering components. Subsequent analyses will attempt to validate the residual stress profiles predicted with a fully coupled thermo-mechanical weld model in ABAQUS, using measurements of the NeT TG5 samples via the Kowari stress diffractometer at ANSTO [5]. Once the model has been fully validated, studies may be conducted to predict the susceptibility of such welds to cracking, and to ascertain what effect the presence of welds may have to safety inspection schedules and the remaining-life assessment of welded structures. Ultimately, these weld models may be used to optimise the welding process used for ferritic steels, in an attempt to extend the service life of welded components.

Figure 2

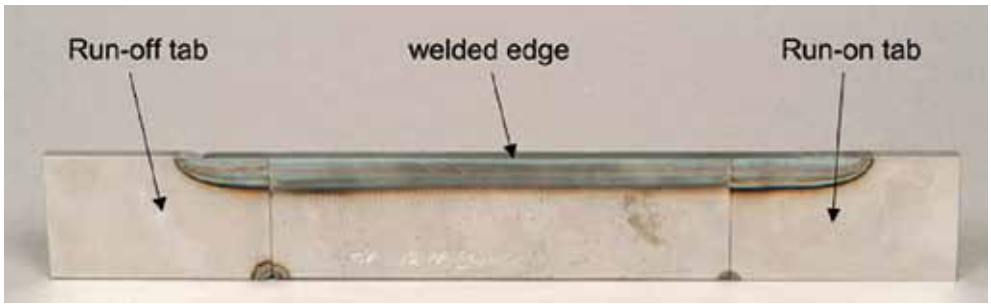

Representative TG5 sample: an autogenous beam weld in SA508 Gr.3 Cl.1 steel, with run-on and run-off tabs to ensure a uniform weld bead is laid on the specimen. Dimensions are 180 x 10 x 50 mm^3 (l x w x h).

Figure 3

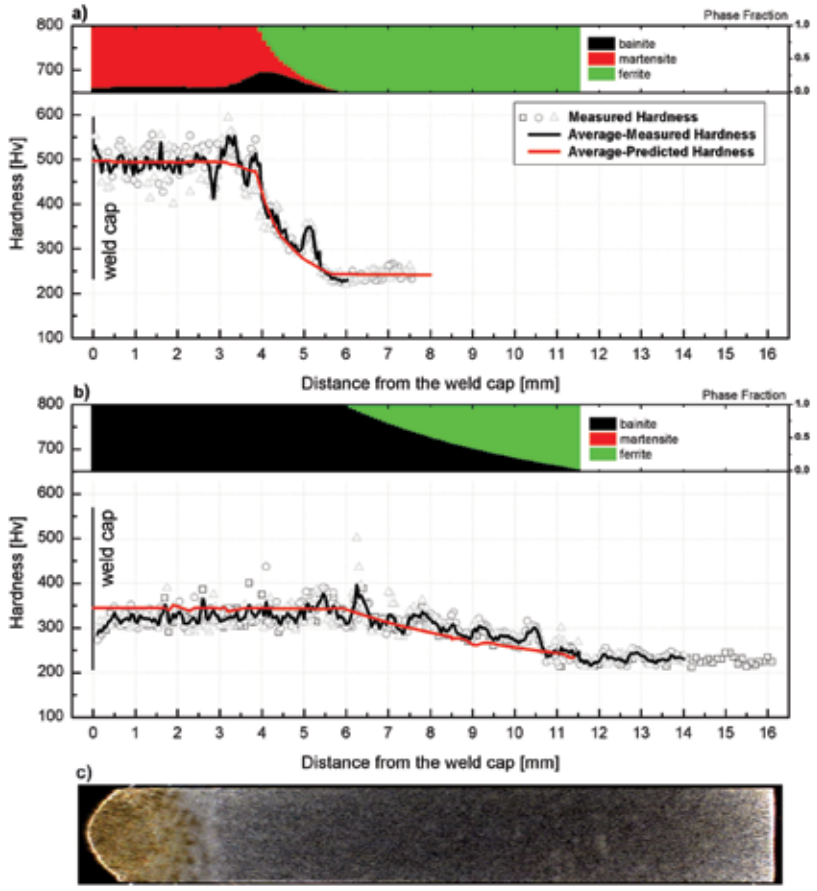

Predicted post-weld steady-state phase compositions with torch speeds of: (a) 5.00 mm/s; and (b) 1.25 mm/s. Phases are validated via hardness profiles. (c) A representative steady-state beam weld profile in SA508 steel (not to scale).

References

[1] J.S. Kirkaldy and D. Venugopalan, in: Phase Transformations in Ferrous Alloys, edited by A.R. Marder and J.I. Goldstein, TMS Publications, Warrendale PA, 125-148 (1984).

[2] O. Muránsky, C.J. Hamelin, M.C. Smith, P.J. Bendeich and L. Edwards, The effect of plasticity theory on predicted residual stress fields in numerical weld analyses, Computational Materials Science, 54, 125-134 (2012).

[3] P. Maynier, J. Dollet and P. Bastien, in: Hardenability Concepts with Applications to Steels, edited by D.V. Doane and J.S. Kirkaldy, AIME, New York, NY, 518-544 (1978).

[4] C.J. Hamelin, O. Muránsky, P.J. Bendeich, K. Short and L. Edwards, Predicting solid-state phase transformations during welding of ferritic steels, Materials Science Forum, 706-709, 1403-1408 (2012).

[5] O. Kirstein, V. Luzin, A. Brule, H. Nguyen and D. Tawfik, Kowari – OPAL's residual stress diffractometer and its application to materials science and engineering, Advanced Materials Research, 41-42, 439-444 (2008).

Understanding residual stress in insulated rail points is vital for rail maintenance and extending service lives.

An investigation of residual stresses in insulated rail joints

David Wexler[2], Chandrahas Rathod[2], Huijun Li[2], Manicka Dhanasekar[3], Vladimir Luzin[1]
[1]ANSTO, [2]University of Wollongong, [3]Queensland University of Technology, CRC for Rail Innovation

Insulated rail joints (IRJs) are an integral part of any rail track system, as they split a continuous rail track into electrically isolated sections for signalling and easy detection of rail track damage. Bonded IRJs are safety-critical components that must satisfy requirements for structural integrity as well as the isolation function for both railway signalling and track condition monitoring systems.

In heavy haul corridors in Australia and around the world, IRJs are periodically replaced due to accumulated damage in their railhead, often within 10-20% of the useful life of other rail components.

Their replacement is the single largest track maintenance cost in New South Wales, apart from track ballast work. Neutron diffraction can tell us what happens to material and residual stresses within used rails and trace down accumulation of damage caused by stresses throughout rail service history.

The study is helping railway engineers better understand how residual stress fields evolve in service and enable them to develop IRJs with longer service lives, as well as determine the most appropriate rail maintenance and replacement schedules for safe and economic operation.

Role of stress in rail damage

A number of serious incidents, including fatal derailments and train-on-train impacts, have been attributed to rail and rail-end failures resulting from rolling-contact fatigue. Most of the various mechanisms of rail failure are related to the interaction between defects and the residual stress field at and below the rail surface. Residual stresses are generated in rails first as a result of the manufacturing processes, which include hot-rolling (shaping rails from a billet), roller-straightening (final cold rolling through multiple rollers to achieve geometrical tolerance) and head-hardening (heat treatment to achieve high hardness). In service, the running surfaces of rails are subjected to repeated rolling-contact loading through interaction with train wheels, and the rail itself is subject to a variety of complex stresses and strains. Stresses are usually so high that they can cause plastic deformation around the contact surface and modify the stress field and material properties near the running line and internally in the railhead. Track fracture can result from one or more progressive defects, the propagation of which is also influenced by residual and contact stresses in the rail.

IRJs and their damage

The above mentioned effects change significantly in IRJs because they are somewhat different from continuous rail. Essentially IRJs comprise two rail ends and a narrow gap in the rail filled with insulator, and a support structure including bolted fishplates on both sides of the rails, which are electrically isolated from the track by a layer of glue and help add rigidity to the IRJ, as shown in Fig. 1. IRJs represent a different support structure to standard tracks as they endure an additional impact-forces distribution arising from the wheel-to-rail contact in special conditions of the rail gap and the rail ends. For example, failure can occur when metal flows over the insulated rail gap (typically 6-8 mm width) breaks the electrically isolated section of track and results in malfunction of the track signalling system. This can happen well before any other defects, such as cracks or surface voids, start to develop. Therefore, a significant amount of track maintenance work is dedicated to the inspection of rail ends. As a maintenance procedure the head of the rail may be ground periodically to restore the correct head profile, to remove surface cracks before they grow too big, or to move the wheel-rail contact position

Figure 1

Left: 4-bolt square ended IRJ: two rail sections are connected by means of bolted fishplates on both sides of the rail; an insulator, placed in the gap between two rail sections, forms a rail-post. Right: Metal flow in damaged end-post.

across the vicinity of the end-post in order to extend the life of the IRJs. In case of severe damage, when the rail is approaching an unsafe condition, rail sections containing IRJs are replaced. In heavy haul rail systems, IRJs' periodical replacement due to accumulated damage in their railhead may be necessary after only 2-3 years of service or within 10% of the useful life of other rail components. Apart from track ballast work, IRJ replacement represents the most significant track maintenance expense in the rail network.

Researching IRJs

A research project was initiated by the Cooperative Research Centre for Rail Innovation to address this problem and supported by industrial partners (the Australian Track and Rail Corporation, Queensland Rail) and academic institutions (University of Wollongong, Queensland University of Technology, University of Central Queensland). We use neutron diffraction to investigate the material stress accumulation at rail ends in the vicinity of the insulated gap in IRJs - this is the area of rail subjected to the most damage.

By selecting a series of samples with different service histories the investigation provided fundamental information about residual stresses accumulation, material properties evolution and how these might change during degradation of IRJs. The samples selected for this investigation are rail ends from square-ended IRJs made from the same steel type (Australian standard A1085.1 60 kg grade) and manufacturer. Rail ends from IRJs described as 'partly damaged' and 'badly damaged' will be compared with a rail end in the 'not damaged', as-manufactured, condition.

Neutron stress measurements

Neutron diffraction is particularly suited to the non-destructive mapping of complex internal stress fields within dense materials such as steel, because of the high penetration. For neutrons the penetration depth in steel is 100 times greater than that of X-rays. There are a handful of known examples of use of neutron diffraction to investigate residual stresses in rail and most of the studies have been performed on rail slices because the railhead thickness of 70 mm is still too great even for neutrons. Although stresses are partially eliminated by slicing, this approach allows stresses to be mapped much faster, more accurately and over larger areas. In our study one transverse slice and one longitudinal slice was machined out of each rail sample. They were studied in residual stress experiment with gauge volume (probing volume) of 2 x 2 x 2 mm^3, accuracy of ±30 MPa and using the iron (211) Bragg reflection.

Mapping the stress

(1) Drastic changes in residual stress state were found in the rail head of the selected samples, see Fig. 2. Compressive stress (shown as blue areas) immediately under the top surface, which is induced due to the service load from train movement, is counteracted by a wide zone of tension (red areas) that potentially can cause defect growth (Fig. 2a). The rail material also undergoes transformation as shown in Fig. 2b changing from harder steel (shown in red) to softer (shown in blue). This happens differently across railhead and evolves noticeably with the service span.

(2) The distributions of stresses close to the end-posts are different from the bulk parts because of different loading conditions and this is demonstrated in Fig. 3a. The material close to the IRJ rail end-post is more damaged then material in the continuous rail as shown in Fig. 3b by a differential stress map for the longitudinal component. Damage accumulation is mostly happening 5-10 mm beneath the surface and progresses with rail service (can be seen as enhancement of the features in Fig. 3b).

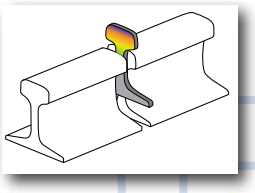

Figure 2

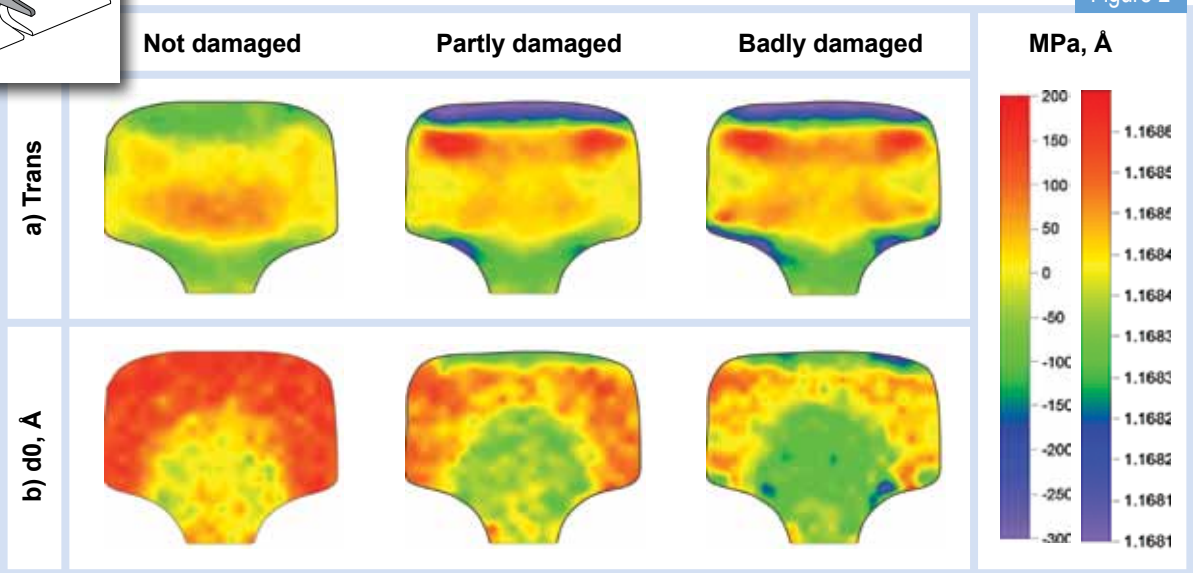

Evolution of the residual stress and material lattice parameter in rails of different service history. The railhead is 70 mm across. a) In the stress maps, the red areas represent high tensile stress while the blue areas correspond to high compressive stress. b) In the lattice parameter maps, larger d-spacing are shown in red while small d-spacing values are blue.

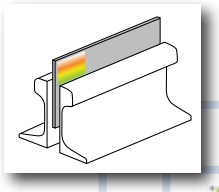

Figure 3

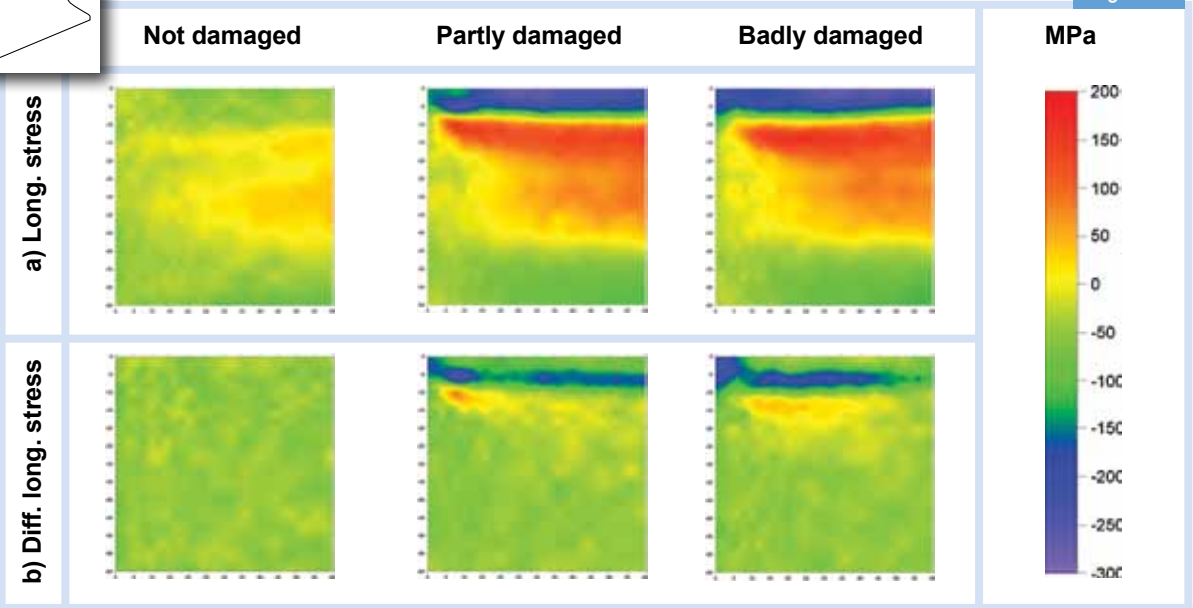

a) Evolution of the residual stress longitudinal component in rails of different service history obtained on longitudinal slices (maps top left corner corresponds to the top corner of the end-post). Patch size is 60 x 60 mm^2. b) Differential longitudinal stress component maps are obtained by subtracting stress values representing bulk material from the values representing material of IRJ.

Projected outcomes

The stress distributions determined experimentally can be used to validate finite-element simulations carried out at Queensland University of Technology to assess progressive damage accumulation in material of IRJ through elastic-plastic deformation history and residual stress evolution. Our detailed stress maps will allow us to narrow the selection of the correct material mechanical models and damage mechanisms. The combined experimental and modelling efforts will help railway engineers to better understand how residual stress fields evolve in service and enable them to develop IRJs with longer service lives, as well as to determine the most appropriate rail maintenance and replacement schedules for safe and economic operation.

New technologies for national security

New technologies for national security

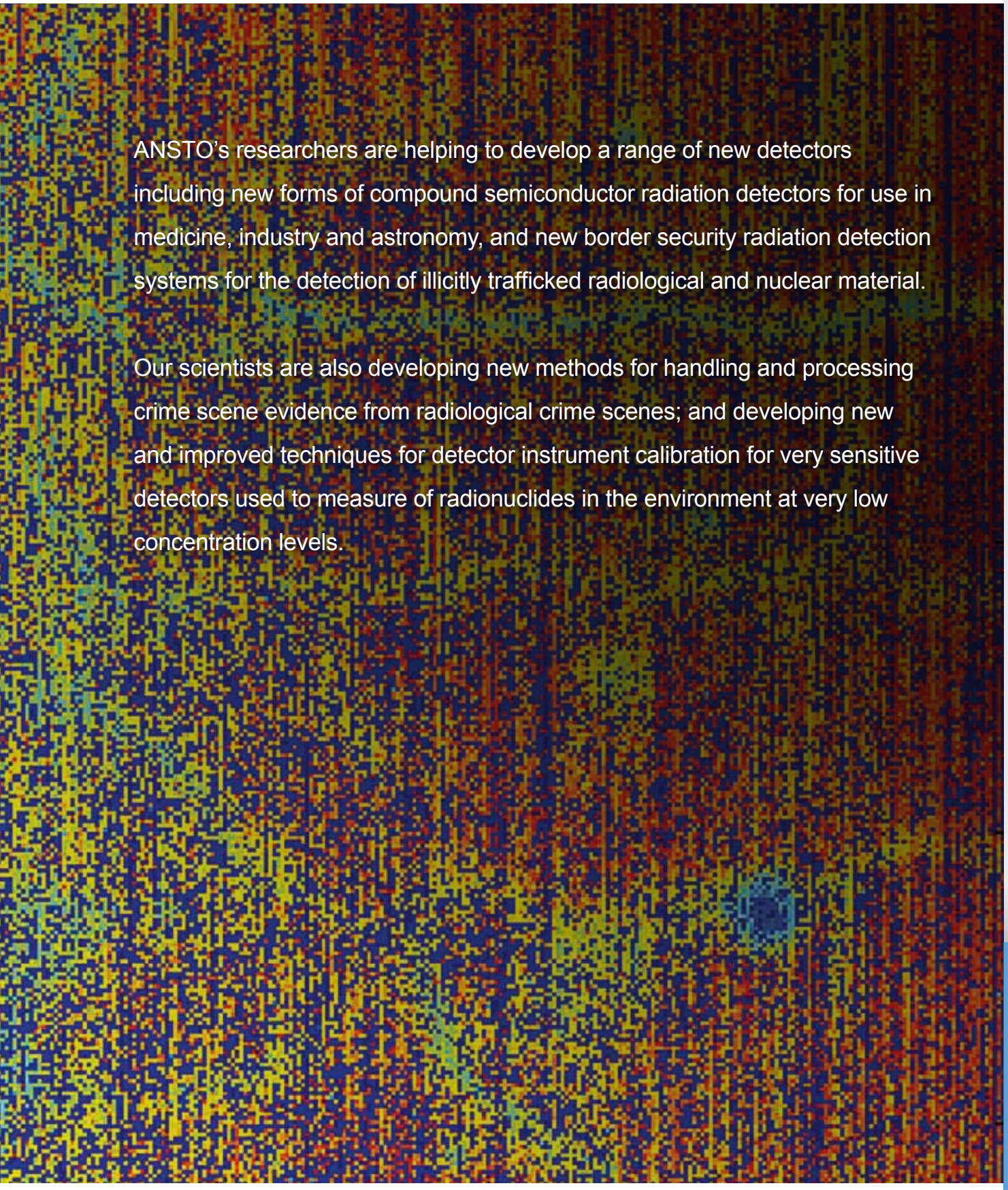

ANSTO's researchers are helping to develop a range of new detectors including new forms of compound semiconductor radiation detectors for use in medicine, industry and astronomy, and new border security radiation detection systems for the detection of illicitly trafficked radiological and nuclear material.

Our scientists are also developing new methods for handling and processing crime scene evidence from radiological crime scenes; and developing new and improved techniques for detector instrument calibration for very sensitive detectors used to measure of radionuclides in the environment at very low concentration levels.

Tegan Evans is working within the confines of a glove box to enhance a contaminated fingermark under 505 nm light.

Investigating the impact of radiation and radioactive contamination on forensic trace evidence

Tegan Evans[1], Daniel Brew[1], Kaitlyn Toole[1], Michael Colella[1], Chris Lennard[2], Claude Roux[3], Simon Walsh[4]
[1]ANSTO, [2]University of Canberra, [3]University of Technology, Sydney, [4]Australian Federal Police, Forensic and Data Centres

The collection, handling and analysis of forensic evidence from a radiological crime scene presents significant challenges. The potential for the use of radioactive materials in a malevolent act has been heightened in recent years, and it is highly likely that some or all of the physical evidence recovered after such an event may have been exposed to ionising radiation or contaminated with radioactive material. Authorities need a way to safely collect, handle and examine potential evidence contaminated with radioactive material. This research explores the impact that high-energy alpha particles have on traditional evidence types including fingermarks, DNA, hairs and fibres. The study also assesses existing methods and develops new forensic procedures for handling and processing traditional evidence contaminated with alpha emitting radioactive material.

What is nuclear forensics?

Nuclear forensic science, internationally referred to as 'nuclear forensics', is the comprehensive scientific analysis of nuclear or other radioactive materials or contaminated materials in the context of a State's obligations under international law, including criminal or civil proceedings [1]. The Nuclear Forensics Research Facility at ANSTO has been established to accommodate the requirements for handling radioactive or nuclear material or contaminated materials that require forensic exploitation. A traditional forensic laboratory does not possess the facilities to handle radioactive material and therefore a facility such as that developed at ANSTO is required to ensure a national capacity to deal with a radiological crime scene.

What is the impact of alpha radiation on forensic trace evidence?

Alpha radiation is a type of ionising radiation in the form of particles, namely helium nuclei, with very low penetration but high energy. If contaminants containing alpha-particle emitters are inhaled or ingested, they can cause damage to cells. We set out to explore the impact of alpha-radiation on forensic trace evidence.

ANSTO's 2 MV Tandetron STAR accelerator was used to expose fingermarks, hairs and fibres to helium ions, representative of the energies and doses that may occur through exposure to common alpha-emitting sources. It was identified that alpha radiation inflicted damage on forensic trace evidence that may affect the ability to analyse and interpret the evidence types studied.

Fingermarks

Exposure of a porous surface such as paper to alpha radiation, either before or after the deposition of fingermarks, was detrimental to the ability to develop fingermarks when doses were greater than 250 kGy. In Fig. 1, the alpha-beam track is observed through the centre of the developed fingermark. It can be seen that the damage incurred at 1000 kGy significantly impedes the ability to recognise identifiable features that are required for fingermark comparison.

Hairs and fibres

Using a range of analytical techniques, it was observed that the surface and chemical structures of hairs and fibres were mostly resistant to alpha radiation at the energies and doses employed. Minimal effects were identified in dyed hair as well as acrylic, cotton and wool fibres. Nylon and polyester fibres showed significant resistance to alpha radiation-induced damage.

What is the impact of contamination on forensic trace evidence?

We have also been able to demonstrate effective laboratory methods for the processing of evidence contaminated with radioactive material. In the nuclear industry, glove boxes are commonly used for the isolation of alpha contamination. Although external contamination with alpha-emitting radioisotopes poses little health risk (due to their low penetration), should they enter the body then the high ionising power of alpha particles means that significant cellular damage may occur. A glove box enables the handling of contaminated evidence whilst maintaining a safe

Figure 1

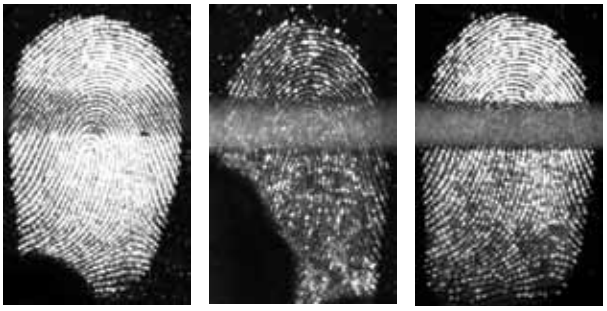

Developed (using indanedione-zinc) fingermarks on paper exposed to alpha radiation at (l-r) 50, 250, and 1000 kGy prior to fingermark deposition.

Figure 2

Glove boxes used for examination of forensic trace evidence in ANSTO's Nuclear Forensics Research Facility.

Figure 3

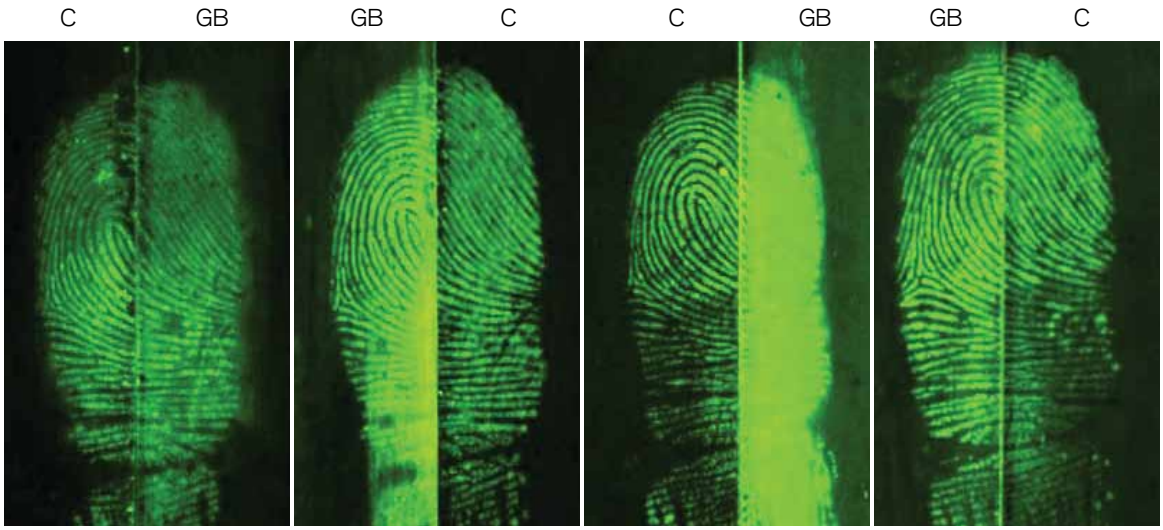

Fingermarks on glass developed using cyanoacrylate fuming with Rhodamine 6G stain solution. Imaged under 505 nm Polilight® and a KV550 long-pass barrier filter.

user environment, but the restricted environment of a glove box was particularly challenging for examining contaminated evidence. However the trialled techniques proved successful for most evidence types that were investigated.

Fingermarks

The introduction of two bench-top fingermark development and enhancement techniques to the glove box was successful. To allow these techniques to be employed, an essential modification to the glove box was the inclusion of a variable wavelength light source (Polilight®) and camera system to allow image capture *in situ*.

The first technique, for non-porous surfaces such as glass, requires superglue to be heated to 100°C. This produces cyanoacrylate fumes which react with the fingermark residue to form a white deposit along the ridges of the fingermark. To visualise the fingermark, a dye, known as Rhodamine 6G stain solution, is applied. This enables visual enhancement using specific lighting and filters. To employ this technique in the glove box, a modified fuming chamber with a hotplate was retrofitted and a secondary ventilation system installed to vent the cyanoacrylate fumes.

The second technique requires the porous sample (paper) to be submerged in a prepared solution, dried and then heated in a heat press. Due to size constraints imposed by the glove box a commercially available hair straightener was successfully substituted for the heat press. Comparison of the results of the bench-top (C) and glove box (GB) techniques for cyanoacrylate fuming is provided.

Fibres

In general, the contamination and the ensuing decontamination of fibres had no impact on subsequent forensic analysis. The decontamination procedure, an optimised technique developed in previous research [2], was the immersion of the sample in a detergent and water solution (2% Decon 90™) and cleaning for 5 minutes using ultrasonication to loosen particles adhering to the sample surface, before rinsing. This procedure resulted in satisfactory decontamination without damaging the fibre.

Figure 4

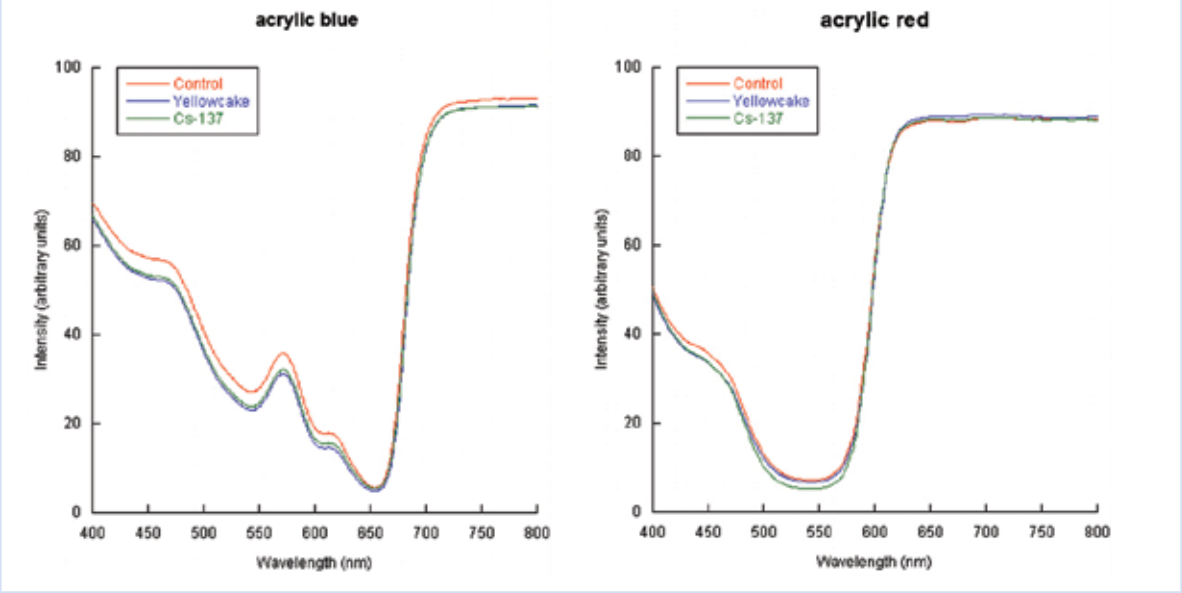

Microspectrophotometry spectra of a blue acrylic fibre (left) and a red acrylic fibre (right). The control sample is overlayed with the treated samples showing no discernible difference as a result of contamination and subsequent decontamination.

Figure 5

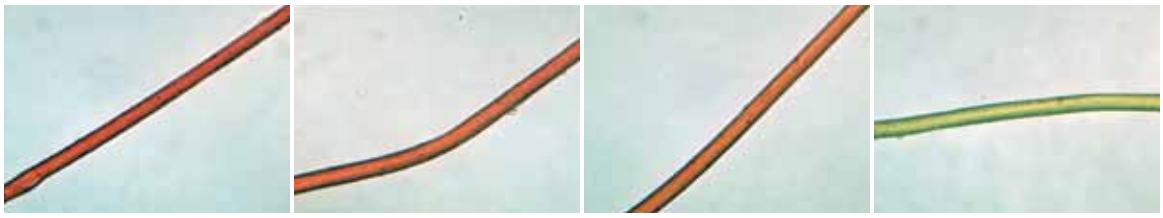

Colour changes observed in red polyester fibres with increasing doses. Shown fibres exposed to (l-r) 0, 10, 100, 1000 kGy.

What about other types of radiation?

In 2007, we completed a project assessing the impact of gamma radiation on forensic trace evidence [3-7], identifying the impact on specific evidence types at particular dose intervals. These results indicated that some types of evidence, such as human hair, paint chips and fingermarks, are not degraded by gamma radiation whilst others, such as fibres, glass and trace DNA, demonstrated damage to various degrees.

Fig. 5 shows the impact gamma radiation had on red polyester fibres as a function of dose: the intensity of the colour of the red polyester fibre diminishes with increasing dose, almost to a point of bleaching at the 1000 kGy exposure. This highlights the importance of understanding the effects of radiation on forensic evidence.

Acknowledgements

This work is supported by the Department of Prime Minister and Cabinet, National Security Science and Technology Branch, under contract PR07-0093, the Australian Federal Police and Australian Emergency Management.

References

[1] Office of Nuclear Security, draft non-paper Development of National Nuclear Forensics Libraries, 2011, International Atomic Energy Agency: Vienna.

[2] Parkinson, A., Evans, T., Roux, C., Abbondante, S., Hill, D., and Colella, M., NSST 06-032 Project: The Assessment of Post-Incident Radiological Decontamination Materials, 2008, Australian Nuclear Science and Technology Organisation: Sydney.

[3] Abbondante, S.F., The Effect of Radioactive Materials on Forensic DNA Evidence: Procedures and Interpretation, 2009, University of Canberra.

[4] Colella, M., Evans, T., Parkinson, A., Roux, C., Lennard, C., Robertson, J., Abbondante, S., and Hill, D., NSST 06-031 Project: The Impact of Ionising Radiation on Forensic Trace Evidence, 2009, Australian Nuclear Science and Technology Organisation: Sydney.

[5] Colella, M., Parkinson, A., Evans, T., Robertson, J., Roux, C., The Effect of Ionizing Gamma Radiation on Natural and Synthetic Fibers and its Implications for the Forensic Examination of Fiber Evidence, Journal of Forensic Sciences, 56(3), 591-605 (2011).

[6] Parkinson, A., Colella, M. and Evans, T., The Development and Evaluation of Radiological Decontamination Procedures for Documents, Document Inks, and Latent Fingermarks on Porous Surfaces, Journal of Forensic Sciences, 55(3), 728-734 (2010).

[7] Colella, M., Parkinson, A., Evans, T., Lennard, C., Roux, C., The Recovery of Latent Fingermarks from Evidence Exposed to Ionising Radiation, Journal of Forensic Sciences, 54(3), 583-590 (2009).

Meet a new generation radiation detector. Its future promises applications ranging from medical imaging to national security.

Towards realisation of novel semiconductor radiation detectors

Ramin Rafiei[1], David Boardman[1], Mark I. Reinhard[1], Adam Sarbutt[1], Dale A. Prokopovich[1], KiHyun Kim[2], Aleksey E. Bolotnikov[2], Ralph B. James[2]
[1]ANSTO, [2]Brookhaven National Laboratory, USA

Semiconductor gamma-ray and X-ray detectors are being used increasingly in medicine, industry, astronomy and national security. Conventional semiconductor detectors are manufactured from germanium and silicon. Such materials have become less useful in many emerging applications due to their physical limitations such as low detection efficiency or their need to operate at cryogenic temperatures.

This research contributes towards the development of compound semiconductor radiation detectors based on cadmium manganese telluride (CdMnTe) that operate at room temperature and with a high stopping power. With continued improvements in crystal quality and detector fabrication, this research could lead to the development of a new generation of radiation detectors for use in medical imaging and in national security applications.

Compound semiconductors: CdMnTe a promising candidate

CdMnTe is a promising compound semiconductor. While previously investigated for applications in optical isolators (transmission of light in only one direction using the Faraday effect), infra-red detectors and tuneable solid state lasers, its application as a radiation detector was first investigated in 1999 [1]. Its distinct advantages of good compositional homogeneity and a highly tuneable band-gap (energy difference between the top of the valence band and the bottom of the conduction band in insulators and semiconductors) compared to CdZnTe and CdTe, which have been leading room temperature detector candidates for over three decades, have encouraged CdMnTe detector developments in recent years.

A detailed understanding of the fundamental charge transport properties of CdMnTe radiation detectors is essential for detector developments. The most useful figure of merit is the mobility-lifetime product which quantifies the charge carrier transport through the detector. While for silicon and germanium this figure is greater than unity, for compound semiconductors this figure is up to 100,000 times less. The main cause of this performance shortfall can be traced to trapping centres caused by impurities and lack of stoichiometry in the material. Low mobility-lifetime product results in short carrier drift lengths and limits the maximum detector thickness and hence its application. It is also imperative to measure the uniformity of the charge-transport properties across the detector, allowing for the identification of surface and bulk features which affect charge transport through the device.

ANSTO and Brookhaven National Laboratory jointly investigate and improve the performance of CdMnTe detectors [2] and their properties. The CdMnTe crystals were grown by the vertical Bridgman technique [2]. A manganese fraction of 5 %, corresponding to a band-gap of 1.59 eV, was chosen for optimum room temperature spectral performance. To grow high-resistivity CdMnTe, the crystal was doped with indium. Indium, which is a donor compensates for the high concentration of Cd vacancies which act as acceptor centres in CdMnTe.

The samples were cut to a size of 10 x 10 x 1.9 mm^3. Infrared imaging of the CdMnTe samples prior to their clean-room fabrication revealed networks of tellurium inclusions distributed throughout their bulk, as shown in Fig. 1, and at an average concentration of 4.6 x 10^5 cm^{-3}.

Clean-room CdMnTe detector fabrication

Each sample was mechanically polished with a deionised water-based slurry of alumina powder in order of decreasing alumina particle sizes of 1 µm, 0.3 µm and 0.05 µm until extremely smooth surfaces were achieved.

Figure 1

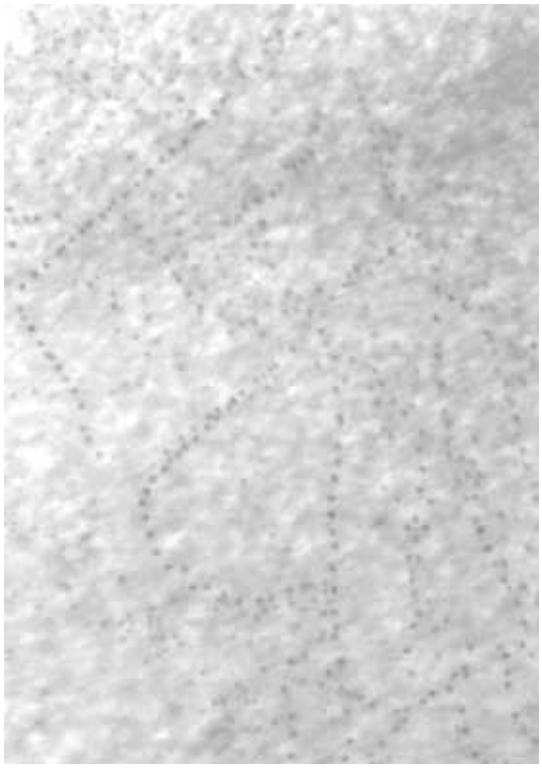

An infrared image of a 1.2 x 2.0 mm^2 area just beneath the CdMnTe surface. The dark dots are tellurium inclusions. The image shows a network of tellurium inclusions which extend from one side of the crystal to the other.

Figure 2

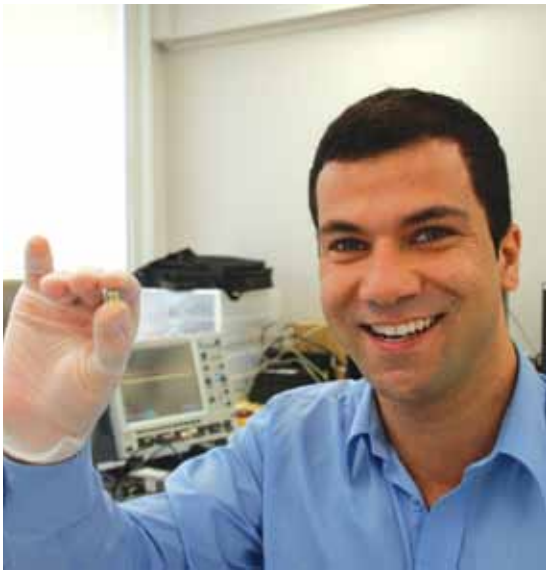

Ramin Rafiei holding a 10 x 10 x 1.9 mm^3 CdMnTe radiation detector.

To prepare the CdMnTe crystal surfaces for metal contact deposition, each sample was etched in an optimum 0.1% bromine-methanol solution for 5 minutes. Prior to metal deposition, the four contacts on the front surface of the sample were patterned by photolithography. To ensure excellent adhesion strength of the gold to the CdMnTe surface, we adopted a two-step thermal deposition of 5 nm chromium followed by a 150 nm gold layer. The detector test structures consist of a 2 x 2 array of evenly spaced 4 mm^2 squares and π mm^2 circles, both with and without guard rings. A single uniform contact covers the entire rear side. A fabricated CdMnTe detector is shown in Fig. 2.

Charge-transport properties of CdMnTe

Time-resolved transient current measurements and alpha-spectroscopy measurements have been used to measure the charge-collection efficiency of CdMnTe detectors. Fig. 3 shows the dependence of the charge-collection efficiency on the applied bias voltage. The average charge-collection efficiency across the detector increases with higher bias values and approaches 100% at the highest applied bias of 1000 V. The fit to the data points follows the Hecht analysis [3] and produces an average electron mobility-lifetime product of $8.5(\pm0.4) \times 10^{-4}$ cm^2V^{-1}.

Uniform charge-carrier transport is critical to the spectroscopic performance of CdMnTe detectors. Ion beam induced charge (IBIC) measurements, utilising $4He^{2+}$ beams from the ANTARES accelerator at ANSTO, have revealed the charge transport of these devices down to micron scale resolution. Fig. 4 (top panel) is an IBIC image showing the charge collection efficiency across an area of 1449 x 1449 μm^2 and at an applied bias of 400 V. Such images have quantified how major impurities such as tellurium inclusions present within the detector bulk (and clearly visible in Fig. 4 as areas of reduced charge collection), affect the charge collection of these devices. These measurements have also shown that the role of tellurium inclusions in degrading charge collection is reduced with increasing values of bias voltage. In contrast to the top panel of Fig. 4, the bottom panel is an IBIC image showing uniform charge collection at a value approaching 100%. The edges of the contact and the guard ring structure are clearly visible.

Single charge-transient measurements provided the drift time of the electrons across the detector. Using these transit times the drift velocity of the electrons has been calculated and is shown in Fig. 5, as a function of the applied electric field. From the region of proportionality in Fig. 5, the room temperature mobility of the CdMnTe sample was found to be 718(±55) cm^2/Vs. Knowing the electron mobility-lifetime product the electron carrier lifetime is 1.2(±0.1) µs.

Figure 3

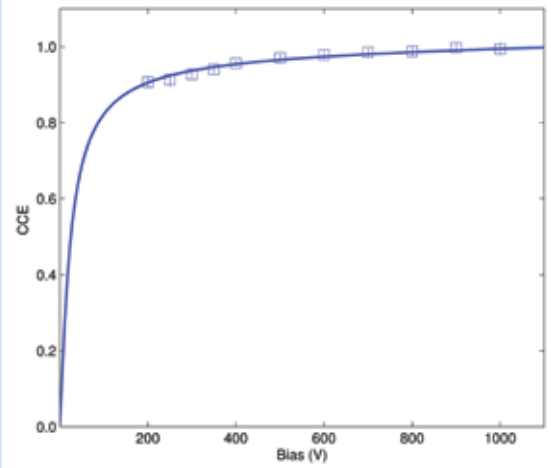

The evolution of the average charge-collection efficiency across the CdMnTe detector with applied bias voltage. The efficiency approaches 100% for the highest bias measurement. The measured data points have been fitted using the Hecht model to obtain the mobility-lifetime product.

Summary and path ahead

The ANSTO-Brookhaven detector collaboration covers the areas of crystal growth, detector fabrication and characterisation. Knowledge gained from our recent measurements has already led to the growth of CdMnTe crystals with modified stoichiometry. These crystals have been fabricated into radiation detectors and initial measurements on these generation II devices show an order of magnitude improvement in the electron mobility-lifetime product. Continued improvements in crystal quality and detector fabrication will be required for the realisation of state-of-the-art radiation detectors in medical and national security applications.

Figure 4

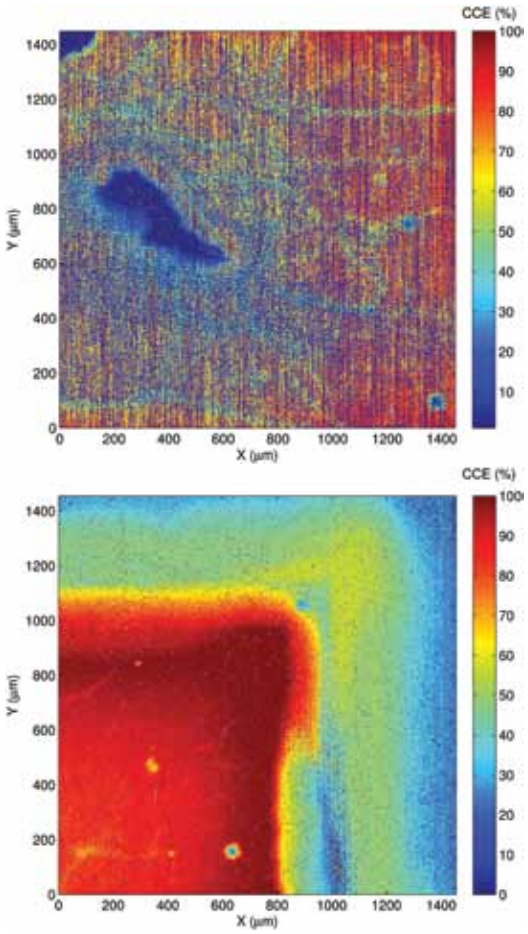

Spatially resolved charge-collection efficiency maps of the CdMnTe detector. On this colour scale blue signifies low charge collection, while regions of high charge collection are represented in red. In the top panel regions of poor efficiency are spread throughout the bulk and are associated with the tellurium network. In contrast, a region with uniform charge collection approaching 100% is presented in the bottom panel. The edges of the contact and the guard ring structure (green coloured) are clearly visible

Figure 5

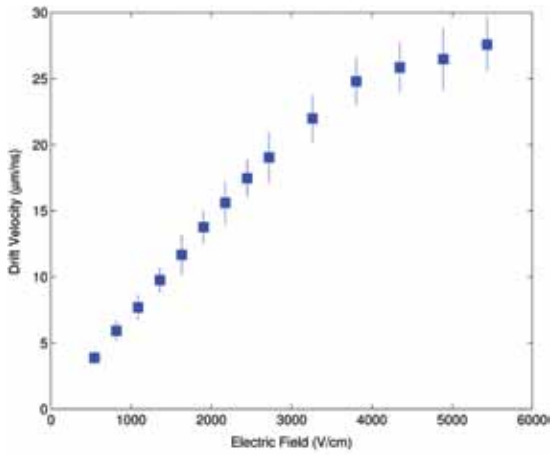

Carrier-drift velocity as a function of the applied electric field. From the region of proportionality the carrier mobility has been extracted.

References

[1] A. Burger et al., Crystal growth, fabrication and evaluation of cadmium manganese telluride gamma ray detectors, J. Cryst. Growth, 198/199, 872-876 (1999).

[2] R. Rafiei et al., Investigation of the charge collection efficiency of CdMnTe radiation detectors, IEEE Trans. Nucl. Sci., 59, 634-641 (2012).

[3] Y. Nemirovsky, A. Ruzin, G. Asa, and J. Gorelik, Study of the charge collection efficiency of CdZnTe radiation detectors, J. Electron. Mater, 25, 1221-1231 (1996).

In cool climate rainforests moss is an indication of pure uncontaminated air.

Improving low-level gamma spectrometric measurements to study contamination in environmental samples

Aimee McNamara[2], Henk Heijnis[1], Daniela Fierro[1], Mark Reinhard[1]
[1]ANSTO, [2]University of Sydney,

Measuring radionuclides in the environment at very low concentration levels is of increasing importance to ensuring we have a proper means of minitoring the impact of nuclear activities on the environment.

Many aspects of environmental monitoring require very sensitive detection techniques for precise measurement of the very low levels of radionuclides found in the environment.

This need has driven the development of new detector instrumentation, which in turn has prompted the need for more complex techniques for instrument calibration. ANSTO has developed new techniques based on Monte-Carlo simulation to determine accurate calibrations of a specialised high-resolution gamma-ray spectrometer used to measure radionuclides at environmental levels in a variety of sample matrices and geometries.

Introduction to the technique used

High-resolution gamma-ray spectrometry is routinely used for measuring radionuclides in a variety of purposes. In environmental contexts the presence of radionuclides is typically at very low concentrations challenging the performance of traditional approaches. Reducing the spectral background to allow better detection of small gamma-ray signatures in environmental samples can be achieved using Compton-suppression techniques [2]. Compton scattering is a type of scattering that gamma rays undergo in matter; its inelastic scattering results in a decrease in energy of a gamma-ray photon, called the Compton effect.

In the Compton-suppression approach the addition of a secondary outer detector to the normally employed spectroscopy inner detector allows for the detection of Compton-scattered photons which emerge from the inner detector. Anti-coincident circuitry allows these Compton-scattered events to be rejected from the measured spectrum thereby greatly improving the ability to identify gamma-ray peaks which would otherwise be hidden behind the Compton continuum. The International Atomic Energy Agency and many practitioners have identified that the calibration of Compton-suppressed gamma-ray spectrometers for the various sample matrices and measurement geometries used for environmental samples is complicated, time consuming and costly [1].

We used Monte Carlo simulations as an alternative to empirical calibration to assess the correction factors specific to the detector design and overall energy calibration of a Compton-suppressed spectrometer specific to radionuclides in environment contexts.

Detector specifications

Measurements were performed with a Compton-suppressed reverse-electrode high-purity germanium (HPGe) detector (Model GR5022 from the company Canberra), specified as having a relative efficiency of 50.9% to a 3 inch by 3 inch NaI(Tl) detector at 1.33 MeV. The components and dimensions of the HPGe detector were taken from manufacturer-provided documents. A sketch of the HPGe detector, is shown in Fig. 1 and an X-ray radiograph of the detector is shown in Fig. 2. The reverse-electrode HPGe detector, which acts as the primary spectrometer, is surrounded by two NaI(Tl) detectors in the form of an annulus and plug. The plug is positioned above the inner detector adjacent to the annulus. The detector annulus is further contained in a thin aluminium holder with an inner and outer radius of 41.25 mm and 140.5 mm, respectively. The full length of the surrounding annulus is 162.5 mm. The entire suppression system is placed in a graded lead case shield (w115 mm thick) with an inner copper and tin lining (each w1.5 mm thick) to protect against environmental radiation (e.g. cosmic rays, building materials radiation).

Figure 1

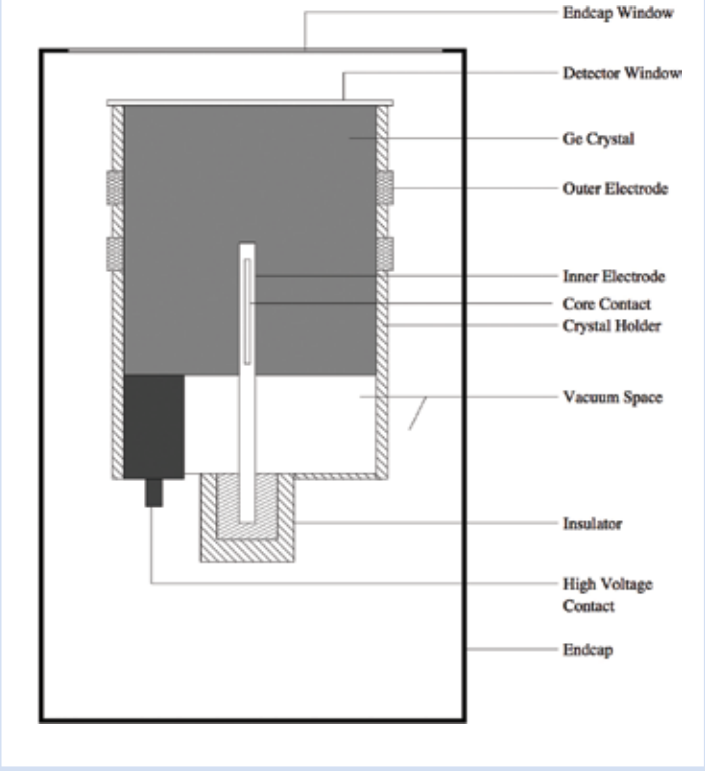

Schematic illustration of the HPGe detector not drawn to scale.

Figure 2

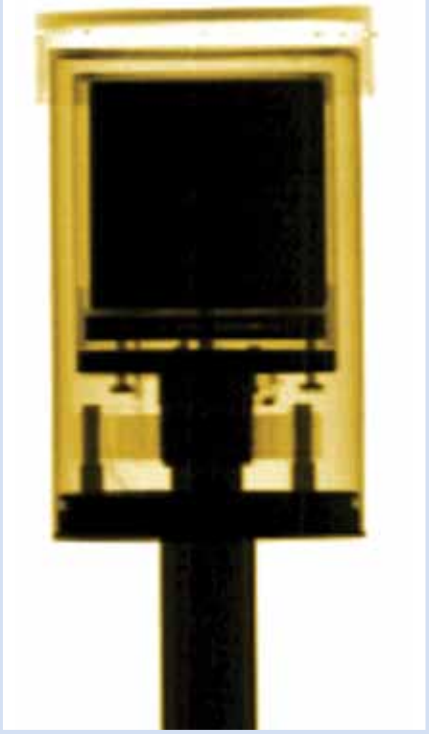

X-ray radiograph taken of the HPGe detector to verify the geometric structure.

Simulation of detection processes

The Compton-suppressed HPGe detector system as described was modelled using the Monte Carlo simulation package Geant4 (version 9.4) [3]. The Geant4 Low Energy Electromagnetic Physics processes based on the Livermore libraries, valid for energies of 250 eV-100 GeV, were used to model the photon interactions within the detector. The physics processes activated included Compton scattering, Rayleigh scattering, pair production and the photoelectric effect for photons. Bremsstrahlung and ionisation processes for secondary particles were also activated. The gamma-emitting radionuclides were generated using the radioactive-decay module [4], which allows the user to generate all possible decay components emitted for a particular radionuclide.

For comparison of the simulated results, the detector system energy calibration was conducted using a traceable multi-nuclide standard source (QSA Global RF929), which covers a gamma-ray energy range of 60 to 2000 keV. The standard sample configuration used was a 65 mm diameter plastic petri-dish containing the compacted soil sample, positioned directly on the detector end-cap.

The calibration

The detection efficiencies for the standard source sample, RF929, were calculated with Monte Carlo simulations for the suppressed and unsuppressed modes of operation and compared to the experimental efficiencies (see Fig. 3 for the suppressed mode data). The experimental and the simulated values agree relatively well for high energies but deviate at lower energies. Low-energy photons would be more susceptible to absorption in the inactive detector components and sample. If these components are not correctly modelled, it can affect the calculated efficiencies. The summation effects within the HPGe detector seem to be mostly well accounted for by the Geant4 radioactive-decay models for the unsuppressed mode.

The simulations show that the full energy peak efficiency in the suppressed detector mode is radionuclide dependent. This is largely due to the coincidence detection of two different photons from the same source, in a time frame shorter than the timing resolution of the detector system. In this case, an unscattered photon may be falsely labelled as a scattered photon and discarded. Some radionuclides are associated with summation effects in the suppression system and may be better evaluated in the unsuppressed mode of operation or with validated simulation efficiencies.

Figure 3

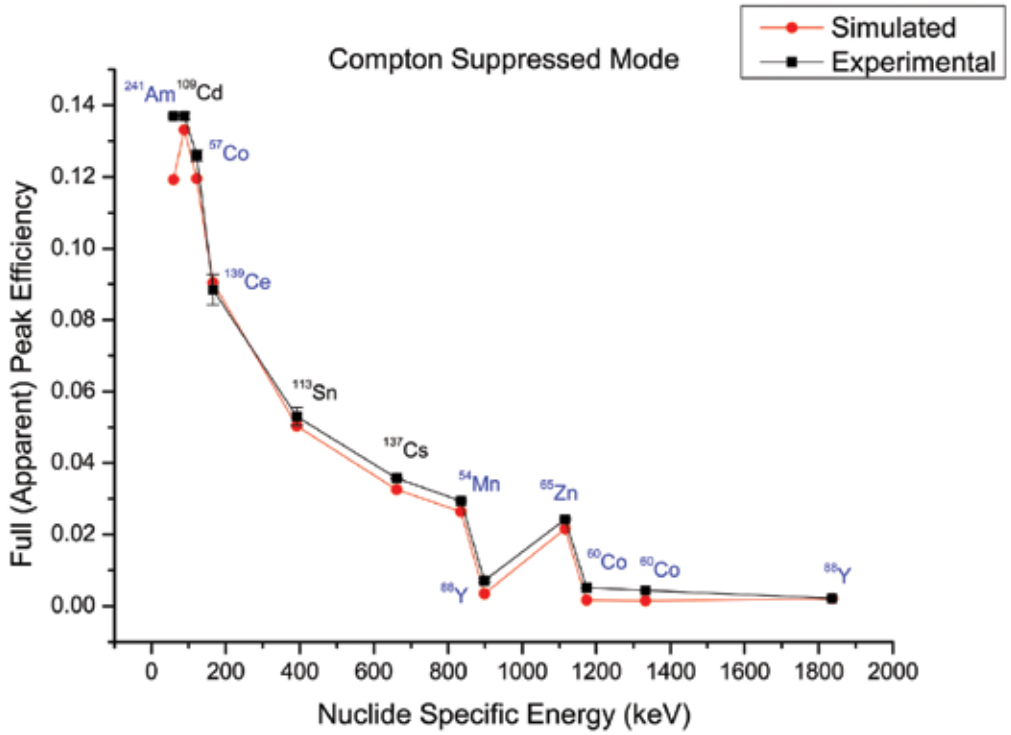

Simulated and experimental full energy peak efficiencies as a function of radionuclide gamma-ray energy, for the detector system in the suppressed mode.

Our model

The model developed can assist environmental scientists with the measurement of very low concentrations of radionuclides in the environment via an improved tool to perform measurements on a large variety of sample matrices and geometries. The model reduces the need for complicated, time consuming and costly manufacture of radionuclide calibration samples as well as providing important insights into the measurement process for particular sample types.

Acknowledgements

This work was carried out at ANSTO as part of the IAEA CRP entitled “Benchmarking calibration for low-level gamma spectrometric measurements of environmental samples” (IAEA-CRP1471-01).

References

[1] Hult, M., Low-level gamma-ray spectrometry using Ge-detectors, Metrologia 44 (S87) (2007).

[2] Knoll, G.F., Radiation Detection and Measurement, third ed. John Wiley and Sons Inc. (1999).

[3] Agostinelli, S., et al., Geant3 a simulation toolkit, Nucl. Instrum. Methods A. 506, 250. (2003).

[4] Truscott, P., et al., Development of a spacecraft radiation shielding and effects toolkit based on Geant4, Proc. Computing in High Energy and Nuclear Physics A123. (2000).

David Boardman, Alison Flynn and Mark Reinhard are helping Australia meet its international requirements for radiation screening.

Improving the identification of radiological and nuclear materials

David Boardman, Alison Flynn, Mark Reinhard
ANSTO

The illicit trafficking of radiological and nuclear material is a major concern for the international community. In the near future the United States will require all trade partners to perform passive radiation screening on 100% of cargo at the country of origin. However, the high false or nuisance alarm rates of current radiation detection systems negatively impact the flow of legitimate trade through the ports. Furthermore, the potential failure to detect the presence of illicit radioactive material is of even greater concern. Our research has led to the development and evaluation of a new technology in the form of identification algorithms that address these issues and maintains a high true positive alarm rate whilst minimising the false positive alarm rate. This research will contribute directly to national and international security.

Evaluations of commercially available radiation portal monitors for detecting radioactivity have demonstrated a high rate of false alarm [1, 2]. This is mainly due to short measurement acquisition times required for broader security applications. The small detector volumes imposed by cost restraints can also limit the statistical quality of the measured gamma-ray spectra. Fig. 1 shows an example of the low statistic sodium iodide spectra that have been obtained from a handheld radionuclide identifier. Traditional radionuclide identification software based on peak search algorithms is unable to detect the presence of ^{137}Cs, due to the low number of counts in the ^{137}Cs peak at 662 keV.

Using a special computation method: FLDA algorithm

Fisher Linear Discriminant Analysis (FLDA) is a multivariate statistical analysis technique that has typically been used as a classification and/or dimensionality-reduction technique and is used in pattern recognition. The dimensionality reduction properties of FLDA mean that the original data with 512 energy bins (variables) can be represented in a new single variable (i.e. reducing 512 dimensions down to 1). FLDA can generate loading coefficients (weighting factors) that maximise the separation between user-defined classes. For our work, a multiple two class FLDA approach was used in order to generate the energy-bin weighting factors that maximise the separation between one source and all other sources in a training data library. Each of these loading coefficients are subsequently used to project (or transform) the unknown measured spectra.

Fig. 2 illustrates the projection of various gamma-ray spectra by the loading coefficients for ^{137}Cs and ^{133}Ba. If a particular source is present then it is separated from all the other sources along its corresponding loading-coefficient axis. All the other sources, which do not contain ^{137}Cs or ^{133}Ba, tend to cluster around a single point. The standard deviation in the cluster distribution varies as the inverse square-root of the mean gross-counts, so the source separation becomes more pronounced as the number of counts increase.

Performance validation

The North American standard (ANSI N42.34) for handheld radionuclide identifiers requires that each radionuclide must be identified in 8 out of 10 trials in a minimum of 120 s for a dose rate of 0.5 μSv/h [3]. The validation of the algorithm performance, against these requirements, has been done with experimental and semi-empirical synthetic spectra. Table 1 shows the identification performance for 100 spectra of each of the given radionuclides. The analysed spectra were for a 10 s acquisition time of a radionuclide dose rate of 0.05 μSv/h in the presence of a 0.1 μSv/h background. For the threat radionuclides, the identification performance typically meets the ANSI N42.34

Figure 1

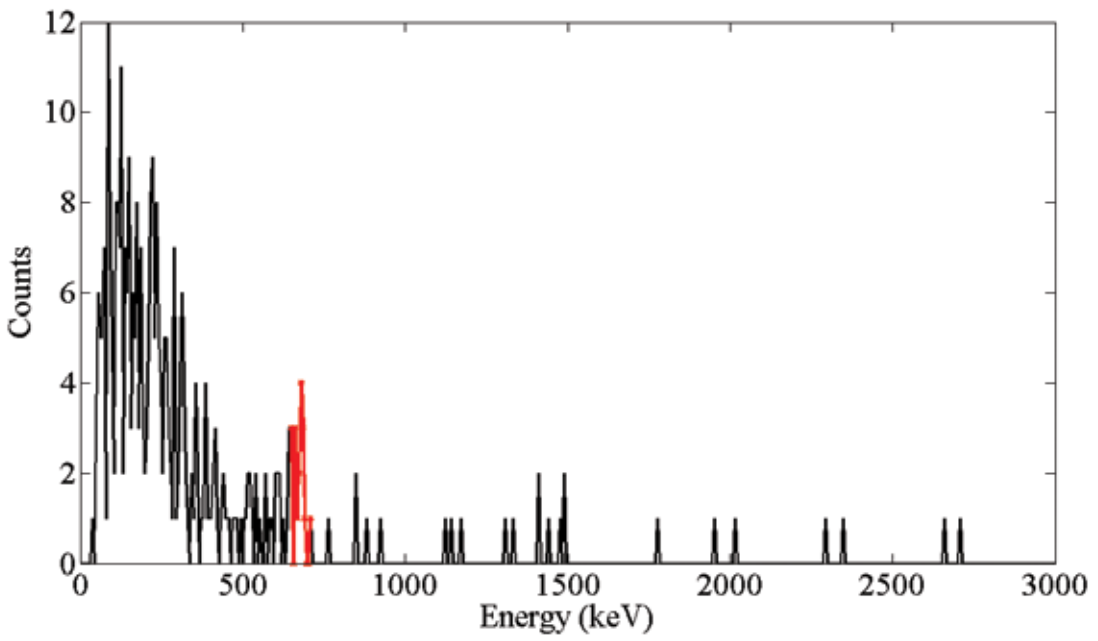

A typical low count ^{137}Cs spectrum acquired by a NaI detection system. The red highlighted region shows where the ^{137}Cs peak occurs.

requirements for a dose rate and acquisition time that are an order of magnitude lower. There were also no false alarms in the analysed spectra.

The results presented are for a NaI detector, however the FLDA algorithm performance has shown an improved identification performance for lanthanum bromide and high-purity germanium detectors that have an improved energy resolution. The FLDA algorithm has shown high potential for the accurate identification of threat radionuclides which is maintained for count starved spectra. The algorithm could be used in border monitoring applications that require a high sensitivity to threats, but also require low false and nuisance alarm rates which will maintain the flow of commerce at ports of entry.

References

[1] J. M. Blackadar, S. E. Garner, J. A. Bounds, W. H. Casson, and D. J. Mercer, "Evaluation of Commercial Detectors," Los Alamos National Laboratory 2003.

[2] L. Pibida, M. Unterweger, and L. R. Karam, "Evaluation of handheld radionuclide identifiers," Journal of Research of the National Institute of Standards and Technology, vol. 109, pp. 451-456, 2004.

[3] ANSI, "American National Standard Perofrmance Criteria for Hand-Held Instruments for the Detection and Identification of Radionuclides," vol. N42.34, 2006.

Figure 2

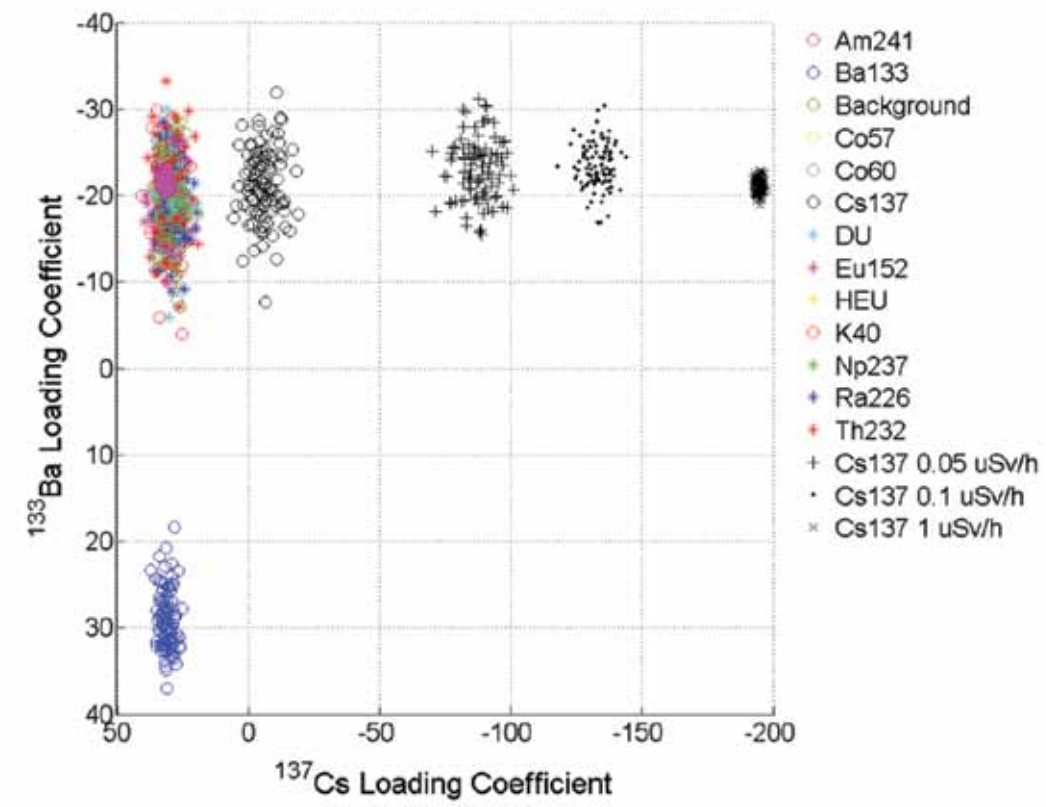

The projection of various gamma-ray spectra by the loading coefficients for ^{137}Cs and ^{133}Ba. If a particular source is present then it is separated from all the other sources along its corresponding loading-coefficient axis. All the other sources, which do not contain ^{137}Cs or ^{133}Ba, tend to cluster around a single point.

Table 1

Dose rate (μSv/h)	^{241}Am	^{133}Ba	^{57}Co	^{60}Co	^{137}Cs	DU	HEU	^{40}K	^{237}Np	^{226}Ra	^{90}Sr	^{232}Th
0.05	100	100	100	100	100	96	100	100	100	26	100	0

The true positive identification results for 0.05 mSv/h and an acquisition time of 10 s. No false positive alarms were recorded.

ANSTO facts and figures 2011

Financial Statement ($AUD'000)

	2011 Research		2011 Total ANSTO	
Expenditure				
Operations	57,809	75%	235,688	76%
Investments	19,600	25%	74,979	24%
Total	77,409	100%	310,667	100%
Exp according to source of income				
Federal Govt. funding	70,142	91%	240,451	77%
Third Party	7,267	9%	70,216	23%
Third Party revenue				
Private Industry	5,249	72%	67,849	97%
Grants #1	2,018	28%	2,367	3%
Total	7,267	100%	70,216	100%

#1 Includes grants from Government, Universities and CRCs

The total expenditure by ANSTO for the calendar year 2011 was AUD $310.7 million. This represents a ~5% increase from the previous year. Of this total amount, AUD $77.4 million or 24.9% was utilised in scientific research. Federal Government (block) funding represented 91% of this revenue and 9% came from third parties. These third parties include significant private investment (72%) while the rest came through grants and Government, Universities and Cooperative Research Centres (CRCs).

ANSTO employees

At the end of 2011, ANSTO had 1,140 full time equivalent employees of whom 27.9% were women. The chart below shows ANSTO's continued reliance on Technical and Engineering Staff (53.5%) for a successful user-based research facility.

ANSTO employment categories

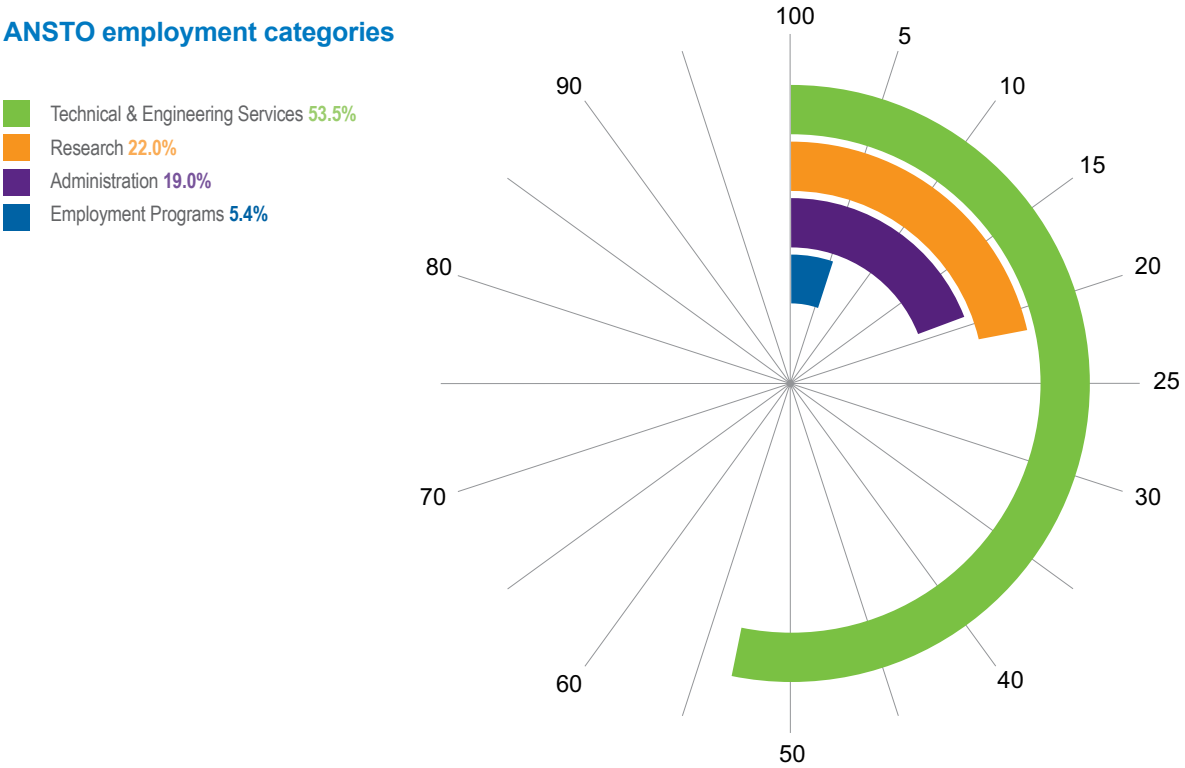

User facilities

In 2011,the OPAL beam lines and the two accelerators (ANTARES and STAR) attracted a total of over 500 users with more than 1570 visits. These users came from more than 95 institutions in over 25 countries.

Invention Disclosures

In 2011, there were 4 'invention disclosures' to IP Australia for the purposes of securing provisional patents.

- Next Generation of Sarcophagines/ Cryptates for Imaging and Therapy
- Filling devices: Systems and methods for transferring hazardous waste material into a sealable container
- Modularized process flow facility plan for storing hazardous waste material
- Filling container and method for storing hazardous waste material.

Awards

- Ms Leena Burgess – 1st Prize for presentation at 2011 Inorganic Chemistry (IC11) RACI meeting in Perth
- Mr Paris Constantine – elected as a Fellow of the Institute of Engineers, Australia
- Institute of Materials Engineering – WTIA Company of the Year 2010 (Welding Technology Institute of Australia awarded in 2011)
- Dr Robert Robinson – elected as vice-president of the Executive to the Australian Institute of Physics
- Mr Michael Saleh - Industry Partnership Award by DMTC (Defence Materials Technology Centre)
- Ms Jessica Veliscek Carolan – United Uranium Scholarship recipient.

Grants awarded in which ANSTO collaborates

ARC Discovery Grants

- Diffusion – the key to performance in organic optoelectronic devices (University of Queensland)
- Cementitious Gel: The Missing Link in Understanding the Ageing of Built Infrastructure (Monash University and National University of Singapore).

ARC Linkage Infrastructure, Equipment and Facilities (LIEF) Grants

- A State-of-the-art Magnetic Property Measurement Facility for the Development of Advanced Materials and Biomedical Technologies in the Sydney Basin (University of NSW, University of Sydney, University of Wollongong, University of Western Sydney)
- Automated preparative gas chromatograph for isolating unique and important organic components for structural identification (Curtin University and UWA)
- An Australian fluid-inclusion facility for climate-change science (University of Melbourne and UNSW)
- An aberration-corrected analytical Transmission Electron Microscope for nanoscale characterisation of materials (UoW, Blue Scope Steel, Deakin University, University of Newcastle, DMTC).

NHMRC Grants

- Improving the use of chemotherapy (University of Sydney)
- Mephedrone ("Meow", 4-Methylmethcathinone): examining the effects of a novel "party drug" on brain and behaviour (University of Sydney).

CSIRO – Science and Industry Endowment Fund (SIEF)

- Solving the Energy Waste Roadblock: Addressing one of the foremost challenges for reducing greenhouse gas emissions on a national and international scale, namely, the development of new materials and processes for the capture and utilisation of carbon dioxide.(University of Sydney).

2011 National Science Week (DIISR)

- Science - Fact or Fiction.

US - National Science Foundation (NSF)

- East Asia and Pacific Summer Institutes (EAPSI) fellowship program (Australian Academy of Science).

Partnerships

Cooperative Research Centres (CRCs) and their equivalents are an integral part of the scientific research landscape in Australia today. From their inception, ANSTO has been involved in these centres, and our current involvements are described below.

CRC for Infrastructure and Engineering Asset Management (CIEAM)

- Sustainability and Organisational Performance
- Integration and Operability
- Capability Optimisation
- Structural Integrity

CRC for Biomedical Imaging and Development

- Protein Biosynthetic Pathway Targeting
- Neuroreceptor Ligand Targeting
- Development of Novel Receptor Based Radio-Pharma
- Apoptotic Pathway Targeting
- Development of Synthesis Mods for Tracer Product
- General
- CRC Revenue and Contributions
- Evaluation and Characterisation of Detector Materials

CRC for Polymers III

- Functional Polymers for Photovoltaic devices
- Degradable Polymer films

Defence Materials Technology Centre (DMTC) - non CRC Partnership

- Maritime Platforms Programme
- Armour Applications Programme
- Personnel Survivability Programme

Partnerships and collaborations

As reflected by the research presented in Research Selections, collaboration is vital to productive and innovative science. Cooperation among the scientific community enables research institutions to combine and thus perform beyond individual capabilities and provide greater outcomes for society.

ANSTO continues to pursue collaborative agreements and memoranda of understanding with leading science and research institutions within Australia and around the world. The Australian Institute for Nuclear Science and Engineering (AINSE) is a key facilitator of collaboration between ANSTO and Australasian universities. Through AINSE, university scientists and researchers can access ANSTO's world class facilities, supporting high quality research, education and training in nuclear science and engineering.

Since the beginning of 2011, ANSTO has broadened Australia's scientific reach, entering into formal co-operation with national and international research organisations including:

- National Measurement Institute, 22 March 2011
- Universiti Teknologi Mara, Malaysia, 20 May 2011
- University of Sydney, 7 September 2011
- Monash University, 28 September 2011
- European Molecular Biology Laboratory (EMBL) Australia, 29 November 2011

Schools, workshops, reviews

Schools

- Science in the Suburbs at ANSTO, 10 February 2011 (joint event between ANSTO and the Australian Museum – 100 students attended)
- ANSTO Science: 'Fact or Fiction', 20 July 2011, held at UTS
- 5th Annual Neutron School for PhD students and Post-Doctoral Fellows, 15-19 August, 2011 (31 participants) to learn about and perform experiments, using ANSTO's neutron instrumentation.
- 'Marine Benchmark Study on the Possible Impact of the Fukushima Radioactive Releases in the Asia-Pacific Region'. The project is an IAEA Technical Cooperation (TC) activity evaluating the extent and possible impact of the releases of radioactivity from the Fukushima Daiichi nuclear power plant accident in March 2011 into the marine environment in the Asia-Pacific region through the RCA. First workshop 29 August-2 September, 2011, in Cronulla. 33 participants from 20 Asia-Pacific nations.
- Foundations in PET/CT School for International Users. 5-16 September 2011 (10 participants).
- 4th Asia-Oceania Neutron Scattering Association (AONSA) Neutron School 12-17 November 2011, ANSTO, Sydney (due to unavailability of the neutron-scattering facilities in Tokai, Japan, following the disaster of the Great East Japan Earthquake in March 2011).
- Individual professional development days for secondary teachers: 74 teachers attended the 3 day course. Overview of all areas of the science curriculum including Chemistry, Physics, Biology as well as Earth & Environmental Science that are covered (at a HSC level).
- 47 ANSTO scientists were lecturing at Universities and higher education establishments across New South Wales and Australia.

Workshops

- ANSTO-SINAP workshop Shanghai Institute of Applied Physics (SINAP), 17-18 February 2011, Shanghai, China.
- Italian-Australian Archaeology and Cultural Heritage Workshop: New Scientific Techniques in Archaeology, Palaeo-Anthropology and Cultural Heritage 14-17 March 2011, Rydges Hotel, Cronulla, Sydney.
- Synchrotron and Neutron New Users Symposium, 8 July 2011 at UNSW.
- 2nd Australian Cyclotron Users' Workshop 15 July 2011, Darwin, (ANZSNM conference).
- ANSTO-BMRI Molecular Imaging Workshop 24 August 2011, University of Sydney's Brain and Mind Research Institute (BMRI), Sydney.(pictured **2**)
- FNCA Workshop on Neutron Activation Analysis Project, 21 – 24 November 2011, ANSTO.

Reviews

- Bragg Institute – Advisory Committee Meeting. This committee provides strategic advice to the Institute under its chair, Professor Peter Colman (Walter and Eliza Hall Institute) 11-12 April 2011.
- Institute of Environmental Research (IER) Review. The review of this Institute considered its performance and facility, quality and impact of its research, project structure, its overall strategic direction, governance and safety. It took place in May 2011 and the review panel included, Professor Jim Williams (ANU), Professor Mary Edwards (University of Southampton,UK), Professor A. Tim Jull (University of Arizona, Tucson) Dr Greg Storr (ANSTO, Nuclear Operations) .
- Bragg Institute - Beam Instrument Advisory Group met on 28-29 July to review the major capital projects. The committee was chaired by Dr Dan Neumann (NIST Center for Neutron Research, USA).
- A Final Progress Review Meeting for the RCA project on 'Assessment of Trends in Freshwater Quality Using Environmental Isotopes and Chemical Techniques for Improved Resource Management'. IAEA Technical Cooperation (TC) activity promoting the utilisation of isotope techniques for improving freshwater resources management in the region was held 11-14 November, 2011, at ANSTO. 18 participants from 14 Asia-Pacific nations.

4th Asia-Oceania Neutron Scattering Association (AONSA) Neutron School

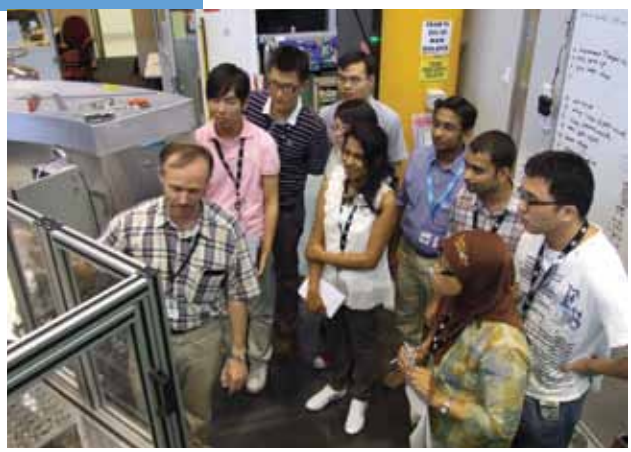

Italian-Australian Archaeology and Cultural Heritage Workshop

ANSTO-BMRI Molecular Imaging Workshop

ANSTO Executive Team

Mr Peter Arambatzis – Chief Financial Officer

Mr Michael Beckett – General Manager, Support Services & Chief Information Officer

Mr Robert (Rob) Blissett – General Manager, Human Resources

Mr Douglas (Doug) Cubbin – General Manager, Business Development and Commercialisation

Professor John Dodson – Head, Institute of Environmental Research

Professor Lyndon Edwards – Head, Institute of Materials Engineering

Dr Marie Claude Gregoire – Head, ANSTO LifeSciences

Mr Hefin Griffiths – General Manager, Safety, Environmental & Radiological Assurance

Mr Shaun Jenkinson – General Manager, Commercial Operations

Mr Paul Jones – General Manager, Security and Safeguards

Ms Nadia Levin – General Manager, Government, International and External Affairs

Mr Con Lyras – General Manager, Engineering and Capital Programs

Dr Adi Paterson – ANSTO CEO

Dr Robert (Rob) Robinson – Head, Bragg Institute

Dr Greg Storr – General Manager, Nuclear Operations

By Invitation:

Professor Richard Banati – Distinguished Research Fellow and ANSTO LifeSciences

Ms Stephanie Cole – Legal Counsel

Mr Kobus Naude – Senior Manager, Strategy and Planning

Pictured from left to right (back row) Peter Arambatzis, Kobus Naude, Stephanie Cole, Michael Beckett, Rob Blissett, Con Lyras, Rob Robinson, John Dodson, Hefin Griffiths, Paul Jones, Richard Banati.

(front row), Shaun Jenkinson, Marie-Claude Gregoire, Adi Paterson, Greg Storr, Nadia Levin.

Not present: Doug Cubbin, Lyndon Edwards.

Australian Institute of Nuclear Science and Engineering (AINSE) - facts and figures 2011

Background

The Australian Institute of Nuclear Science and Engineering (AINSE) provides a platform for training and cooperation in the nuclear science and engineering fields. Its membership comprises 46 Australian and New Zealand universities and science organisations, including ANSTO, making it one of few scientific institutions with such a wide membership. AINSE facilitates access to ANSTO's and other associated nuclear capabilities through research grants, fellowships and support for conferences and workshops.

Research Awards

Access to ANSTO's nuclear science and technology is the primary purpose of these awards. They require close cooperation between ANSTO research scientists and university-based researchers and their students. They involve a substantial use of both the accelerators and the OPAL research reactor.

In 2011, 234 projects were supported and they had a total value of $1,850,319.

International Travel Awards and Scholarships

AINSE provided $94,523 for this purpose. Half of the funding went to students presenting AINSE supported research at an international meeting, and the other half primarily supported travel for researchers conducting research at ISIS, UK.

Postgraduate Research Awards

In 2011, 11 of the 72 AINSE postgraduate research award holders received an award for the first time and 12 doctoral theses were received. A further 71 theses, where students conducted experiments under a research award in the name of their supervisor, are recorded in the publications list. The AINSE postgraduate research award holders accessed the facilities for a total of 1097 days. In addition, another 135 students gained access to the facilities via awards held by their supervisors, for a total of 1252 days.

Research Fellowships

These are three-year fellowships which can be extended to a total of five years where appropriate. In 2011, one new fellow was appointed. Dr Alison Blyth will join Curtin University of Technology and work with ANSTO's Institute of Environmental Research on a project entitled Molecular, stable isotopic and radiocarbon analyses of organic matter preserved in terrestrial records.

Dr Lizhong He concluded his fellowship at the end of the 2011 when he was appointed to a senior lectureship in the School of Chemical Engineering at Monash University.

At the end of 2011, the total number of current AINSE Research Fellows was seven.

Schools, Workshops and Reviews

The following events were run and/or supported by AINSE. Other events were supported in a minor way and are not reported here.

- 17th AINSE Conference on Nuclear and Complementary Techniques of Analysis & 10th Vacuum Society of Australia Congress
- Quaternary Techniques Short-course
- Synchrotron and Neutron New Users Symposium
- ANSTO Breakfast Briefing
- Bragg Institute IAT and PAC meetings
- Powder Diffraction at Large Scale Facilities Workshop
- 4th Asia Oceania Neutron Scattering Association Neutron School
- 1st Asia Oceania Conference on Neutron Scattering
- Australian Synchrotron Users Meeting
- OZ-INTIMATE 2011

In 2011, Professor Robert Norris conducted a review of the AINSE Research Fellowships program. His recommendation that the program continue was accompanied by more than 30 recommendations on suggestions for improvements.

Publications

During 2011, notification was given of 602 publications that reported the results from AINSE supported research projects. Of these, 361 are articles in refereed journals and 167 include an ANSTO co-author. The remainder are conference papers/abstracts (148), books/book chapters (10) and theses (83).

ANSTO publications 2011

Refereed Journal Publications

Abaffy, N., McCulloch, D. G., Partridge, J. G., Evans, P. J. and Triani, G., Engineering titanium and aluminium oxide composites using atomic layer deposition. Journal of Applied Physics, 110(12), 123514-123518. (2011).

Ahmed, R., Faisal, N.H., Paradowska, AM., Fitzpatrick, M.E. and Khor, K.A., Neutron diffraction residual strain measurements in nanostructured hydroxyapatite coatings for orthopaedic implants. Journal of the Mechanical Behavior of Biomedical Materials, 4(8), 2043-2054 (2011).

Andersen, K.H., Bentley, P.M., Cussen, L.D., The ABC of powder diffractometer detector coverage. Journal of Applied Crystallography, 44(Part 2), 295-298. (2011).

Anderson, K.M., Goeta, A.E., Martin, J.E., Mason, S.A., McIntyre, G.J., Sansam, B.C.R., Wilkinson, C., Steed, J.W., Dominance of Charge-Assisted Hydrogen Bonding on Short Contacts and Structures that Crystallize with Z ' > 1. Crystal Growth and Design, 11(11), 4904-4919. (2011).

Arrachart G., Karatchevtseva, I., Heinmann, A., Cassidy, D. and Triani, G., Synthethis and characterisation of nanocomposite materials prepared by dispersion of functional TiO2 nanoparticles in PMMA matrix. Journal of Materials Chemistry, 21(34), 13040-13036. (2011).

Atahan, P., Dodson, J., Li, X. Q., Zhou, X. Y., Hu, S. M., Bertuch, F., Sun, N., Subsistence and the isotopic signature of herding in the Bronze Age Hexi Corridor, NW Gansu, China. Journal of Archaeological Science, 38(7), 1747-1753. (2011).

Atahan, P., Dodson, J., Li, X. Q., Zhou, X. Y., Hu, S. M., Chen, L., Bertuch, F., Grice. K., Early Neolithic diets at Baijia, Wei River valley, China: stable carbon and nitrogen isotope analysis of human and faunal remains. Journal of Archaeological Science, 38(7), 2811-2817. (2011).

Avdeev, M., Thorogood, G.J., Carter, M.L., Kennedy, B.J., Ting, J., Singh, D.J., Wallwork, K.S., Antiferromagnetism in a Technetium Oxide Structure of $CaTc_{O3}$. Journal of the American Chemical Society, 133(6), 1654-1657. (2011).

Bacon, D.H., Edwards, L., Moffatt, J.E. and Fitzpatrick M.E., Synchrotron X-ray diffraction measurements of internal stresses during loading of steel-based metal matrix composites reinforced with TiB_2 particles. Acta Matrialia, 59(9), 3373-3383. (2011).

Baczmanski, A., Le Joncour, L., Panicaud, B., Francois, M., Braham, C., Paradowska, A.M., Wronski, S., Amara, S. and Chiron, R., Neutron time-of-flight diffraction used to study aged duplex stainless steel at small and large deformation until sample fracture, Journal of Applied Crystallography, 44(5), 966-982 (2011).

Bartkowiak, M., Kearley, G. J., Yethiraj, M., and Mulders, A. M., Symmetry of ferroelectric phase of $SrTi^{18}O^3$ determined by ab initio calculations. Physical Review B, 83(6), 064102. (2011).

Batlle, J.V. I., Vives-Lynch, S., Beaugelin-Seiller, K., Beresford, N., Hosseini, A., Kamboj, S., Yu, C., Copplestone, D., Newsome, L., Horyna, J., Johansen, M., Keum, D. K., Kurosawa, N., The estimation of absorbed dose rates for non-human biota: an extended inter-comparison. Radiation and Environmental Biophysics, 50(2), 231-251. (2011).

Beecham, C.J., Boag, S., Frost, C.D., McKetterick, T.J., Stewart, J.R., Andersen, K.H., Bentley, P.M., Jullien, D., ^{3}He polarization for ISIS TS2 phase I instruments. Physica B-Condensed Matter, 406(12), 2429-2432. (2011).

Begum, B. A., Bisws, S. K., Pandit, G. I., Saradhi, I. V., Waheed, S., Siddique, N., Seneviratn, M. C. S., Cohen, D. D., Markwitz, A. and Hopke, P. K., Long Range Transport of Soil Dust and Smoke Pollution in the South Asian Region. Atmospheric Pollution Research, 2(2), 151-157. (2011).

Bentley, P.M., Fouquet, P., Bohm, M., Sutton, I., Dewhurst, C.D., Andersen, K.H., Global optimization of an entire neutron guide hall. Journal of Applied Crystallography, 44(3), 483-488. (2011).

Bhatia, V. K., Kealley, C. S., Prior, M. J., Cortie, M. B., Martensite destabilization in $Au_7Cu_5Al_4$ shape-memory alloy. Acta Materialia, 59(5), 2193-2200. (2011).

Bhattacharyya, D., Mara, N.A., Dickerson, P., Hoagland, R.G. and Misra, A., Compressive flow behaviour of Al-TiN multilayes at nanometer scale layer thickness. Acta Materialia, 59(10), 3804-3816. (2011).

Bilus, A. N., McCulloch, D. G., Partridge, J. G., Evans, P. J. and Triani, G., Engineering titanium and aluminium oxide composites using atomic layer deposition. Journal of Applied Physics, 110(12), Article No. 123514. (2011).

Bird, D.K., Chagué-Goff, C. and Gero, A. Human response to extreme events: A review of three post-tsunami disaster case studies. Australian Geographer, 42 (3), 225-239. (2011).

Blazek, J., Gilbert, E.P., Application of small-angle X-ray and neutron scattering techniques to the characterisation of starch structure: A review. Carbohydrate Polymers, 85(2), 281-293. (2011).

Blazek, J., Gilbert, E.P., Copeland, L., Effects of monoglycerides on pasting properties of wheat starch after repeated heating and cooling. Journal of Cereal Science, 54(1), 151-159. (2011).

Bloch, E.D., Murray, L.J., Queen, W.L., Chavan, S., Maximoff, S.N., Bigi, J.P., Krishna, R., Peterson, V.K., Grandjean, F., Long, G.J., Smit, B., Bordiga, S., Brown, C.M., Long, J.R., Selective Binding of O(2) over N(2) in a Redox-Active Metal-Organic Framework with Open Iron(II) Coordination Sites. Journal of the American Chemical Society, 133(37), 14814-14822. (2011).

Boeer, A.B., Barra, A.L., Chibotaru, L.F., Collison, D., McInnes, E.J.L., Mole, R.A., Simeoni, G.G., Timco, G.A., Ungur, L., Unruh, T., Winpenny, R.E.P., A Spectroscopic Investigation of Magnetic Exchange Between Highly Anisotropic Spin Centers. Angewandte Chemie-International Edition, 50(17), 4007-4011. (2011).

Boland, D. D., Collins, R. N., Payne, T. E., and Waite, T. D., Effect of amorphous Fe(III) oxide transformation on the Fe(II)-mediated reduction of U(VI). Environmental Science and Technology, 45(4), 1327-1333. (2011).

Boldeman, J. W., Banati, R. Options for a light ion facility for hadron therapy and research. Journal and proceedings of the royal society of New South Wales, 144(441-442), 58-65. (2011).

Boland, D.D., Collins, R.N., Payne, T.E. and Waite, T.D., The inhibitory effect of silicate on the Fe(II)-catalysed crystallisation of Fe(III) minerals and the associated sequestration of uranium. Environmental Science and Technology, 45(4), 1327-1333. (2011).

Bourdier, T., Greguric, I., Roselt, P., Jackson, T., Faragalla, J., Katsifis, A., Fully-automated one-pot radiosynthesis of O-(2-[^{18}F]fluoroethyl)-L-tyrosine on the TracerLab FXFN module. Nuclear Medicine and Biology, 38(5), 645-651. (2011).

Bourdier, T., Shepherd, R., Berghofer, P., Jackson, T., Fookes, C. J., Denoyer, D., Dorow, D., Greguric, I., Gregoire, M-C., Hicks, R. J., Katsifis, A., Radiosynthesis and biological evaluation of L and D S-(3-[18F]Fluoropropyl)-homocysteine for tumor imaging using positron emission tomography. Journal of Medicinal Chemistry, 54(6), 1860-1870. (2011).

Bowman, D. M.J.S., Prior, L. D., Tng, D., Hua, Q., Brodribb, T. J., Continental-scale climate drivers of growth ring variability in an Australian conifer. Trees – Structure and Function. 25(5), 925-934.

Callaghan, M.D., Humphries, S.R., Law, M., Ho, M., Yan, K., Yeung, W.Y., Specimen-size dependency and modelling of energy evolution during high-temperature low-cycle fatigue of pressure vessel steel. Scripta Materialia, 65(4), 308-311. (2011).

Carolan, J. V., Hughes, C.E. and Hoffman, E.L., Dose Assessment for marine biota and humans from discharge of ^{131}I to the marine environment and uptake by algae in Sydney, Australia. Journal of Environmental Radioactivity, 102(10), 953-963. (2011).

Cavaye, H., Shaw, P.E., Smith, A.R.G., Burn, P.L., Gentle, I.R., James, M., Lo, S.C., Meredith, P., Solid State Dendrimer Sensors: Effect of Dendrimer Dimensionality on Detection and Sequestration of 2,4-Dinitrotoluene. Journal of Physical Chemistry C, 115(37), 18366-18371. (2011).

Chague-Goff, C., Schneider, J.L., Goff, J.R., Dominey-Howes, D., Strotz, L., Expanding the proxy toolkit to help identify past events - Lessons from the 2004 Indian Ocean Tsunami and the 2009 South Pacific Tsunami. Earth-Science Reviews, 107(SI. 1-2), 107-122. (2011).

Chambers, S., Williams, A.G., Zahorowski, W., Griffiths, A., Crawford, J., Separating remote fetch and local mixing influences on vertical radon measurements in the lower atmosphere. Tellus Series B Chemical and Physical Meteorology, 63(5), 843-859. (2011).

Chan, R. T. H., Garvey, C. J., Marcal, H., Russell, R. A., Manipulation of Polyhydroxybutyrate Properties through Blending with Ethyl-Cellulose for a Composite Biomaterial. International Journal of Polymer Science, 2011(2011), Art. No. 651549. (2011).

Chan, R. T. H., Marcal, H., Russell, R. A., Holden, P. J., Foster, L. J. R., Application of Polyethylene Glycol to Promote Cellular Biocompatibility of Polyhydroxybutyrate Films. International Journal of Polymer Science, 2011(2011), Art. No. 473045. (2011).

Chan, W.K., Haverkate, L.A., Borghols, W.J.H., Wagemaker, M., Picken, S.J., van Eck, E.R.H., Kentgens, A.P.M., Johnson, M.R., Kearley, G.J., Mulder, F.M., Direct View on Nanoionic Proton Mobility.Advanced Functional Materials, 21(8), 1364-1374. (2011).

Chan, Y. C., Hawas, O., Hawker, D., Vowles, P., Cohen, D. D., Stelcer, E., Simpson, R., Golding, G., Christensen, E., Using multiple type composition data and wind data in PMF analysis to apportion and locate sources of air pollutants. Atmospheric Environment, 45(2), 439-449. (2011).

Chen, J., Katsifis, A., Hu, C., Huang, X. F., Insulin decreases therapeutic efficacy in colon cancer cell line HT29 via the activation of the PI3K/Akt pathway. Current Drug Discovery Technologies, 8(2), 119-125. (2011).

Ciampi, S., James, M., Darwish, N., Luais, E., Guan, B., Harper, J.B., Gooding, J.J., Oxidative acetylenic coupling reactions as a surface chemistry tool. Physical Chemistry Chemical Physics, 13(34), 15624-15632. (2011).

Ciampi, S., James, M., Michaels, P., Gooding, J.J., Tandem "Click" Reactions at Acetylene-Terminated Si(100) Monolayers. Langmuir, 27(11), 6940-6949. (2011).

Clark, M.W., Harrison, J.J., and Payne, T.E., The pH-dependence and reversibility of uranium and thorium binding on a modified bauxite refinery residue using isotopic exchange techniques. Journal of Colloid and Interface Science, 356(2), 699-705. (2011).

Clements, R., Hester, J.R., Kennedy, B.J., Ling, C.D., Stampfl, A.P.J., The fluorite-pyrochlore transformation of $Ho2_{-y}Nd_yZr_2O_7$. Journal of Solid State Chemistry, 84(8), 2108-2113. (2011).

Cohen, D. D., Stelcer, E., Garton, D., Crawford, J., Fine Particle Characterisation, Source Apportionment and Long Range Dust Transport into the Sydney Basin: A long term study between 1998 and 2009. Atmospheric Pollution Research, 2(2), 182-189. (2011).

Cohen, T. J., Nanson, G. C., Jansen, J. D., Jones, B. G., Jacobs, Z., Treble, P., et al. Continental aridification and the vanishing of Australia's megalakes. Geology, 39(2), 167-170. (2011).

Cole, J.M., Burgi, H.B., McIntyre, G., Distinction of disorder, classical and quantum vibrational contributions to atomic mean-square amplitudes in dielectric pentachloronitrobenzene. Physical Review B, 83(22), Pages: Art. No. 224202. (2011).

Colella, M., Parkinson, A., Evans, T., Robertson, J. and Roux, C., The Effect of Ionizing Gamma Radiation on Natural and Synthetic Fibres and Its Implications for the Forensic Examination of Fibre Evidence. Journal of Forensic Sciences, 56(3), 591-605. (2011).

Collins, R. N., Saito, T., Aoyagi, N., Payne, T. E., Kimura, T., and Waite, T. D., Applications of Time-Resolved Laser Fluorescence Spectroscopy to the Environmental Biogeochemistry of Actinides. Journal of Environmental Quality, 40(3), 731-741. (2011).

Comarmond, M. J., Payne, T. E., Harrison, J. J., Thiruvoth, S., Wong, H. K., Aughterson, R. D., Lumpkin, G. R., Müller, K., Foerstendorf, H., Uranium sorption on various forms of titanium dioxide – influence of surface area, surface charge and impurities. Environmental Science and Technology, 45(13), 5536-5542. (2011).

Cortie, D.L. and Lewis, R.A., Role of vanguard counter-potential in terahertz emission due to surface currents explicated by three-dimensional ensemble Monte Carlo simulation. Physical Review B, 84(15), Art. No. 155328. (2011).

Cortie, M.B., Kealley, C.S., Bhatia, V., Thorogood, G.J., Elcombe, M. M. and Aveev, M., High temperature transformations of the $Au_7CU_5Al_4$ shape memory alloy. Journal of Alloys and Compounds, 509(8), 3502-3508. (2011).

Crawford, J., Cohen, D.D., Zahorowski, W., Chambers, S., Stelcer, E., A new method to combine IBA of fine aerosols with Radon-222 to determine source characteristic. Nuclear Instruments and Methods In Physics Research Section B-Beam Interactions With Materials And Atoms, 269(19), 2041-2051. (2011).

Crow, L., Robertson, L., Bilheux, H., Fleenor, M., Iverson, E., Tong, X., Stoica, D., Lee, W.T., The CG1 instrument development test station at the high flux isotope reactor. Nuclear Instruments and Methods in Physics Research Section a-Accelerators Spectrometers Detectors and Associated Equipment, ,634 (Suppl. 1), S71-S74. (2011).

Dalton, V. S., Long, L., Weickert, C. S., Zavitsanou, K., Paranoid schizophrenia is characterized by increased cannabinoid CB1 receptor binding in the dorsolateral prefrontal cortex. Neuropsychopharmacology, 36(8), 1620-1630. (2011).

Dalton, V. S., Zavitsanou, K., Rapid changes in D1 and D2 dopamine receptor binding in striatal subregions after a single dose of phencyclidine. Clinical Psychopharmacology and Neuroscience, 9(2), 67-72. (2011).

Daly, H. L., Hall, M. D., Failes, T. W., Zhang, M., Foran, G. J. and Hambley, T. W., Stabilization of Triam(m) inechloridoplatinum complexes by oxidation to PtIV. Australian Journal of Chemistry, 64(3), 273-278. (2011).

Danilkin, S.A., Avdeev, M., Sakuma, T., Macquart, R., Ling, C.D., Neutron diffraction study of diffuse scattering in $Cu_{2-\delta}$ Se superionic compounds. Journal of Alloys and Compounds, 509(18), 5460-5465. (2011).

Danilkin, S.A., Avdeev, M., Sakuma, T., Macquart, R., Ling, C.D., Rusina, M., Izaola, Z., Neutron scattering study of short-range correlations and ionic diffusion in copper selenide. Ionics, 17(1), 75-80. (2011).

Darwish, T. A., Evans, R. A., James, M. and Hanley, T. L., Spiropyran-Amidine: A Molecular Canary for Visual Recognition of Carbon Dioxide Gas. Chemistry: A European Journal, 17(41), 11399-11404. (2011).

Davis, M., Matmon, A., Fink, D., Ron, H., Niederniann, S., Dating Pliocene lacustrine sediments in the central Jordan Valley, Israel - Implications for cosmogenic burial dating. Earth and Planetary Science Letters, 305(3-4), 317-327. (2011).

Dearling, J. L. J., Voss, S. D., Dunning, P., Snay, E., Fahey, F., Smith, S. V., et al., Imaging cancer using PET - the effect of the bifunctional chelator on the biodistribution of a ^{64}Cu-labeled antibody. Nuclear Medicine and Biology, 38(1), 29-38. (2011).

del Rio, M.S., Garcia-Romero, E., Suarez, M., da Silva, I., Fuentes-Montero, L. and Martinez-Criado, G., Variability in sepiolite: Diffraction studies, American Mineralogist, 96(10), 1443-1454, (2011).

Deng, G.C., Pomjakushin, V., Petricek, V., Pomjakushina, E., Kenzelmann, M., Conder, K., Structural evolution of one-dimensional spin-ladder compounds $Sr_{14-x}Ca_xCu_{24}O_{41}$ with Ca doping and related evidence of hole redistribution. Physical Review B, 84(14), Art. No. 144111. (2011).

Deng, G.C., Radheep, D.M., Thiyagarajan, R., Pomjakushina, E., Wang, S., Nikseresht, N., Arumugam, S., Conder, K., High oxygen pressure single crystal growth of highly Ca-doped spin ladder compound $Sr_{14-x}Ca_xCu_{24}O_{41}$ (x > 12). Journal of Crystal Growth, 327(1), 182-188. (2011).

Denoyer, D., Potdevin, T., Roselt, P., Neels, O. C., Kirby, L., Greguric, I. et al., Improved detection of regional melanoma metastasis using 18F-6-Fluoro-N-[2-(Diethylamino)Ethyl] Pyridine-3-Carboxamide, a Melanin-specific PET probe, by perilesional administration. Journal of Nuclear Medicine, 52(1), 115-122. (2011).

Dikundwar, A. G., Venkateswarlu, C., Piltz, R. O., Chandrasekaran, S., Row, T. N. G., et al., Crystal structures of fluorinated aryl biscarbonates and a biscarbamate: a counterpoise between weak intermolecular interactions and molecular symmetry. Crystengcomm, 13(5), 1531-1538. (2011).

Du, G.D., Sharma, N., Peterson, V.K., Kimpton, J.A., Jia, D.Z. and Guo, Z.P., Br-Doped Li4Ti5O12 and Composite TiO2 Anodes for Li-ion Batteries: Synchrotron X-Ray and *in situ* Neutron Diffraction Studies. Advance Functional Materials, 21(20), 3990-3997. (2011).

Duan, X. Y., Cheung, S. C. P., Yeoh, G. H., Tu, J. Y., Krepper, E., and Lucas, D., Gas-liquid flows in medium and large vertical pipes. Chemical Engineering Science, 66(5), 872-883. (2011).

Dunstan, M.T., Southon, P.D., Kepert, C.J., Hester, J., Kimpton, J.A., Ling, C.D., Phase diagram, chemical stability and physical properties of the solid-solution $Ba_4Nb_{2-x}Ta_xO_9$. Journal of Solid State Chemistry, 184(10), 2648-2654. (2011).

Dutta, N.K., Truong, M.Y., Mayavan, S., Choudhury, N.R., Elvin, C.M., Kim, M., Knott, R., Nairn, K.M., Hill, A.J., A Genetically Engineered Protein Responsive to Multiple Stimuli. Angewandte Chemie-International Edition, 50(19), 4428-4431. (2011).

Edwards, A.J., Neutron Diffraction - Recent Applications to Chemical Structure Determination. Australian Journal of Chemistry, 64(7), 869-872. (2011).

Etienne, S., Buckley, M., Paris, R., Nandasena, A.K., Clark, K., Strotz, L., Chague-Goff, C., Goff, J., Richmond, B., The use of boulders for characterising past tsunamis: Lessons from the 2004 Indian Ocean and 2009 South Pacific tsunamis. Earth-Science Reviews, 107(1-2), 76-90. (2011).

Fischer M.J., Baldini L. M. A climate-isotope regression model with seasonally-varying and time-integrated relationships. Climate Dynamics, 37(11-12), 2235-2251. (2011).

Flores-Johnson, E. A. and Li, Q.M., Experimental study of the indentation of sandwich panels with carbon fibre-reinforced polymer face sheets and polymeric foam core. Composites Part B: Engineering, 42(5), 1212-1219. (2011).

Flores-Johnson, E. A.and Li, Q.M., Low velocity impact on polymeric foams. Journal of Cellular Plastics, 47(1), 45-63. (2011).

Flores-Johnson, E.A., Saleh, M., and Edwards, L., Ballistic performance of multi-layered metallic plates impacted by a 7.62-mm APM2 projectile. International Journal of Impact Engineering, 38(12), 1022-1032. (2011).

Flores-Johnson, E.A., Vázquez-Rodríguez, J.M., Herrera-Franco, P.J. and González-Chi, P.I., Photoelastic evaluation of fiber surface-treatments on the interfacial performance of a polyester fiber/epoxy model composite. Composites Part A: Applied Science and Manufacturing, 42 (8), 1017-1024. (2011).

Ford, S.J., Delamore, O.J., Evans, J.S.O., McIntyre, G.J., Johnson, M.R. and Radosavljević E. I., Giant Deuteron Migration During the Isosymmetric Phase Transition in Deuterated 3,5-Pyridinedicarboxylic Acid. Chemistry - A European Journal, 17(52), 14942-14951. (2011).

Foreman, A. L., Phillips, L., Kanellis, V. G., Hammoudeh, D., Naumann, C., Wong, H., Chisari, R., Hibbert, D. B., Lee, G. S. H., Patra, R., Julli, M., Chapman, J., Cooke, A. R., dos Remedios, C. G., A DNA-Based Assay For Toxic Chemicals In Wastewater. Environmental Toxicology And Chemistry, 30 (8), 1810-1818. (2011).

Freund, A.K., Rehm, C., Phase space optimisation of the USANS instrument Kookaburra at the ANSTO OPAL reactor. Nuclear Instruments and Methods in Physics Research Section a-Accelerators Spectrometers Detectors and Associated Equipment, 634(Suppl. 1), S81-S89. (2011).

Freund, A.K., Yu, D.H., Optimisation and fabrication of a composite pyrolytic graphite monochromator for the Pelican instrument at the ANSTO OPAL reactor. Nuclear Instruments and Methods in Physics Research Section a-Accelerators Spectrometers Detectors and Associated Equipment, 634(Suppl. 1), S75-S80. (2011).

Friend, A. J., Ayoko, G. A., Stelcer, E. and Cohen, D. Source apportionment of PM2.5 at two receptor sites in Brisbane, Australia. Environmental Chemistry, 8(6), 569-580. (2011).

Fruchter, N., Matmon, A., Avni, Y., Fink, D., Revealing sediment sources, mixing, and transport during erosional crater evolution in the hyperarid Negev Desert, Israel. Geomorphology, 134(3-4), 363-377. (2011).

Fuentes-Montero, L., Montero-Cabrera, M.E., Fuentes-Cobas, L., The software package ANAELU for X-ray diffraction analysis using two-dimensional patterns. Journal of Applied Crystallography, 44(Part 1), 241-246. (2011).

Ganguly, S., Edwards, L. and Fitzpatrick, M.E., Problems in using a comb sample as a stress-free reference for the determination of welding residual stress by diffraction. Materials Science and Engineering: A, 528(3), 1226-1232. (2011).

Garces, P., Glasser, F.P., Brew, D.R.M., Zornoza, E. and Paya, J., Pozzolanic Activity of a Spent Fluid Catalytic Cracking Catalyst Residue. Advances in Cement Research, 23(3), 105-111. (2011).

García-Veigas J., Cendón D.I., Pueyo J.J. and Peryt T. Zechstein saline brines in Poland, evidence of overturned anoxic ocean during the Late Permian mass extinction event. Chemical Geology, 290(3-4), 189-201. (2011).

Gardberg, A.S., Potter, B.S., Palmer, R.A., McIntyre, G.J. and Myles, D.A.A., The Neutron Structure of the Formyl Peptide Receptor Antagonist Cyclosporin H (CsH) Unambiguously Determines the Solvent and Hydrogen-Bonding Structure for Crystal Form II. Journal of chemical crystallography, 41(4), 470-480. (2011).

Gatta, G.D., McIntyre, G.J., Sassi, R., Rotiroti, N., Pavese, A., Hydrogen-bond and cation partitioning in muscovite: A single-crystal neutron-diffraction study at 295 and 20 K. American Mineralogist, 96(1), 34-41. (2011).

Gault, B., Chen, Y. M., Moody, M. P., Ohkubo, T., Hono, K. and Ringer, S. P., Influence of the wavelength on the spatial resolution of pulsed-laser atom. Journal of Applied Physics, 110(9), Article No. 094901. (2011).

Goff, J., Chagué-Goff, C., Dominey-Howes, D., McAdoo, B., Cronin, S., Bonte-Grapetin, M., Nichol, S., Horrocks, M., Cisternas, M. Lamarche, G., Pelletier, B., Jaffe, B., Dudley, W., Palaeotsunamis in the Pacific Islands. Earth-Science Reviews, 107(1-2, SI), 141-146. (2011).

Goff, J., Lamarche, G., Pelletier, B., Chagué-Goff, C., Strotz, L., Predecessors to the 2009 South Pacific tsunami in the Wallis and Futuna archipelago. Earth-Science Reviews, 107(1-2, SI), 91-106. (2011).

Gorjiara, T., Hill, R., Kuncic, Z., Bosi, S., Davies, J. B., Baldock, C., Radiological characterization and water equivalency of genipin gel for x-ray and electron beam dosimetry. Physics in Medicine and Biology, 56(15), 4685-4699. (2011).

Goto, K., Chagué-Goff, C., Fujino, S., Goff, J., Jaffe, B., Nishimura, Y., Richmond, B., Sugawara, D., Szczuciski, W., Tappin, D.R., Witter, R. and Yulianto, E. New insights of tsunami hazard from the 2011 Tohoku-oki event. Marine Geology, 290(1-4), 46-50. (2011).

Grage, S.L., Keleshian, A.M., Turdzeladze, T., Battle, A.R., Tay, W.C., May, R.P., Holt, S.A., Contera, S.A., Haertlein, M., Moulin, M., Pal, P., Rohde, P.R., Forsyth, V.T., Watts, A., Huang, K.C., Ulrich, A.S., Martinac, B., Bilayer-Mediated Clustering and Functional Interaction of MscL Channels. Biophysical Journal, 100(5), 1252-1260. (2011).

Greguric, I., Taylor, S., Pham, T., Wyatt, N., Jiang, D., Bourdier, T., Loc'h, C., Roselt, P., Neels, O., Katsifis, A., Radiosynthesis of a novel PET fluoronicotinamide for melanoma tumour PET imaging; ^{18}F MEL050. Australian Journal of Chemistry, 64, 873-879. (2011).

Griffith, M.J., James, M., Triani, G., Wagner, P., Wallace, G.G., Officer, D.L., Determining the Orientation and Molecular Packing of Organic Dyes on a TiO_2 Surface Using X-ray Reflectometry. Langmuir, 27(21), 12944-12950. (2011).

Griffiths, M.L., Drysdale, R.N., Vonhof, H.B., Gagan, M.K., Zhao, J.X., Ayliffe, L.K., Hantoro, W.S., Hellstrom, J.C., Cartwright, I., Frisia, S., Suwargadi, B.W., High-resolution stalagmite reconstructions for Australian-Indonesian monsson rainfall variability during Heinrich stadial 3 and Greenland interstadial 4. Earth And Planetary Science Letters, 303(1-2), 133-142. (2011).

Guralnik, B., Matmon, A., Avni, Y., Porat, N., and Fink, D., Constraining the evolution of river terraces with integrated OSL and cosmogenic nuclide data. Quaternary Geochronology, 6(1), 22-32. (2011).

Hackett, M.J., McQuillan, J.A., El-Assaad, F., Aitken, J.B., Levina, A., Cohen, D.D., Siegele, R., Carter, E.A., Grau, G.E., Hunt, N.H., Lay, P.A., Chemical alterations to murine brain tissue induced by formation fixation: implications for biospectroscopic imaging and mapping studies of disease pathogenesis. Analyst, 136(14), 2941-2952. (2011).

Hamelin, C.J., Diak, B.J., Pilkey, K., Multiscale modelling of the induced plastic anisotropy in bcc metals. International Journal of Plasticity, 27(8), 1185-1202. (2011).

Hanaor D., Triani, G., Sorrell, C., Morphology and Photocatalytic Activity of Highly Oriented Mixed Phase Titanium Dioxide Thin Films. Surface and Coatings Technology, 205(12), 3658-3664. (2011).

Haverd, V., Cuntz, M., Griffith, D., Keitel, C., Tadros, C., Twining, J., Measured deuterium in water vapour concentration does not improve the constraint on the partitioning of evapotranspiration in a tall forest canopy, as estimated using a soil vegetation atmosphere transfer model. Agricultural and forest meteorology, 151(6), 645-654. (2011).

He, L.Z., Onaizi, S.A., Dimitrijev-Dwyer, M., Malcolm, A.S., Shen, H.H., Dong, C.C., Holt, S.A., Thomas, R.K., Middelberg, A.P.J., Comparison of positional surfactant isomers for displacement of rubisco protein from the air-water interface. Journal of Colloid and Interface Science, 360(2), 617-622. (2011).

Herzog, G.F., Albrecht, A., Ma, P.X., Fink, D., Klein, J., Middleton, R., Bogard, D.D., Nyquist, L.E., Shih, C.Y., Garrison, D.H., Reese, Y., Masarik, J., Reedy, R.C., Rugel, G., Faestermann, T., Korschinek, G., Cosmic-Ray Exposure History of the Norton Country Enstatite Achondrite. Meteritics and Planetarty Science, 46(2), 284-310. (2011).

Hodge, E., McDonald, J., Fischer, M., Redwood, D., Hua, Q., Levchenko, V., Drysdale, R., Waring, C., Fink, D., Using the ^{14}C Bomb Pulse to date young speleothems. Radiocarbon, 53(2), 345-357. (2011).

Hoile, R., Banos, C., Colella, M., Roux, C. Bioterrorism: The effects of biological decontamination on the recovery of electronic evidence. Forensic Science International, 209(1-3), 143-148. (2011).

Hollins, S.E., Harrison, J.J., Jones, B.G., Zawadzki, A., Heijnis, H., Hankin, S., Reconstructing recent sedimentation in two urbanised coastal lagoons (NSW, Australia) using radioisotopes and geochemistry. Journal of Paleolimnology, 46(4), 579-596. (2011).

Holmes, R. L., Campbell, J.A., Linser, R., Hook, J.M., Burford, R.P., *In situ* preparation of poly(2-hydroxyethyl methacrylate)-titania hybrids using γ -radiation. Polymer, 52(20), 4471-4479. (2011).

Hopke, P., Cohen, D. D., Application of receptor modeling methods. Atmospheric Pollution Research, 2(2), 122-125. (2011).

Hudspeth, J.M., Stewart, G.A., Studer, A.J. and Goossens, D.J., Crystal and magnetic structures in Perovskite-related $La_{1-x}Ca_xFeO_{3-\delta}$ (x=0.2, 0.33). Journal of Physics Chemistry Solids, 72(12), 1543-1547. (2011).

Hunt, G. E., McGregor, I. S., Cornish, J. L., Callaghan, P. D., MDMA-induced c-Fos expression in oxytocin-containing neurons is blocked by pretreatment with the 5-HT-1A receptor antagonist WAY 100635. Brain Research Bulletin, 86(1-2), 65-73. (2011).

Huson, M.G., Strounina, E.V., Kealley, C.S., Rout, M.K., Church, J.S., Appelqvist, I.A.M., Gidley, M.J., Gilbert, E.P., Effects of Thermal Denaturation on the Solid-State Structure and Molecular Mobility of Glycinin. Biomacromolecules, 12(6), 2092-2102. (2011).

Ide, A., Drisko, G.L., Scales, N., Luca, V., Schiesser, C.H. and Caruso, R.A., Monitoring Bisphosphonate Surface Functionalization and Acid Stability of Hierarchically Porous Titanium Zirconium Oxides. Langmuir, 27(21), 12985 – 12995. (2011).

Jacques, D. A., Langley, D. B., Hynson, R. M. G., Whitten, A. E., Kwan, A., Guss, J. M., et al., Novel structure of an antikinase and its inhibitor. Journal of Molecular Biology, 405(1), 214-226. (2011).

Jacques, D.A., Langley, D.B., Kuramitsu, S., Yokoyama, S., Trewhella, J., Guss, J.M., The structure of TTHA0988 from Thermus thermophilus, a KipI-KipA homologue incorrectly annotated as an allophanate hydrolase. Acta Crystallographica Section D-Biological Crystallography, 67(Part 2), 105-111. (2011).

James, M., Ciampi, S., Darwish, T.A., Hanley, T.L., Sylvester, S.O., Gooding, J.J., Nanoscale Water Condensation on Click-Functionalized Self-Assembled Monolayers. Langmuir, 27(17), 10753-10762. (2011).

James, M., Darwish, T.A., Ciampi, S., Sylvester, S.O., Zhang, Z.M., Ng, A., Gooding, J.J., Hanley, T.L., Nanoscale condensation of water on self-assembled monolayers. Soft Matter, 7(11), 5309-5318. (2011).

James, M., Nelson, A., Holt, S.A., Saerbeck, T., Hamilton, W.A., Klose, F., The multipurpose time-of-flight neutron reflectometer “Platypus” at Australia’s OPAL reactor. Nuclear Instruments and Methods in Physics Research Section a-Accelerators Spectrometers Detectors and Associated Equipment, 632(1), 112-123. (2011).

Jeffries, C.M., Lu, Y.L., Hynson, R.M.G., Taylor, J.E., Ballesteros, M., Kwan, A.H. and Trewhella, J., Human Cardiac Myosin Binding Protein C: Structural Flexibility within an Extended Modular Architecture. Journal of Molecular Biology, 414(5), 735-748. (2011).

Johansen, D., Jeffries, C.M.J., Hammouda, B., Trewhella, J., Goldenberg, D.P., Effects of Macromolecular Crowding on an Intrinsically Disordered Protein Characterized by Small-Angle Neutron Scattering with Contrast Matching. Biophysical Journal, 100(4), 1120-1128. (2011).

Kabra, S., Yan, K., Mayer, S., Schmoelzer, T., Reid, M., Dippenaar, R., Clemens, H., Liss, K.D., Phase transition and ordering behavior of ternary Ti-Al-Mo alloys using *in situ* neutron diffraction. International Journal of Materials Research, 102(6, SI), 697-702. (2011).

Karanges, E., Li, K., Motbey, C., Callaghan, P., Katsifis, A., McGregor, I., Differential behavioural and neurochemical outcomes from chronic paroxetine treatment in adolescent and adult rats: a model of adverse antidepressant effects in human adolescents? International Journal of Neuropsychopharmacology, 14(4), 491-504. (2011).

Katsifis, A., Loc’h, C., Henderson, D., Bourdier, T., Pham, T., Greguric, I., et al., Rapid solid-phase extraction method for measurement of non-metabolised peripheral benzodiazepine receptor ligands, ^{18F}PBR102 and ^{18F}PBR111, in rat and primate plasma. Nuclear Medicine and Biology, 38(1), 137-148. (2011).

Kawaguchi, D., Nelson, A., Masubuchi, Y., Majewski, J.P., Torikai, N., Yamada, N.L., Sarah, A.R.S., Takano, A. and Matsushita, Y., Precise Analyses of Short-Time Relaxation at Asymmetric Polystyrene Interface in Terms of Molecular Weight by Time-Resolved Neutron Reflectivity Measurements, Macromolecules, 44(23), 9424-9433. (2011).

Kench, P. L., Lin, J., Gregoire, M-C., Meikle, S. R., An investigation of inconsistent projections and artefacts in multi-pinhole SPECT with axially aligned pinholes. Physics in Medicine and Biology, 56(23), 7487-7503. (2011).

Kennedy, B. J., Avdeev, M., Structure of C-type Gd_2O_3; A powder neutron diffraction study using enriched ^{160}Gd. Australian Journal of Chemistry, 64(1), 119-121. (2011).

Kennedy, B.J., and Avdeev, M., The structure of B-type Sm_2O_3; A powder neutron diffraction study using enriched 154Sm, Solid State Science, 13(9), 1701-1703, (2011).

Kennedy, B. J., Zhou, Q. D., The ferroelectric phase of $CdTiO_3$: A powder neutron diffraction study. Journal of Solid State Chemistry, 184(11), 2987-2993. (2011).

Kennedy, B.J., Zhou, Q.D., Avdeev, M., Neutron diffraction studies of $Gd_2Zr_2O_7$ pyrochlore. Journal of Solid State Chemistry, 184(7), 1695-1698. (2011).

Khan, M.K., Fitzpatrick, M.E., Hainsworth, S. V. and Edwards, L., Effect of residual stress on the nanoindentation response of aerospace aluminium alloys. Computational Materials Science, 50(10), 2967-2976. (2011).

Khan, M.K., Fitzpatrick, M.E., Hainsworth, S.V., Evans, A.D. and Edwards, L., Application of synchrotron X-ray diffraction and nanoindentation for the determination of residual stress fields around scratches. Acta Matrialia, 59(22), 7508-7520. (2011).

Kinsela, A. S., Collins, R. N., and Waite, T. D., Speciation and transport of arsenic in an acid sulfate soil-dominated catchment, eastern Australia. Chemosphere, 82(6), 879-887. (2011).

Kirstein, O., Zhang, J.F., Kisi, E.H. and Riley, D.P., Ab Initio Phonon Dispersion Curves Used to Check Experimentally Determined Elastic Constants of the MAX Phase Ti_3SiC_2. Advanced Materials Research, 275, 135-138. (2011).

Kjallman, T.H.M., Nelson, A., James, M., Dura, J.A., Travas-Sejdic, J., McGillivray, D. J., A neutron reflectivity study of the interfacial and thermal behaviour of surface-attached hairpin DNA. Soft Matter, 7(10), 5020-5029. (2011).

Ko, J. H., Reilhac, A., Ray, N., Rusjan, P., Bloomfield, P., Pellecchia, G., Houle, S., Strafella, A. P., Analysis of variance in neuroreceptor ligand imaging studies. Public Library of Science, 6(8), e23298. (2011).

Kobayashi, T., Ryder, D.S., Ralph, T.J., Mazumder, D., Saintilan, N., Iles, J., Knowles, L., Thomas, R., Hunter, S., Longitudinal spatial variation in ecological conditions in an in-channel floodplain river system during flow pulses. River Research and Applications, 27(4), 461-472. (2011).

Koo, H.J., Lee, C., Whangbo, M.H., McIntyre, G.J., Kremer, R.K., On the Nature of the Spin Frustration in the CuO_2 Ribbon Chains of $LiCuVO_4$: Crystal Structure Determination at 1.6 K, Magnetic Susceptibility Analysis, and Density Functional Evaluation of the Spin Exchange Constants. Inorganic Chemistry, 50(8), 3582-3588. (2011).

Kuperkar, K.C., Mata, J.P., Bahadur, P., Effect of 1-alkanols/salt on the cationic surfactant micellar aqueous solutions-A dynamic light scattering studyJournal. Colloids and Surfaces a-Physicochemical and Engineering Aspects, 380(1-3), 60-65. (2011).

Larsen, J. R. Was evaporation lower during the Last Glacial Maximum? Quaternary Australasia, 28(1), 11-13. (2011).

Law, M., Luzin, V., Effect of spatial variation of stress-free lattice spacings on measured residual stresses. Journal of Strain Analysis for Engineering Design, 46(8), 837-841. (2011).

Le Brun, A.P., Holt, S.A., Shah, D.S.H., Majkrzak, C.F., Lakey, J.H., The structural orientation of antibody layers bound to engineered biosensor surfaces. Biomaterials, 32(12), 3303-3311. (2011).

Le Brun, A.P., Shah, D.S.H., Athey, D., Holt, S.A., Lakey, J.H., Self-Assembly of Protein Monolayers Engineered for Improved Monoclonal Immunoglobulin G Binding. International Journal of Molecular Sciences, 12(8), 5157-5167. (2011).

Le, V. S., Specific radioactivity of neutron induced radioisotopes: assessment methods and application for medically useful ^{177}Lu production as a case. Molecules, 16(1), 818-846. (2011).

Lee, K H, Schwenn, P E, Smith, A R. G., Cavaye, H., Shaw, P. E., and James, M., et al., Morphology of all-solution-processed “bilayer” organic solar cells. Advanced Materials, 23(6), 766-770. (2011).

Lehnert, W., Gregoire, M-C., Reilhac, A., Meikle, S. R., Analytical positron range modelling in heterogeneous media for PET Monte Carlo simulation. Physics in Medicine and Biology, 56(11), 3313-3335. (2011).

Li, Q.M. and Flores-Johnson, E.A., Hard projectile penetration and trajectory stability. International Journal of Impact Engineering, 38(10), 815-823. (2011).

Li, X.L., Cai, K.F., Yu, D.H. and Wang, Y.Y., Electrodeposition and characterization of thermoelectric Bi_2Te_2Se/Te multilayer nanowire arrays. Superlattices and Microstructures, 50(5), 557-562. (2011).

Li, X.Q., Sun, N., Dodson, J., Ji, M., Zhao, K.L., Zhou, X.Y., The impact of early smelting on the environment of Huoshiliang in Hexi Corridor, NW China, as recorded by fossil charcoal and chemical elements. Palaeogeography Palaeoclimatology Palaeoecology, 305 (1-4), 329-336. (2011).

Li, X.Q., Zhao, K., Dodson, J., Zhou, X. Y., Moisture dynamics in central Asia for the last 15 kyr: new evidence from Yili Valley, Xinjiang, NW China. Quaternary Science Reviews, 30(23-24), 3457-3466. (2011).

Lin, H. Q., Meriaty, H., Katsifis, A., Prediction of synergistic antitumour effect of gefitinib and radiation in vitro. Anticancer Research, 31(9), 2883-2888. (2011).

Liu, J., Yuan, L.X., Yang, X.S., Elbert, A., Harris, A.T., Synthesis of vertically aligned carbon nanotube arrays on polyhedral Fe/Al_2O_3 catalysts. Chemical Communications, 47(22), 6434-6436. (2011).

Low, I. M., Pang, W. K., Kennedy, S. J., Smith, R. I., High-temperature thermal stability of Ti_2AlN and Ti_4AlN_3: a comparative diffraction study. Journal of the European Ceramic Society, 31(1-2), 159-166. (2011).

Lu, Y.L., Jeffries, C.M., Trewhella, J., Invited Review: Probing the Structures of Muscle Regulatory Proteins Using Small-Angle Solution Scattering. Biopolymers, 95(8, SI), 505-516. (2011).

Luzin, V., Spencer, K., Zhang, M.X., Residual stress and thermo-mechanical properties of cold spray metal coatings. Acta Materialia, 59(3), 1259-1270. (2011).

Mackintosh, A., Golledge, N., Domack, E., Dunbar, R., Leventer, A., White, D., et al., Retreat of the East Antarctic ice sheet during the last glacial termination. Nature Geoscience, 4(3), 195-202. (2011).

Marsilius, M., Granzow, T., Jones, J.L., Quantitative comparison between the degree of domain orientation and nonlinear properties of a PZT ceramic during electrical and mechanical loading. Journal of Materials Research, 26(9), 1126-1132. (2011).

Mata, J.P., Udabage, P., Gilbert, E.P., Structure of casein micelles in milk protein concentrate powders via small angle X-ray scattering. Soft Matter, 7(8), 3837-3843. (2011).

Mattner, F., Bandin, D. L., Staykova, M., Berghofer, P., Gregoire, M-C., Ballantyne, P., Quinlivan, M., Fordham, S., Pham, T., Willenborg, D. O., Katsifis, A., Evaluation of [^{123}I]-CLINDE as a potent SPECT radiotracer to assess the degree of astroglia activation in cuprizone-induced neuroinflammation. European Journal of Nuclear Medicine and Molecular Imaging, 38(8), 1516-1528. (2011).

Mazumder, D., Saintilan, N., Williams, R. J., and Szymczak, R., Trophic importance of a temperate intertidal wetland to resident and itinerant taxa: evidence from multiple stable isotope analyses. Marine and Freshwater Research, 62(1), 11-19. (2011).

McGregor H. V., Fischer M. J., Gagan M. K., Fink, D., Woodroffe, C.D., Environmental control of the oxygen isotope composition of Porites coral microatolls. Geochimica Et Cosmochimica Acta, 75(14), 3930-3944. (2011).

McGregor, H. V, Hellstrom, J., Fink, D., Hua, Q., Woodroffe, C. D., Rapid U-series dating of young fossil corals by laser ablation MC-ICPMS. Quaternary Geochronology, 6(2), 195-206. (2011).

Miao, M.H., Hawkins, S.C., Cai, J.Y., Gengenbach, T.R., Knott, R., Huynh, C.P., Effect of gamma-irradiation on the mechanical properties of carbon nanotube yarns. Carbon, 49(14), 4940-4947. (2011).

Mihalik, M., Prokleska, J., Kamarad, J., Prokes, K., Isnard, O., McIntyre, G.J., Donni, A., Yoshii, S., Kitazawa, H., Sechovsky, V., de Boer, F.R., NdRhSn: A ferromagnet with an antiferromagnetic precursor. Physical Review B, 83(10), Art. No.104403. (2011).

Miiller, W., Avdeev, M., Zhou, Q., Studer, A.J., Kennedy, B.J., Kearley, G.J. and Ling, C.D., Spin-gap opening accompanied by a strong magnetoelastic response in the S=1 magnetic dimer system $Ba_3BiRu_2O_9$. Physical Review B, 84(22), Art. No. 220406. (2011).

Miiller, W., Christensen, M., Khan, A., Sharma, N., Macquart, R. B., Avdeev, M., et al., $YCa_3(VO)_3(BO_3)_4$: a kagom compound based on vanadium(III) with a highly frustrated ground state. Chemistry of Materials, 23(5), 1315-1322. (2011).

Minakshi, M., Blackford, M.G. and Ionescu, M., Characterization of alkaline earth oxide additions to the MnO_2 cathode in an aqueous secondary battery. Journal of Alloys and Compounds, 509(20), 5974-5980. (2011).

Minakshi, M., Sharma, N., Ralph, D., Appadoo, D., Nallathamby, K., Synthesis and Characterization of $Li(Co_{0.5}Ni_{0.5})PO_4$ Cathode for Li-Ion Aqueous Battery Applications. Electrochemical and Solid State Letters, 14(6), A86-A89. (2011).

Minakshi, M., Singh, P., Sharma, N., Blackford, M., and Ionescu, M., Lithium extraction-insertion from/into $LiCoPO_4$ in aqueous batteries. Industrial and Engineering Chemistry Research, 50(4), 1899-1905. (2011).

Mitchell, M. R., Reader, S. W., Johnston, K. E., Pickard, C. J., Whittle, K. R. and Ashbrook, S. E., ^{119}Sn MAS NMR and first-principles calculations for the investigation of disorder in stannate pyrochlores. Physical Chemistry Chemical Physics, 13(2), 488-497. (2011).

Mole, R.A., Stride, J.A., Henry, P.F., Hoelzel, M., Senyshyn, A., Alberola, A., Garcia, C.J.G., Raithby, P.R., Wood, P.T. , Two Stage Magnetic Ordering and Spin Idle Behavior of the Coordination Polymer $Co\text{-}3(OH)_{2(}C_4O_4)_2 \cdot 3H_2O$ Determined Using Neutron Diffraction. Inorganic Chemistry, 50(6), 2246-2251. (2011).

Mooney, S. D., Harrison, S. P., Bartlein, P. J., Daniau, A. -L., Stevenson, J., Brownlie, K. C., et al., Late Quaternary fire regimes of Australasia. Quaternary Science Reviews, 30(1-2), 28-46. (2011).

Morgan, D. L., Triani, G., Blackford, M. G., Raftery, N. A., Frost, R. L., and Waclawik, E. R., Alkaline hydrothermal kinetics in titanate nanostructure formation. Journal of Materials Science, 46(2), 548-557. (2011).

Mulders, A.M., Bartkowiak, M., Hester, J.R., Pomjakushina, E., Conder, K., Ferroelectric charge order stabilized by antiferromagnetism in multiferroic $LuFe_2O_4$. Physical Review B, 84(14), Art. No. 140403. (2011).

Mume, E., Lynch, D. E., Uedono, A., Smith, S. V., Investigating the binding properties of porous drug delivery systems using nuclear sensors and Positron Annihilation Lifetime Spectroscopy – predicting conditions for optimum performance. Dalton Transactions, 40(23), 6278-6288. (2011).

Muransky, O., Smith, M.C., Bendeich, P.J., Edwards, L., Validated numerical analysis of residual stresses in Safety Relief Valve (SRV) nozzle mock-ups. Computational Materials Science, 50(7), 2203-2215. (2011).

Muscheler, R. and Heikkila, U., Constraints on long-term changes in solar activity from the range of variability of cosmogenic radionuclide records. Astrophysics and Space Sciences Transactions, 7(3), 355-364. (2011).

Nadeem, M.A., Thornton, A.W., Hill, M.R., Stride, J.A., A flexible copper based microporous metal-organic framework displaying selective adsorption of hydrogen over nitrogen. Dalton Transactions, 40(13), 3398-3401. (2011).

Naidoo-Variawa, S., Lehnert, W., Banati, R. B., and Meikle, S. R., Scatter correction for large non-human primate brain imaging using microPET. Physics in Medicine and Biology, 56(7), 2131-2143. (2011).

Nguyen, T.-H., Hanley, T., Porter, C. J. H., Boyd, B. J., Nanostructured liquid crystalline particles provide long duration sustained-release effect for a poorly water soluble drug after oral administration. Journal of Controlled Release, 153(2), 180–186. (2011).

Noked, O., Yakovlev, S., Greenberg, Y., Garbarino, G., Shuker, R., Avdeev, M., Sterer, E., Pressure-induced amorphization of $La_{1/3}NbO_3$. Journal of Non-Crystalline Solids, 357(18), 3334-3337. (2011).

Nuhiji, B., Attard, D., Thorogood, G., Hanley, T., Magniez, K. Fox, B., The effect of alternate heating rates during cure on the structure-property relationships of epoxy/MMT clay nanocomposites. Composites Science and Technology, 71(15), 1761-1768. (2011).

Okal, E.A., Borrero, J.C., Chague-Goff, C. (2011). Tsunamigenic predecessors to the 2009 Samoa Earthquake. Earth-Science Reviews, 107(1-2), 128-140. (2011).

Ouladdiaf, B., Archer, J., Allibon, J.R., Decarpentrie, P., Rodriguez-Carvajal, J., Lemée-Cailleau, M.H., Hewat, A.W., York, S., Brau, D. and McIntyre, G.J., CYCLOPS - a reciprocal-space explorer based on CCD neutron detectors. Journal of applied crystallography, 44, 392-397. (2011).

Pang, W. K., Low, I. M., O'Connor, B. H., Peterson, V. K., Studer, A. J., Palmquist, J. P., *In situ* diffraction study of thermal decomposition in Maxthal Ti_2AlC. Journal of Alloys and Compounds, 509(1), 172-176. (2011).

Pappas, C., Lelievre-Berna, E., Bentley, P., Falus, P., Fouquet, P., Farago, B., Magnetic fluctuations and correlations in MnSi: Evidence for a chiral skyrmion spin liquid phase. Physical Review B, 83(22), Art. No. 224405. (2011).

Paskevicius, M., Sheppard, D.A., Chaudhary, A.L., Webb, C.J., Gray, E.M., Tian, H.Y., Peterson, V.K., Buckley, C.E., Kinetic limitations in the Mg-Si-H system. International Journal of Hydrogen Energy, 36(17), 10779-10786. (2011).

Pastuovic, Z., Vittone, E., Capan, I., Jaksic, M., Probability of divacancy trap production in silicon diodes exposed to focused ion beam irradiation. Applied Physics Letters, 98(9), Article No., 092101. (2011).

Patwardhan, S. V., Holt, S. A., Kelly, S. M., Kreiner, M., Perry, C. C. and van der Walle, C. F., Silica Condensation by a Silicate in alpha Homologue Involves Surface-Induced Transition to a Stable Structural Intermediate Forming a Saturated Monolayer. Biomacromolecules, 11(11), 3126-3135. (2011).

Payten, W. M., Wei, T., Snowden, K. U., Bendeich, P., Law, M., and Charman, D., Crack initiation and crack growth assessment of a high pressure steam chest. International Journal of Pressure Vessels and Piping, 88(1), 34-44. (2011).

Payten, W., Charman, D., Chapman, A., Bashiri, K. and Bendeich, P., Life Assessment and Inspection of a Hot Reheat Turbine Bifurcation. Engineering Failure Analysis, 18(6), 1445-1457. (2011).

Pearson, S., Hua, Q.A., Allen, K., Bowman, D.M.J.S., Validating putatively cross-dated Callitris tree-ring chronologies using bomb-pulse radiocarbon analysis. Australian Journal Of Botany, 59(1), 7-17. (2011).

Peterson, V.K., Brown, C.M., Liu, Y., Kepert, C.J., Structural Study of D_2 within the Trimodal Pore System of a Metal Organic Framework. Journal of Physical Chemistry C, 115(17), 8851-8857. (2011).

Peterson, V.K., Shoko, E., Kearley, G.J., The effect of host relaxation and dynamics on guest molecule dynamics in H_2/tetrahydrofuran-hydrate. Faraday Discussions, 151, 37-46. (2011).

Phan, S., Fong, W.K., Kirby, N., Hanley, T. and Boyd, B. J., Evaluating the link between self-assembled mesophase structure and drug release. International Journal of Pharmaceutics, 421(1), 176-182. (2011).

Pogson R.E., Osborne R.A.L., Colchester D.M. and Cendón D.I., Sulfate and phosphate-sulfate speleothemes at Jenolan Caves, New South Wales. Acta Carsologica, 40(2), 239–254. (2011).

Pojprapai, S., Simons, H., Studer, A.J., Luo, Z.H., Hoffman, M., Temperature Dependence on Domain Switching Behavior in Lead Zirconate Titanate Under Electrical Load via *In situ* Neutron Diffraction. Journal of the American Ceramic Society, 94(10), 3202-3205. (2011).

Popa, M.E., Vermeulen, A.T., van den Bulk, W.C.M., Jongejan, P.A.C., Batenburg, A.M., Zahorowski, W., Rockmann, T., H_2 vertical profiles in the continental boundary layer: measurements at the Cabauw tall tower in The Netherlands. Atmospheric Chemistry And Physics, 11(13), 6425-6443. (2011).

Princep, A.J., Mulders, A.M., Staub, U., Scagnoli, V., Nakamura, T., Kikkawa, A., Lovesey, S.W., Balcar, E., Triakontadipole and high-order dysprosium multipoles in the antiferromagnetic phase of DyB_2C_2. Journal of Physics-Condensed Matter, 23(26), Art. No. 266002. (2011).

Qasim, I., Kennedy, B.J., Zhang, Z. M., Avdeev, M. and Jang, L. Y., X-ray absorption near edge structure and crystallographic studies of the mixed valence oxide $SrRu_{0.8}Ni_{0.2}O_3$. Journal of Physics: Condensed Matter , 23(43), Art. No. 435401. (2011).

Qin, J., Taylor, D., Atahan, P., Zhang, X., Wu, G., Dodson, J., et al., Neolithic agriculture, freshwater resources and rapid environmental changes on the lower Yangtze, China. Quaternary Research, 75(1), 55-65. (2011).

Qu, D.D., Liss, K.D., Yan, K., Reid, M., Almer, J.D., Wang, Y.B., Liao, X.Z., Shen, J., On the Atomic Anisotropy of Thermal Expansion in Bulk Metallic Glass. Advanced Engineering Materials, 13(9), 861-864. (2011).

Queen, W. L., Brown, C. M., Britt, D. K., Zajdel, P., Hudson, M. R. and Yaghi, O. M., Site-Specific CO2 Adsorption and Zero Thermal Expansion in an Anisotropic Pore Network. The journal of physical chemistry C, 115(50), 24915-24919. (2011).

Rajkhowa, R., Naik, R., Wang, L., Smith, S. V., Wang, X., An investigation into transition metal ion absorption properties of silk fibres and particles using radioisotopes. Journal of Applied Polymer Science, 119(6), 3630-3639. (2011).

Randau, C., Garbe, U., Brokmeier, H.G., StressTextureCalculator: a software tool to extract texture, strain and microstructure information from area-detector measurements. Journal of Applied Crystallography, 44(Part 3), 641-646. (2011).

Ratcliff, W., Kan, D., Chen, W.C., Watson, S., Chi, S.X., Erwin, R., McIntyre, G.J., Capelli, S.C., Takeuchi, I., Neutron Diffraction Investigations of Magnetism in $BiFeO_3$ Epitaxial Films. Advanced Functional Materials, 21(9), 1567-1574. (2011).

Reddy, M.V., Raju, M.J.S., Sharma, N., Quan, P.Y., Nowshad, S.H., Emmanuel, H.E.C., Peterson, V.K., Chowdari, B.V.R., Preparation of $Li_{1.03}Mn_{1.97}O_4$ and $Li_{1.06}Mn_{1.94}O_4$ by the Polymer Precursor Method and X-ray, Neutron Diffraction and Electrochemical Studies. Journal of the Electrochemical Society, 158(11), A1231-A1236. (2011).

Reehuis, M., Ulrich, C., Prokes, K., Mat'as, S., Fujioka, J., Miyasaka, S., et al., Structural and magnetic phase transitions of the orthovanadates RVO_3 (R= Dy, Ho, Er) as seen via neutron diffraction. Physical Review B, 83(6), 064404. (2011).

Ricco, M., Pontiroli, D., Mazzani, M., Choucair, M., Stride, J. A. and Yazyev, O. V., Muons Probe Strong Hydrogen Interactions with Defective Graphene. Nano Letters, 11(11), 4919-4922. (2011).

Richmond, B.M., Buckley, M., Etienne, S., Chague-Goff, C., Clark, K., Goff, J., Dominey-Howes, D., Strotz, L., Deposits, flow characteristics, and landscape change resulting from the September 2009 South Pacific tsunami in the Samoan islands. Earth-Science Reviews, 107(1-2, SI), 38-51. (2011).

Rizwan, S. B., Assmus, D., Boehnke, A., Hanley, T., Boyd, B. J., Rades, T., Hook, S., Preparation of phytantriol cubosomes by solvent precursor dilution for the delivery of protein vaccines. European Journal of Pharmaceutics and Biopharmaceutics, 79 (1, SI), 15-22. (2011).

Rodriguez, D.M., Kennedy, S.J., Bentley, P.M., Properties of elliptical guides for neutron beam transport and applications for new instrumentation concepts. Journal of Applied Crystallography, 44(Part 4), 727-737. (2011).

Rodriguez, E. E., Poineau, F., Llobet, A., Kennedy, B. J., Avdeev, M., Thorogood, G. J., et al., High temperature magnetic ordering in the 4d perovskite SrTcO3. Physical Review Letters, 106(6), 067201. (2011).

Roest, R., Latella, B. A., Heness, G., Ben-Nissan, B., Adhesion of sol-gel derived hydroxyapatite nanocoatings on anodised pure titanium and titanium (Ti6Al4V) alloy substrates. Surface and Coatings Technology, 205(11), 3520-3529. (2011).

Saerbeck, T., Loh, N., Lott, D., Toperverg, B.P., Mulders, A.M., Rodriguez, A.F., Freeland, J.W., Ali, M., Hickey, B.J., Stampfl, A.P.J., Klose, F., Stamps, R.L., Spatial Fluctuations of Loose Spin Coupling in CuMn/Co Multilayers. Physical Review Letters, 107(12), 7201-7201. (2011).

Saines, P.J., Yeung, H.H.M., Hester, J.R., Lennie, A.R., Cheetham, A.K., Detailed investigations of phase transitions and magnetic structure in Fe(III), Mn(II), Co(II) and Ni(II) 3,4,5-trihydroxybenzoate (gallate) dihydrates by neutron and X-ray diffraction. Dalton Transactions, 40(24), 6401-6410. (2011).

Salamakha, L., Bauer, E., Michor, H., Hilscher, G., Muller, H., Svagera, R., Sologub, O., Rogl, P., Hester, J., Roisnel, T., Giester, G., Mudryi, S., First-Order Phase Transition in a New $CaCu_5$-Related Antimonide, $CePt_5Sb$. Chemistry of Materials, 23(17), 4016-4024. (2011).

Schmoelzer, T., Liss, K.D., Staron, P., Mayer, S., Clemens, H., The Contribution of High-Energy X-Rays and Neutrons to Characterization and Development of Intermetallic Titanium Aluminides. Advanced Engineering Materials, 13(8), 685-699. (2011).

Schmoelzer, T., Liss, K.D., Rester, M., Yan, K., Stark, A., Reid, M., Peel, M. and Clemens, H., Dynamic Recovery and Recrystallization During Hot-Working in an Advanced TiAl Alloy. Praktische Metallographie-Practical Metallography, 48(12), 632-642 (2011).

Schmoelzer, T., Mayer, S., Sailer, C., Haupt, F., Guther, V., Staron, P.,; Liss, K.D., Clemens, H., *In situ* Diffraction Experiments for the Investigation of Phase Fractions and Ordering Temperatures in Ti-44 at% Al-(3-7) at% Mo Alloys. Advanced Engineering Materials, 13(4), 306-311. (2011).

Schokker, E.P., Church, J.S., Mata, J.P., Gilbert, E.P., Puvanenthiran, A., Udabage, P., Reconstitution properties of micellar casein powder: Effects of composition and storage. International Dairy Journal, 21(11), 877-886. (2011).

Shamba, P., Debnath, J.C., Zeng, R., Wang, J.L., Campbell, S.J., Kennedy, S.J., Dou, S.X., Reduction of hysteresis losses in the magnetic refrigerant $La_{0.8}Ce_{0.2}Fe_{11.4}Si_{1.6}$ by the addition of boron. Journal of Applied Physics, 109(7), Art. No. 07a940. (2011).

Sharma, N., Du, G. D., Studer, A. J., Guo, Z. P., Peterson, V. K., *In situ* neutron diffraction study of the MoS_2 anode using a custom-built Li-ion battery. Solid State Ionics, 199-200, 37-43. (2011).

Sharma, N., Reddy, M.V., Du, G.D., Adams, S., Chowdari, B.V.R., Guo, Z.P., Peterson, V.K. , Time-Dependent *in situ* Neutron Diffraction Investigation of a $LiCo_{0.16}Mn_{1.84}O_4$ Cathode. Journal of Physical Chemistry C, 115(43), 21473-21480. (2011).

Shen, H.H., Hartley, P.G., James, M., Nelson, A., Defendi, H., McLean, K.M., The interaction of cubosomes with supported phospholipid bilayers using neutron reflectometry and QCM-D. Soft Matter, 7(18), 8041-8049. (2011).

Shiga, Y., Greene, R.S.B., Scott K. M.and Stelcer, E., Recognising terrestrially-derived salt (NaCl) in SE Australian dust. Aeolian Research, 2(4), 215-220. (2011).

Shima, T., Luo, Y., Stewart, T., Bau, R., McIntyre, G.J., Mason, S.A., Hou, Z.M., Molecular heterometallic hydride clusters composed of rare-earth and d-transition metals. Nature Chemistry, 3(10), 814-820. (2011).

Shoko, E., Smith, M. F. and McKenzie, R. H., Charge distribution and transport properties in reduced ceria phases: A review. Journal of Physics and Chemistry of Solids, 72(12), 1482-1494. (2011).

Simons, H., Daniels, J., Jo, W., Dittmer, R., Studer, A., Avdeev, M., et al., Electric-field-induced strain mechanisms in lead-free 94%($Bi_{1/2}Na_{1/2}$)TiO_3-6%$BaTiO_3$. Applied Physics Letters, 98(8), 082901. (2011).

Sloss, C.R., Jones, B. G., Brooke, B. P., Heijnis, H., Murray-Wallace, C. V., Contrasting sedimentation rates in Lake Illawarra and St Georges Basin, two large barrier estuaries on the southeast coast of Australia. Journal of Paleolimnology, 46(4), 561-577. (2011).

Smith, A.R.G., Ruggles, J.L., Cavaye, H., Shaw, P.E., Darwish, T.A., James, M., Gentle, I.R., Burn, P.L., Investigating Morphology and Stability of Fac-tris (2-phenylpyridyl)iridium(III) Films for OLEDs. Advanced Functional Materials, 21(12), 2225-2231. (2011).

Smith, H.G., Sheridan, G.J., Lane, P.N.J., Noske, P.J., Heijnis, H., Changes to sediment sources following wildfire in a forested upland catchment, southeastern Australia. Hydrological Processes, 25(18), 2878-2889. (2011).

Solanki, R.S., Singh, A.K., Mishra, S.K., Kennedy, S.J., Suzuki, T., Kuroiwa, Y., Moriyoshi, C., Pandey, D., Ground state of ($Pb_{0.94}Sr_{0.06}$)($Zr_{0.53}Ti_{0.47}$)O_3 in the morphotropic phase boundary region: Evidence for a monoclinic C c space group. Physical Review B, 84(14), Art. No. 144116. (2011).

Sowada, K., Jacobsen, G.E., Bertuch, F., Palmer, T., Jenkinson, A., Who's that lying in my coffin? An imposter exposed by ^{14}C dating. Radiocarbon, 53(2), 221-228. (2011).

Spindler, M. W. and Payten, W M, Advanced Ductility Exhaustion Methods for the Calculation of Creep Damage During Creep-Fatigue Cycling. Journal of ASTM International, 8(7), Paper ID: JAI103806. (2011).

St John, A. M., Stephen P. Best, S. P., Wang, Y. D., Tobin, M., Puskar, L., Siegele, R., Cattrall, R. W. and Kolev, S. D., Micron-scale 2-D Mapping of the Composition and Homogeneity of Polymer Inclusion Membranes. Australian Journal of Chemistry, 64(7), 930-938. (2011).

Stroeven, A.P., Fabel, D., Harbor, J.M., Fink, D., Caffee, M.W., Dahlgren, T., Importance of sampling across an assemblage of glacial landforms for interpreting cosmogenic ages of deglaciation. Quaternary Research, 76(1), 148-156. (2011).

Taguchi, S., Law, R.M., Rödenbeck, C., Patra, P.K., Maksyutov, S., Zahorowski, W., Sartorius, H., and Levin, I., TransCom continuous experiment: comparison of ^{222}Rn transport at hourly time scales at three stations in Germany. Atmospheric Chemistry and Physics. 11(19), 10071–10084. (2011).

Tallon, C. Slater, S., Gillen A., Wood, C. and Turner, J., Ceramic Materials for Hypersonic Applications. Materials Australia, 2011(July), 28-32. (2011).

Taraban, M.B., Ramachandran, S., Gryczynski, I., Gryczynski, Z., Trewhella, J., Yu, Y.H.B., Effects of chain length on o ligopeptide hydrogelation. Soft Matter, 7(6), 2624-2631. (2011).

Telford, A. M., Thickett, S. C., James, M. and Neto, C., Competition between Dewetting and Cross-Linking in Poly(N-vinylpyrrolidone)/Polystyrene Bilayer Films. Langmuir, 27(23), 14207-14217. (2011).

Thorogood, G. J., Avdeev, M., Carter, M. L., Kennedy, B. J., Ting, J. and Wallwork, K. S., Structural phase transitions and magnetic order in $SrTcO_3$. Dalton Transactions, 40(27), 7228-7233. (2011).

Thorogood, G. J., Kennedy, B.J., Avdeev. M., Peterson, V.K., Hanna. J.V. and Luca, V., Cation disorder in $NaW_2O_{6+\delta}$• $nH_{2-z}O$ post-ion exchange with K, Rb, Sr, and Cs. Journal of Physics and Chemistry of Solids, 72(6), 692-700. (2011).

Thorogood, G. J., Orain, P-Y., Ouvry, M., Piriou, B., Tony, T., Wallwork, K. S., Herrmann, J. and James, M., Structure, crystal chemistry and magnetism of rare earth calcium-doped cobaltates: $Ln_{2-x}Ca_xCoO_{4+d}$ (Ln = Pr, Nd, Sm, Eu And Gd). Solid State Sciences, 13(12), 2113-2123. (2011).

Thorogood, G.J., Zhang, Z.M., Hester, J.R., Kennedy, B.J., Ting, J., Glover, C.J., Johannessen, B., Structure and cation ordering in spinel-type $TcCo_2O_4$. An example of a trivalent technetium oxide. Dalton Transactions, 40(41), 10924-10926. (2011).

Tillett, B.J., Meekan, M.G., Field, I. C., Hua, Q., Bradshaw, C.J.A, Similar life history traits in bull (Carcharhinus leucas) and pig-eye (C. amboinensis) sharks. Marine and Freshwater Research, 62(7), 850-860. (2011).

Toudic, B., Rabiller, P., Bourgeois, L., Huard, M., Ecolivet, C., McIntyre, G.J., Bourges, P., Breczewski, T. Janssen, T., Temperature-pressure phase diagram of an aperiodic host guest compound. Europhysics Letters, 93(1), Art. No.16003. (2011).

Twining, J. R., Hughes, C. E., Harrison, J. J., Hankin, S., Crawford, J., Johansen M., Dyer, L., Biotic, temporal and spatial variability of tritium concentrations in transpirate samples collected in the vicinity of a near-surface low-level nuclear waste disposal site and nearby research reactor. Journal of Environmental Radioactivity, 102(6), 551-558. (2011).

Vance, E.R., Zhang, Y., McLeod, T. and Davis, J., Actinide valences in xenotine and monazite. Journal of Nuclear Materials, 409(3), 221-224. (2011).

Velinov, T., Ahtapodov, L., Nelson, A., Gateshki, M., Bivolarska, M., Influence of the surface roughness on the properties of Au films measured by surface plasmon resonance and x-ray reflectometry. Thin Solid Films, 519(7), 2093-2097. (2011).

Wacklin, H.P., Composition and Asymmetry in Supported Membranes Formed by Vesicle Fusion. Langmuir, 27(12), 7698-7707. (2011).

Wagemaker, M., Singh, D.P., Borghols, W.J.H., Lafont, U., Haverkate, L., Peterson, V.K., Mulder, F.M., Dynamic Solubility Limits in Nanosized Olivine $LiFePO_4$. Journal of the American Chemical Society, 133(26), 10222-10228. (2011).

Wagner, K., Griffith,M.J., James M., Mozer, A.J., Wagner, P., Triani, G., Officer, D.L. and Wallace, G.G., Significant performance improvement of porphyrin-sensitised TiO_2 solar cells under prolonged illumination. Journal Physical Chemistry C, 115(1), 317-326. (2011).

Wakeham, D., Nelson, A., Warr, G. G. and Atkin, R., Probing the protic ionic liquid surface using X-ray reflectivity. Physical Chemistry Chemical Physics, 13(46), 20828-20835. (2011).

Wang, J. L., Studer, A. J., Campbell, S. J., Kennedy, S. J., Zeng, R., Dou, S. X., Wu, G. H., Magnetic Structures of $Pr_{0.8}Lu_{0.2}Mn_2Ge_2$ and $Pr_{0.6}Lu_{0.4}Mn_2Ge_2$. IEEE Transactions on Magnetics, 47(10), 2893-2896. (2011).

Wang, J., Liu, Y., Withers, R.L., Studer, A., Li, Q., Noren, L., Guo, Y.P., A correlated electron diffraction, *in situ* neutron diffraction and dielectric properties investigation of poled (1-x) $Bi_{0.5}Na_{0.5}TiO_3$-$xBaTiO_3$ ceramics. Journal of Applied Physics, 110(8), Art. No. 084114. (2011).

Wang, J.L., Campbell, S.J., Cadogan, J.M., Studer, A.J., Zeng, R., Dou, S.X., Magnetocaloric effect in layered $NdMn_2Ge_{0.4}Si_{1.6}$. Applied Physics Letters, 98(23), Art. No. 232509. (2011).

Wang, J.L., Campbell, S.J., Kennedy, S.J., Zeng, R., Dou, S.X., Wu, G.H., Critical magnetic transition in $TbNi_2Mn$-magnetization and Mössbauer spectroscopy. Journal of Physics: Condensed Matter, 23(21), Art. No. 216002. (2011).

Wang, J.L., Campbell, S.J., Zeng, R., Dou, S.X., Kennedy, S.J., Magnetic phase transition and Mossbauer spectroscopy of $ErNi_2Mnx$ compounds. Journal of Applied Physics, 109(7), Art. No. 07E304. (2011).

Wang, S.H., Sun, Y.S., Chiang, A.S.T., Hung, H.F., Chen, M.C., Wood, K., Carboxylic Acid-Directed Clustering and Dispersion of ZrO_2 Nanoparticles in Organic Solvents: A Study by Small-Angle X-ray/Neutron Scattering and NMR. Journal of Physical Chemistry C, 115(24), 11941-11950. (2011).

Webster, N.A.S., Hartlieb, K.J., Saines, P.J., Ling, C.D., Lincoln, F.J., New quenched-in fluorite-type materials in the Bi_2O_3-La_2O_3-PbO system: Synthesis and complex phase behaviour up to 750 degrees C. Materials Research Bulletin, 46(4), 538-542. (2011).

Webster, N.A.S., Loan, M.J., Madsen, I.C., Knott, R.B., Kimpton, J.A., An investigation of the mechanisms of goethite, hematite and magnetite-seeded $Al(OH)_3$ precipitation from synthetic Bayer liquor. Hydrometallurgy, 109(1-2), 72-79. (2011).

Weir, M.P., and Parnell, A.J., Water Soluble Responsive Polymer Brushes, Polymers, 3(4), 2107-2132.(2011).

Weir, M.P., Heriot, S.Y., Martin, S.J., Parnell, A.J., Holt, S.A., Webster, J.R.P., Jones, R.A.L., Voltage-Induced Swelling and Deswelling of Weak Polybase Brushes. Langmuir, 27(17), 11000-11007. (2011).

Werry, E. L., Liu, G. J., Lovelace, M. D., Nagarajah, R., Hichie, I. B., and Bennett, M. R., Lipopolysaccharide-stimulated interleukin-10 release from neonatal spinal cord microglia is potentiated by glutamate. Neuroscience, 175, 93-103. (2011).

White, C. E., Provis, J. L., Kearley, G. J., Riley, D. P., and van Deventer, J. S. J., Density functional modelling of silicate and aluminosilicate dimerisation solution chemistry. Dalton Transactions, 40(6), 1348-1355. (2011).

White, D. A., Fink, D., and Gore, D. B., Cosmogenic nuclide evidence for enhanced sensitivity of an East Antarctic ice stream to change during the last deglaciation. Geology, 39(1), 23-26. (2011).

Whittle, K. R., Blackford, M G., Aughterson, R. D., Lumpkin, G R., and Zaluzec, N. J., Ion irradiation of novel yttrium/ytterbium-based pyrochlores: The effect of disorder. Acta Materialia, 59(20), 7530-7537. (2011).

Williams, A.G., Zahorowski, W., Chambers, S., Griffiths, A., Hacker, J.M., Element, A., Werczynski, S., The vertical distribution of radon in clear and cloudy daytime terrestrial boundary layers. Journal Of The Atmospheric Sciences, 68(1), 155-174. (2011).

Williams, M. and Jacobsen, G. E., A wetter climate in the desert of northern Sudan 9700 -7600 years ago. Sahara, 22, 1-14. (2011).

Winton, B. R., Ionescu, M., Lukey, C., Wilson, Nevirkovets, I. P., Dou, S. X., Micro-patterned Surface Modifications of Poly(dimethylsiloxane) (PDMS) substrates for Tissue Engineering. Advanced Science Letters 4(2), 431-436. (2011).

Wood, S.W., Hua, Q., Bowman, D.M.J.S. (2011). Fire-patterned vegetation and the development of organic soils in the lowland vegetation mosaics of south-west Tasmania. Australian Journal Of Botany, 59(2), 126-136. (2011).

Woodward, C., Chang, J., Zawadzki, A., Shulmeister, J., Collecut, S., Jacobsen, G., Haworth, R., Evidence against early nineteenth century major European induced environmental impacts by illegal settlers in the New England Tablelands, south eastern Australia. Quaternary Science Reviews, 30(27-28), 3743-3747. (2011).

Wyatt, A. R., Yerbury, J. J., Berghofer, P., Greguric, I., Katsifis, A., Dobson, C. M., Wilson, M. R., Clusterin facilitates in vivo clearance of extracellular misfolded proteins. Cellular and Molecular Life Sciences, 68(23), 3919-3931. (2011).

Xia, Y., Conen, F., Haszpra, L., Ferenczi, Z., Zahorowski, W. (2011). Evidence for Nearly Complete Decoupling of Very Stable Nocturnal Boundary Layer Overland. Boundary-layer Meteorology, 138(1), 163-170. (2011).

Yamada, M., Iwashita, Y., Kanaya, T., Ichikawa, M., Tongu, H., Kennedy, S.J., Shimizu, H.M., Mishima, K., Yamada, N.L., Hirota, K., Carpenter, J.M., Lal, J., Andersen, K., Geltenbort, P., Guerard, B., Manzin, G., Hino, M., Kitaguchi, M., Bleuel, M., The performance of magnetic lens for focusing VCN-SANS. Nuclear Instruments and Methods in Physics Research Section a-Accelerators Spectrometers Detectors and Associated Equipment, 634(Suppl.), S156-S160. (2011).

Yan, K, Carr, D.G., Kabra, S., Reid, M, Studer, A, Harrison, R.P., Dippenaar R. and Liss, K-D., *In situ* Characterization of Lattice Structure Evolution during Phase Transformation of Zr-2.5Nb. Advanced Engineering Materials, 13(9), 882-886. (2011).

Yan, T., Zheng, F.F., Yu, Y.G., Qin, S.B., Liu, H., Wang, J.Y., Yu, D.H., Formation mechanism of black $LiTaO_3$ single crystals through chemical reduction. Journal of Applied Crystallography, 44(part 1) 158-162. (2011).

Yang, D., Sarina, S., Zhu, H., Liu, H., Zheng, Z., Xie, M., Smith, S. V., Komarneni, S., Capture of radioactive cesium and iodide Ions from water by using titanate nanofibers and nanotubes. Angewandte Chemie International Edition, 50(45), 10594–10598.(2011).

Yang, X.S., Yuan, L.X., Peterson, V.K., Yin, Y.B., Minett, A.I. Harris, A.T., Open-Ended Aligned Carbon Nanotube Arrays Produced Using CO_2-Assisted Floating-Ferrocene Chemical Vapor Deposition. Journal of Physical Chemistry C, 115(29), 14093-14097. (2011).

Yang, Z.X., Du, G.D., Guo, Z.P., Yu, X.B., Chen, Z.X., Guo, T.L., Sharma, N., Liu, H.K., TiO_2B@anatase hybrid nanowires with highly reversible electrochemical performance. Electrochemistry Communications, 13(1), 46-49. (2011).

Yao, S.H., Wang, J.Y., Liu, H., Yan, T., Yu, D.H., Chen, Y.F., Mechanism of the abnormal thermal expansion of nearly stoichiometric $LiNbO_3$. Journal of Crystal Growth, 318(1), 951-953. (2011).

Yaron, P.N., Scott, A.J., Reynolds, P.A., Mata, J.P., White, J.W., High Internal Phase Emulsions under Shear. Co-Surfactancy and Shear Stability. Journal of Physical Chemistry B, 115(19), 5775-5784. (2011).

Yeoh, W.K., Gault, B., Cui, X.Y., Zhu, C. Moody, M. P., Li, L., Zheng, R.K., Li, W.X., Wang, X.L., Dou, S.X., Sun, G.L., Lin, C.T., and Ringer, S.P., Direct Observation of Local Potassium Variation and its Correlation to Electronic Inhoogeneity in $BA_{1-x}K_x$. Physical Review Letters, 106(24), Article No. 247002. (2011).

Zeng, R., Debnath, J.C., Chen, D.P., Shamba, P., Wang, J.L., Kennedy, S.J., Campbell, S.J., Silver, T., Dou, S.X., Magnetic properties in polycrystalline and single crystal Ca-doped $LaCoO_3$. Journal of Applied Physics, 109(7), Art. No. 07E146. (2011).

Zeng, R., Dou, S. X., Wang, J. L., and Campbell, S. J., Large magnetocaloric effect in re-entrant ferromagnet $PrMn_{1.4}Fe_{0.6}Ge_2$. Journal of Alloys and Compounds, 509(7), L119-L123. (2011).

Zhang, J.F., Kisi E. H., Kirstein O., Quantitative neutron diffraction texture measurement applied to alpha-phase alumina and Ti_3AlC_2. Journal of Applied Crystallography, 44(Part 5), 1062-1070. (2011).

Zhang, K., Feichter, J., Kazil, J., Wan, H., Zhuo, W., Griffiths, A.D., Sartorius, H., Zahorowski, W., Ramonet, M., Schmidt, M., Yver, C., Neubert, R.E.M., Brunke, E.G., Radon activity in the lower troposphere and its impact on ionization rate: a global estimate using different radon emissions. Atmospheric Chemistry And Physics, 11(15), 7817-7838. (2011).

Zhang, X. R., Heijnis, H., Dodson, J., Zawadzki, A., Buchanan, G., Environmental changes indicated by grain-size and trace-metal analysis over the past 700 years at Annaburroo Billabong, NT, Australia. Quaternary Australasia, 28(1), 3. (2011).

Zhou, Q.D., Kennedy, B.J., Avdeev, M., Thermal expansion behaviour in the oxygen deficient perovskites $Sr_2BSbO_{5.5}$ (B=Ca, Sr, Ba). Competing effects of water and oxygen ordering. Journal of Solid State Chemistry, 184(9), 2559-2565. (2011).

Zhou, X. Y., Li, X. Q., Zhao, K. L., Dodson, J., Sun, N., Yang, Q., Early agricultural development and environmental effects in the Neolithic Longdong basin (East Gansu). Chinese Science Bulletin, 56(1-6), 1-10. (2011).

Zhu, H., Couper, M.J. and Dahle, A.K., Effect of Process Variables on Mg-Si Particles and Extrudability of 6xxx Series Alumium Extrusions. Journal of Minerals, Metals and Materials Society, 63(11), 66-71. (2011).

Books, Edited Book Chapters, Special Journal Issues and Theses

Book Chapters

Hughes, C.E., Cendon, D.I., Johansen, M.P., Meredith, K.T., Climate Change and Groundwater. In Johes, J.A.A. (Ed.), Sustaining Groundwater Resources: A Critical Element in the Global Water Crisis (pp. 97-117). New York: Springer. (2011).

*Peterson, V. K., Studying the Hydration of Cement Systems in Real Time using Quasielastic and Inelastic Neutron Scattering. In Studying Kinetics with Neutrons - Prospects for Time-Resolved Neutron Scattering. Eds. G. Eckold, H. Schober and S. E. Nagler, pp. 19-75. Springer, Heidelberg. (2010).

Voskoboinikov, R. E., Recent Advances in Molecular Dynamics Modelling of Radiation Effects in a-Zr. In M. P. Hemsworth (Ed.), Nuclear Materials. Nova Publishers. Pages, 177-216. (2011).

Technical Reports

Carton, D., Vacuum Technology and Vacuum Design Handbook for Accelerator Technicians. ANSTO External Report ANSTO/E-775. (2011).

Chagué-Goff, C., Goff, J.R., Dominey-Howes, D., Nott, J., Sloss, C., Shaw, W. & Law, L., Tropical Cyclone Yasi and its predecessors. Australian Tsunami Research Centre Miscellaneous Report No. 5, 16 pp. (2011).

Cohen, D., Crawford, J., Siegele, R, Description of ANSTO's Confocal Microprobe Simulation Program, ANSTO External Report E-722. (2011).

Crawford, J., Cohen, D., Doherty, G., Atanacio, A., Calculated K, L, and M shell X-ray line intensities for light ion impact on selected targets from Z=6 to 100. ANSTO External Report ANSTO/E-774. (2011).

Sugawara, D., Goto K., Chagué-Goff, C., Fujino, S., Goff, J., Jaffe, B., Nishimura, Y., Richmond, B., Szczucinski, W., Tappin, D.R., Witter, R., Yulianot, E., Initial field survey report of the 2011 East Japan Tsunami in Sendai, Natori adn Iwanuma Cities. UNESCO-IOC International Tsunami Survey Team. Report to UNESCO, 16 pp. (2011).

Editing of Special Journals

Buttner, H. G. (Ed.) Neutron News, 22 (1-4). Philadelphia, USA: Taylor and Francis Group. (2011)

Theses

Freire, T. "Iso-electric points of modified and unmodified Bauxite Refinery Residues" (Honours Thesis)- Southern Cross University, Australia (2011).

(* not included in previous year's research selections report)

Published Conference Proceedings

Andersen, M.S., Rau, G.C., McCallum, A., Meredith, K., Acworth, R.I., Groundwater recharge and geochemical processes in a semi-arid losing stream using heat, isotopes and geochemistry. 11th Australasian Environmental Isotope Conference and 4th Australasian Hydrogeology Research Conference, 12th-14th July 2011. Cairns, Australia. In 11th Australasian Environmental Isotope Conference and 4th Australasian Hydrogeology Research Conference Proceedings, pp. 18. (2011).

Atanacio, A. J., Stelcer, E., Cohen, D. D., Ion Beam Analysis, Positive Matrix Factorisation and Wind Back Trajectories, Tools for PM2.5 Particle Research in Australia. 20th International Clean Air and Environment Conference (CASANZ 2011), 31 July-2nd August 2011, Auckland, New Zealand. (2011).

Atuchin, V. V., Borosov, S. V.,Pervukhina, N. V. & Zhang, Z., Structural and electronic parameters of complex niobates and tantalates. 2010 International Conference on Nano Science and Technology, 18th -19th December 2010, Emei, China. In International Journal of Applied Physics and Mathematics, 1, pp. 38-42. (2011).

Azcurra, C. S., Hughes, C. E., Parkes, S., Hollins, S. E., Gibson, J.J., McCabe, M.F., Evans, J.P. A comparison between direct and pan-derived measurements of the isotopic composition of atmospheric waters.The 19th International Congress on Modelling and Simulation (MODSIM2011), 12th-16th December 2011. Perth, Western Australia. In F. Chan et al, eds. MODSIM2011, 19th International Congress on Modelling and Simulation. Modelling and Simulation Society of Australia and New Zealand, pp.3279-3285. (2011).

Bartle, C.M., Edgar, A.,Dixie, L., Varoy, C., Piltz, R., Buchanan, S. and Rutherford, K., Novel methods for measuring afterglow in developmental scintillators for X-ray and neutron detection, The Ninth World Conference on Neutron radiography (WCNR-9), 3rd-8th October 2010, Kwa Maritane, North-West, South Africa. In Nuclear Instruments and Methods in Physics Research Section A: Accelerators, Spectrometers, Detectors and Associated Equipment, 651(1), 105-109. (2011).

Bhatia, V., Thorogood, G., Dowd, A. & Cortie, M.B., Thins Films of AuCuAl Shape Memory Alloy for Use in Plasmonic Nano-acturators. 2010 MRS Fall Meeting: Symposium N – Intermetallic Based Alloys for Structural and Functional Application, 29th November – 3rd December 2010, Boston, Massachusetts, USA. In M. Palm, B. P. Bewlay, K. S. Kumar, K. Yoshimi (Eds), Intermetallic-Based Alloys for Structural and Functional Applications: MRS Proceedings Volume 1295 (p. mrsf10-1295-n-01-08), Cambridge University Press (2011).

Cadogan, J. M., Avdeev, M., Kumar, P., Suresh, K., D., Ryan, D. H., Neutron powder diffraction determination of the magnetic structure of Nd2Al, Joint European Magnetic Symposia (JEMS 2010), 23th-28th August 2010, Krakow, Poland. In Journal of Physics: Conference Series, 303(1), Art. No. 012026. (2011).

Chagué-Goff, C., Goff, J.R., Dudley, W., Nichol, S., Mooney, S., Zawadzki, A., Bennett, J.W., Heijnis, H., Courtney, C. & Dominey-Howes, D., Multi-proxy analysis of an enigmatic sand layer in Pololu Valley, Hawaii: tsunami or storm deposit? European Geosciences Union General Assembly, 3th-8th April 2011. Vienna, Austria. In Geological Research Abstracts, Vol. 13, EGU2011-1476. (2011).

Chambers, S., Williams, A. G., Zahorowski, W., Griffiths, A., Crawford, J., Separating remote fetch and local mixing influences on near-surface radon gradient measurements. The atmosphere and incorporating the Cape Grim Annual Science Meeting (The fifith CAWCR Workshop), 15th-17th Noverber 2011. Melbourne, Australia. In Keith, A. D. and Holis, A. J. (Eds). Composition of the atmosphere - abstracts of the fifth CAWCR Workshop, CAWCR Technical Report No. 044, pp.6. (2011).

Chamizo, E., Garcia-León, M., Garcia-Tenorio, R., Hotchkis, M. Measurement of Pu and U isotopes on the 1 MV AMS system at the Centro Nacional de Aceleradore. 12th International Conference on Accelerator Mass Spectrometry (AMS 12), 20th - 25th March 2011. Museum of New Zealand: Te Papa Tongarewa, Wellington, New Zealand. (2011).

Child, D. and Hotchkis, M., Plutonium and uranium contamination is soils from the former nuclear weapon tests in Australia. 12th International Conference on Accelerator Mass Spectrometry (AMS 12), 20th - 25th March 2011. Museum of New Zealand: Te Papa Tongarewa, Wellington, New Zealand. (2011).

Child, D. and Simon, K., A new method for separation and purification of beryllium and aluminium using the Eichrom DIPEX® resin. 12th International Conference on Accelerator Mass Spectrometry (AMS 12), 20th - 25th March 2011. Museum of New Zealand: Te Papa Tongarewa, Wellington, New Zealand. (2011).

Darwish, T., Luks, E., Moraes, G., Gillon, M., Hunt, T., Hanley, T., James, M. & Holden, P., Deuteration of Oleic Acid, Lipids and Other Molecules for Neutron Studies. XXII International Congress and General Assembly of the International Union of Crystallography (IUCr2011), 22th – 30th August 2011, Madrid, Spain. In Acta Crystallographica Section A: Foundations of Crystallography, A67 (Supplement), pp. C182. (2011).

Evans, P.J., Nambiar, M., Triani, G., Shapter, J.G. & Losic, D., Fabrication of Titania Nanotube Membranes by Atomic Layer Deposition Using Nanoporous Alumina as a Template. Chemca 2011: Engineering a Better World, 18th – 21th September, 2011, Sydney, New South Wales, Australia, In Proceedings of Chemca 2011, pp. 092. (2011).

Fainerman-Melnikova, M., Ho, E.M. and Soldenhoff, K., Impact of sulphate media on the extraction of rare earths with organophosphorous reagents. 19th International Solvent Extraction Conference (ISEC), 3th -7th October 2011. Santiago, Chile. In Proceedings of the 19th International Solvent Extraction Conference, Chapter 3, Paper 102. (2011).

Fink, D., Fujioka, T., Mifsud, C., Nanson, G., Felton, A., Overturned mega boulders on coastal cliff-tops and in bedrock river channels : can cosmogenic nuclides constrain tsunami and palaeo-flood events in Australia? 12th International Conference on Accelerator Mass Spectrometry (AMS 12), 20th - 25th March 2011. Museum of New Zealand: Te Papa Tongarewa, Wellington, New Zealand. (2011).

Fink, D., Fujioka, T., Mifsud, C., Nanson, G., Felton, A., Quantifying the response of Australian landscapes to climatic and tectonic forcing using cosmogenic isotope analysis. 12th International Conference on Accelerator Mass Spectrometry (AMS 12), 20th - 25th March 2011. Museum of New Zealand: Te Papa Tongarewa, Wellington, New Zealand. (2011).

Fink, D., Storey, B., Joy, K., Shulmeister, J. Constraints on ice volume changes of the West Antarctic Ice Sheet and Ross Ice Shelf since the LGM based on cosmogenic exposure ages. 12th International Conference on Accelerator Mass Spectrometry (AMS 12), 20th - 25th March 2011. Museum of New Zealand: Te Papa Tongarewa, Wellington, New Zealand. (2011).

Fong, N., Guagliardo, P., Williams, J., Musumeci, A., Martin, D., Smith, S. V., Clay particles - potential of Positron Annihilation Lifetime Spectroscopy (PALS) for studying interlayer spacing. 12th International Workshop on Slow Positron Beam Techniques (SLOPOS 12), 1st - 6th August, 2010. Magnetic Island, Australia. In Journal of Physics: Conference Series 262, 12022. (2011).

Fujioka, T., Fink, D., Mifsud, C., Improving the accuracy of aluminium assay in purified quartz for *in situ*, 12th International Conference on Accelerator Mass Spectrometry (AMS 12), 20th - 25th March 2011. Museum of New Zealand: Te Papa Tongarewa, Wellington, New Zealand. (2011).

Goff, J., Chagué-Goff, C. & Dominey-Howes, D. Tracking the extent of the Kuwae. European Geosciences Union General Assembly, 3th-8th April 2011. Vienna, Austria. In Geological Research Abstracts, Vol. 13, EGU2011-85. (2011).

Hackett, M. J., Siegele, R., El-Assad, F., McQuillan, J. A., Aitken, J. B., Carter, E. A., Grau, G. E., Hunt, N. H., Cohen, D. and Lay, P. A., Investigation of the Mouse Cerebellum Using STIM and μ -PIXE Spectrometric and FTIR Spectroscopic Mapping and Imaging. 12th International Conference on Nuclear Microprobe Technology and Applications (ICNMTA 2010), 26th-30th July 2010. Leipzing, Germany. In Nuclear Instruments and Methods in Physics Research Section B: Beam Interactions with Materials and Atoms, 269(20), 2260-2263. (2011).

Harrison, J. J., Zawadzki, A. W., Chisari, R.and Wong, H., Rapid determination of uranium, thorium, plutonium, americium and strontium activities in water, soil and vegetation. South Pacific Environmental Radioactivity Association 2008 conference (SPERA 2008), 23th-27th November 2008. Christchurch, New Zealand. Journal of Environmental Radioactivity, 102(10), 896-900. (2011).

Hotchkis, M. A. C., Child, D., Fink, D. and Wallner, A., Investigation of gas stripping at 4MV for high mass negative ions. 12th International Conference on Accelerator Mass Spectrometry (AMS 12), 20th - 25th March 2011. Museum of New Zealand: Te Papa Tongarewa, Wellington, New Zealand. (2011).

Hua, Q., Ulm, S., Levchenko, V., Fash, W. L., Agurcia, R., Sharer, R., Traxler, L., Petchey, F., Reliable AMS ages for Mayan structures at Copán, Honduras based on Spondylus sp. marine shells. 12th International Conference on Accelerator Mass Spectrometry (AMS 12), 20th - 25th March 2011. Museum of New Zealand: Te Papa Tongarewa, Wellington, New Zealand. (2011).

Hua, Q., Webb, G., Zhao, J-x., Nothdurft, L., Price, G., Variations in marine reservoir corrections for the Great Barrier Reef during the last 7000 years. 12th International Conference on Accelerator Mass Spectrometry (AMS 12), 20th - 25th March 2011. Museum of New Zealand: Te Papa Tongarewa, Wellington, New Zealand. (2011).

Hughes, C.E., Cendon, D.I., Harrison, J.J., Hankin, S., Johansen, M.P. Payne, T.E., Vine, M., Collins, R.N., Hoffmann, E., Loosz, T.M., Movement of a tritium plume in shallow groundwater at a legacy low level radioactive waste disposal site in eastern Australia. South Pacific Environmental Radioactivity Association 2008 conference (SPERA 2008), 23th-27th November 2008. Christchurch, New Zealand. In Journal of Environmental Radioactivity, 102(10), 943-952. (2011).

Hughes, C.E., Crawford, J., Hollins, S.E. Precipitation isotopes in the Sydney Region. 11th Australasian Environmental Isotope Conference and 4th Australasian Hydrogeology Research Conference, 12th-14th July 2011, Cairns, Australia. In 11th Australasian Environmental Isotope Conference and 4th Australasian Hydrogeology Research Conference Proceedings, pp. 38. (2011).

Jacobsen, G., Bertuch, F., Sowada, K., Palmer, T. and Jenkinson, A., Radiocarbon dating of linen from an Eqyptian mummy. 12th International Conference on Accelerator Mass Spectrometry (AMS 12), 20th - 25th March 2011. Museum of New Zealand: Te Papa Tongarewa, Wellington, New Zealand. (2011).

Joseph, D., Scott, K., Greene, R., Stelcer, E., Assessment of Aeolian Dust Properties in the Port Hedland Area and Implications for Future Air Quality Management Strategies. 20th International Clean Air and Environment Conference (CASANZ 2011), 31 July-2nd August 2011, Auckland, New Zealand. (2011).

Joy, K., Carson, N., Fink, D., Storey, B., *In situ* cosmogenic exposure dating in the Meirs and Garwood valleys, Denton Hills, Antarctica, 12th International Conference on Accelerator Mass Spectrometry (AMS 12), 20th - 25th March 2011. Museum of New Zealand: Te Papa Tongarewa, Wellington, New Zealand. (2011).

Keywood, M., Galbally, I., Cope, M., Boast, K., Chambers, S., Cheng, M., Dunne, E., Fedele, R., Gillett, R., Griffiths, A., Lawson, S., Miljevic, B., Molloy, S., Powell, J., Reisen, F., Ristovski, Z., Selleck, P., Ward, J., Sydney Particle Study: overview and motivations. The atmosphere and incorporating the Cape Grim Annual Science Meeting (The fifith CAWCR Workshop), 15th-17th Noverber 2011. Melbourne, Australia. In Keith, A. D. and Holis, A. J. (Eds). Composition of the atmosphere - abstracts of the fifth CAWCR Workshop, CAWCR Technical Report No. 044, pp.42. (2011).

Kirstein, O., Zhang, J. F., Kisi, E. H., Riley, D. F., Ab Initio Phonon Dispersion Curves Used to Check Experimentally Determined Elastic Constants of the MAX Phase Ti3SiC2. International Conference on Structural Integrity and Failure (SIF2010), 4th - 7th July 2010. University of Auckland, Auckland, New Zealand. In Advanced Materials Research, 275, 135-138. (2011).

Le V.S., Izard M., Pellegrini P., Zaw M., Development of 68Ga Generator at ANSTO. 1st World Congress on Ga-68 and Peptide Receptor Radionuclide Therapy, THERANOSTICS, 23th -26th June 2011. Bad Berka, Germany. In World Journal of Nuclear Medicine, Abstracts of Poster Presentations (Chemistry), 10(1), 73-89, P-023. (2011).

Loh, Z. M., Law, R. M., Corbin, K. D., Steele, L. P., Krummel, P. B., Fraser, P. J., Zahorowski, W., Methane simulations at Cape Grim to assess methane flux estimates for South east Australia. The atmosphere and incorporating the Cape Grim Annual Science Meeting (The fifith CAWCR Workshop), 15th-17th Noverber 2011. Melbourne, Australia. In Keith, A. D. and Holis, A. J. (Eds). Composition of the atmosphere - abstracts of the fifth CAWCR Workshop, CAWCR Technical Report No. 044, pp.48. (2011).

McLean, W., Meredith, K., McPhail, D. C., Norman, M. D., Horner, K. N., McDonald, J. G., Impacts of extraction on radiocarbon ages in the Lower Murrumbidgee catchment. 11th Australasian Environmental Isotope Conference and 4th Australasian Hydrogeology Research Conference, 12th-14th July 2011. Cairns, Australia. In 11th Australasian Environmental Isotope Conference and 4th Australasian Hydrogeology Research Conference Proceedings, pp. 44. (2011).

Meredith, K., McLean, W., Norman, M., Identifying groundwater end-members using stable isotopes of silica (δ30Si) in the Lower Namoi Valley, New South Wales. 11th Australasian Environmental Isotope Conference and 4th Australasian Hydrogeology Research Conference, 12th-14th July 2011. Cairns, Australia. In 11th Australasian Environmental Isotope Conference and 4th Australasian Hydrogeology Research Conference Proceedings, pp. 46. (2011).

Mifsud C., Fujioka T., Fink D., Extraction and Purification of Quartz Using Phosphoric Acid. 12th International Conference on Accelerator Mass Spectrometry (AMS 12), 20th - 25th March 2011. Museum of New Zealand: Te Papa Tongarewa, Wellington, New Zealand. (2011).

Minakshi, M., Singh, P., Martin, D., Appadoo, D., Blackford, M. and Ionescu, M., LiNiP04 Aqueous Rechargeable Battery, 219th International ECS Meeting, 1st-6th May 2011,Montreal, Canada. In ECS Transactions, Vol.35(32), 281-292. (2011).

Minami, M., Miyata, Y., Nakamura, T., Hua, Q., A first step toward small-mass AMS radiocarbon analysis at Nagoya University. 12th International Conference on Accelerator Mass Spectrometry (AMS 12), 20th - 25th March 2011. Museum of New Zealand: Te Papa Tongarewa, Wellington, New Zealand. (2011).

Morrision, A. N., Peter, F., Stelcer, E., Cohen D., Haberlah, D., Quantifying Respirable Crystalline Silica in the Ambient Air of the Hunter Valley, Nsw – Sorting The Silica From The Silicon. 20th International Clean Air and Environment Conference (CASANZ 2011), 31 July-2nd August 2011, Auckland, New Zealand. (2011).

Morrison, T., Rayburg, S., Hughes, C., A combined hydrodynamic and mixing model approach to quantify small saline groundwater input into rivers. The XXV IUGG General Assembly Earth ob the edge: Science for a sustainable planet (IUGG 2011), 28th June-7th July 2011. Melbourne, Australia. In Abesser , C. et al (Eds) Conceptual and Modelling Studies of Integrated Groundwater, Surface Water, and Ecological Systems, IAHS Publication Vol,345. pp69-74. IAHS Press, Wallingford Oxfordshire, UK. (2011).

Mume, E., Uedono, A., Mizunaga, G., Lynch, D. E., Smith, S. V., The role of Positrons Annihilation Lifetime Studies and nuclear sensors for characterising porous materials. 12th International Workshop on Slow Positron Beam Techniques (SLOPOS12), 1st-6th August 2010. Magnetic Island, Australia. In Journal of Physics: Conference Series 262, 12040. (2011).

Murugaraj, P., Kumar, N., Jakubov, T. S., Mainwaring, D. E. and Siegele, R., Probing the structure of nanochannal arrays by electrostatic force microscopy, International Conference Nanomeeting-2011, 24th-27th May 2011. Minsk, Belarus. In Physics, Chemistry and Applications of Nanostructures: Proceedings of International Conference Nanomeeting-2011, pp.241-244. (2011).

Nambiar, M., Evans, P. J., Triani, G., Shaper, J. G., Losic, D. Study of titania modified porous alumina membranes for protein transport and separation, Chemca 2011: Engineering a Better World, 18th – 21th September, 2011, Sydney, New South Wales, Australia, In Proceedings of Chemca 2011, pp. 584. (2011).

Olivero, P., Forneris, J., Jaksic, M., Pastuovic, Z., Picollo, F., N. Skukan, N., Vittone, E., Focused ion beam fabrication and IBIC characterisation of a diamond detector with buried electrodes. 12th International Conference on Nuclear Microprobe Technology and Applications Nuclear Instruments and Methods (ICNMTA 2010), 26th-30th July 2010. Leipzing, Germany. In Nuclear Instruments and Methods in Physics Research Section B: Beam Interactions with Materials and Atoms, 269(20), 2340-2344. (2011).

Olivero, P., Forneris, J., Gamarra, P., Jaksic, M., Giudice, A. L., Manfredotti, C., Pastuovic, Z., Skukan, N., Vittone, E., Monte Carlo analysis of a lateral IBIC experiment on a 4H-SiC Schottkey diode. 12th International Conference on Nuclear Microprobe Technology and Applications Nuclear Instruments and Methods (ICNMTA 2010), 26th-30th July 2010. Leipzing, Germany. In Nuclear Instruments and Methods in Physics Research Section B: Beam Interactions with Materials and Atoms, 269(20), 2350-2354. (2011).

Payne, T. E., Brendler, V., Nebelung, C. and Comarmond, M. J., Applicability of surface area normalised distribution coefficients (Ka) in interpreting measurements of radionuclide sorption. South Pacific Environmental Radioactivity Association 2008 conference (SPERA 2008), 23th-27th November 2008. Christchurch, New Zealand. In Journal of Environmental Radioactivity, 102(10), 888-895. (2011).

Pham, B., Guagliardo, P., Williams, J., Samarin, S., Smith, S. V., A study of porosity of synthetic polymer nanoparticles using PALS. 12th International Workshop on Slow Positron Beam Techniques (SLOPOS 12), 1st - 6th August, 2010. Magnetic Island, Australia. In Journal of Physics: Conference Series 262, 12048. (2011).

Reardon-Smith, K.M., Le Brocque, A.F., Hollins, S., Silburn, D.M. Using stable isotopes to identify soil moisture sources of key species in riparian woodlands of the northern Murray-Darling Basin. 11th Australasian Environmental Isotope Conference and 4th Australasian Hydrogeology Research Conference, 12th-14th July 2011, Cairns, Australia. In 11th Australasian Environmental Isotope Conference and 4th Australasian Hydrogeology Research Conference Proceedings, pp. 122. (2011).

Ryan, M., Newnham, R. M., Dunbar, G., Vandergoes, M., Neil, H., Bostock, H., Mid-Late Quaternary vegetation and climate change reconstructed from palynology of marine cores off southwestern New Zealand. 18th International Union for Quaternary Research Congress, 21th-27th July 2011, Berne Switzerland.(2011).

Salim, N. V., Hanley, T., Guo, Q. Microphase separation in double crystalline poly (ethylene oxide)-block-poly (caprolactone)/poly (4-vinyl phenol) blends. The Fifth International Symposium on the Separation and Characterization of Natural and Synthetic Macromolecules, 26th – 28th January 2011, Rhône Congress Centre, Amsterdam, The Netherlands, In P.G. Verschuren and T. Aalbers (Eds), SCM-5 Fifth International Symposium on the Separation and Characterization of Natural and Synthetic Macromolecules: Book of Abstracts. (2011).

Sellaiyan, S., Smith, S. V., Hughes, A.E., Miller, A., Jenkins, D. R., Uedono, A., Understanding the effect of nanoporosity on optimizing the performance of self-healing materials for anti-corrosion applications. 12th International Workshop on Slow Positron Beam Techniques (SLOPOS 12), 1st - 6th August, 2010. Magnetic Island, Australia. In Journal of Physics: Conference Series 262, 12054. (2011).

Simon K., Pedro J., Smith A.M., Child D., Fink D., Reprocessing of 10B-contaminated 10Be AMS targets. 12th International Conference on Accelerator Mass Spectrometry (AMS 12), 20th - 25th March 2011. Museum of New Zealand: Te Papa Tongarewa, Wellington, New Zealand. (2011).

Smith, S. V., The role of nuclear sensors and positrons for engineering nano and microtechnologies. 12th International Workshop on Slow Positron Beam Techniques (SLOPOS 12), 1st - 6th August, 2010. Magnetic Island, Australia. In Journal of Physics: Conference Series 262, 12055. (2011).

Stelcer, E., Morrison, M. A., Atanaciao, A. J. and Cohenhe, D. D., PIXE ANALYSIS OF MOUDI FILTERS. 20th International Clean Air and Environment Conference (CASANZ 2011), 31 July-2nd August 2011, Auckland, New Zealand. (2011).

Varasanec, M., I. Radovic, I. B., Pastuovic, Z., Jaksic, M., Creation of microstructures using heavy ion beam lithography. 12th International Conference on Nuclear Microprobe Technology and Applications Nuclear Instruments and Methods (ICNMTA 2010), 26th-30th July 2010. Leipzing, Germany. In Nuclear Instruments and Methods in Physics Research Section B: Beam Interactions with Materials and Atoms, 269(20), 2413-2416. (2011).

Vorontsov, V.A., Voskoboinikov, R.E. & Rae, C.M.F., Prediction of Mechanical Behaviour in Ni-Base Superalloys Using the Phase Field Model of Dislocations. 2010 European Symposium on Superalloys and their Applications, 25th-28th May, 2010. Wildbach Kreuth, Germany. In Advanced Materials Research, 278, 150. (2011).

Wallner, A., Buczak, K., Plompen, A., Schumann, D., Semkova, V., New exotic and non-standard radionuclides in AMS. 12th International Conference on Accelerator Mass Spectrometry (AMS 12), 20th - 25th March 2011. Museum of New Zealand: Te Papa Tongarewa, Wellington, New Zealand. (2011).

Wang, J. L., Campbell, S.J., Cadogan, J. M., Studer, A.J., Zeng, R. and Dou, S.X., Neutron diffraction study of the magnetic order in NdMn2Ge1.6Si0.4. Joint European Magnetic Symposia (JEMS 2010), 23th-28th August 2010. Krakow, Poland. In Journal of Physics: Conference Series, 303(1), Art. No. 012022. (2011).

Waring, C., Falahat, S. and Watt, G., What can you measure with neutron activation analysis? Global Workshop Proximal Soil Sensing, 15th-18th May 2011. Montreal, Canada. In Proceedings 2nd Global Workshop Proximal Soil Sensing, V.I. Adamchuk, R.A. Viscarra-Rossel (Ed.), pp. 120-123. (2011).

Whitfield, R., Studer, A. and Goossens, D., Temperature Dependence of Diffuse Scattering in PZN. Meeting 2011 TMS Annual Meeting and Exhibition: Symposium Neutron and X-ray Studies of Advanced Materials IV, 27th February-3rd March 2011. San Diego Convention Center, San Diego, California, Metallurgical and Materials Transactions A, 43(5), 1429-1433. (2011).

Williams, S., Goff, J., Chagué -Goff, C., Prasetya, G., Cheung, K.F., Davies, T., Wilson, T., Characterising diagnostic proxies for identifying palaeotsunamis in a tropical climatic regime, Samoan Islands. OCEANS '11 MTS/IEEE KONA (Oceans of Opportunity: International cooperation and partnership across the Pacific), 19th-22th September 2011. Hilton Waikoloa Village, Kona, Hawaii. In Proceedings of the MTS/IEEE Oceans 2011 Conference, INSPEC Accession Number: 12485352. (2011).

Wilson, A., Fainerman-Melnikova, M. and Soldenhoff, K.,, What are the Options for an Integrated IX Process to Recover Uranium from Saline and Hypersaline Liquors. ALTA 2011 Uranium Conference, 23th-27th May 2011. Burswood Convention Centre in Perth, Western Australia. In ALTA 2011 Uranium - 7 Proceedings, p. 116, published by ALTA Metallurgical Services. (2011).

Yang, B., Smith, A., Hua, Q. A cold finger cooling system for the efficient graphitisation of microgramsized carbon samples. 12th International Conference on Accelerator Mass Spectrometry (AMS 12), 20th - 25th March 2011. Museum of New Zealand: Te Papa Tongarewa, Wellington, New Zealand. (2011).

Zahorowski, W., Williams, A. G., Chambers, S., Griffiths, A., Crawford, J., Werczynski, S., Element., A., Vertical radon-222 profiles in the atmospheric boundary layer. The atmosphere and incorporating the Cape Grim Annual Science Meeting (The fifith CAWCR Workshop), 15th-17th Noverber 2011. Melbourne, Australia. In Keith, A. D. and Holis, A. J. (Eds). Composition of the atmosphere - abstracts of the fifth CAWCR Workshop, CAWCR Technical Report No. 044, pp.98. (2011).

Zhao, M., Yang, X., Church, T.L. and Harris, A.T., Interaction between a bimetallic Ni-Co catalyst and micrometer-sized CaO for enhanced H2 production during cellulose decomposition. 11th International Conference: Hydrogen Materials Science & Chemistry of Carbon Nanomaterials (ICHMS'2009), 25th-31th August 2009. Yalta-Crimea, Ukraine. In International Journal of Hydrogen Energy, 36(1), 421-431. (2011).

Zhu, H., Wei, T., Harrison, R., Edwards, L., & Maruyama, K., Development of oxide dispersion strengthened steels for high temperature nuclear structural applications, Fifth World Congress on Engineering Asset Management (WCEAM-AGIC 2010), 25th -27th 2010, Brisbane Queensland, Australia. in Mathew. J; Ma. M; Tan. A; Weijnen. Lee, J (Eds). Engineering Asset Management and Infrastructure Sustainability, pp. 1147 -1160, Springer-Verlag London. (2011).

Front cover images (clockwise from bottom right): the OPAL research reactor pool; Karina Meredith working in the Isotope Ratio Mass Spectrometry Laboratory (p.34); Ramin Rafiei with a new generation radiation detector (p.96); an artist's impression (David S. Goodsell 1999) of molecules in a slice of an E. coli cell (p.12); Tegan Evans working within the confines of a glove box (p.93); James Doutch (left) and Elliot Gilbert preparing the Rapid Visco Analysis for use on the Quokka SANS instrument (p.28).

Back cover images (clockwise from bottom right): the OPAL research reactor building; Winnie Kam in the laboratory studying the effect of the translocator protein in diseases such as schizophrenia and psychosis (p.20); Michael Hotchkis in front of the ANTARES accelerator (p.46); ANSTO staff viewing the OPAL reactor pool; (centre) part of the titanium roofing of the OPAL reactor building.

ANSTO Research Selections 2012

Published by
The Australian Nuclear Science and Technology Organisation (ANSTO)

Available from
PDF version is available on the ANSTO website
www.ansto.gov.au

ANSTO August 2012

www.ansto.gov.au